To the Graduate Council:

I am submitting a thesis written by James L. Kalbas entitled "Geology of part of the southwestern Brushy Mountains, Inner Piedmont, North Carolina, and the geochemistry of western Inner Piedmont migmatite." I have examined the final paper copy of this thesis for form and content and recommend that it be accepted in partial fulfillment of the requirements for the degree of Master of Science, with a major in Geology.

Robert D. Hatcher Jr., Major Professor

We have read this thesis and recommend its acceptance:

Karla C. Mora

Lawrence A. Taylor

Acceptance for the Council:

Vice Provost and Dean of Graduate Studies

Geology of part of the southwestern Brushy Mountains, Inner Piedmont, North Carolina, and the geochemistry of western Inner Piedmont migmatite

A Thesis
Presented for the
Master of Science Degree
University of Tennessee, Knoxville

James L. Kalbas
May, 2003

U.T. Archives
Thesis
2003
.K25

to my wife, Jennifer,
for her support, encouragement, and love
Thank You!

Acknowledgments

My first thanks goes to Professor Robert D. Hatcher, Jr. His support, encouragement, and advice during my tenure at the University of Tennessee have been vital not only to my success in completing this thesis, but also in completing departmental requirements. Dr. Hatcher's enthusiasm for field geology and dedication to his students have made him an always available resource. Many thanks also go to my thesis committee members, Dr. Lawrence Taylor and Dr. Kula Misra, who provided helpful feedback and constructive criticism. Additional thanks go to Dr. Taylor for providing access to the electron microprobe facility at the University of Tennessee.

I also send a heartfelt thank you to my colleagues in the Tectonics and Structural Geology Research Group at the University of Tennessee. Technical support and constructive advice on countless topics and occasions came from Chris and Jennifer Whisner and David Settles. My classmate and fellow Brushy Mountain mapper, Arthur Merschat, played an integral role in keeping me sane on long, hot, tick-infested days in the backcountry. My fellow tectonic geochemist and co-author, Brendan Bream, however, deserves my utmost gratitude. Collaboration with Brendan, whether it was for editing, scholarly discussions, or just blowing off steam proved to be the most educative times for me in the past two years. Nancy Meadows (a.k.a., "mom") has been key to the success of essentially all of our work in the Hatchery. Her careful editing on numerous occasions for this study is most appreciated. Her heart, enthusiasm, and genuine care for all of us makes the "Hatchery" a wonderful place to work every day.

My parents Bill and Jackie Kalbas, and siblings Katie and Jay Norton, have always encouraged me to be passionate about my research and persistent in pursuing my

goals. Moreover, they have all helped me laugh and see the lighter side of life even in times of frustration and mental exhaustion. Finally, I thank my wife, Jennifer. Without her love, patience, and usually gentle encouragement I think I never would have finished.

My research was supported for two field seasons by the National Cooperative Geologic Mapping Program, EDMAP component, administered by the U. S. Geological Survey. Additional financial support came from Dr. Hatcher and the University of Tennessee Science Alliance Center of Excellence Distinguished Scientist stipend.

Abstract

The newly defined boundary between the western and eastern Inner Piedmont belts has been the focus of several recent tectonic studies in the southern Appalachians. Specifically, the Brindle Creek fault was recognized in southwestern North Carolina as a thrust that juxtaposed Siluro-Devonian-age paragneisses (now-known) and Devonian and Mississippian granites atop Neoproterozoic- to Cambrian-age paragneisses, Middle Ordovician volcanic and metasedimentary rocks, and Ordovician intrusive units.

Detailed geologic mapping in the Kings Creek 7.5-minute quadrangle, southwestern Brushy Mountains, Caldwell County, North Carolina, revealed the northeastern continuation of the thrust. Recognition of the northeastern extension of the fault, and analysis of small-scale map compilations indicate the thrust is a major (crustal-scale) boundary.

Structural data denote six deformation events in the southwestern Brushy Mountains. Penetrative and partially penetrative fabrics are attributed to syn-peak and post-peak metamorphic deformation (Neoacadian and earliest Alleghenian; D_2 and D_3, respectively). Changes in the orientations of D_2 and D_3 structures were observed in the study area; foliations, mineral stretching lineations, and isoclinal and tight fold axes in the northwestern two thirds of the quadrangle are strongly oriented northeast-southwest. Structural orientations in the southeastern corner of the quadrangle vary, but are dominantly oriented east-west, southeast-northwest, and north-south. The structural transition represents Neoacadian transpressional flow caused by buttressing of plastically deforming thrust sheets against the primordial Brevard fault zone. Mylonites immediately adjacent to a second thrust fault (the Green Mountain/Mill Spring thrust)

also confirm a significant component of dextral strike-slip displacement. Two episodes of post-Neoacadian folding (F_4 and F_5) complexly refolded F_2 (isoclinal) and F_3 (tight) folds. Multiple joint sets are also attributed to Alleghanian and Mesozoic-Cenozoic deformation.

A zone of intensely migmatized amphibolite and biotite-hornblende granodiorite was identified in the immediate footwall of the Brindle Creek thrust in the Kings Creek quadrangle and extrapolated ~110 km to the southwest. Detailed geologic mapping has locally placed the migmatite in the same tectonostratigraphic position as the Poor Mountain Formation; intense migmatization, however, has obscured virtually all primary sedimentological evidence that could establish an unequivocal migmatite protolith.

U-Pb ion microprobe (SHRIMP RG) geochronology of zoned zircons indicate the migmatite protolith has a Middle Ordovician crystallization age (zircon cores), and was subsequently metamorphosed at 342 Ma and 330 Ma (zircon rims). The crystallization age is coeval with the Poor Mountain Quartzite member. Whole-rock trace and rare earth element chemical data from melanocratic and leucocratic constituents of the migmatite also suggest partial derivation from the Poor Mountain Amphibolite. The highly fractionated migmatite leucosome, an *in situ* anatectic melt, is enriched in low compatibility trace elements and depleted in high compatibility trace elements. A subset of melanocratic samples has similar concentrations of low compatibility trace elements as the Poor Mountain Amphibolite, but is depleted in higher compatibility elements. The same samples have nearly identical flat REE trends as Poor Mountain Amphibolite samples, but are slightly REE depleted. Emplacement of the hot Brindle Creek thrust

sheet in the Neoacadian likely resulted in intense migmatization of the already hot Poor Mountain Formation and adjacent units.

Table of Contents

Overview **1**

Part I: Lithologic and Metamorphic Relationships of the Kings Creek 7.5-minute Quadrangle **4**

Abstract **5**

Introduction **6**

Geologic Setting **12**

Structural Patterns 12

Regional Lithologic Succession 13

Metamorphism and Deformation 16

The Kings Creek Quadrangle 17

Methods **18**

Lithologic Units **20**

Brindle Creek Fault Hanging Wall 20

Brindle Creek Fault Footwall 42

Green Mountain Fault Footwall 55

Metamorphism **61**

Brindle Creek Fault Footwall 63

Brindle Creek Fault Hanging Wall 67

Discussion **67**

Timing of Metamorphism and Deformation 67

Petrogenesis of the Walker Top Gneiss 69

Petrogenesis of the Hibriten gneiss 69

Conclusions **72**

References Cited **73**

Part II: Structural Geology of the Kings Creek Quadrangle, North Carolina **80**

Abstract **81**

Introduction **82**

Methods **85**

Structural and Tectonic Framework **86**

Map Patterns 86

Deformation Hierarchy 89

Structural Interpretation **106**

Section A-A′ 106

Section B-B′ 108

Section C-C′ 109

Brindle Creek Thrust Sheet in theKings Creek Quadrangle 109

Synthesis **112**

Conclusions **116**

References Cited **117**

Part III: Intense Migmatization Beneath the Brindle Creek Thrust Separating the Eastern and Western Inner Piedmont, North Carolina: Distribution, Geochronology, Geochemistry, and Petrogenesis 122

Abstract **123**

Introduction **124**

Macroscopic Relationships **127**

Mesoscopic Relationships **132**

Petrography **135**

Sampling and Analytical Methods **137**

Whole-rock Chemistry 137

Zircon Geochronology 138

Chemical Relationships **139**

Chemistry of the Migmatite 139

Tectonic affinity of the Poor Mountain Amphibolite 147

Geochronology 155

Discussion **159**

Petrogenesis 159

Timing of Migmatization 163

Migmatite Protolith 163

Tectonic Implications of fault-related anatexis in the Inner Piedmont 169
Conclusions **172**
Acknowledgments **173**
References Cited **174**
Appendices **181**
Appendix A: Structural and Rock Type Data for the Kings Creek Quadrangle **182**
Vita **208**

List of Figures

PART I

Figure 1-1. Generalized tectonic map of the southern Appalachian orogen. 7

Figure 1-2. Index map showing the location of the study area in western North Carolina 9

Figure 1-3. Metamorphic isograd map of part North and South Carolina..... 10

Figure 1-4. Location and reconnaissance maps of the Brushy Mountain study area..... 11

Figure 1-5. Detailed geologic map of the Kings Creek 7.5 minute quadrangle, Caldwell County, North Carolina..... 19

Figure 1-6. Generalized lithologic column for the study area..... 21

Figure 1-7. Sillimanite schist on U. S. 64 near its intersection with McRary Creek Road..... 23

Figure 1-8. Outcrop exposure of migmatitic biotite gneiss (metagraywacke) at station KC-3 on U. S. 64 at the western boundary of the Kings Creek quadrangle..... 24

Figure 1-9. Saprolitic exposures of the Brindle Creek thrust hanging wall sillimanite schist..... 25

Figure 1-10. Sillimanite schist from the Brindle Creek thrust hanging wall..... 27

Figure 1-11. Brindle Creek fault hanging wall sillimanite schist in thin section 28

Figure 1-12. Metagraywacke (biotite gneiss) in scanned thin section 30

Figure 1-13. Walker Top Granite in outcrop and hand specimen..... 32

Figure 1-14. Walker Top Granite in thin section..... 35

Figure 1-15. IUGS modal classification (Streckeisen, 1976) of Brindle Creek fault hanging wall gneisses.... 36

Figure 1-16. Hibriten orthogneiss from station KC-536, located ~1.94 km south of the clubhouse at the Cedar Rock Country Club..... 39

Figure 1-17. Topographic maps showing the proposed type locality for the Hibriten orthogneiss in the Kings Creek 7.5 minute quadrangle..... 40

Figure 1-18. Hibriten orthogneiss in scanned thin section 41

Figure 1-19. Western Inner Piedmont stromatic migmatite 45

Figure 1-20. Topographic maps showing the proposed type locality for the Lenoir Quarry migmatite in the Kings Creek 7.5 minute quadrangle 47

Figure 1-21. Stromatic Lenoir Quarry migmatite at the Vulcan Materials Company Lenoir Quarry on North Carolina 18 near Lenoir 48

Figure 1-22. Lenoir Quarry migmatite at the Vulcan Materials Company Lenoir Quarry on North Carolina 18 49

Figure 1-23. Scanned thin section in cross-polarized light showing the texture of Lenoir Quarry migmatite from station KC-504, ~0.45 km east of Hibriten High School 51

Figure 1-24. Textures in the Lenoir Quarry migmatite 52

Figure 1-25. Mylonitic Tallulah Falls migmatite from the footwall of the Green Mountain thrust at station KC-1792, ~1.3 km east of Moses Knob 56

Figure 1-26. Mylonitic metagraywacke from the Tallulah Falls Formation 58

Figure 1-27. Type II S-C mylonite from the Tallulah Falls Formation 60

Figure 1-28. IUGS modal classification (Streckeisen, 1976) of the Henderson Gneiss 62

Figure 1-29. Petrogenetic grids for aluminous rocks with metamorphic P-T conditions plotted from various IP studies 64

Figure 1-30. Chemical variation diagram for calcium-rich amphibole 66

PART II

Figure 2-1. Generalized tectonic map of the southern Appalachian orogen 84

Figure 2-2. Detailed geologic map of the Kings Creek quadrangle, Caldwell County, North Carolina 87

Figure 2-3. Lower hemisphere, equal area scatter plot and Kamb contoured projections of poles to foliations and dip histograms 90

Figure 2-4. Backscatter electron image of localized truncations of biotite into a quartz layer in sillimanite schist 95

Figure 2-5. Cross sections A-A', B-B', and C-C' (section lines referenced in Plate 1)..... 96

Figure 2-6. Lower hemisphere, equal area scatter plot and contoured fabric diagrams of lineation orientations and plunge histograms 98

Figure 2-7. Lower hemisphere, equal area scatter plots of fold axis and axial surface orientations 99

Figure 2-8. Structures in migmatites of the Green Mountain thrust sheet..... 100

Figure 2-9. Mineral lineation and fold axis orientations in Domains I and II 101

Figure 2-10. Systematic joint orientations in the Kings Creek quadrangle 107

PART III

Figure 3-1. Generalized tectonic map of the southern Appalachian orogen 126

Figure 3-2. Generalized lithotectonic map 128

Figure 3-3. Migmatitic structures from the study area 131

Figure 3-4. Typical Poor Mountain Amphibolite at station PMA-1.0 (Fig. 3-2) located in the Mill Spring thrust footwall ~4 km south of Glenwood on North Carolina 18..... 133

Figure 3-5. Sketch of structures in migmatite adjacent to the Brindle Creek thrust ~2 km east of the Vulcan Materials Company Lenoir Quarry in the Kings Creek quadrangle 136

Figure 3-6. Two-element variation diagrams of major oxide and select trace element concentrations vs. Zr... 142

Figure 3-7. Two-element variation diagrams of major oxide and select trace element compositions vs. Mg # for the Brindle Creek footwall migmatite, Poor Mountain Amphibolite, Tallulah Falls metagraywacke, Poor Mountain Quartzite, Dysartsville Tonalite, Toluca Granite, Toccoa granitoid, and granitoid in the Henderson Gneiss..... 143

Figure 3-8. Chondrite-normalized trace element concentrations of migmatite..... 145

Figure 3-9. Chondrite-normalized REE concentrations of migmatite 146

Figure 3-10. Mg, c, al-alk-ortho-and para-amphibolite discrimination diagram (after Leake, 1964)..... 150

Figure 3-11. AFM ternary diagrams 151

Figure 3-12. Ti-Zr-Y tectonic discrimination diagrams for basalt (after Pearce and Cann, 1973) 152

Figure 3-13. Zr/Y-Zr tectonic discrimination diagrams for basalts (after Pearce and Norry, 1979) 153

Figure 3-14. Ti/Zr tectonic discrimination diagrams for basalts (after Pearce and Cann, 1973) 154

Figure 3-15. Backscattered electron and cathodoluminescence images from the migmatite leucosome 156

Figure 3-16. Concordia and summed probability plot of SHRIMP RG data. a) Concordia diagram showing all data from the migmatite leucosome 160

Figure 3-17. Chondrite-normalized trace element concentrations of migmatite sample groups compared with concentration reference points and fields from Poor Mountain Amphibolite and select eastern and western Inner Piedmont orthogneisses 165

Figure 3-18. Chondrite-normalized REE concentrations 166

List of Tables

PART I

Table 1-1. Modal mineralogy of Brindle Creek thrust hanging wall metagraywacke and sillimanite schist 26

Table 1-2. Modal mineralogy of the Walker Top Granite 34

Table 1-3. Modal mineralogy of the Hibriten orthogneiss 43

Table 1-4. Modal mineralogy of the Lenoir Quarry migmatite 50

Table 1-5. Composite amphibole and epidote analyses from Lenoir Quarry migmatite sample KC-VQ-1, collected from the Vulcan Materials Company Lenoir Quarry 54

Table 1-6. Modal mineralogy of the Tallulah Falls Formation metagraywacke-schist 59

PART II

Table 2-1. The relative timing and nature of deformation events in the central and western IP, North Carolina (modified from Davis, 1993; Yanagihara, 1994; Bream, 1999; Hill, 1999; Giorgis, 1999; Williams, 2000; and Bier, 2001). BCT = Brindle Creek thrust; BFZ = Brevard fault zone; MST = Mill Spring thrust; SMT = Sugarloaf Mountain thrust; TCT = Tumblebug Creek thrust 91

PART III

Table 3-1. Concentrations of major and trace elements in Poor Mountain Formation and migmatitic amphibolite andgranodiorite 140

Table 3-2. Normative mineralogy of the migmatite 141

Table 3-3. Concentrations of major and trace elements in Poor Mountain Formation 148

Table 3-4. Ion microprobe (SHRIMP RG) data for zircons from the Vulcan Materials Company Lenoir quarry (sample LVQ1) 158

List of Plates

Plate 1. Geologic map of part of the Inner Piedmont, south-central and southwestern North Carolina.

Plate 2. Geologic map and cross sections of the Kings Creek 7.5 minute quadrangle, Caldwell County, North Carolina.

Plate 3. Station locations within the Kings Creek 7.5 minute quadrangle, North Carolina.

Overview

This thesis presents work completed in two years of study of the eastern and western Inner Piedmont, North Carolina. Research centered on geologic mapping (at 1:12,000- and 1:24,000-scales) of the Kings Creek 7.5-minute quadrangle, Caldwell County, North Carolina. This first-ever detailed geologic mapping and structural/geochemical study in the Brushy Mountains, an area of moderate topographic relief northeast of the Morganton Basin (Plate 1), is complemented by the work of Arthur J. Merschat in the adjacent Ellendale and Boomer 7.5-minute quadrangles. A primary goal of our combined research was to trace the Brindle Creek fault northeastward from the South Mountains, where it was originally recognized as a thrust fault. My field research yielded 1872 field stations collected during 9 months of work. Data and interpretations presented here provide greater insight into the tectonic history of this part of the Inner Piedmont.

This thesis contains three chapters. Each is intended to be a free-standing, potentially publishable work, and therefore contains a separate abstract, introduction, synthesis, conclusions, and references. For this reason, certain introductory and reference notations are duplicated, but each section centers upon unique themes, perspectives, and interpretations. Part I describes lithotectonic units in the Kings Creek quadrangle, and includes all data collected in the field and laboratory that pertain to lithologic relationships observed in rock units from the study area. Part I is largely a data report that includes mineralogic and petrographic descriptions of the eight major lithologic units in the study area. A discussion of the timing and nature of metamorphism in the study area and in laterally adjacent areas (the South Mountains, North Carolina) is also included.

One important unit, an intensely migmatitic amphibolite and biotite-hornblende granodiorite in the footwall of the Brindle Creek thrust, is informally named the Lenoir Quarry migmatite in Part I. This nomenclature is based on the lithologic relationships in the study area, and allows petrogenetic objectivity (i.e., no statements are made here about possible migmatite protoliths).

Part II presents an analysis of the structural geology of the Kings Creek quadrangle. Relationships documented at micro-, meso-, and macroscales in the Brushy Mountains are representative of macroscopic trends along the boundary between the western and eastern Inner Piedmont throughout western North Carolina. The timing, nature, and magnitude of successive deformation events are addressed in light of new absolute age constraints from rocks in the study area.

Part III addresses the lithotectonic, temporal, and chemical character of intensely migmatized rocks (the Lenoir Quarry migmatite of Part I) in the immediate footwall of the Brindle Creek fault. The spatial distribution, age, and chemical character of the migmatite are documented, and the data are used to discriminate between potential source rocks from adjacent units.

Appendix A is a table of all primary structural data and field lithologic descriptions recorded in the Kings Creek quadrangle. Data from Appendix A correspond to station localities shown in Plate 3.

PART I

Lithologic and Metamorphic Relationships of the Kings Creek 7.5-minute Quadrangle

Abstract

Detailed geologic mapping of the Kings Creek 7.5-minute quadrangle, Caldwell County, North Carolina, revealed the northeastern extension of the Brindle Creek thrust fault, the boundary between the western and eastern Inner Piedmont (IP) belts. The Brindle Creek thrust sheet is composed of two paragneiss units: metagraywacke and sillimanite schist. An inequigranular quartz-biotite-plagioclase gneiss, not previously mapped at 1:24,000 scale, was also recognized in the Brindle Creek thrust hanging wall and informally named the Hibriten orthogneiss. Disconnected bands of Walker Top Granite were also mapped in the hanging wall of the Brindle Creek thrust. The footwall is composed of a migmatitic amphibolite, biotite gneiss, and biotite-hornblende granodiorite unit, herein informally named the Lenoir Quarry migmatite. The migmatite shares a gradational contact with mylonitic muscovite schist near its northwestern termination. The muscovite schist directly overlies mylonitic Tallulah Falls Formation metagraywacke. The lithologic discontinuity and mylonitic rock fabrics indicate the presence of a second fault, probably the Mill Spring thrust, here informally named the Green Mountain fault. The Henderson Gneiss is the northwesternmost unit in the quadrangle.

Rock units in the study area preserve a Neoacadian thermal, metamorphic, and deformational history. Estimates of thermobarometric conditions from mineral assemblages and geochemical analyses were compared to similar, unpublished studies from southwestern North Carolina, and indicate comparable Barrovian metamorphic histories. Rocks in the Kings Creek quadrangle preserve sillimanite grade conditions; no change in metamorphic grade occurs across the Brindle Creek thrust. Moreover, no

retrograde fabrics are preserved along faults in the study area. This suggests early- to synmetamorphic thrust emplacement. Recent geochronologic evidence suggests major thrusting, deformation, and peak prograde metamorphism were coeval with Acadian and Neoacadian-earliest Alleghanian (366 Ma, and 342-330 Ma; Late Devonian-early Mississippian) thermal events.

Introduction

A complete understanding of the tectonic evolution of mountain belts requires interpretations from at least three fundamental reference frames: structure, timing, and geothermobarometry (P-T). Detailed P-T determinations without spatial and temporal contexts have limited effectiveness. Likewise, detailed geologic mapping indicates little about the tectonic history of an area without temporal references and estimates of the conditions of genesis (i.e., temperature and pressure). The southern and central Appalachian IP, despite decades of intense research (Adams, 1933; Griffin, 1971, 1974; Hatcher, 1972; Horton et al., 1989), lacks this integration and is therefore not sufficiently understood.

The IP (Fig. 1-1) is the Acadian (now Neoacadian) metamorphic core of the southern Appalachians (e.g., Hatcher et al., 1999). It is a generally shallowly dipping suite of high-grade metasedimentary, metaigneous, and plutonic rocks. Multiple episodes of intense deformation, anatexis, and plutonism have affected IP rocks. Some primary lithostratigraphic successions, however, are recognizable and traceable for long distances (e.g., Goldsmith et al., 1988; Hatcher, 1989). Despite its large area and tectonic significance, up to 75 percent of the IP remains unexplored. Our knowledge of the

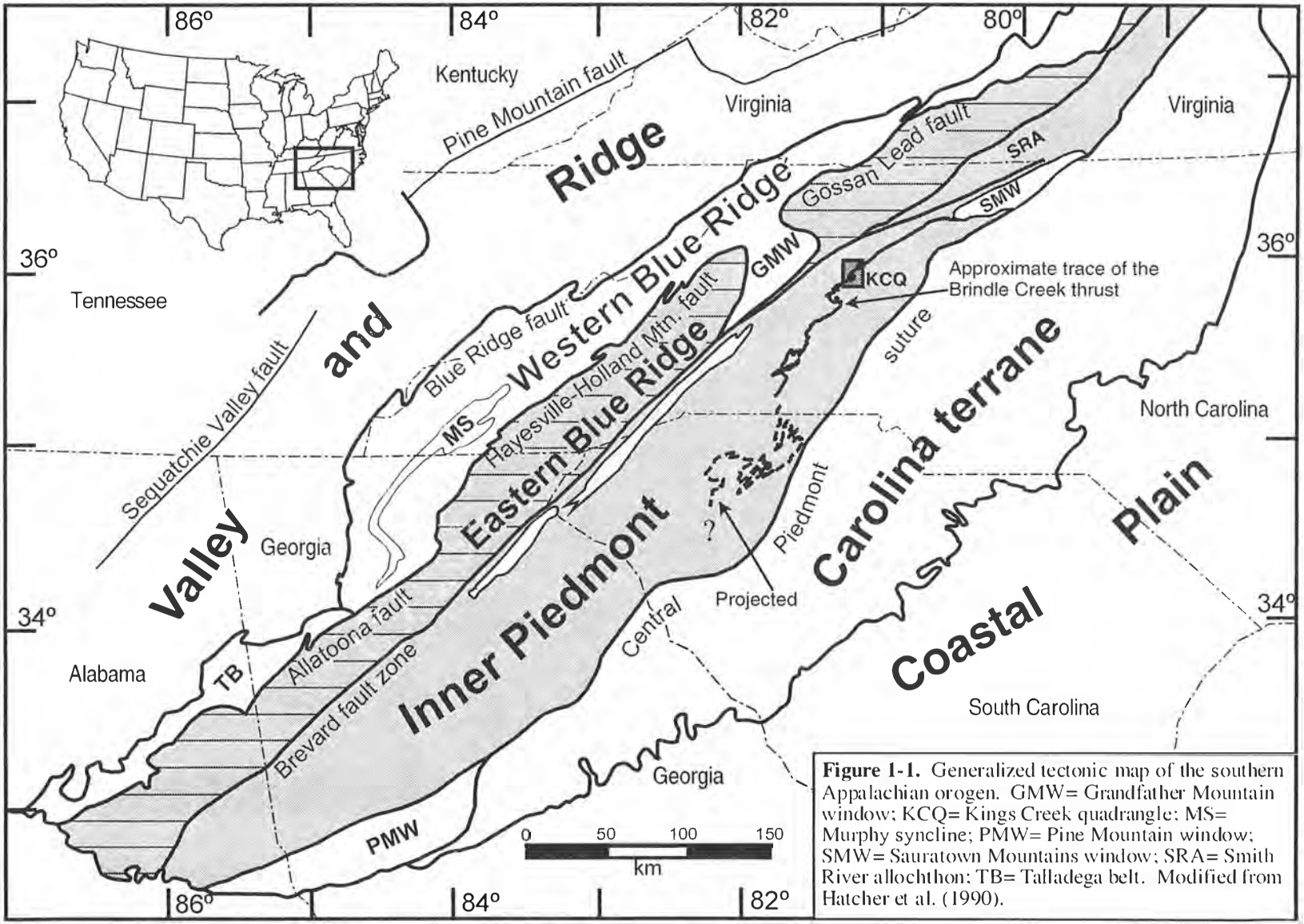

Figure 1-1. Generalized tectonic map of the southern Appalachian orogen. GMW= Grandfather Mountain window; KCQ= Kings Creek quadrangle; MS= Murphy syncline; PMW= Pine Mountain window; SMW= Sauratown Mountains window; SRA= Smith River allochthon; TB= Talladega belt. Modified from Hatcher et al. (1990).

timing and conditions of peak metamorphism and deformation is, to date, understandably limited.

Numerous workers, in attempts to delineate the structural and stratigraphic framework and the timing and conditions of deformation and metamorphism in the IP, have produced detailed studies in southwestern North Carolina (Overstreet et al., 1963a, 1963b; Lemmon and Dunn, 1973a, 1973b; Davis, 1993a, 1993b; Yanagihara, 1994; Bream, 1999; Giorgis, 1999; Hill, 1999; Williams, 2000; Bier, 2001). Those studies focused on areas of high topography southeast of the Brevard fault zone near Hendersonville, Lake Lure, Marion, and Morganton, North Carolina (i.e., the Columbus Promontory and South Mountains; Fig. 1-2). Reconnaissance mapping by Goldsmith et al. (1988) aids in projecting regional trends from the South Mountains to the northeast; tectonic relationships, however, can be difficult to interpret at 1:250,000 scale.

This study contributes to the regional database of detailed (1:12,000- and 1:24,000-scale) mapping (Plate 1) by focusing on the geology of the along-strike area east of Lenoir, North Carolina. The Brushy Mountains in the Kings Creek 7.5-minute quadrangle have moderate relief (300 m/1300 ft) and excellent exposure and trend ~N45°E (Fig. 1-2). Merschat and Kalbas (2002) documented their continuation in the Boomer and Ellendale quadrangles to the east-northeast of the present study area (Figs. 1-2, 1-3, 1-4).

In addition to geologic mapping, an improved understanding of the petrogenetic relationships in the study area was derived from detailed descriptions of lithologic units and estimates of metamorphic conditions from their mineral assemblages. New geochronologic work on rocks from the study area (Part III; Bream et al., 2001a, 2001b)

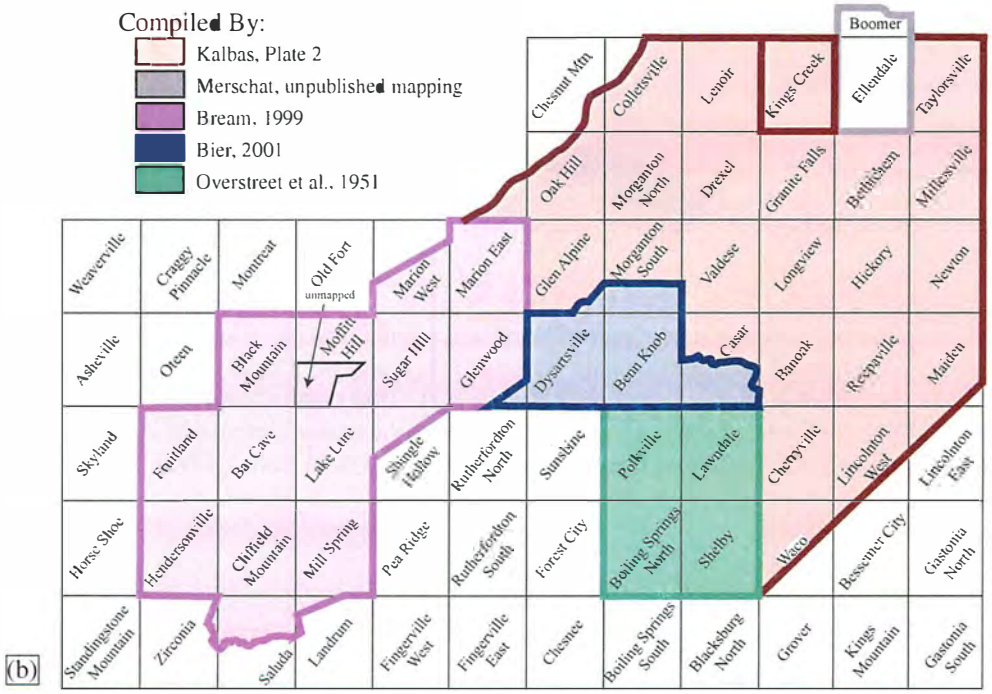

Figure 1-2. Index map showing the location of the study area in western North Carolina. (a) Digital elevation model of western North Carolina with the area of detailed and reconnaissance mapping superimposed (from a compilation by Bream and Bier, unpublished work). (b) 7.5-minute quadrangle mapping index. Note: Plate 1 contains a list of authors for all primary mapping sources used in the compilations indexed above.

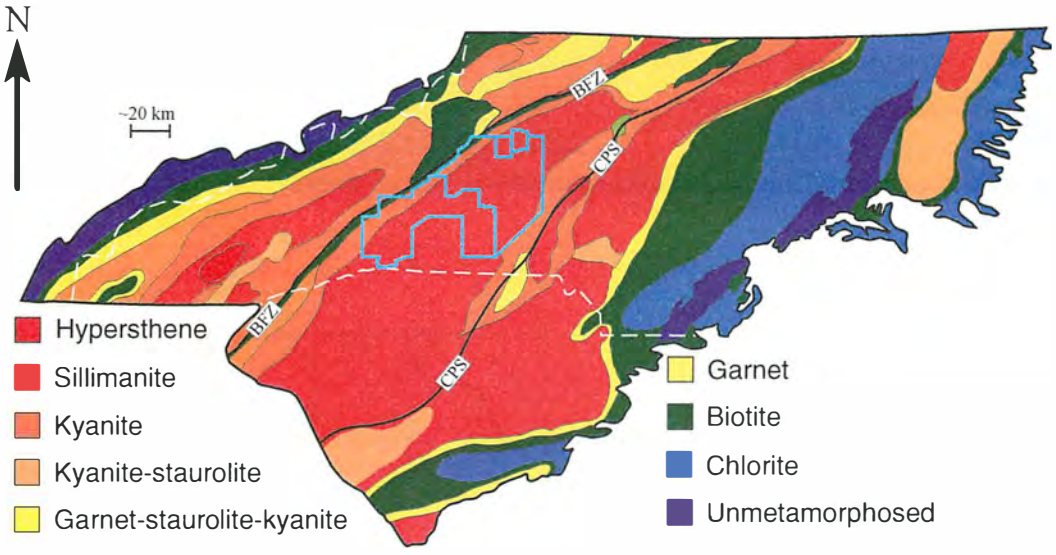

Figure 1-3. Metamorphic isograd map of part of North and South Carolina. Blue outlines represent approximate areas of detailed geologic mapping (various UTK mappers), USGS mapping (Overstreet et al., 1951), and some reconnaissance mapping (Goldsmith et al., 1988) in the southwestern and south-central portions of North Carolina (Plate 1). Isograds represent the first occurrence of index minerals. BFZ= Brevard fault zone; CPS= Central Piedmont suture (modified from Butler, 1991).

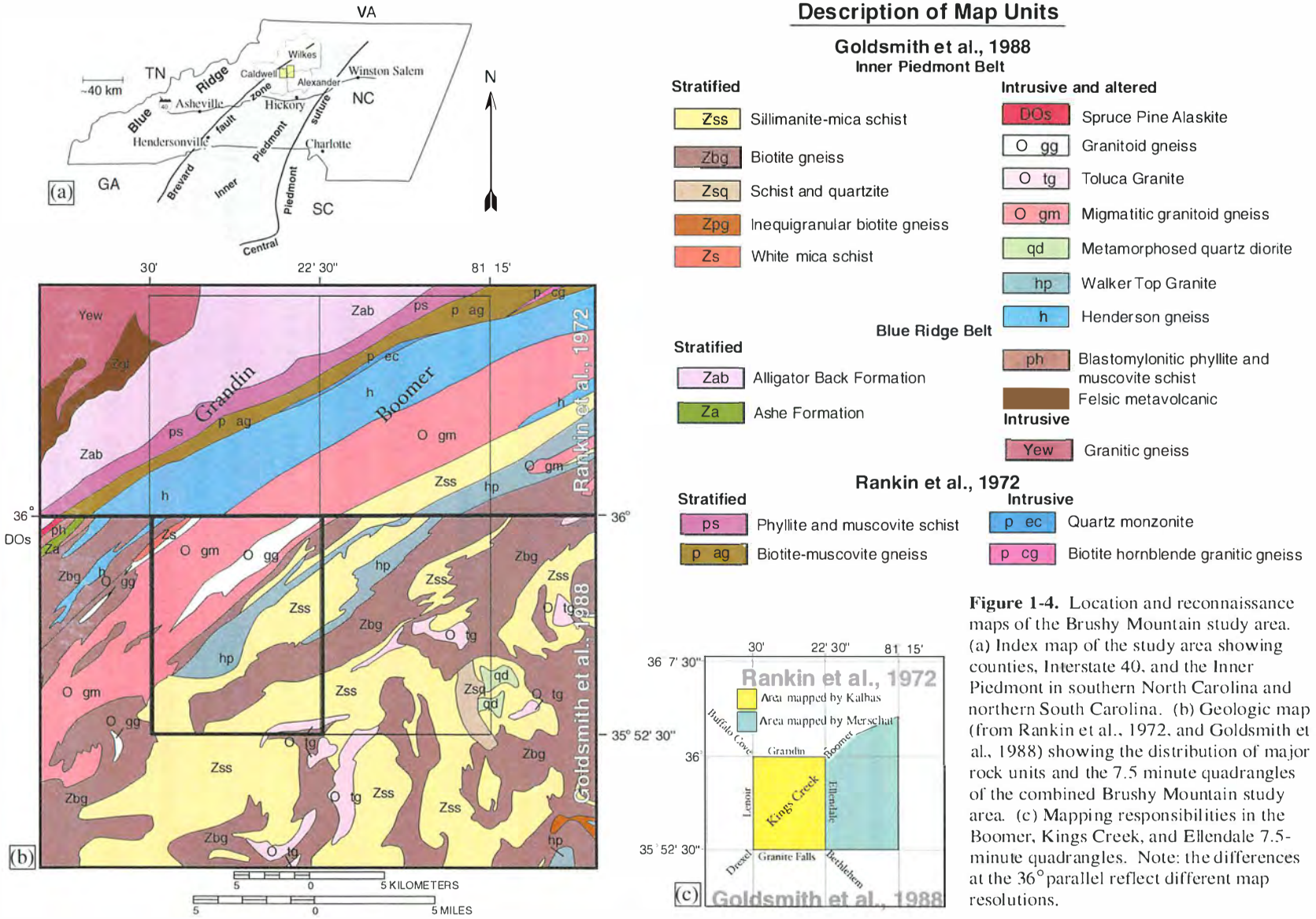

Description of Map Units

Goldsmith et al., 1988

Inner Piedmont Belt

Stratified

- Zss — Sillimanite-mica schist
- Zbg — Biotite gneiss
- Zsq — Schist and quartzite
- Zpg — Inequigranular biotite gneiss
- Zs — White mica schist

Intrusive and altered

- DOs — Spruce Pine Alaskite
- O gg — Granitoid gneiss
- O tg — Toluca Granite
- O gm — Migmatitic granitoid gneiss
- qd — Metamorphosed quartz diorite
- hp — Walker Top Granite
- h — Henderson gneiss

Blue Ridge Belt

Stratified

- Zab — Alligator Back Formation
- Za — Ashe Formation
- ph — Blastomylonitic phyllite and muscovite schist
- Felsic metavolcanic

Intrusive

- Yew — Granitic gneiss

Rankin et al., 1972

Stratified

- ps — Phyllite and muscovite schist
- p ag — Biotite-muscovite gneiss

Intrusive

- p ec — Quartz monzonite
- p cg — Biotite hornblende granitic gneiss

Figure 1-4. Location and reconnaissance maps of the Brushy Mountain study area. (a) Index map of the study area showing counties, Interstate 40, and the Inner Piedmont in southern North Carolina and northern South Carolina. (b) Geologic map (from Rankin et al., 1972, and Goldsmith et al., 1988) showing the distribution of major rock units and the 7.5 minute quadrangles of the combined Brushy Mountain study area. (c) Mapping responsibilities in the Boomer, Kings Creek, and Ellendale 7.5-minute quadrangles. Note: the differences at the 36°parallel reflect different map resolutions.

allows increased precision in quantifying relative events with absolute ages. This treatment is, therefore, a comprehensive tectonic synthesis of observed and derived relationships in the Kings Creek quadrangle.

Geologic Setting

The IP is separated from the eastern Blue Ridge to the northwest by the Brevard fault zone, and from the Carolina terrane to the southeast by the Central Piedmont suture (Fig. 1-1). The IP consists of a polydeformed thrust stack of dominantly metasedimentary and metavolcanic units (biotite gneiss [metagraywacke], pelitic schist, amphibolite, and quartzite) intruded by katazonal plutonic rocks of various compositions (typically tonalitic and granitic; Griffin, 1972, 1974; Goldsmith et al., 1988; Horton and McConnell, 1991).

Structural Patterns

At least five (probably six) deformational episodes (D_1 to D_5; Part II) have affected the IP of North Carolina, South Carolina, and Georgia (Griffin, 1969; Hopson and Hatcher, 1988; Davis et al., 1991; Davis, 1993a; Yanagihara, 1994). D_2 and D_3 are linked as a single contiguous event (Hopson and Hatcher, 1988; Liu, 1991; Davis, 1993a) and are of primary interest because they produced dominant, penetrative and partially penetrative structural trends of northeast-striking, southeast-dipping foliations, and northeast- and southwest-plunging tight and isoclinal folds in the western IP.

Structural and stratigraphic differences between the western and eastern IP (west and east of the Brindle Creek thrust) are readily identifiable on reconnaissance and detailed geologic maps (Plate 1; e.g., Goldsmith et al., 1988; Bier, 2001). Hatcher and Hooper (1992) concluded that westward-vergent Type-F (fold-related) thrust sheets

dominate the structural style of the western IP. This style contrasts with that of the eastern IP, which is dominated by less consistent, variably oriented complex fold patterns of isoclinal recumbent and sheath folds in paragneiss, pelitic schist, and quartz-, feldspar-, and biotite-rich orthogneiss units (Plate 1; Part II; Bier, 2001; Merschat and Kalbas, 2002).

Recent geologic mapping across these two regions of contrasting structural style near Marion, North Carolina, delineated the Brindle Creek thrust (Plate 1; Giorgis, 1999; Giorgis and Williams, 1999). The Brindle Creek thrust, as described in the South Mountains, is a Type-F thrust that juxtaposes migmatitic metasedimentary units (then referred to as Tallulah Falls Formation), Walker Top Granite, and Toluca Granite over "migmatitic Poor Mountain Amphibolite and Quartzite" (Giorgis et al., 1998). The Charlotte 1° x 2° sheet (Goldsmith et al., 1988) and other reconnaissance maps (Brown et al., 1985; Nelson et al., 1998; Horton and Dicken, 2001) depict truncated relationships that suggest the fault is traceable throughout the IP of North and South Carolina; thus it is a major structural feature of the southern Appalachian crystalline core.

Regional Lithotectonic Succession

The overprint from multiple episodes of penetrative deformation and accompanying metamorphism modified primary (S_0) mesoscopic sedimentary and igneous features, but lateral and sequential consistencies have permitted workers (e.g., Hatcher, 1969, 1972; Hatcher and Acker, 1984; Hopson and Hatcher, 1988; Davis, 1993a, 1993b) to delineate lithostratigraphic sequences and major tectonic units. A partially traceable stratigraphy in the southern Appalachian Acadian core consists of a series of paragneiss units interpreted as distal slope-and-rise sediments shed from the Laurentian margin (Plate 1; e.g., Rankin

et al., 1989; Hatcher, 1993). The Tallulah Falls (-Ashe) Formation was originally recognized in the eastern Blue Ridge of southern Virginia, North Carolina, South Carolina, and northeastern Georgia (Hatcher, 1993). Recent work in the western IP indicates the Tallulah Falls Formation is also a prominent unit southeast of the Brevard fault zone (e.g., Hatcher, 1993; Hatcher et al., 1999; Bream, 1999; Hill, 1999). Considerable debate persists, however, over the true areal extent of the Tallulah Falls Formation in successive IP thrust sheets (e.g., Bream et al., 2001b).

The Tallulah Falls stratigraphic sequence, originally subdivided by Hatcher (1971, 1973), was identified in the southwestern North Carolina (Bream, 1999; Giorgis, 1999; Hill, 1999; Williams, 2000; Bier, 2001). The sequence consists of three units: a lower metagraywacke-schist-amphibolite member, a middle aluminous schist member, and an upper metagraywacke-schist member. Upper and lower members have been differentiated by their stratigraphic position relative to the aluminous schist and by a general dearth of amphibolite in the upper unit (Hatcher, 1971; Bier, 2001).

Petrologically similar metasedimentary units of the eastern IP (i.e., southeast of the Brindle Creek thrust) were originally correlated with the Tallulah Falls Formation based on detailed mapping (Giorgis, 1999; Williams, 2000; Bier, 2001). The three distinctive members seen in western IP exposures, however, have not been differentiated in the eastern IP. Specifically, Giorgis (1999) and Bier et al. (2000) documented significant thickness changes in both aluminous schist and metagraywacke units in the hanging wall of the Brindle Creek thrust (Plate 1). Moreover, the amphibolite-rich lower metagraywacke unit is absent in the study area and in the Brindle Creek thrust sheet exposed in the South Mountains (Plate 1), but a similar unit crops out in the eastern IP

(Goldsmith et al., 1988).

Thickness variations and lithologic changes can be reasonably explained by primary (sedimentological) facies changes and/or structural thickening. New detrital zircon U-Pb data (Bream, 2002) preclude correlation of units in the Brindle Creek thrust sheet with the Tallulah Falls Formation. Both western and eastern IP rocks contain Grenville-age (~1.25 to 1.10 Ga) detrital zircons; eastern IP metasedimentary rocks, however, also contain Devonian-age detrital grains, and were likely deposited in a Late Silurian to Early Devonian basin (Bream et al., 2001a, 2001b). Western IP paragneisses and schists suggests their deposition along an earlier Paleozoic continental margin. Although numerous granitoids crop out southeast of the Brindle Creek thrust in North Carolina, all published ages are Devonian (375 Ma for the Toluca Granite, 366 Ma for the Walker Top Granite) or younger (e.g., Mapes, 2002; Mapes et al., 2002).

In this report, the name Tallulah Falls Formation is reserved only for rocks that are laterally connected with previously mapped Tallulah Falls Formation of the western IP and eastern Blue Ridge. Although they bear textural and mineralogical similarities to Tallulah Falls Formation, a different terminology will be employed for rocks of the eastern IP in the Brindle Creek thrust sheet.

Southeast of the Brevard fault zone the Tallulah Falls Formation is overlain by the Chauga River and Poor Mountain Formations (Hatcher, 1972, 1993). A distinct lithologic (metasedimentary and/or metavolcanic) succession has been recognized in the Poor Mountain Formation (Shufflebarger, 1961; Hatcher, 1969). Rocks at the type locality in the Whetstone 7.5-minute quadrangle, South Carolina-Georgia mainly consist of laminated amphibolite, quartzite, and marble. Davis (1993b) documented three

equivalent units in the Columbus Promontory of northwestern South Carolina and southwestern North Carolina: interlayered amphibolite and quartzite; discontinuous garnet-mica schist and quartzite; and laminated amphibolite and hornblende gneiss. The Poor Mountain Formation in South Carolina is overlain by the Ordovician Henderson Gneiss, the most petrologically distinctive and laterally continuous IP orthogneiss (Plate 1).

Orthogneisses can be subdivided into eastern and western IP groups; the former (e.g., Walker Top Granite and Toluca Granite) have Acadian to Neoacadian crystallization ages whereas the later (e.g., Henderson Gneiss and Dysartsville Tonalite) have Ordovician ages (e.g., Mapes, 2002; Bream, 2002). The Henderson Gneiss, a porphyroclastic quartz-K-feldspar-biotite-muscovite orthogneiss, structurally (?) overlies the Tallulah Falls Formation in the Lenoir quadrangle (Reed, 1964). The Walker Top Granite, a texturally similar megacrystic biotite gneiss (see detailed description below), was originally recognized by Goldsmith et al. (1988) as a rapakivi-textured, less deformed version of the Henderson Gneiss in southwestern and central western North Carolina. The Toluca Granite (Verseput, 1980) and Dysartsville Tonalite (Horton and McConnell, 1991; Bream, 2002) represent a series of biotite granitoids and metagranodiorite bodies that intruded IP metasedimentary rocks (Goldsmith et al., 1988).

Metamorphism and Deformation

The core of the IP is dominated by middle- to upper-amphibolite facies (sillimanite grade), prograde, Barrovian to Buchan metamorphic assemblages (Butler, 1991; Merschat and Kalbas, 2002; Fig. 1-3). Along the flanks of the IP, the metamorphic grade generally decreases to kyanite, staurolite, and garnet grade (Butler, 1991; Hatcher,

1993). Geochronologic work has begun to delimit the ages of plutonism, metamorphism, coeval anatexis, and related deformation.

Rb-Sr whole-rock ages indicate the Henderson Gneiss (509-472 Ma) contains deformed younger granitoids with crystallization ages of 438 and 429 $\pm$ 22 Ma in North Carolina (Lemmon, 1973; Odom and Russell, 1975), and 423 $\pm$ 2 Ma in South Carolina (Harper and Fullagar, 1981). The undeformed Cherryville monzogranite has a Rb-Sr whole-rock age of 351 $\pm$ 10 Ma (Kish, 1983). These whole-rock ages were used to delimit the timing of the major prograde metamorphic event in the IP to between 429 and 351 Ma (Davis, 1993a).

More recent geochronologic work in the eastern Blue Ridge and IP revealed Late Devonian and early Mississippian monazite ages (~360 Ma and ~325-330 Ma; Dennis and Wright, 1997) and zircon rim ages (~342 and 330 Ma; Bream et al., 2001b; Carrigan et al., 2001; Part III). If the middle- and late-Mississippian ages represent peak thermal conditions, then Neoacadian/earliest Alleghanian metamorphism is inferred. A retrograde overprint (chlorite grade) has been attributed to movement along the Brevard fault zone and subsequent exhumation of the Blue Ridge-Piedmont thrust sheet during Alleghanian orogenesis (~320 Ma; Hatcher, 1993; Kohn, 2001).

The Kings Creek Quadrangle

The Kings Creek 7.5-minute quadrangle consists of a 159.5 km^2 (61.6 mi^2) area in Caldwell County ~100 km east of Asheville and ~50 km northwest of Hickory, North Carolina (Fig. 1-4). In addition to its moderate relief and superb exposure, the area offers good road access to numerous departure points for foot traverses. Many logging roads are kept clear by hunters and allow relatively easy access to ridge lines and some valleys.

The location of the Kings Creek quadrangle is also tectonically significant. The Brevard fault zone crops out ~2.7 km (1.7 mi) northwest of the northwestern corner of the quadrangle (Reed, 1964; Goldsmith et al., 1988), and separates the high mountains of the Blue Ridge from the rolling hills of the Piedmont (Fig. 1-2). The sillimanite isograd was mapped immediately northwest of the northwestern corner of the quadrangle (Butler, 1991; Fig. 1-3). Macroscopic patterns within the Kings Creek quadrangle (Part II; Figs. 1-4, 1-5) reflect the regional structural change from the western IP to the eastern IP.

Methods

Detailed geologic mapping of the Kings Creek quadrangle began in mid-January, 2001 and continued through mid-August, 2001. Additional field work was conducted in January, 2002. Standard and enlarged USGS 7.5-minute quadrangles were used for base maps at 1:24,000 and 1:12,000 scales. Notes, including textural and mineralogical descriptions, fabric orientations (measured with a Brunton™ pocket transit), and scaled sketches were recorded by station number (Plate 3). Compilation of structural and lithologic data from field maps was accomplished using Adobe Illustrator™ and Adobe Photoshop™ software packages, using techniques described by Bream (1999; Appendix C).

Petrographic analysis of 47 representative samples from the Kings Creek quadrangle was completed. Modal mineralogy was ascertained by point counting both large (5.0 x 7.6 cm) and standard size (2.7 x 4.6 cm) thin sections. Stage step distance varied with the grain size of each sample, but averaged ~0.4 mm for fine-grained samples (< 0.5 mm average grain diameter) and ~0.8 mm for coarse-grained samples (≥ 0.5 mm average grain diameter). Plagioclase compositions (anorthite component) were estimated

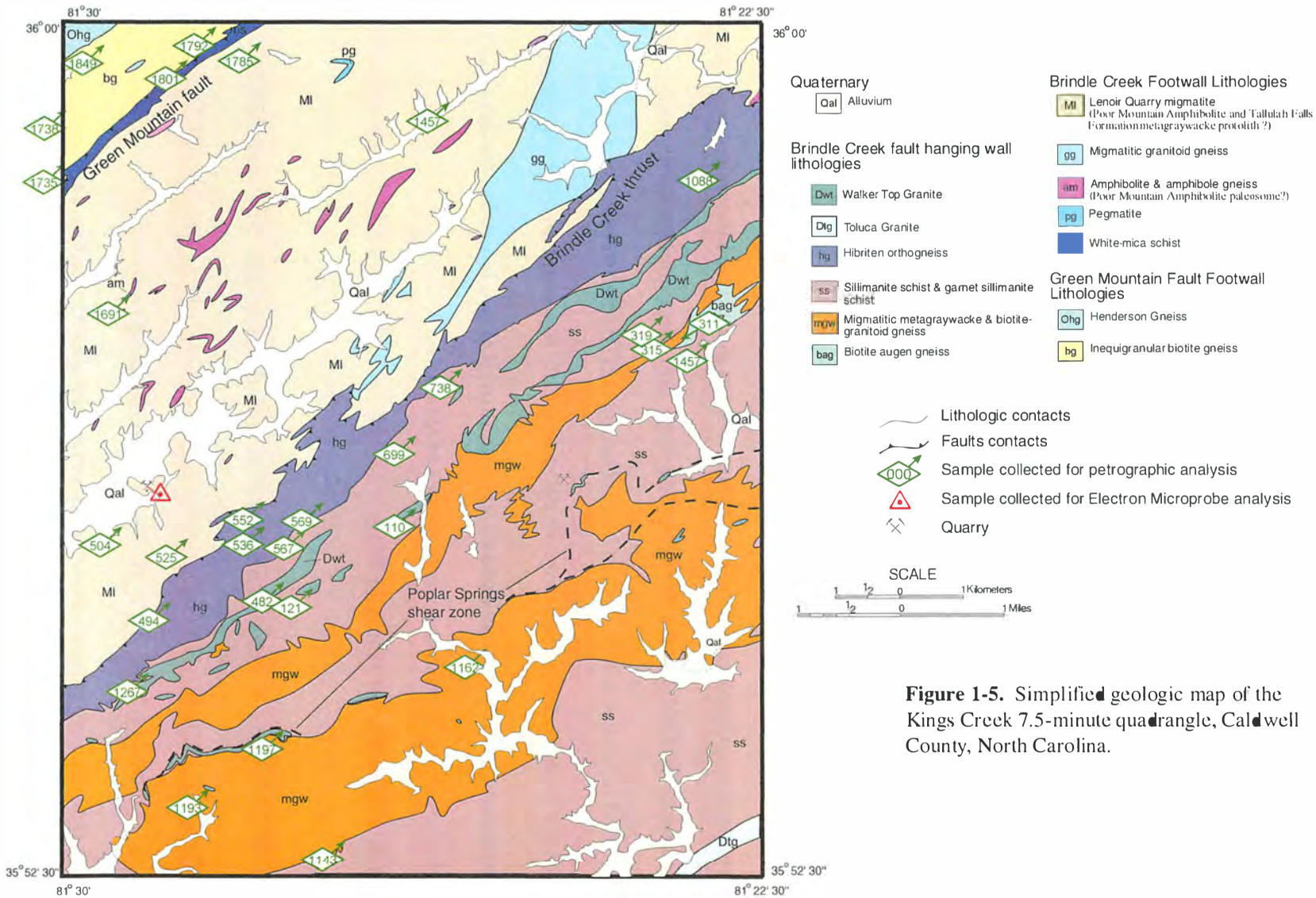

Figure 1-5. Simplified geologic map of the Kings Creek 7.5-minute quadrangle, Caldwell County, North Carolina.

using the Michel-Lévy method (Nesse, 1991). The maximum recorded extinction angle measured parallel to the (010) composition plane of albite twins was determined on a number of grains and compared to the low (plutonic) plagioclase curve of Tobi and Kroll (1975).

Lithologic Units

Detailed geologic mapping in the Brushy Mountains has confirmed the general lithostratigraphic relationships recognized during reconnaissance mapping (Goldsmith et al., 1988), but has revealed significantly greater meso- and macroscale complexity (Plates 1, 2; Figs. 1-4, 1-5). Two faults, the Brindle Creek thrust and a second thrust herein named the Green Mountain fault, probably the Mills Spring fault (see discussion in Part II), package three lithotectonic units composed of ten distinctive lithologic units in the study area (Fig. 1-6). Brushy Mountain lithologic units are correlative with units recognized in south-central western North Carolina and partially correspond to the regionally recognizable stratigraphy of the western IP. Rock unit descriptions begin with the southeasternmost unit and proceed to the northwest (Figs. 1-5, 1-6). Modes for all lithologies are reported in descending order of abundance.

Brindle Creek Thrust Hanging Wall

Sillimanite schist

The first of two metasedimentary rock units that dominate the Brindle Creek thrust sheet is migmatitic biotite-sillimanite-quartz-muscovite-garnet schist (referred to here as sillimanite schist; Fig. 1-5). Three northeast-trending bands of sillimanite schist are exposed in the southwestern Brushy Mountains; lithologies are similar, but a discernable stratigraphy is not evident. In outcrop, the schist is weathered

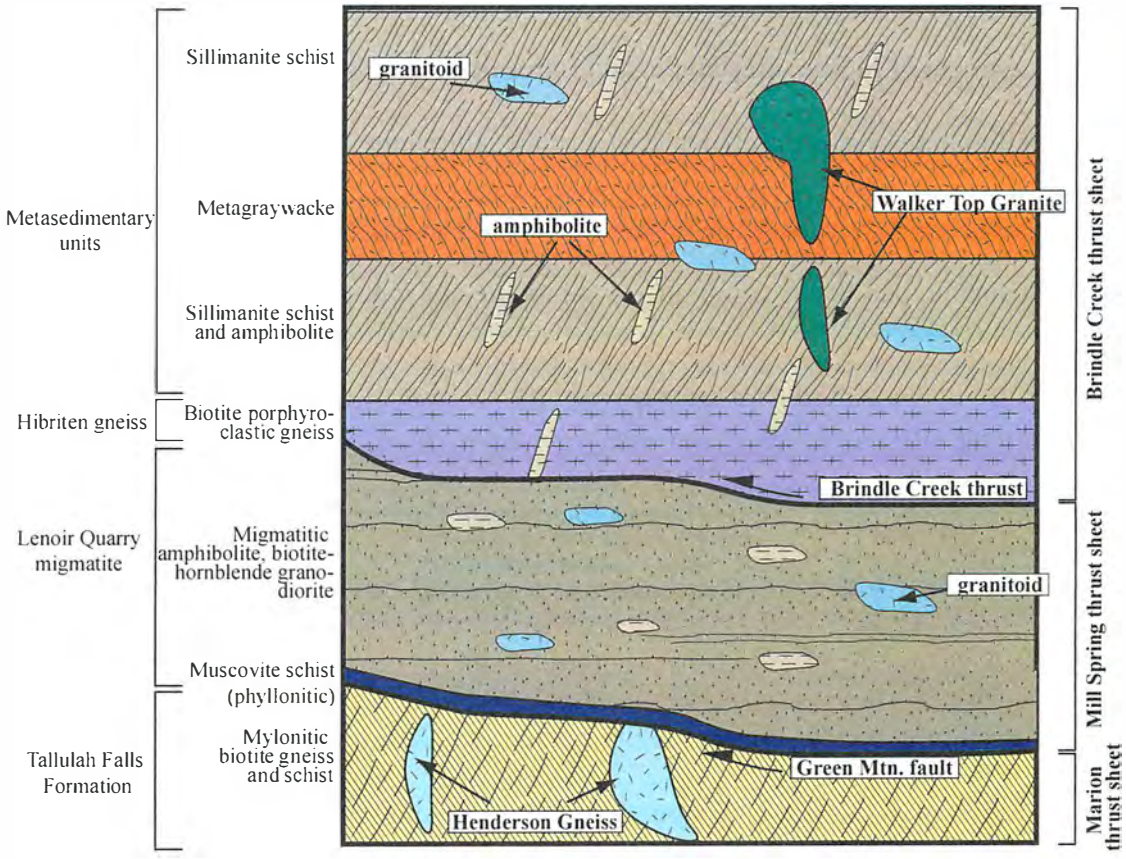

Figure 1-6. Generalized lithologic column for the study area. Note: all rocks in the hanging wall of a thrust such as the Brindle Creek thrust are referred to collectively as a thrust sheet.

along exposed surfaces and degrades to brown and reddish brown saprolite (Fig. 1-7). A well-developed foliation, pervasive throughout the sillimanite schist, is formed by the parallel alignment of biotite, muscovite, and fibrolitic sillimanite. The presence of fibrolitic sillimanite crystals is characteristic of the sillimanite schist and can usually be seen with 10x magnification. Mesoscale compositional banding of micaceous and quartzofeldspathic laminae is common. Amphibolite and calc-silicate float are also present.

Both the sillimanite schist and metagraywacke (discussed below) contain variable percentages of medium- to coarse-grained, quartz and K-feldspar-rich granitoid and pegmatite (Figs. 1-7, 1-8, 1-9). Granitoids and pegmatites can be divided into at least three textural categories: (1) concordant deformed sills, (2) crosscutting deformed bodies, and (3) crosscutting, nondeformed (usually fracture-parallel) bodies (Fig. 1-9). Evidence for mobilization of granitoids and pegmatites is pervasive throughout the Kings Creek quadrangle, and can be most easily seen in the study area in a series of outcrops along U. S. 64 (Fig. 1-9; Plate 2).

Three representative samples (KC-1143, KC-GSS, and KC-699) were chosen for petrographic analysis (Table 1-1). The mineral assemblage of the sillimanite schist (Fig. 1-10) consists of biotite, quartz, sillimanite, muscovite, plagioclase, opaque minerals, $\pm$ garnet. Trace amounts of epidote and < 4 percent chlorite are also present. Trace amounts of needle-like apatite were detected in some biotite and plagioclase crystals. Interstitial sericite is also common in all samples. Minor chloritization is most prevalent in biotite-rich layers. Sillimanite schist samples have an overall medium-grained, lepidoblastic to nematoblastic texture (Figs. 1-10b, 1-11) . In some cases (Fig. 1-11)

Figure 1-7. Sillimanite schist on U. S. 64 near its intersection with McRary Creek Road. The white boudin is pegmatite.

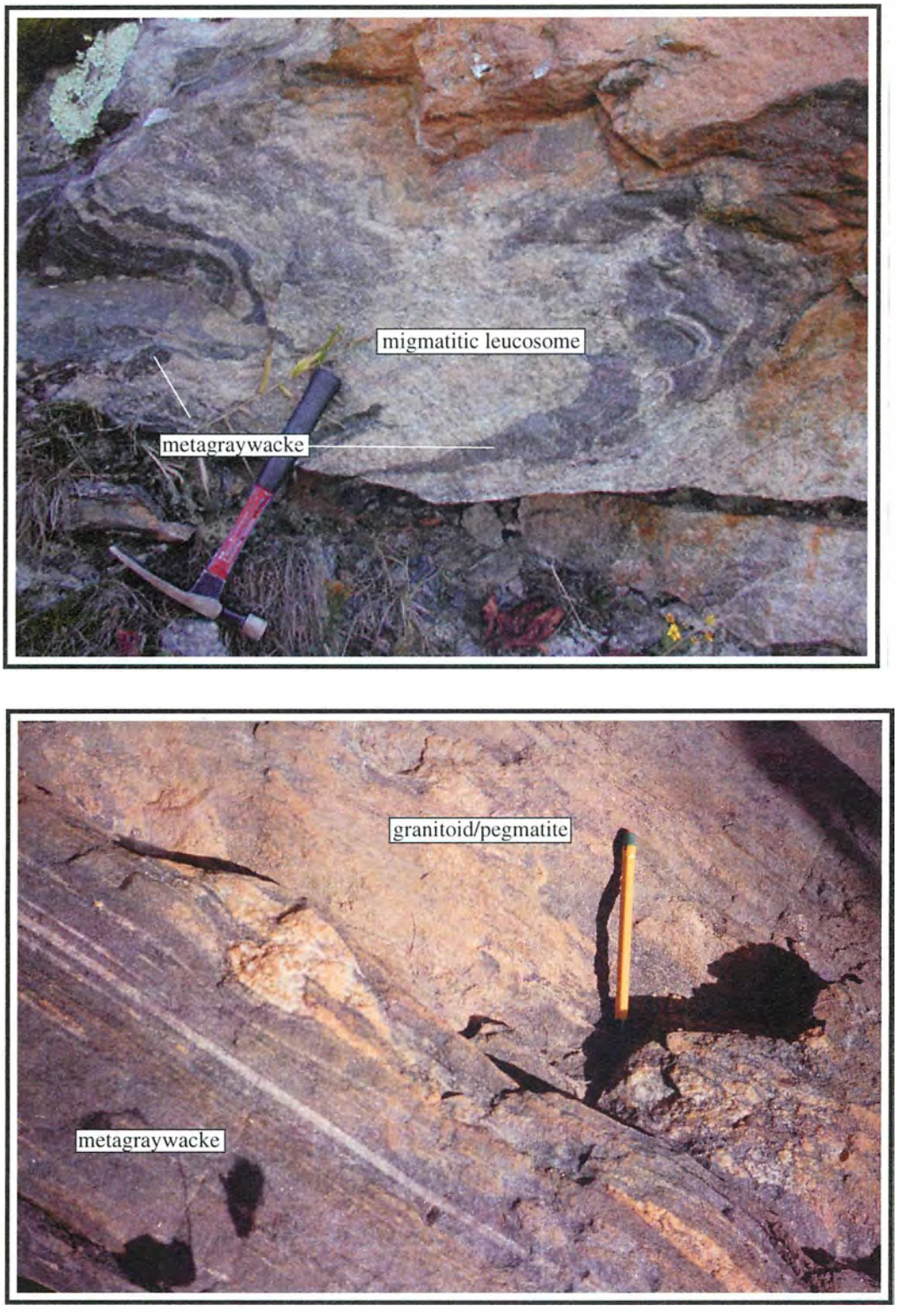

Figure 1-8. Outcrop exposure of migmatitic biotite gneiss (metagraywacke) at station KC-3 on U. S. 64 at the eastern boundary of the Kings Creek quadrangle. (Upper photograph by Robert D. Hatcher, Jr.)

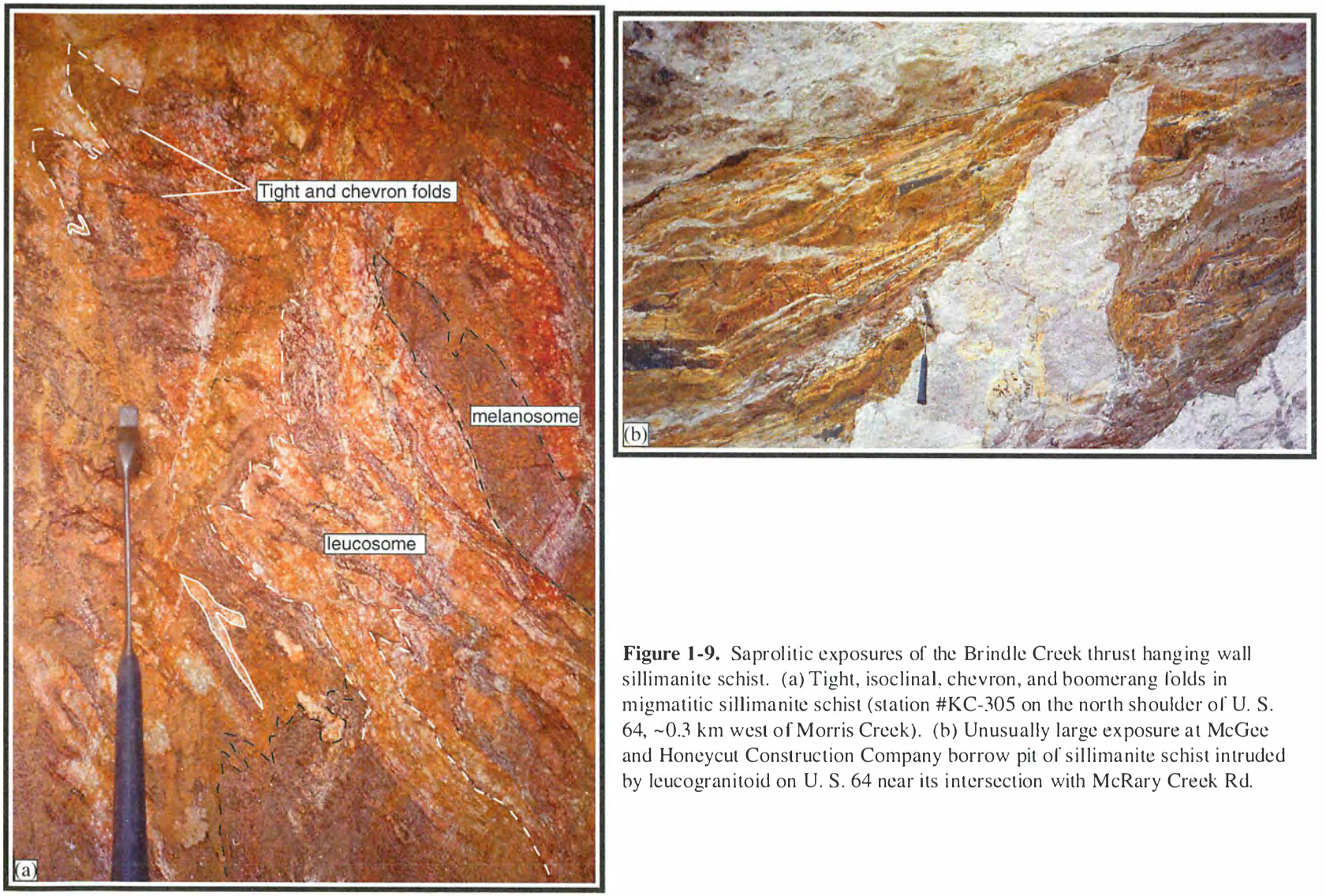

Figure 1-9. Saprolitic exposures of the Brindle Creek thrust hanging wall sillimanite schist. (a) Tight, isoclinal, chevron, and boomerang folds in migmatitic sillimanite schist (station #KC-305 on the north shoulder of U. S. 64, ~0.3 km west of Morris Creek). (b) Unusually large exposure at McGee and Honeycut Construction Company borrow pit of sillimanite schist intruded by leucogranitoid on U. S. 64 near its intersection with McRary Creek Rd.

Table 1-1. Modal mineralogy of Brindle Creek thrust hanging wall metagraywacke and sillimanite schist.

Brindle Creek Fault Hanging Wall

	Sillimanite schist			Metagraywacke	
Sample #	**KC-GSS**	**KC-1143**	**KC-699**	**KC-311**	**KC-1162**
Rock type	sch	sch	sch	bgn	bgn
# Counted	971	1000	1000	1134	1035
Quartz	16.3	12.7	44.9	37.1	48.5
Plagioclase	3.1	—	7.4	12.6	27.5
% Anorthite	—	—	20.0	25.0	31.0
K-Feldspar	tr	—	0.2	32.0	1.8
Hornblende	—	—	—	—	1.6
Biotite	48.0	44.9	27.2	13.1	18.1
Muscovite	5.9	12.1	3.4	4.1	0.2
Chlorite	1.3	3.8	2.8	0.7	0.3
Sericite	tr	5.4	tr	tr	tr
Epi/ clinozo	tr	0.4	—	—	1.2
Kyanite	—	—	—	—	—
Sillimanite	11.5	14.2	9.0	0.3	0.1
Garnet	6.8	0.4	2.7	—	—
Rutile	—	tr	tr	tr	—
Sphene	—	—	—	tr	—
Apatite	tr	—	tr	tr	tr
Limonite	1.0	tr	1.0	—	—
Opaques	6.0	6.0	0.9	tr	0.2
Total	99.9	99.9	99.5	99.9	99.5

Abbreviations: Epi/ clinozo = epidote and clinozoisite, bgn = biotite gneiss, KC-Kings Creek quadrangle, sch = schist, tr < 1.0 %.

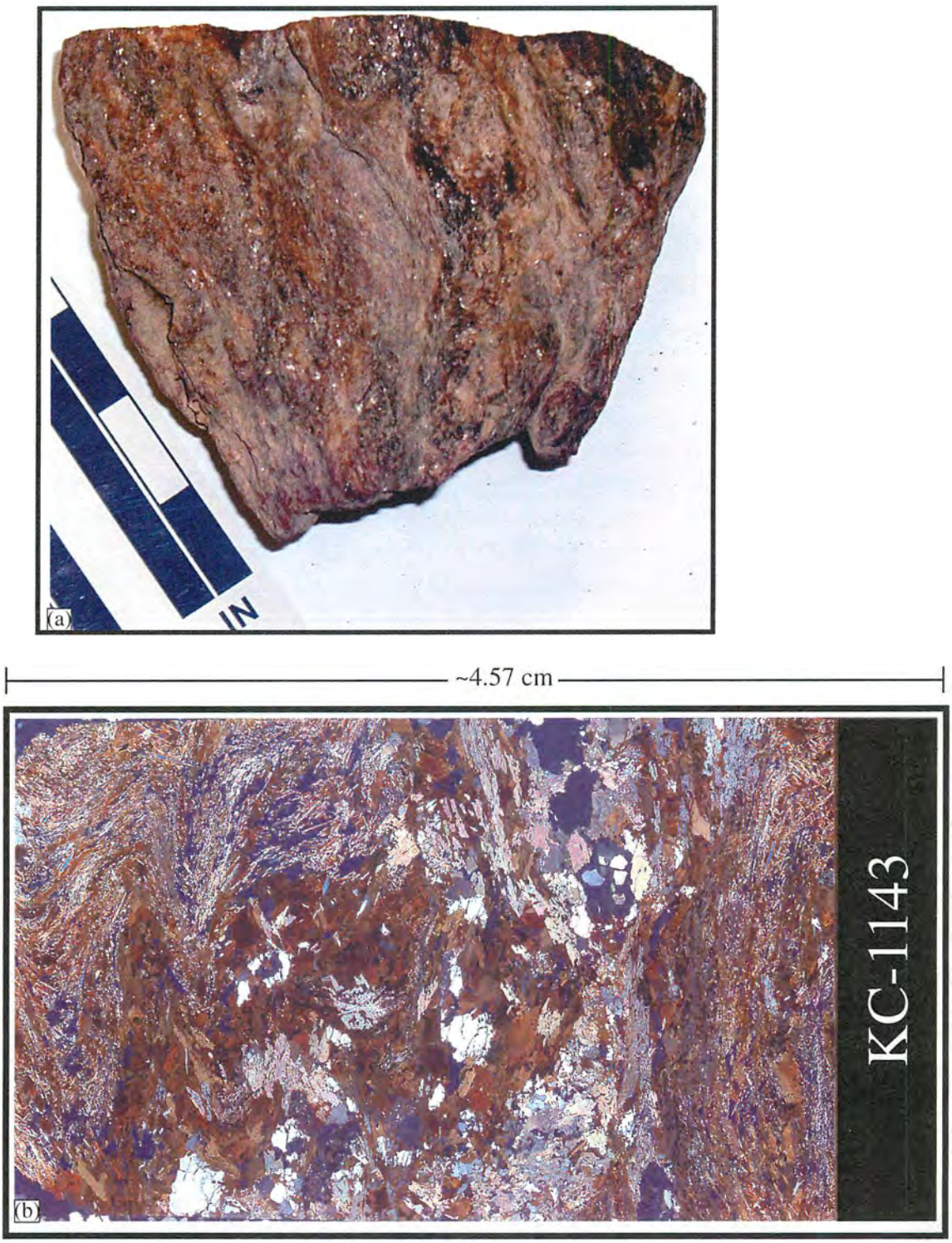

Figure 1-10. Sillimanite schist from the Brindle Creek thrust hanging wall. (a) Weathered sillimanite schist hand specimen from station KC-1148 in a gully on the northern slope of Lick Mountain. (b) Scanned thin section in cross-polarized light from station KC-1143 on the southwestern slope of Pine Mountain in the southern third of the Kings Creek quadrangle. Note the crenulations in a schistosity defined by biotite, sillimanite, and muscovite.

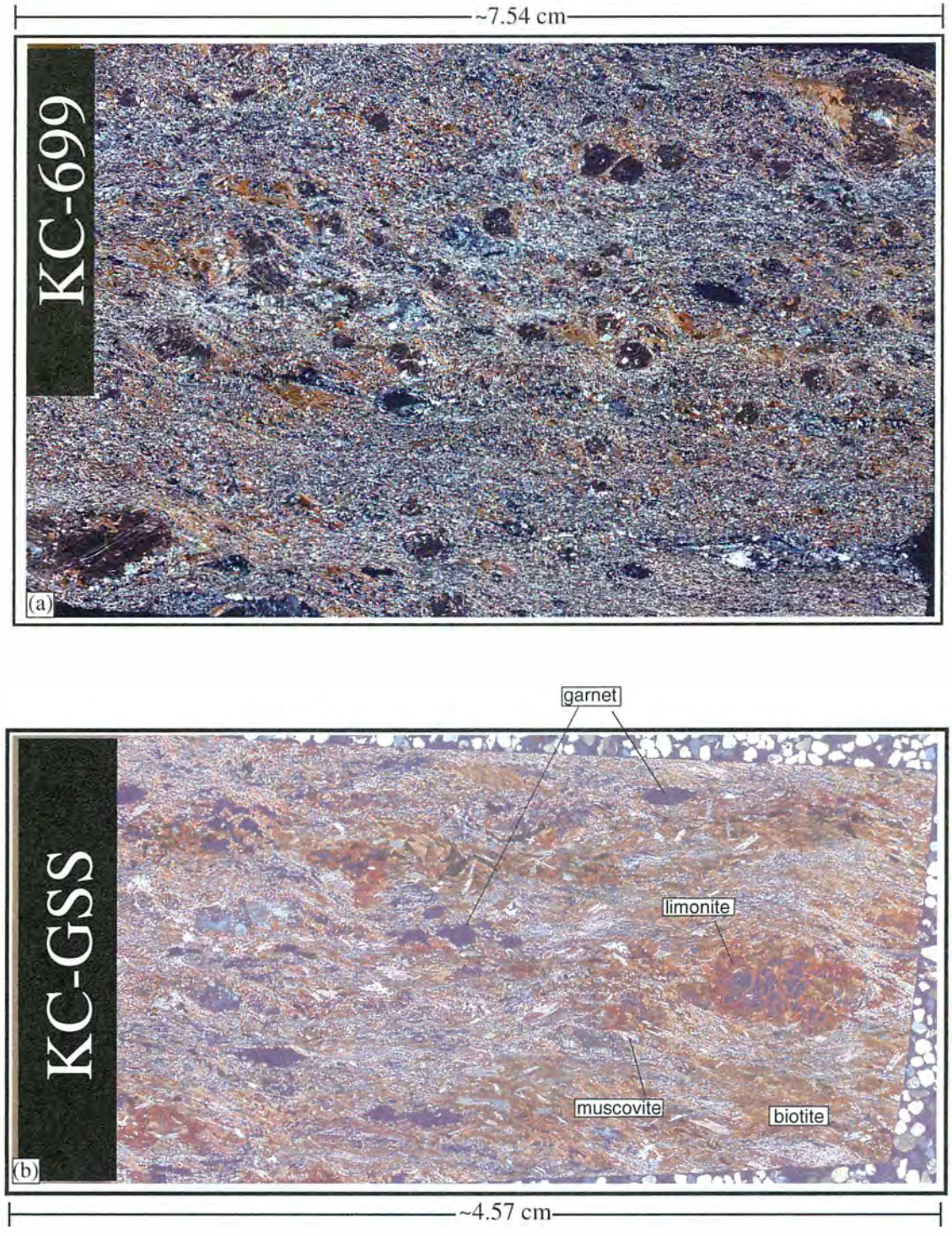

Figure 1-11. Brindle Creek fault hanging wall sillimanite schist. (a) Scanned thin section in cross-polarized light from station KC-699, 1.2 km due north of the north end of McRary Creek Rd. Note the presence of subhedral garnet porphyroblasts. (b) Scanned thin section in cross-polarized light from station KC-GSS, 1.3 km north of Bethel Church in Draco, North Carolina. Note the biotite-dominated schistosity with deformed, weathered garnet porphyroblasts.

rounded and elongate subhedral garnet (almandine) porphyroblasts of varying sizes are present.

Metagraywacke

The second metasedimentary rock unit in the Brindle Creek thrust hanging wall is migmatitic biotite-quartz-plagioclase-K-feldspar gneiss (metagraywacke). The metagraywacke is exposed as two northeast-trending bands that crop out adjacent to the sillimanite schist and Walker Top Granite (Fig. 1-5). It weathers to reddish tan or light to dark gray micaceous saprolite and frequently contains a significant percentage of quartzofeldspathic melt material that degrades to a light tan to white, popcorn-textured saprolite with iron-oxide stain (Fig. 1-9). As with the sillimanite schist, mesoscale compositional banding of micaceous and quartzofeldspathic laminae is common, and amphibolite and calc-silicate float is variably present.

Representative metagraywacke samples (KC-311 and KC-1162) are texturally similar; mineralogical variability exists, however, and may represent differences in protolith composition or degrees of migmatization (Table 1-1). Sample KC-311 contains quartz, K-feldspar, biotite, plagioclase (An_{25}), and muscovite with accessory sillimanite, rutile, sphene, apatite, and opaque minerals. Sample KC-1162 is also dominated by quartz, but contains plagioclase (An_{30}), biotite, K-feldspar, hornblende, and epidote (Table 1-1). Trace minerals in sample KC-1162 are sillimanite, apatite, and opaque minerals (Fig. 1-12).

Walker Top Granite

The Walker Top Granite is an easily recognizable orthogneiss characterized by subhedral to euhedral K-feldspar megacrysts in a medium-grained, medium- to dark-gray

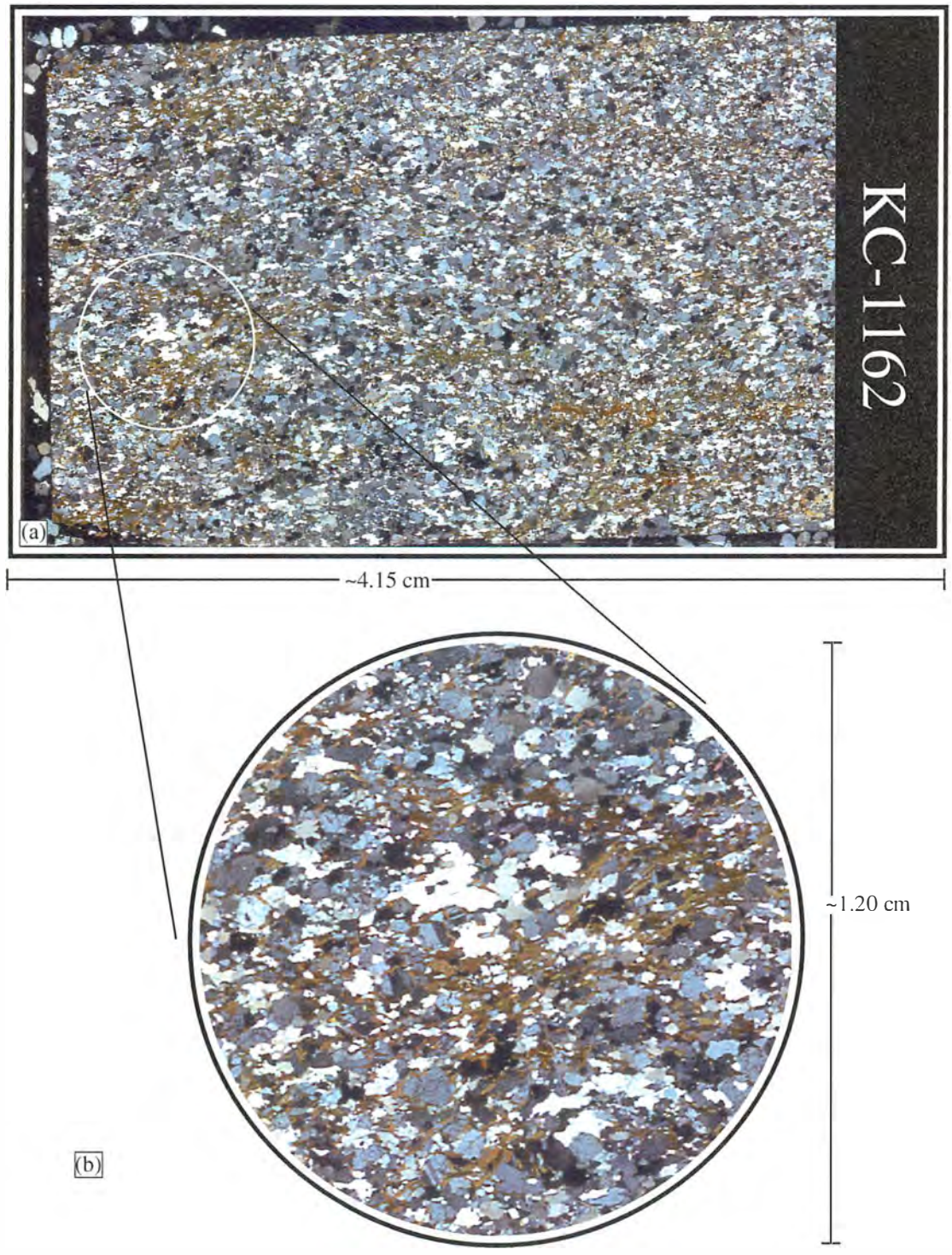

Figure 1-12. Metagraywacke (biotite gneiss). (a) Scanned thin section in cross-polarized light from sample locality KC-1162 on the northeast shoulder of state road #1788 east of Oak Hill. (b) Enlarged image showing the faint, subhorizontal foliation composed of fine-grained quartz, biotite, plagioclase, and microcline.

(CI 25-45 %) biotite, quartz, and plagioclase matrix (Figs. 1-13a, 1-13b; Giorgis, 1999; Vinson and Miller, 1999). Giorgis (1999) proposed a type locality for the Walker Top Granite near Burkemont Mountain Road south of Kaylor Knob and Walker Top in the Morganton South 7.5-minute quadrangle (Plate 1). That name was formalized by Giorgis et al. (2002).

The extent of Walker Top Granite near the northern boundary of the Charlotte 1° x 2° sheet was over-estimated (Fig. 1-4; Goldsmith et al., 1988). It crops out as a series of laterally extensive, but narrow disconnected bodies that parallel the regional structural trend (Fig. 1-5; Plate 2). In the study area, the Walker Top Granite crops out entirely within the sillimanite schist and metagraywacke (Fig. 1-5). Near the eastern boundary of the quadrangle, a biotite augen gneiss with rounded to subhedral K-feldspar megacrysts is distinguished from the Walker Top Granite (Fig. 1-5; Plate 2). The equivalent unit in the Ellendale quadrangle is "sheared Walker Top Granite" (Kalbas et al., 2001). The biotite augen gneiss is petrologically similar to, but not correlative with, the Walker Top Granite. Several small (< 0.1 km thick), discontinuous bodies of Walker Top Granite crop out in the southern third of the Kings Creek quadrangle (Fig. 1-5; Plate 1; Part II). Some outcrops in this band expose rocks with the characteristic megacrystic texture, while others expose rocks with sheared or no megacrysts (Fig. 1-13c; Part II).

The Walker Top Granite typically crops out as bald, pavement surfaces on ridge tops, although smaller exposures were found on hillsides, and in roadcuts and streams. Even in weathered outcrops, megacrysts are usually preserved and easily identifiable. The matrix weathers to an ochre-colored, biotite-bearing schistose saprolite similar to weathered metagraywacke. The contact of the Walker Top Granite and metasedimentary

Figure 1-13. Walker Top Granite. (a) Outcrop at station #KC-110, located at the northern termination of McRary Creek Road. (b) Typical Walker Top Granite texture in hand specimen from station KC-121, ~0.25 km east of St. Johns Church on U. S. 64. (c) Hand specimen from sample locality KC-1193, ~0.3 km southwest of Clearview Church on state road #1712, showing a sheared version of the Walker Top Granite with no discernable megacrysts. Weathered garnet porphyroblasts stand out against the quartz- and K-feldspar-rich matrix.

units can be observed in several locations; the long axes of K-feldspar megacrysts typically parallel both the contact and the foliation.

Modal analyses of three representative samples (KC-121, KC-1197, and KC-1267) indicated mineral assemblages consisting of plagioclase (An_{37-40}), quartz, microcline, biotite, muscovite, $\pm$ garnet, with trace epidote, myrmekite, sericite, apatite, zircon, and opaque minerals (Table 1-2). Samples have a nematoblastic to porphyroblastic schistose texture created by microcline megacrysts in a quartz-, biotite-, plagioclase-rich groundmass. A poorly defined foliation in each sample is delineated by the alignment of biotite crystals parallel to the long axes of microcline megacrysts (Fig. 1-14). Plagioclase crystals in the matrix have albite and Carlsbad twinning, and several grains display undulatory extinction. Microcline megacrysts also have Carlsbad twinning; some megacrysts have irregular cross-hatch twinning (Fig. 1-14b).

The modal mineralogy of the Walker Top Granite was plotted using the IUGS classification system (Fig. 1-15; Streckeisen, 1976). Walker Top samples from the current study area have monzogranitic and granodioritic compositions, and lie in two distinct composition fields, originally reported by Giorgis (1999) and Bier (2001). The apparent bimodality is likely due to mineralogical heterogeneity and an irregular, bimodal grain size distribution (Fig. 1-14). The matrix is enriched in plagioclase, whereas microcline is dominantly megacrystic. Matrix-rich samples (i.e., fewer K-feldspar megacrysts) plot in the granodiorite field while samples with multiple megacrysts plot in the monzogranite field. In this study, samples KC-1267 and KC-1197 have fewer microcline megacrysts than sample KC-121, and thus plot in the granodiorite composition field (Fig. 1-15).

Table 1-2. Modal mineralogy of the Walker Top Granite.

Brindle Creek Fault Hanging Wall

	Walker Top Granite		
Sample #	**KC-121**	**KC-1197**	**KC-1267**
Rock type	bgn	bgn	bgn
# Counted	1131	1018	1006
Quartz	29.6	28.9	30.2
Plagioclase	17.6	39.2	33.7
% Anorthite	40.0	37.0	38.0
K-Feldspar	29.7	20.5	15.6
Hornblende	—	—	—
Biotite	17.5	8.7	13.4
Muscovite	1.6	0.2	4.5
Chlorite	—	—	—
Sericite	1.0	0.4	tr
Epi/ clinozo	tr	0.3	1.3
Myrmekite	0.6	1.6	1.0
Kyanite	—	—	—
Garnet	1.1	—	—
Rutile	—	—	—
Sphene	tr	tr	—
Zircon	tr	tr	tr
Apatite	tr	tr	tr
Opaques	1.0	tr	tr
Total	99.7	99.8	99.7

Abbreviations: Epi/clinozo = epidote and clinozoisite, bgn = biotite gneiss, KC-Kings Creek quadrangle, tr < 1.0 %.

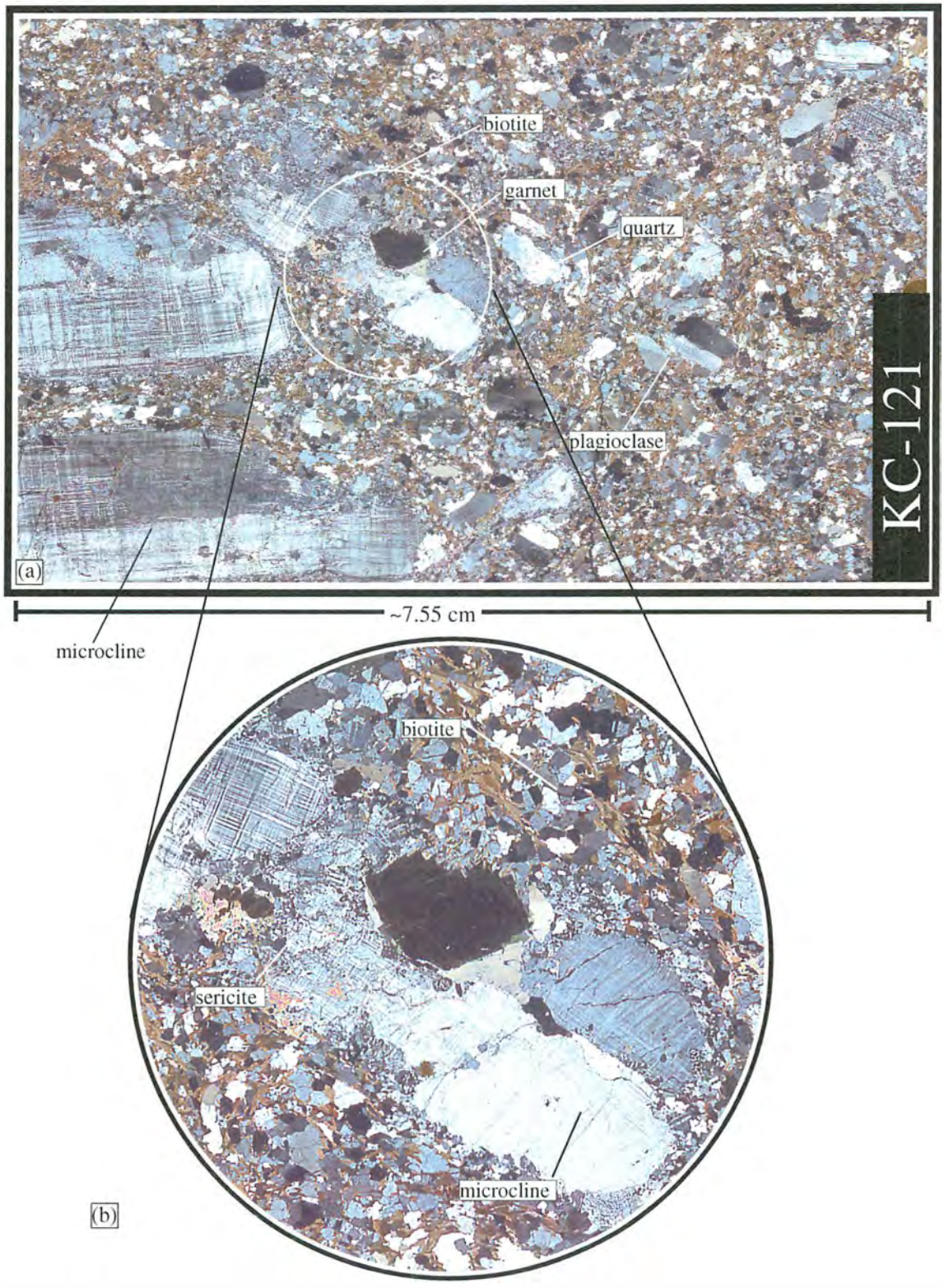

Figure 1-14. The Walker Top Granite. (a) Scanned thin section in cross-polarized light from station KC-121, located 0.25 km east of St. John's Church on U. S. 64. (b) Enlarged image showing a partially retrograded (to sericite) microcline porphyroclast.

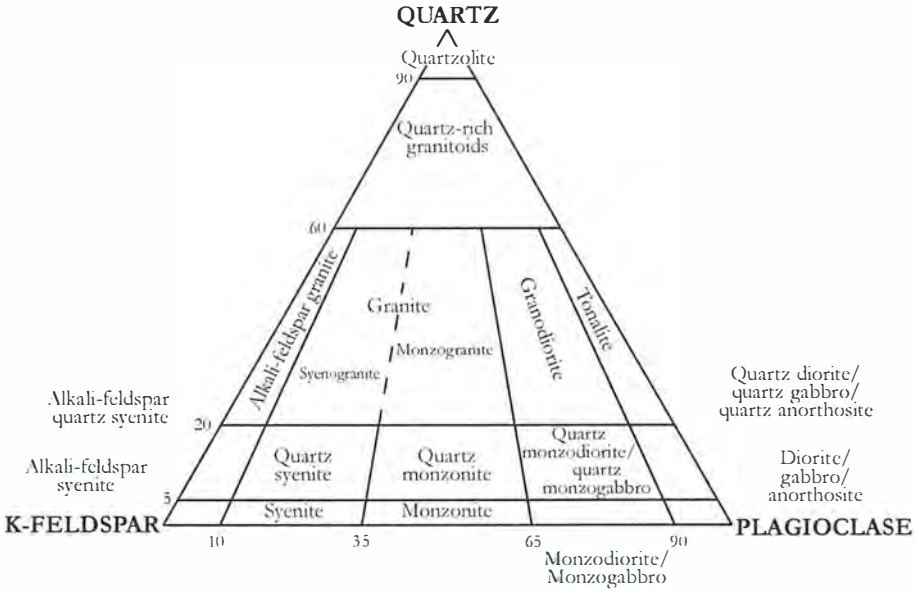

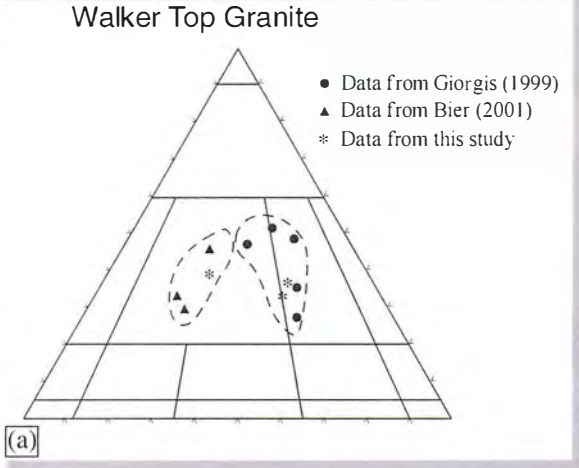

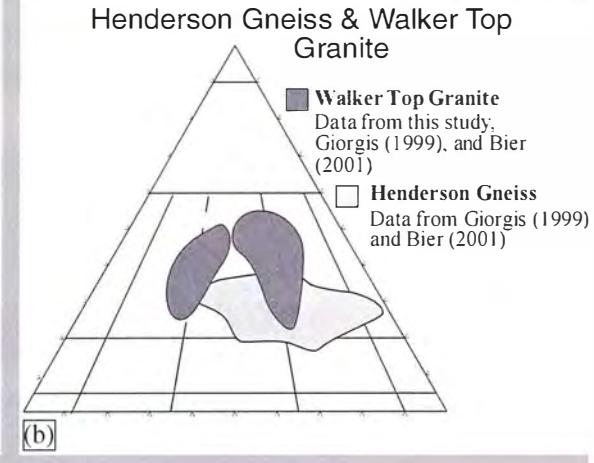

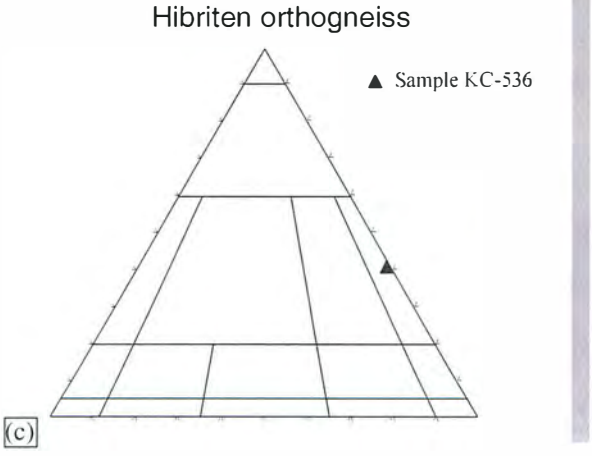

Figure 1-15. IUGS modal classification (Streckeisen, 1976) of Brindle Creek thrust sheet orthogneisses. (a) Walker Top Granite. (b) Composite fields of the Henderson Gneiss and the Walker Top Granite. (c) The Hibriten orthogneiss.

The Walker Top Granite was first distinguished as a poorly to moderately foliated, less sheared, garnetiferous variant of the Henderson Gneiss (Goldsmith et al., 1988). Both are dominated by large (2 cm to > 10 cm) K-feldspar megacrysts with quartz and myrmekite rims. Megacrysts in the Walker Top Granite, however, are typically blocky (subhedral to euhedral); aspect ratios range from 1:2 to 1:8 (Giorgis, 1999; Giorgis et al., 2002), whereas Henderson Gneiss megacrysts are usually augen and less often subhedral. The matrix of the Walker Top Granite here is darker (CI 40-50 %) than Henderson Gneiss matrix (CI 20-40 %). Geochronologic data also discount a genetic relationship between the Walker Top Granite and Henderson Gneiss. Mapes (2002) reported a Neoacadian (366 ± 3 Ma) ion microprobe U-Pb zircon crystallization age for the Walker Top Granite. An Ordovician crystallization age for the Henderson Gneiss is indicated from an ion microprobe U-Pb zircon magmatic age of ~490 Ma (Carrigan et al., 2001).

Hibriten orthogneiss

An inequigranular biotite-quartz-plagioclase gneiss was recognized at several locations in, and to the southwest of, the Brushy Mountains in the Charlotte 1° x 2° geologic map (Plate 1; Goldsmith et al., 1988). Work at 1:62,500-scale in the Lenoir quadrangle did not distinguish this unit from biotite-quartz-plagioclase gneiss and mica-sillimanite schist units seen throughout that study area (Reed, 1964). Although Goldsmith et al. (1988) mapped inequigranular gneiss in the Morganton South 7.5-minute quadrangle, it was grouped on a 1:24,000-scale map with metagraywacke and sillimanite schist (Giorgis, 1999). This grouping is understandable given the textural and

mineralogical similarity of the inequigranular gneiss to overlying metasedimentary rock units. Detailed geologic mapping and thin-section analysis during this study revealed a plagioclase (An_{33})-quartz-biotite, ± hornblende, ± garnet inequigranular gneiss and schist and a plagioclase (An_{34-38})-quartz-hornblende gneiss that is petrologically distinguishable from adjacent sillimanite schist and metagraywacke units (Figs. 1-5, 1-16). This unit is informally named the Hibriten orthogneiss for outcrops on the southeast slopes of Hibriten Mountain (stations KC-1259-1262) adjacent to Hibriten Mountain Road in the Kings Creek 7.5-minute quadrangle (Fig. 1-17; Plate 2).

The Hibriten orthogneiss crops out in the immediate hanging wall of the Brindle Creek thrust throughout the Kings Creek quadrangle, in the adjacent Boomer and Ellendale quadrangles (Merschat, in progress), and in the Charlotte 1° x 2° quadrangle (Goldsmith et al., 1988; Fig. 1-5; Plates 1, 2). A characteristic texture of ~0.25-1.0 cm (diameter) rounded and elongate plagioclase and less common quartz porphyroclasts in a dark gray, biotite-rich matrix is easily recognizable in outcrop (Fig. 1-16). Moderately weathered exposures also retain a characteristic texture; plagioclase degrades first and creates a pattern of rounded dimples on surfaces. More extensive weathering produces reddish-brown schistose saprolite similar to decomposed mica schist of the Brindle Creek thrust hanging wall (Fig. 1-10a). Porphyroclastic biotite gneiss locally grades into porphyroclastic biotite schist. As with the adjacent metasedimentary rock units, local amphibolite layers are common and are identified by sporadic float. Sympathetic and discordant bands of hololeucocratic granitoid and pegmatite are common in outcrop.

Four samples were chosen for petrographic modal analysis of the Hibriten orthogneiss: KC-494, KC-536 (Fig. 1-18), KC-569, and KC-1088. Three samples are

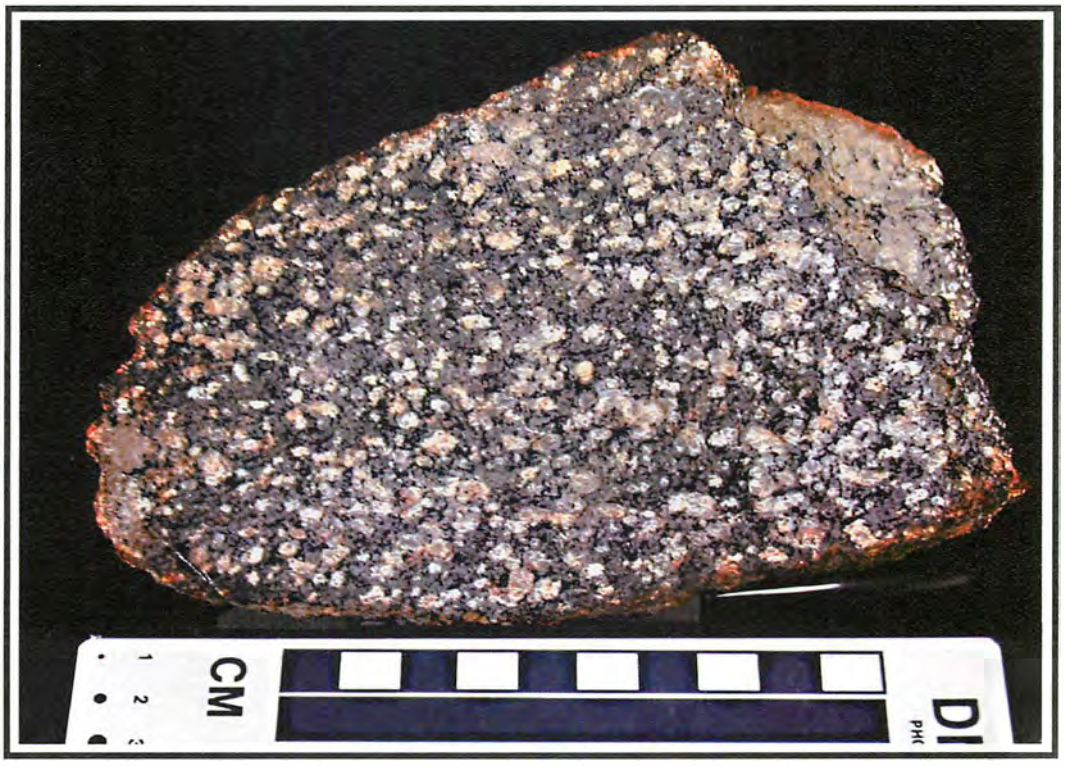

Figure 1-16. Hibriten orthogneiss from station KC-536, located 1.94 km south of the clubhouse at the Cedar Rock Country Club. Note the characteristic distribution of subrounded plagioclase porphyroclasts in a biotite-rich matrix and the weathering rind around the edges of the sample. Note: this sample was chosen to show the characteristic plagioclase porphyroclasts; it lacks the compositional banding frequently observed in outcrop.

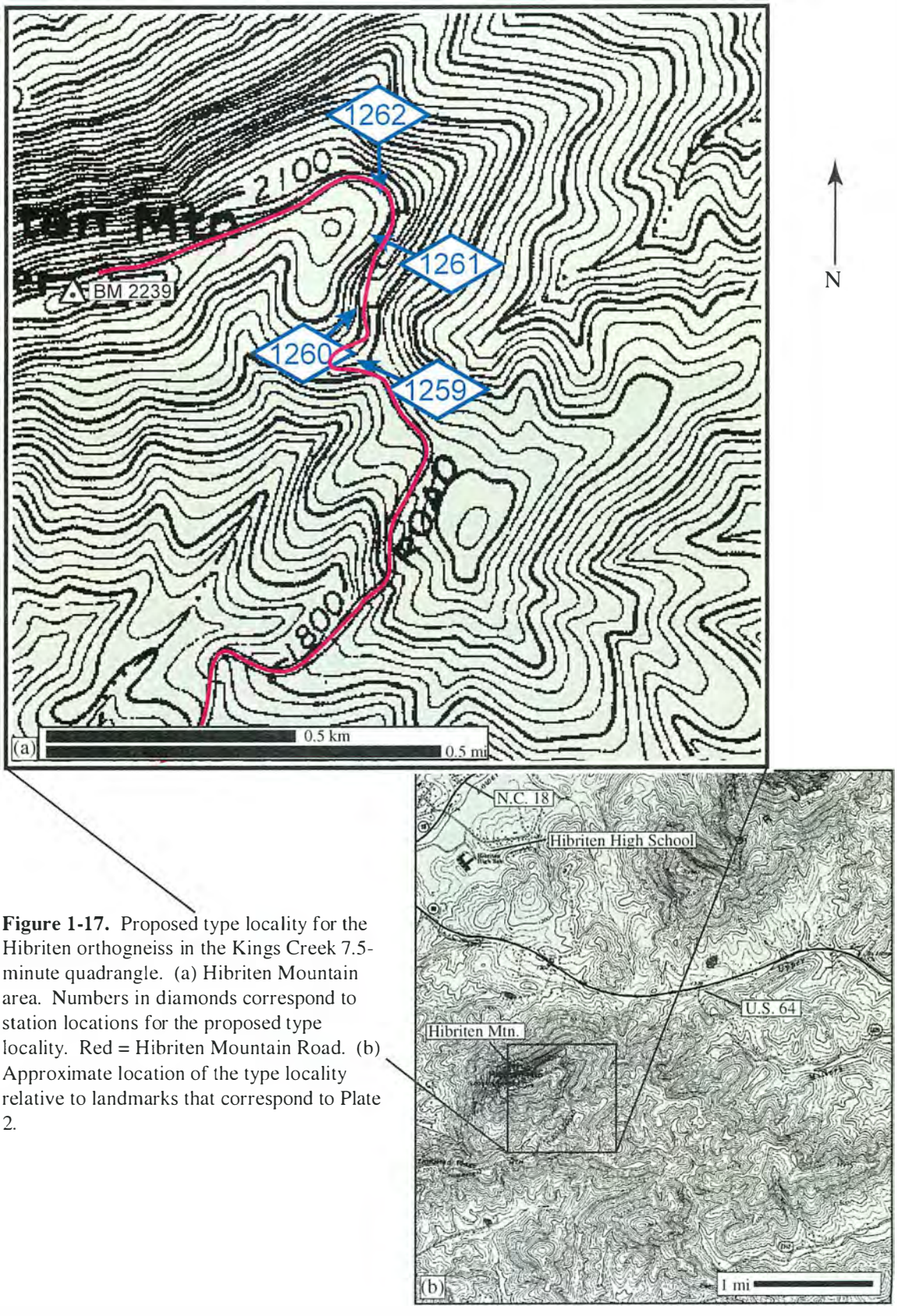

Figure 1-17. Proposed type locality for the Hibriten orthogneiss in the Kings Creek 7.5-minute quadrangle. (a) Hibriten Mountain area. Numbers in diamonds correspond to station locations for the proposed type locality. Red = Hibriten Mountain Road. (b) Approximate location of the type locality relative to landmarks that correspond to Plate 2.

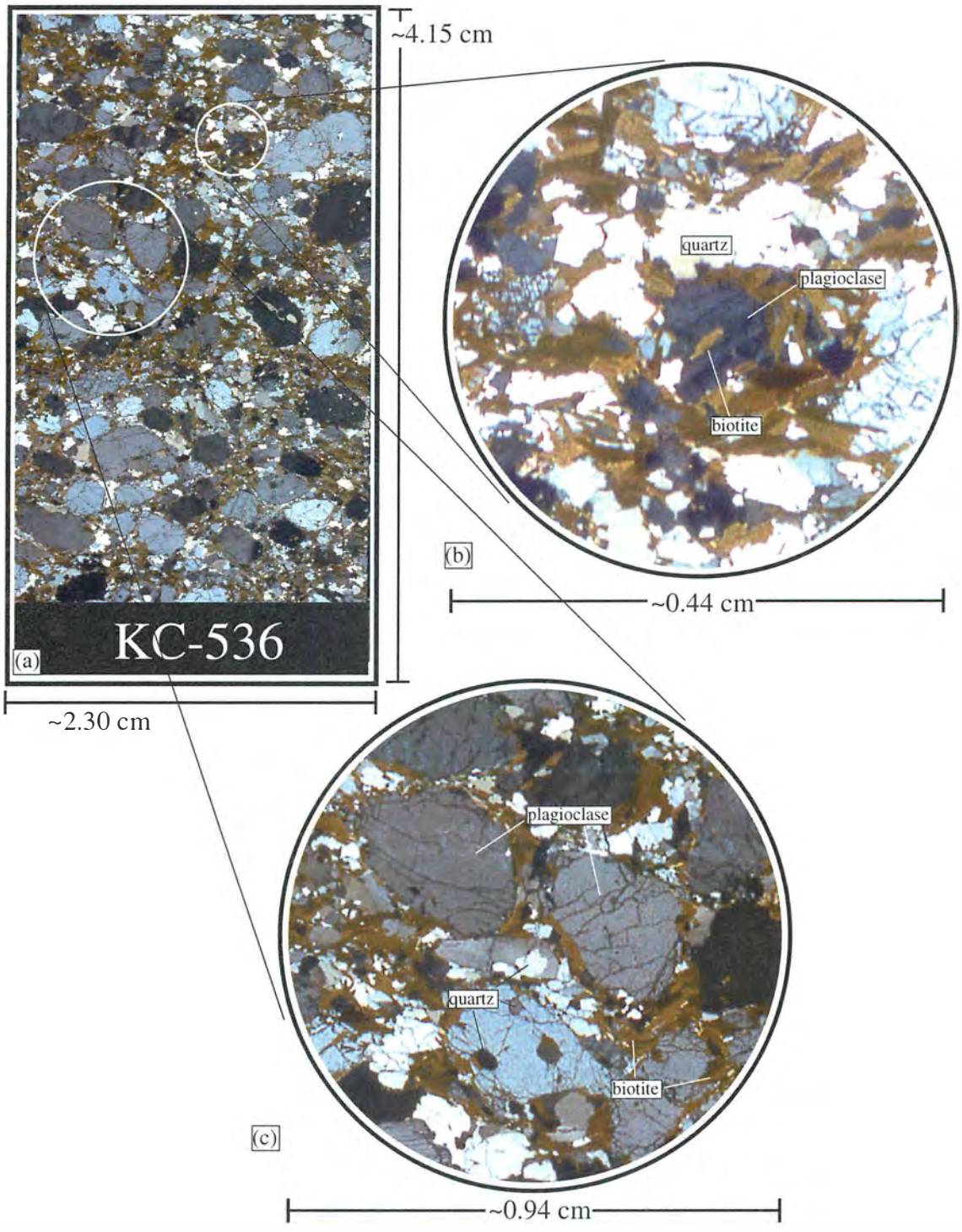

Figure 1-18. Hibriten orthogneiss. (a) Scanned thin section from station KC-536 in cross-polarized light. The sample locality is ~1.94 km south of the clubhouse at the Cedar Rock Country Club. Note the inequigranular texture defined by plagioclase porphyroclasts in a biotite- and quartz-rich matrix. (b) Enlarged image of a weathered plagioclase porphyroclast with interstitial biotite. (c) Enlarged image of cracked weathered plagioclase porphyroclasts bordered by finer-grained biotite and quartz crystals.

hornblende-rich, and may not be representative of the whole rock unit. The Hibriten orthogneiss plots in the tonalite field of the IUGS classification diagram (Fig. 1-15c; Streckeisen, 1976); it typically contains plagioclase (An_{33-38}), quartz, biotite, and muscovite, with accessory hornblende, sericite (replaces plagioclase), garnet, rutile, sphene, apatite, ± epidote, ± sillimanite, ± chlorite, zircon, and opaque minerals. In all four samples much of the plagioclase is partially weathered and clouded (Figs. 1-18a, 1-18c). Samples KC-494, KC-536, and KC-569 have the characteristic porphyroclastic schistose texture, but different matrix mineralogies; KC-536 has a biotite-dominated matrix whereas KC-494 and KC-569 are hornblende gneisses (Table 1-3). Sample KC-1088 is from an amphibolite boudin in Hibriten orthogneiss. It contains hornblende, quartz, plagioclase (An_{39}), and opaque minerals, with accessory sericite (replaces plagioclase), epidote, sphene, apatite, and zircon.

Brindle Creek Thrust Footwall

Lenoir Quarry migmatite

The immediate footwall of the Brindle Creek thrust is dominated by well-foliated, medium- to coarse-grained migmatite. This heterogeneous unit was mapped by Goldsmith et al. (1988) as "migmatitic gneissic biotite granite to quartz diorite" with frequent septa of hornblende amphibolite, biotite gneiss, biotite schist, and blocks of massive amphibolite and metagabbro. Goldsmith et al. (1988) also recognized a granitoid gneiss that locally consists of "gneissic biotite granite, biotite granodiorite, and hornblende-biotite-quartz diorite" (Plate 1). Reed (1964) mapped the migmatitic unit as quartz diorite, granodiorite, and quartz-monzonite gneiss with pods and blocks of amphibolite. Both previous maps document compositional heterogeneity in the

Table 1-3. Modal mineralogy of the Hibriten orthogneiss.

Brindle Creek Fault Hanging Wall

	Hibriten orthogneiss			
Sample #	**KC-536**	**KC-494**	**KC569**	**KC-1088**
Rock type	bgn	amph	amph	amph
# Counted	1130	1005	1008	1126
Quartz	28.8	21.1	1.7	15.8
Plagioclase	41.3	32.4	37.6	16.0
%Anorthite	33.0	34.0	38.0	39.0
K-Feldspar	—	—	—	—
Hornblende	—	32.2	45.5	63.5
Biotite	27.3	10.9	—	—
Muscovite	1.0	—	—	—
Chlorite	0.1	0.1	tr	—
Sericite	tr	tr	tr	tr
Epi/ clinozo	0.4	2.2	11.9	0.5
Myrmekite	—	—	—	—
Sillimanite	tr	—	—	—
Garnet	0.3	tr	—	—
Rutile	tr	tr	tr	—
Sphene	tr	tr	3.0	0.4
Apatite	tr	tr	tr	tr
Opaques	0.3	0.4	tr	3.5
Zircon	tr	tr	tr	tr
Total	99.5	99.3	99.7	99.7

Abbreviations: Epi/ clinozo = epidote and clinozoisite, bgn = biotite gneiss, KC-Kings Creek quadrangle, amph = amphibolite, tr < 1.0 %.

migmatite; Reed (1964), however, attempted to subdivide the unit into leucocratic, mesocratic, and melanocratic members. Detailed mapping of the Dysartsville (Giorgis and Williams, 1999) and Glenwood 7.5-minute quadrangles (Williams, 2000) revealed a texturally similar migmatitic amphibolite in the footwall of the Brindle Creek thrust. The South Mountains unit, a "medium-grained, plagioclase-hornblende-quartz-biotite-muscovite gneiss" (Fig. 1-19a; Giorgis, 1999), was mapped as the Poor Mountain Amphibolite on the basis of its stratigraphic position (above the Tallulah Falls Formation and below the Poor Mountain Quartzite), identification in the sequence, petrologic character, and immobile trace element chemistry (Plate 1). The Poor Mountain Quartzite is medium-grained, quartz- feldspar-muscovite-biotite quartzite interlayered with the upper part and stratigraphically above the amphibolite (Williams, 2000; Giorgis and Williams, 1999). They noted pervasive evidence for anatexis and disruption of textural and mineralogical features characteristic of previously recognized Poor Mountain Formation rocks (e.g., Yanagihara, 1994). Moreover, the migmatite is separated (down sequence) from nonmigmatitic Poor Mountain Formation rocks by migmatitic Tallulah Falls Formation then the Mill Spring thrust (Tabor, 1990; Davis, 1993a; Yanagihara, 1994; Bream, 1999; Hill, 1999; Plate 1).

Detailed geologic mapping during this study revealed a similar migmatite in the Brushy Mountains composed of amphibole-biotite-quartz-plagioclase amphibolite (Fig. 1-19b) and quartz-biotite-K-feldspar-plagioclase granitoid. In the Kings Creek quadrangle the migmatite is exposed as a wide (~6 km), northeast-striking unit that contains large (mappable), disconnected, elliptical amphibolite bodies that parallel the regional structural trend (Fig. 1-5; Plate 2). This unit is informally named the Lenoir

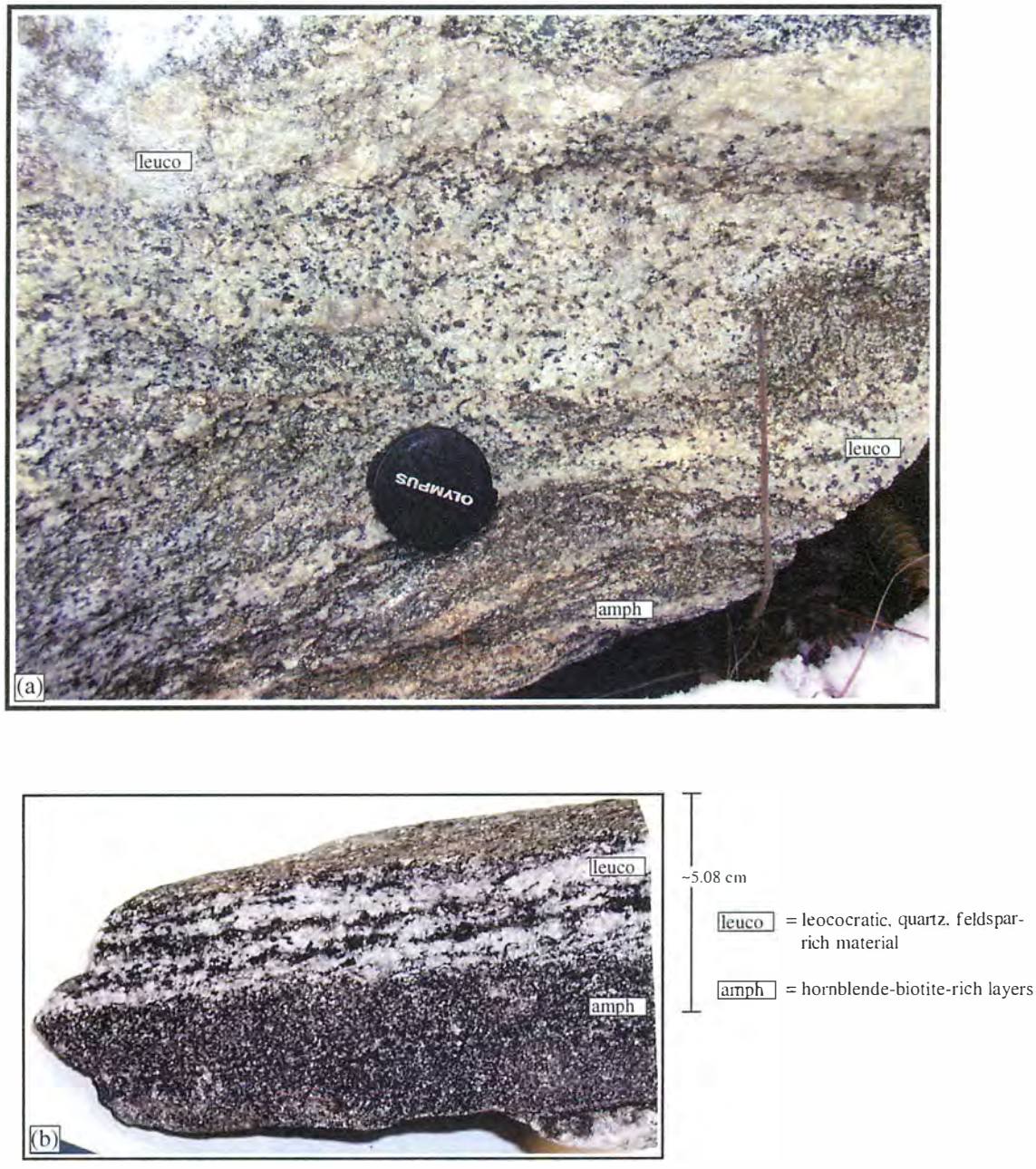

Figure 1-19. Western Inner Piedmont stromatic migmatites. (a) Outcrop of migmatitic "Poor Mountain Amphibolite" from the Dysartsville 7.5-minute quadrangle at sample locality PMA-2.0, adjacent to U. S. 64 near its intersection with state road #226 (Plate 1). The lens cap is ~3 cm in diameter. (b) Hand specimen of stromatic Lenoir Quarry migmatite from sample locality KC-VQ-1 at the Vulcan Materials Company Lenoir Quarry in the Kings Creek 7.5-minute quadrangle (Fig. 1-5; Plate 2). Note the similarity of textures and mineralogy between the two lithologies. In the upper photograph, the foliation in the coarse-grained biotite amphibolite is paralleled and crosscut by hololeucocratic, quartz-feldspar-rich leucosome. In the lower photograph compositional layering parallels the foliation.

Quarry migmatite for outcrop exposures in Vulcan Materials Company Lenoir Quarry, located in the Kings Creek quadrangle on North Carolina 18 ~2 km east of its intersection with U. S. 64 (Fig. 1-20).

The Lenoir Quarry migmatite has a variable texture and composition easily seen at outcrop scale (Fig. 1-21). Amphibolite boudins and thin (~1.5 to 11.0 cm thick; Fig. 1-22), continuous and discontinuous layers and lenses of amphibolite and biotite gneiss contrast with granodioritic, granitic, and pegmatitic, quartz- and K-feldspar-rich leucosome. Leucocratic mobalizates frequently contain large hornblende and biotite porphyroblasts; discordant, post-migmatization pegmatites are also present (Fig. 1-21c). Macroscale amphibolite bodies consist of essentially homogeneous, thin to thick (0.5 to > 30 cm) laminations of hornblende-plagioclase-epidote-quartz amphibolite with thin quartzofeldspathic laminations. Amphibolite weathers to medium-grained, reddish-brown- to ochre-colored saprolite while more felsic portions of the migmatite weather to gray to light orange or tan saprolite.

Eleven representative samples were collected from the Lenoir Quarry migmatite and were subdivided into leuco-, meso-, and melanocratic (amphibolite-dominated) groups. The mineral assemblage of the migmatite neosome consists of quartz, plagioclase (An_{24-34}), biotite, $\pm$ K-feldspar, muscovite, hornblende, myrmekite, and epidote (Table 1-4; Figs. 1-23, 1-24b). Trace accumulations of chlorite, apatite, zircon, sphene, and ilmenite are also present. Two samples, KC-1785 and KC-1691, contain anomalously high concentrations of muscovite (28.3 and 16.1%, respectively; Fig. 1-24a) and represent interlayered schist near the northwestern contact of the Lenoir Quarry migmatite (see discussion of muscovite schist below).

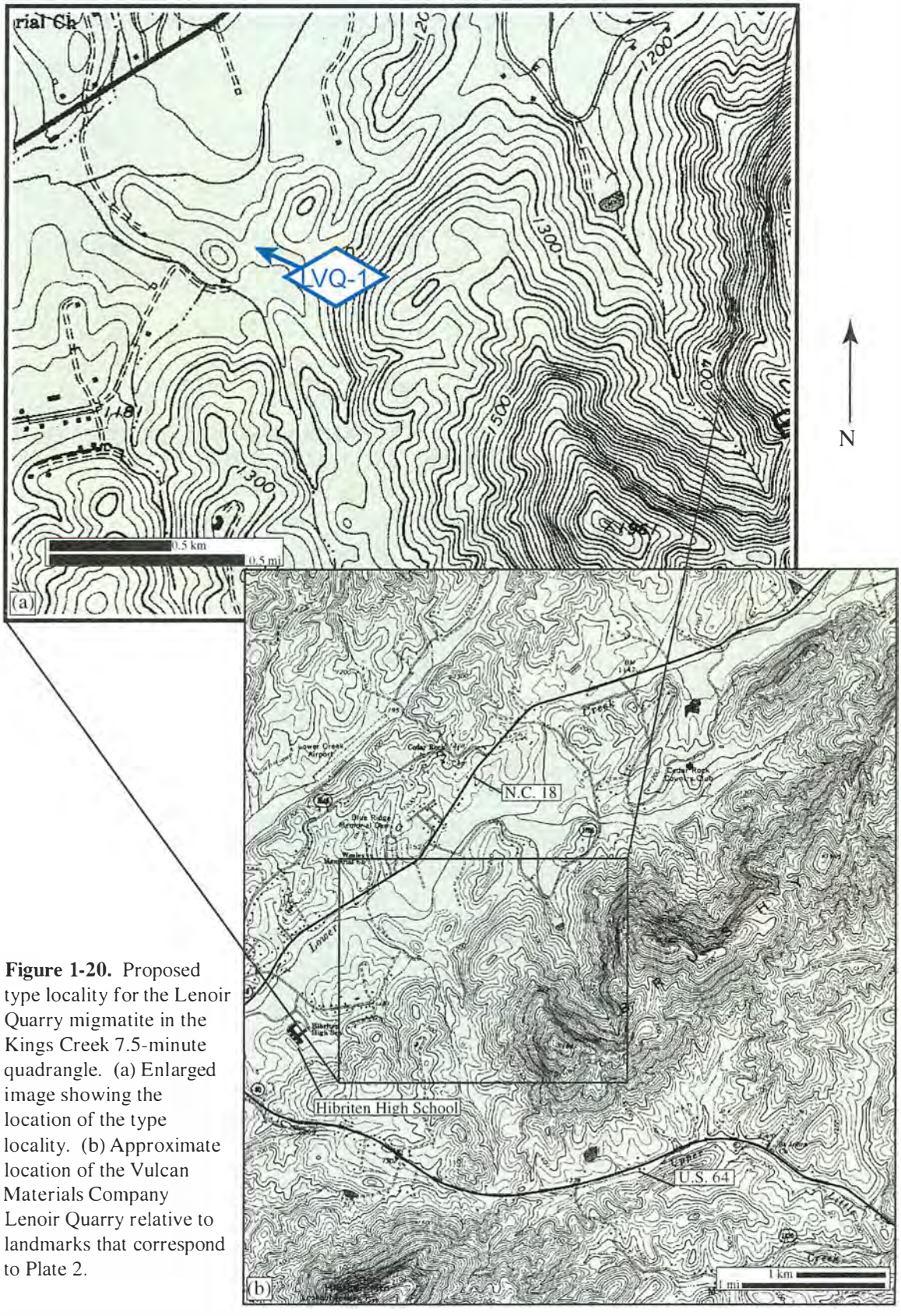

Figure 1-20. Proposed type locality for the Lenoir Quarry migmatite in the Kings Creek 7.5-minute quadrangle. (a) Enlarged image showing the location of the type locality. (b) Approximate location of the Vulcan Materials Company Lenoir Quarry relative to landmarks that correspond to Plate 2.

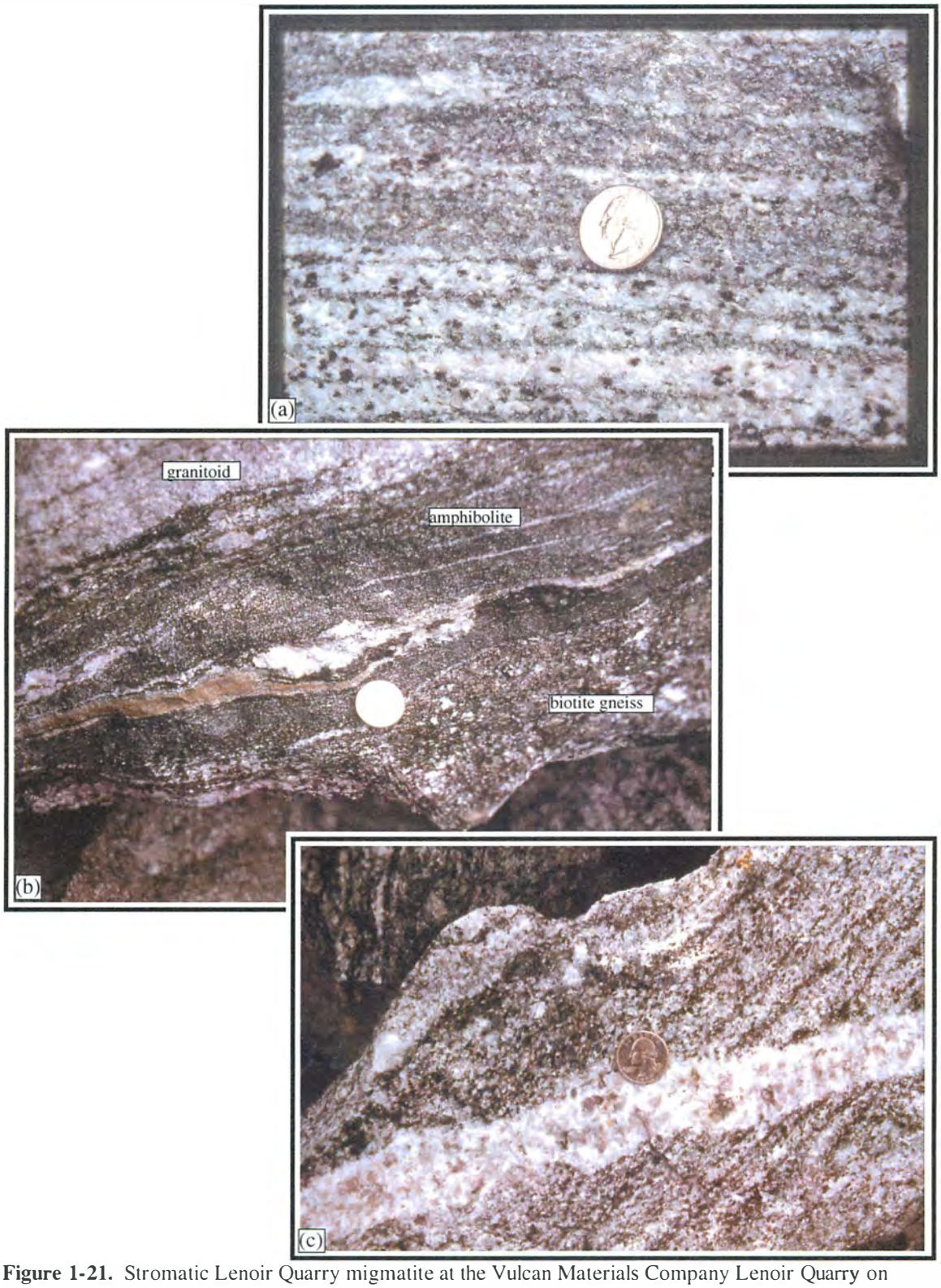

Figure 1-21. Stromatic Lenoir Quarry migmatite at the Vulcan Materials Company Lenoir Quarry on North Carolina 18 near Lenoir. (a) Centimeter-scale compositional layering in a leucocratic specimen. (b) Interlayered coarse-grained granitoid, amphibolite, and biotite gneiss. (c) Pegmatite vein crosscutting a well-developed foliation composed of alternating bands of amphibolite and granitoid.

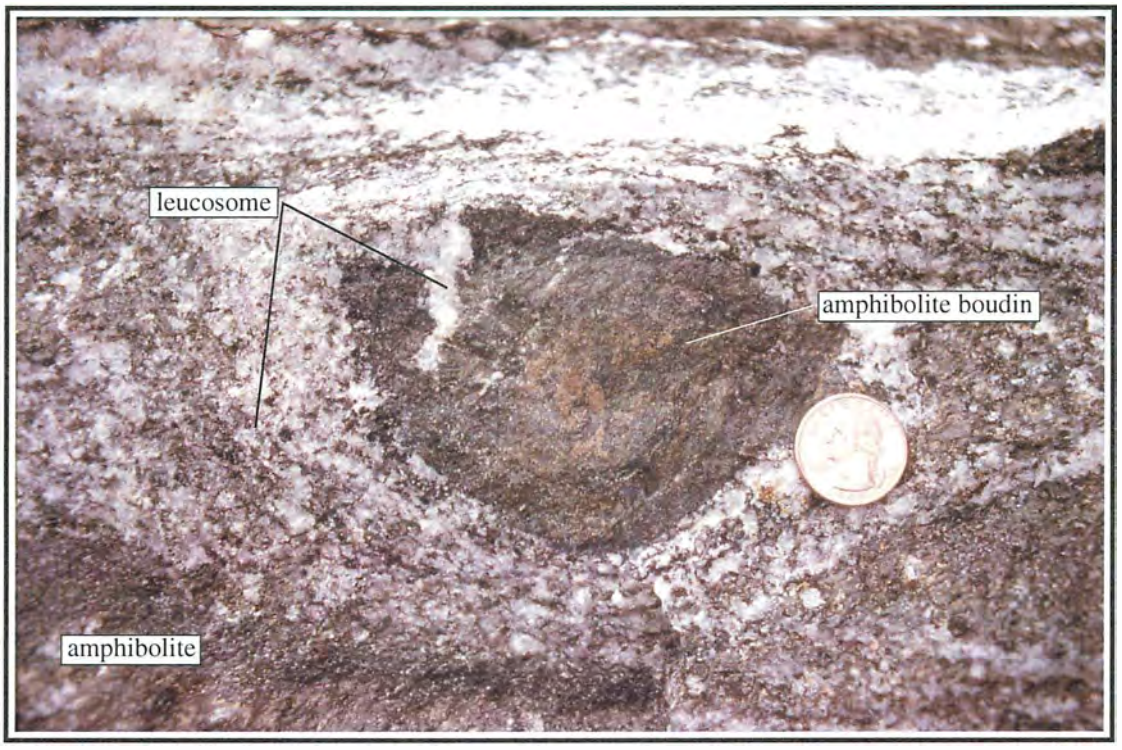

Figure 1-22. Lenoir Quarry migmatite at the Vulcan Materials Company Lenoir Quarry on North Carolina 18. Note early foliation preserved in the boudin.

Table 1-4. Modal mineralogy of Lenoir Quarry migmatite.

Brindle Creek Fault Footwall
Lenoir Quarry migmatite

	Paleosome			Neosome			
Sample #	**KC-1457**	**KC-525**	**KC-Quarry**	**KC-552**	**KC-504**	**KC-1785**	**KC-1691**
Rock type	Amph	Amph	Amph	bgn	bgn	ms	qz
# Counted	NA	1125	1014	1143	1090	1059	1022
Quartz	—	1.6	26.6	37.7	47.5	51.7	67.7
Plagioclase	0.5	25.7	24.2	31.8	36.0	5.3	4.2
% Anorthite	—	44	24.0	34.0	24.0	—	—
K-Feldspar	—	3.4	tr	9.6	—	tr	3.0
Hornblende	99.0	59.4	33.3	4.5	—	tr	—
Biotite	—	—	12.2	11.9	13.2	13.2	2.8
Muscovite	—	tr	—	—	0.8	28.3	16.1
Chlorite	—	—	—	0.1	tr	tr	—
Sericite	—	1.8	—	—	—	tr	tr
Epi/ clinozo	0.2	7.3	2.6	1.8	1.4	—	0.1
Kyanite	—	—	—	—	—	—	—
Myrmekite	—	tr	—	2.4	—	—	—
Sillimanite	—	—	—	—	0.5	0.9	1.4
Garnet	—	—	—	tr	—	—	—
Rutile	tr	—	—	—	tr	—	—
Sphene	—	tr	0.6	—	—	0.2	—
Apatite	—	tr	tr	tr	tr	tr	0.1
Zircon	—	tr	tr	tr	tr	tr	0.2
Opaques	0.1	0.3	0.1	—	0.3	0.2	4.3
Total	99.8	99.5	99.6	99.8	99.7	99.8	99.9

Abbreviations: Epi/ clinozo = epidote and clinozoisite, bgn = biotite gneiss, ms= muscovite schist, amph = amphibolite, qz = quartzite, tr < 1.0 %.

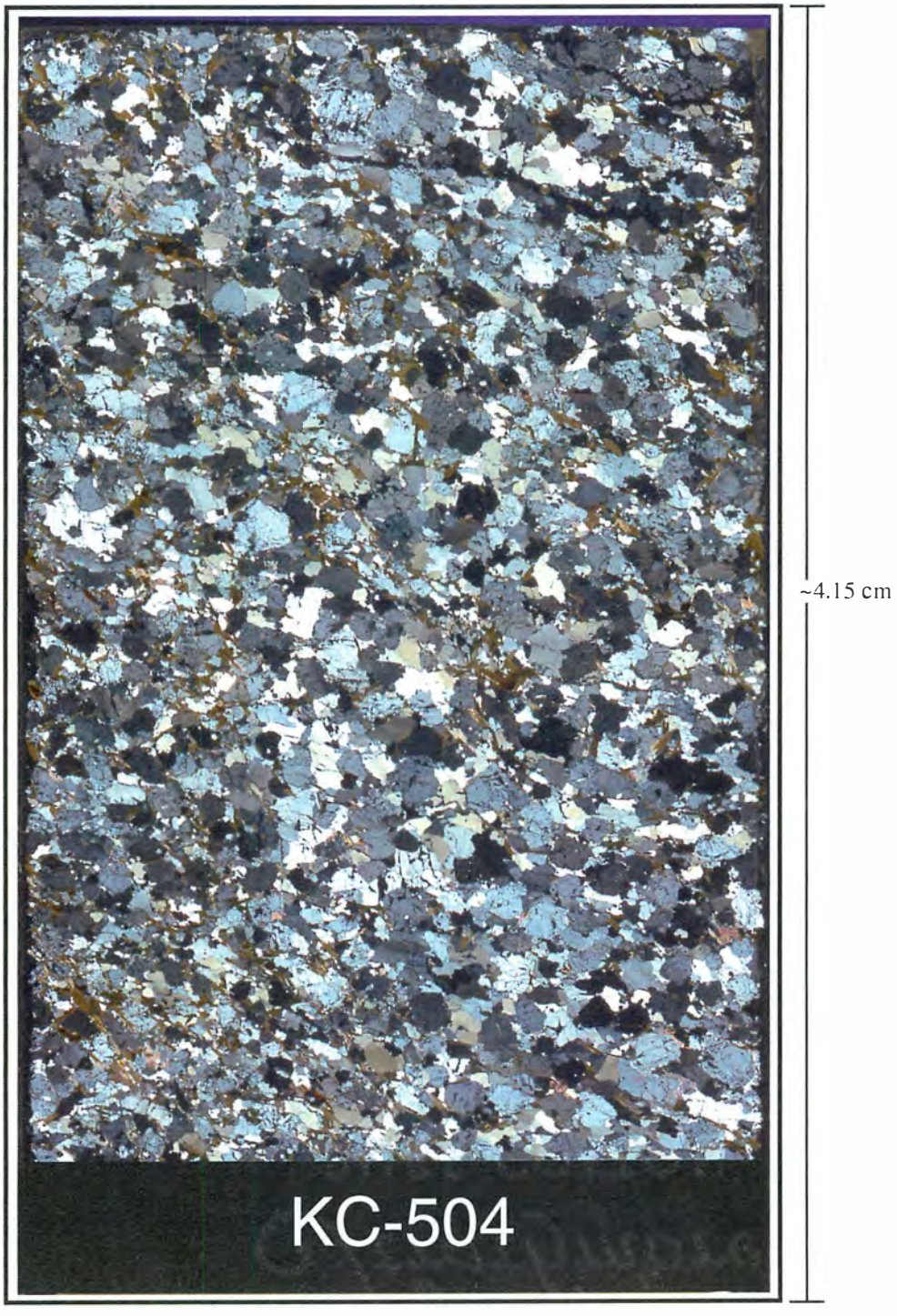

Figure 1-23. Scanned thin section in cross-polarized light showing the texture of Lenoir Quarry migmatite from station KC-504, ~0.45 km east of Hibriten High School. The equigranular-tabular to diablastic texture seen here is typical in both hornblende- and biotite-dominated samples of the Lenoir Quarry migmatite. Note: muscovite is both parallel and sub-perpendicular to the poorly defined foliation dominated by quartz, plagioclase, and biotite.

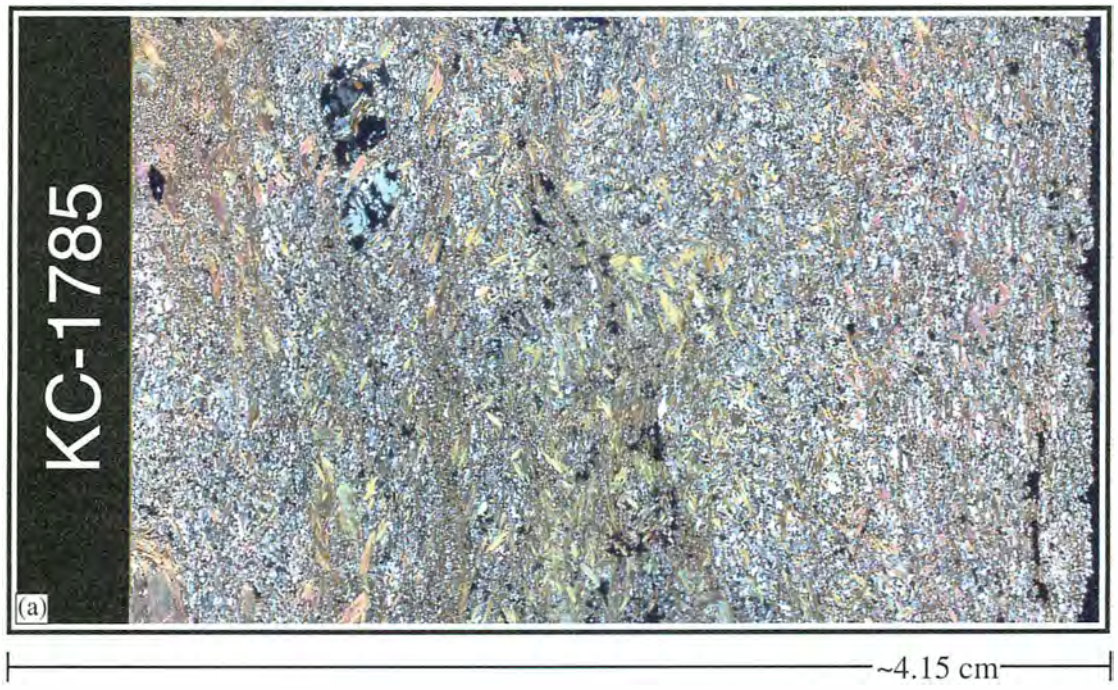

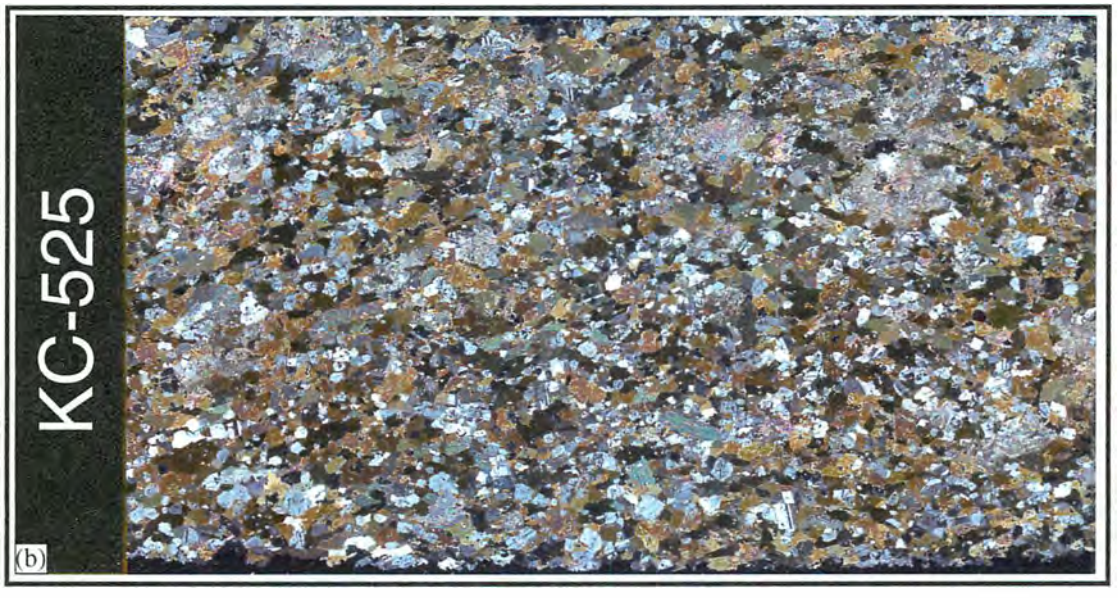

Figure 1-24. Textural variabilityin samples from the Lenoir Quarry migmatite. (a) Scanned thin section in cross-polarized light of sample KC-1785, a quartz-K-feldspar-muscovite-biotite-plagioclase schist from its sample locality ~1.02 km northwest of Little Kings Creek. Note the fine-grained, well-foliated, equigranular texture. The yellow tabular mineral is muscovite. (b) Scanned thin section in cross-polarized light of sample KC-525, a migmatitic amphibolite from its sample locality ~1.62 km east of Hibriten High School. Note the medium-grained, equigranular texture.

Mineralogical variability is also common in hornblende-rich melanosome. The dominant mineral assemblage consists of hornblende, plagioclase (An_{24-44}), quartz, ± biotite, and epidote (Table 1-4) with accessory muscovite, sericite, sphene, apatite, and opaque minerals. Hornblende grains are typically euhedral to subhedral and have average dimensions of ~0.62 x 0.30 mm; medium-grained amphibolites were also observed. Hornblende compositions were obtained with an electron microprobe (EMP) (Table 1-5); spot analyses revealed an asymmetric chemical zonation with respect to SiO_2, TiO_2, and Al_2O_3 in several hornblende grains.

Muscovite Schist

Near its northwestern contact, the Lenoir Quarry migmatite grades into thin, laterally traceable pelitic schist (Fig. 1-5; Plate 2). Goldsmith et al. (1988) recognized this heterogeneous unit as a "yellowish-gray to bluish-gray, medium- to coarse-grained" white mica-quartz-biotite schist with accessory garnet, tourmaline, and chlorite.

In the Brushy Mountains, a schist similar to that described by Goldsmith et al. (1988) is poorly exposed in streams and on logging road cuts on the south-facing slope (dip slope) of Green Mountain (Plate 2). This unit is recognized in the study area as variably garnetiferous, muscovite-biotite-quartz-feldspar schist, quartz-muscovite-biotite schist, and quartzitic schist. It is migmatitic and commonly contains lenses of medium- to coarse-grained quartzofeldspathic material deformed into a Type-II S-C mylonitic fabric (Lister and Snoke, 1984). Sample KC-1785 (Fig. 1-24a; Table 1-4), a fine-grained, quartz-K-feldspar-muscovite-biotite-plagioclase schist, was collected from within the Lenoir Quarry migmatite near its contact with the muscovite schist. It is petrologically

Table 1-5. Averaged hornblende analyses from Lenoir Quarry migmatite sample KC-VQ-1, collected from the Vulcan Materials Company Lenoir Quarry.

	Amph-1	Amph-3	Amph-4
# of Analyses	3	3	3
SiO_2	39.9 (1)	41.5 (1)	42.5 (2)
TiO_2	0.13 (1)	0.08 (4)	0.86 (5)
Al_2O_3	14.5 (1)	11.7 (1)	11.6 (1)
Cr_2O_3	0.01 (1)	<0.03	0.06 (1)
MgO	7.6 (2)	9.98 (5)	9.91 (7)
CaO	11.4 (1)	11.7 (1)	11.5 (1)
MnO	0.42 (1)	0.35 (1)	0.42 (3)
FeO	20.1 (2)	17.7 (2)	17.4 (1)
Na_2O	1.69 (1)	1.44 (1)	1.36 (1)
K_2O	1.13 (4)	1.42 (2)	1.35 (5)
H_2O	1.94 (1)	1.95 (1)	1.97 (1)
Σ	98.8	98.5	99.2
Cations based on 23 oxygens			
Si	6.171	6.378	6.460
Ti	0.014	0.095	0.098
Al	2.648	2.111	2.078
Cr	0.001	0.000	0.007
Mg	1.758	2.286	2.245
Ca	1.881	1.927	1.913
Mn	0.055	0.046	0.054
Fe	2.598	2.274	2.213
Na	0.505	0.428	0.401
K	0.222	0.278	0.262
H	0.000	0.000	0.000
Σ	15.853	15.823	15.731

a Units in ( ) represent one standard deviation of replicate analyses in terms of least units cited

b All Fe calculated as FeO

Amph-1= KCVQ-6, KCVQ-9, and KCVQ-10
Amph-2= KCVQ-37, KCVQ-40, and KCVQ-41
Amph-3= KCVQ-42, KCVQ-43, and KCVQ-44

Procedural note:

Geochemical analyses of several mineral phases in one sample (KC-VQ-1) were conducted using the CAMECA SX-50 electron microprobe at the University of Tennessee, Knoxville. An acceleration voltage of 15 keV, and 20 second counting times were standard for most analyses. A count time of 30 seconds was used for Ca and Mn in biotite. The beam diameter was 5 mm. The beam current was set to 20 nA for most mineral phases; a reduced beam current (10 nA), however, was used for plagioclase. All data were fully reduced using the Cameca ZAF "PAP" software. Analytical precision was validated by comparisons with a set of well characterized natural standards.

indistinguishable from rocks within the muscovite schist unit and may indicate a gradational contact. A medium-grained, quartz-feldspar-biotite gneiss with a salt-and-pepper texture was locally identified in the schist unit.

Green Mountain Fault Footwall

Tallulah Falls metagraywacke and schist

The muscovite schist is in thrust contact (Part II) with mylonitic, dark gray, fine- to medium-grained, biotite gneiss (metagraywacke) and biotite-muscovite schist (Fig. 1-25). Reconnaissance mapping linked this mylonitic metagraywacke and schist with metasedimentary units of the Brindle Creek thrust hanging wall (Reed, 1964; Goldsmith et al., 1988); they are, however, restricted to the western IP. Giorgis and Williams (1999) mapped the unconformable contact between migmatitic Poor Mountain Amphibolite and the upper member of the Tallulah Falls Formation (Plate 1). Compilation of reconnaissance work (Goldsmith et al., 1988) with detailed work (Giorgis, 1999; this study) indicates lateral continuity between the migmatitic Poor Mountain Amphibolite in the South Mountains and the Lenoir Quarry migmatite. Thus, a similar tectonostratigraphic relationship may exist in the northwestern quarter of the Kings Creek quadrangle (Plate 1).

Tallulah Falls Formation rocks in the Kings Creek quadrangle are characterized by a mesomylonitic (Passchier and Trouw, 1998), inequigranular texture composed of 13 to 24 percent subhedral and sheared plagioclase and less commonly quartz porphyroclasts in a fine- to medium-grained biotite-quartz-plagioclase-rich matrix (Fig. 1-25). Porphyroclasts are generally smaller than those in the Hibriten orthogneiss (0.1 to < 1.0

Figure 1-25. Mylonitic Tallulah Falls migmatite in the footwall of the Green Mountain fault at station KC-1792, ~1.3 km east of Moses Knob. Note the characteristic feldspar porphyroclasts in a variably mylonitic, biotite-rich matrix. Also note the weathered lithology in the upper portion of the photograph.

cm), but produce a similar dimpled pattern on weathered surfaces (Fig. 1-26). More intense weathering produces a reddish-brown schistose saprolite.

The dominant mineralogy consists of quartz, biotite, plagioclase (An_{34-44}), muscovite, chlorite, and sillimanite, with accessory K-feldspar, epidote, hematite, ± sericite, ± zircon, and opaque minerals (Table 1-6). A bimodal grain-size distribution is present in both hand specimens and thin sections. Concentrations of muscovite and biotite flank composite plagioclase-quartz porphyroclasts (Figs. 1-26b, 1-27b). Samples KC-1735 and KC-1849 also have large (up to 0.24 x 0.07 cm) muscovite fish that partially define a Type-II S-C mylonitic fabric (Fig. 1-27). The mica fish are parallel to the sillimanite mineral lineation. The foliation in each sample is defined by parallel alignment of fine-grained quartz, biotite, muscovite, and less commonly by plagioclase grains (Figs. 1-26, 1-27). A significant percentage (~10%) of the plagioclase in samples KC-1738 and KC-1849 occurs in the matrix.

Henderson Gneiss

The northwesternmost unit in the Kings Creek quadrangle is the Henderson Gneiss (Plate 1; Fig. 1-5). It was named by Keith (1905, 1907) as Henderson Granite; Reed and Bryant (1964) later characterized it as an easily recognizable orthogneiss that is traceable from near the South Carolina-Georgia border in South Carolina into central North Carolina (Lemmon, 1973; Lemmon and Dunn, 1975). It crops out entirely within the western IP and attains its greatest outcrop width in the type area located in Henderson County (Plate 1). Northeast of Marion, North Carolina, Henderson Gneiss occurs as a series of lenticular outliers (Reed, 1964). The Brushy Mountains body crops out ~45 km northeast of and along strike with the main body (Plate 1).

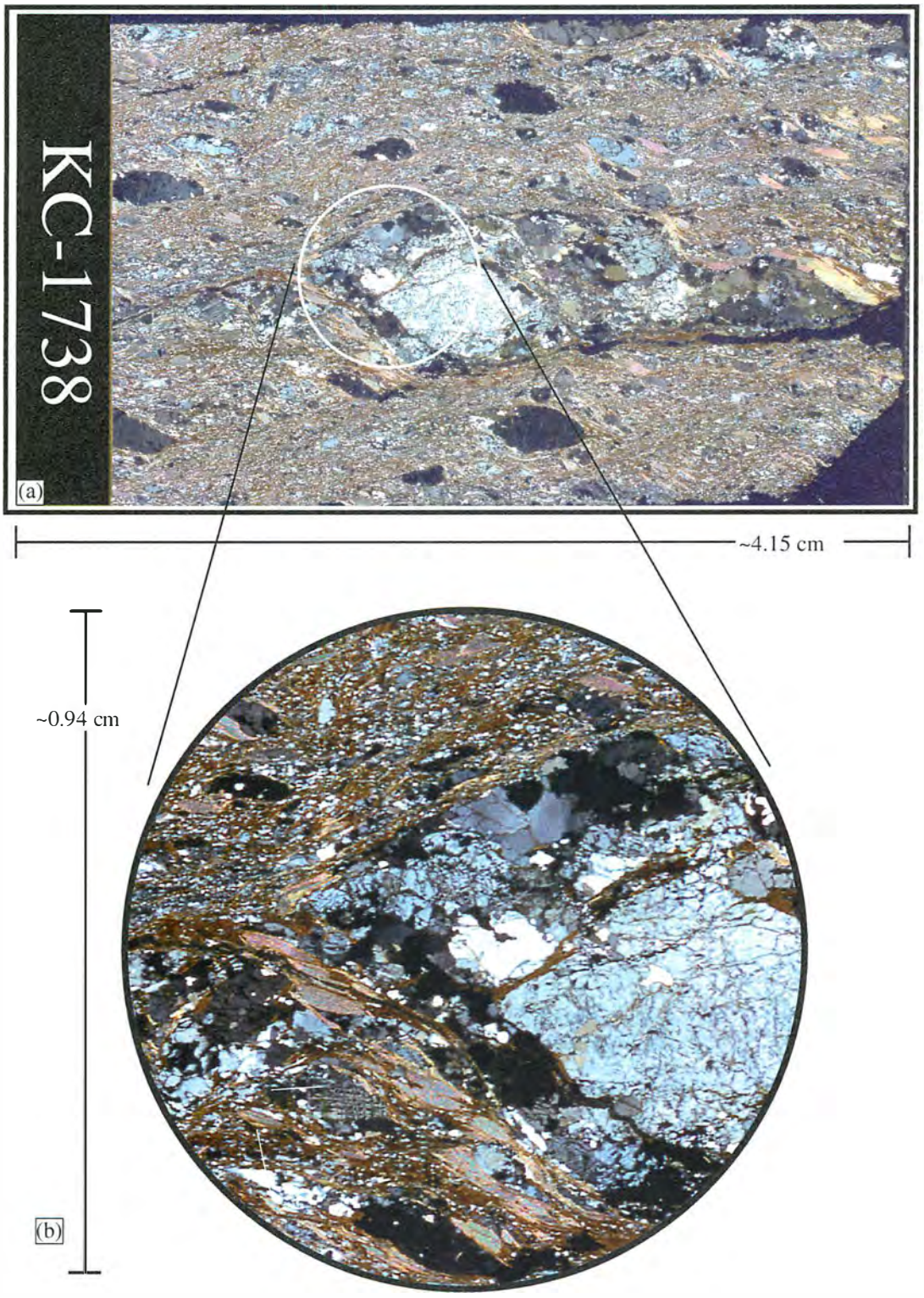

Figure 1-26. Mylonitic metagraywacke from the Tallulah Falls Formation. (a) Scanned thin section in cross-polarized light from station KC-1738 on Green Mountain. The composite porphyroclast has multiple quartz inclusions. The matrix is dominantly biotite, muscovite, quartz, and plagioclase. (b) Enlarged image of a sheared plagioclase porphyroclast.

Table 1-6. Modal mineralogy of Tallulah Falls Formation metagraywacke-schist.

Green Mountain fault footwall

	Tallulah Falls metagraywacke-schist		
Sample #	**KC-1738**	**KC-1849**	**KC-1792**
Rock type	bgn	bgn	bgn
# Counted	1021	1020	1050
Quartz	37.1	33.7	35.4
Plagioclase	21.7	25.3	15.0
%Anorthite	—	44.0	34.0
K-Feldspar	3.2	—	—
Hornblende	—	—	—
Biotite	22.5	32.9	29.1
Muscovite	10.9	7.6	15.0
Chlorite	0.7	0.2	tr
Sericite	tr	—	—
Epi/ clinozo	0.5	0.2	0.8
Myrmekite	—	—	—
Sillimanite	2.8	tr	2.6
Garnet	—	—	—
Rutile	—	—	—
Sphene	—	—	—
Apatite	—	—	0.2
Zircon	tr	—	tr
Opaques	0.3	tr	1.7
Total	99.7	99.9	99.8

Abbreviations: Epi/ clinozo = epidote and clinozoisite, bgn = biotite gneiss, tr < 1.0 %. Note: albite twins in sample KC-1738 are deformed; the Michele-Lévy method yielded spurious An contents (An68).

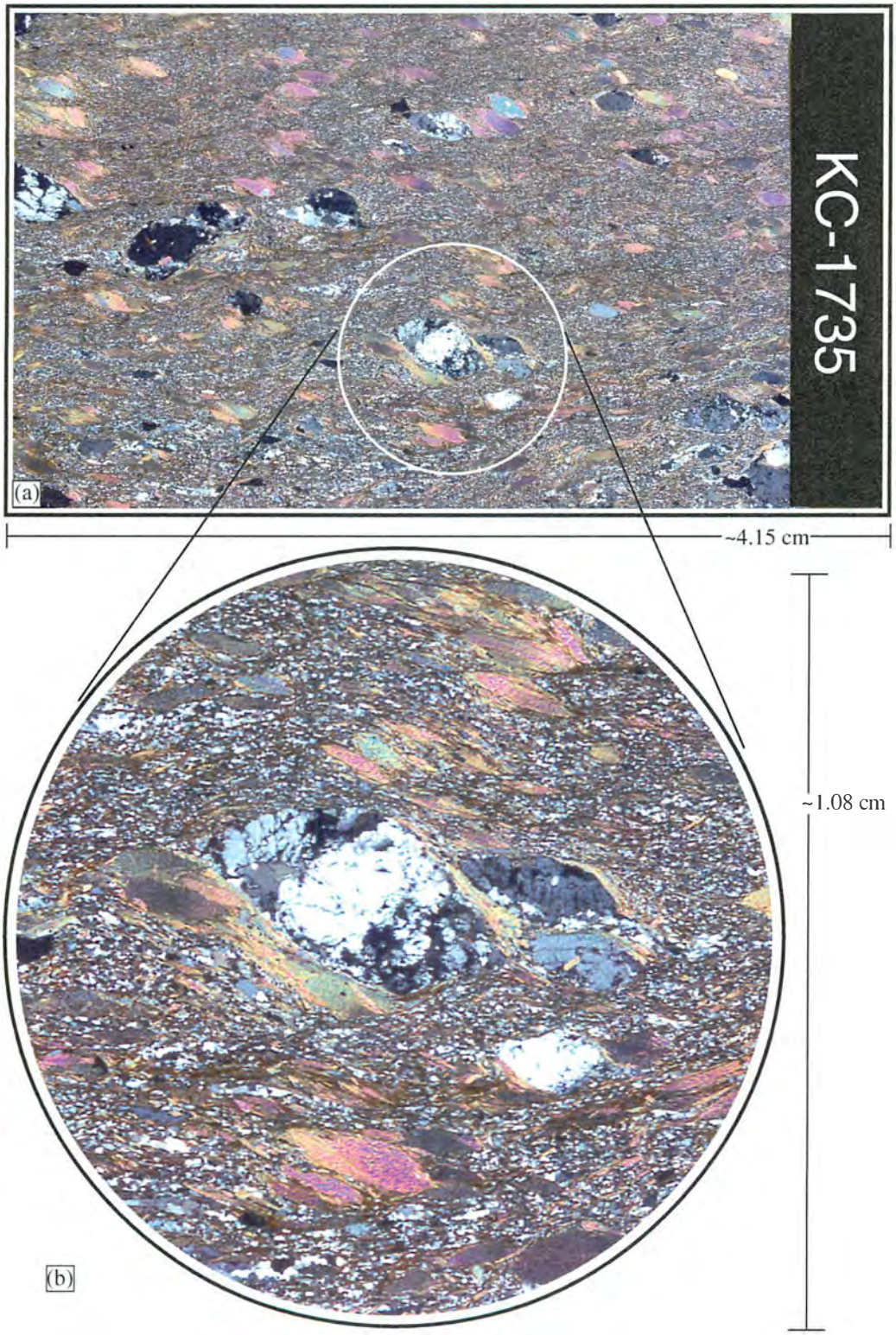

Figure 1-27. Type II S-C mylonite from the Tallulah Falls Formation. (a) Scanned thin section in cross-polarized light from station KC-1735, ~2.0 km north of Zacks Fork Road (state road #1511). The section contains sheared composite plagioclase porphyroclasts and muscovite fish in a fine-grained, quartz-dominated matrix. (b) Enlarged image showing a sinistral shear sense in the mylonitic fabric.

The Henderson Gneiss is a coarse-grained, porphyroclastic augen gneiss composed of microcline, oligoclase, quartz, biotite, and muscovite (Hatcher, 1993). Microcline augen are characteristically rimmed by myrmekite and are typically ~3 cm or less in diameter (Hatcher, 1993). The modal mineralogy of the Henderson Gneiss from several studies in southwestern North Carolina was plotted using the IUGS classification system (Fig. 1-28; Lemmon, 1973; Whisnant, 1975; Streckeisen, 1976; Yanagihara, 1994; Bream, 1999). The Henderson Gneiss plots mainly in the monzogranite field, but also overlaps the granodiorite, quartz monzonite, and quartz monzodiorite/quartz monzogabbro fields (Fig. 1-28).

The crystallization age of the Henderson Gneiss has been debated by southern Appalachian geologists for decades. A variety of ages, derived from both Rb-Sr and conventional U-Pb techniques, have been reported by several workers (Odom and Fullagar, 1973; Odom and Russell, 1975; Sinha et al., 1989). The most recent, and probably most reliable age is a $^{206}Pb/^{238}U$ ion microprobe age of ~490 Ma (Carrigan et al., 2001) from zoned zircons.

Metamorphism

The IP of the Carolinas is dominated by a > 60 km wide expanse of sillimanite-grade (first and less commonly second sillimanite zone) ortho- and paragneiss (e.g., Butler, 1991; Fig. 1-3). A well-documented, fault-related inversion of metamorphic isograds along the western flank of the IP places sillimanite-grade rocks over kyanite (or lower) grade assemblages southeast of the Brevard fault zone (Lemmon and Dunn, 1973a, 1973b; Griffin, 1974; Lemmon, 1982; Nelson et al., 1998; Hatcher, 1987; Hopson

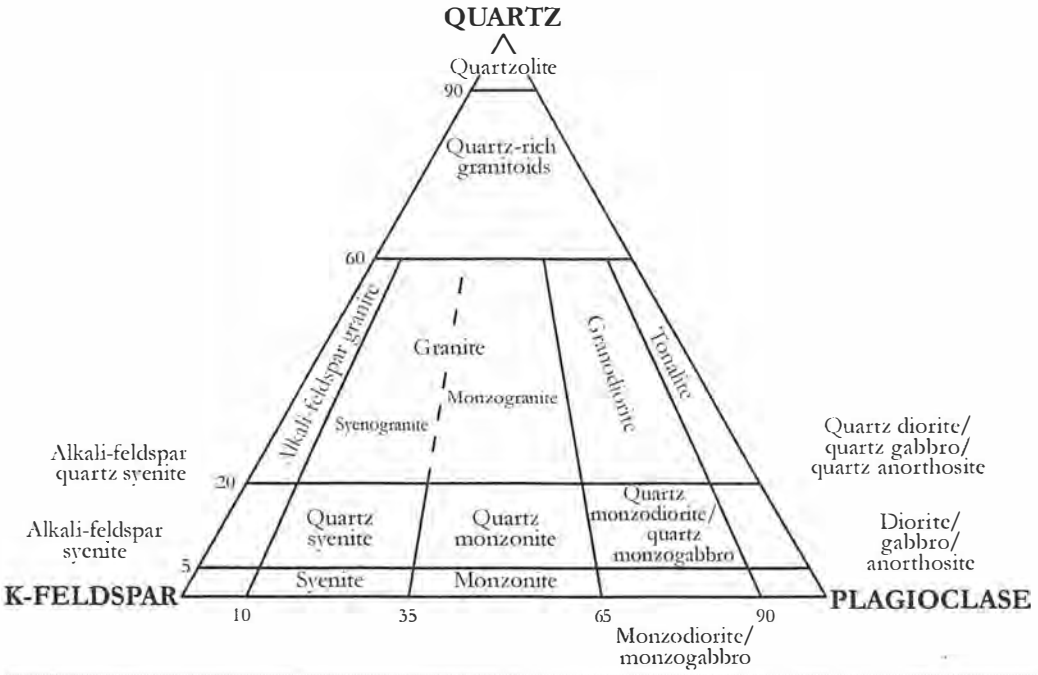

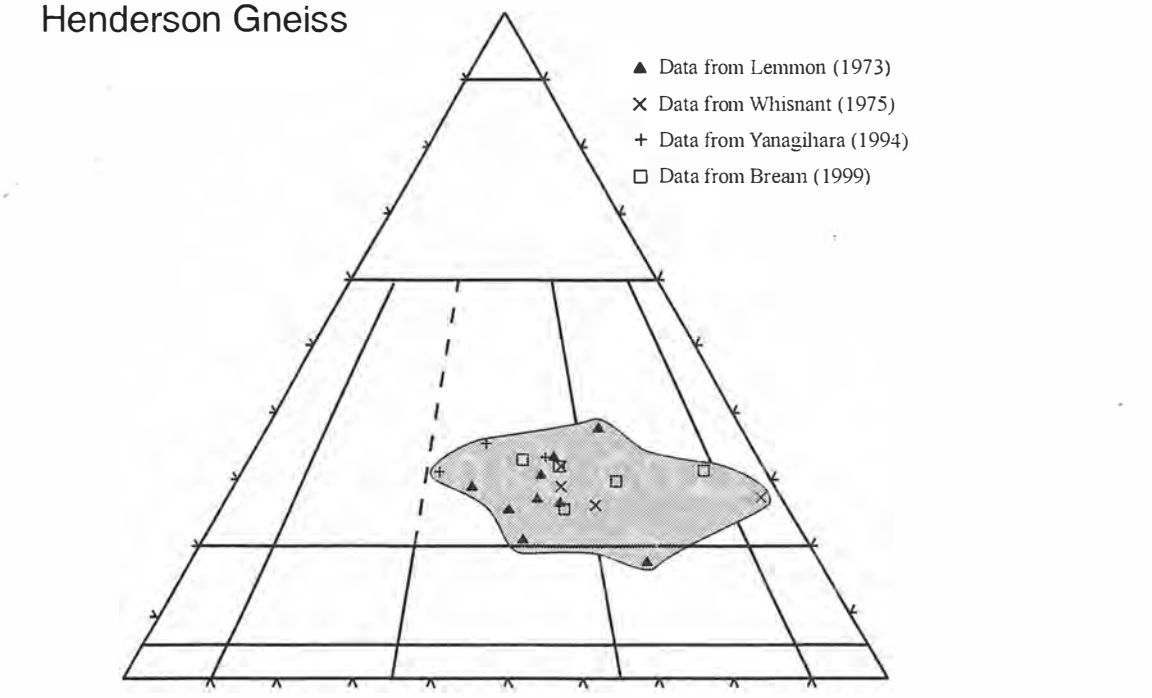

Figure 1-28. IUGS modal classification (Streckeisen, 1976) of the Henderson Gneiss.

and Hatcher, 1988; Butler, 1991; Davis, 1993a; Hatcher, 1993). Part of the kyanite-sillimanite isograd coincides with the Mill Spring thrust in southwestern North Carolina (Bream, 1999; Bier et al., 2002). Along the eastern flank of the IP, upright isograd surfaces are indicated by kyanite-grade rocks over sillimanite-grade assemblages (Fig. 1-3).

Davis (1993a) and Yanagihara (1994), working in the Sugarloaf Mountain and Mill Spring thrust sheets (structurally below the Brindle Creek thrust), documented sillimanite grade mineral assemblages (Fig. 1-29; Plate 1). Similar rock types and metamorphic grades were recorded by Giorgis (1999), Williams (2000), and Bier (2001) in the Brindle Creek thrust sheet in the South Mountains (Fig. 1-29). Estimates of metamorphic conditions were made for the present study further northeast in North Carolina. A weathered aluminous schist sample and a fresh Lenoir Quarry migmatite sample were collected from both sides of the Brindle Creek thrust for mineralogical analysis. Electron microprobe analysis of the Lenoir Quarry migmatite revealed valuable compositional information; data from the weathered aluminous schist, however, were concluded to be spurious and are not included. Comparisons of mineral assemblages in Brushy Mountain Brindle Creek hanging wall units with those in the South Mountains (where detailed P-T studies of unaltered samples were performed; Bier, 2001) are used to approximate P-T conditions for the hanging wall.

Brindle Creek Thrust Footwall

The footwall amphibolite is represented by sample KC-VQ-1, a hornblende-quartz-plagioclase gneiss. The sample has a dominantly equigranular-tabular texture (Raymond, 1995) and contains euhedral and subhedral grains that average ~0.62 x 0.30

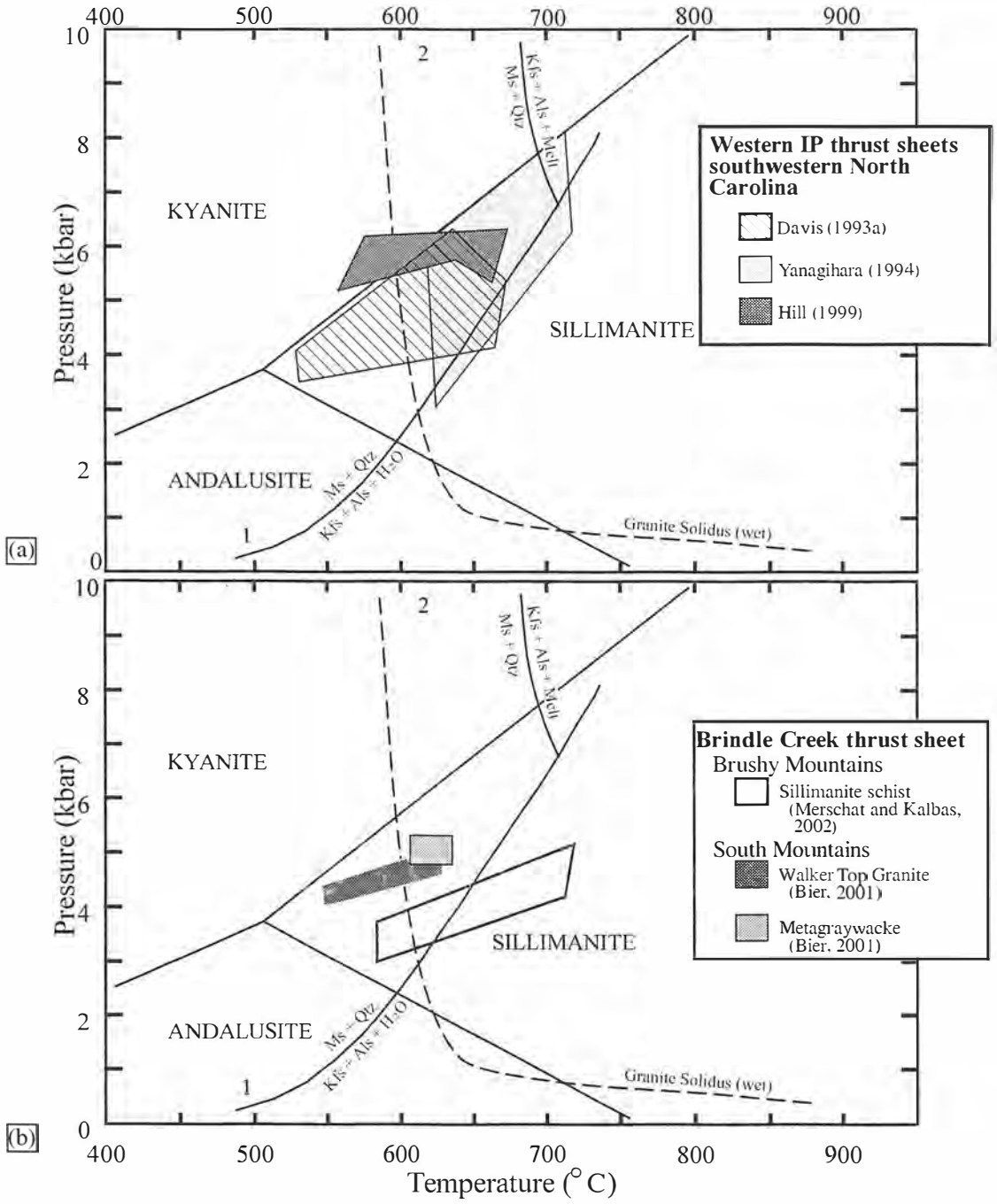

Figure 1-29. Petrogenetic grids for aluminous rocks with metamorphic P-T conditions plotted from various IP studies. Pressure and temperature estimates are derived from mineral assemblages and/ or from idealized equilibrium Fe-Mg exchange between garnet and biotite (Ferry and Spear, 1978; Hodges and Spear, 1982; Bohlen et al., 1983a, 1983b; Holdaway et al., 1988; Bergman, 1990). Estimates from Bier (2001) were based on several reaction sources: Chatterjee and Johannes (1974), Thompson (1982), and Raymond (1995). Ms = muscovite, Qtz = quartz, Kfs = K-feldspar, Als = aluminum silicate. Estimates by Meraschat and Kalbas (2002) were based on: Luth et al. (1964); Holdaway (1971); Chatterjee and Johannes (1974); and Thompson (1982).

mm. Major phases are: hornblende, quartz, plagioclase (~An_{25-47}), biotite, K-feldspar, and epidote, with accessory sphene, pyrite, and ilmenite/titaniferous magnetite.

A reliable thermobarometric calculation was not found for a system devoid of garnet; P-T constraints, however, were inferred from the mineral assemblage. The presence of hornblende, plagioclase, quartz, epidote, and ilmenite is characteristic of the amphibolite facies (e.g., Spear, 1995). A range of pressures and temperatures is inferred from the coexistence of hornblende (Fig. 1-30) and primary epidote in the footwall migmatite and the presence of sillimanite in aluminous footwall specimens. Coexisting plagioclase compositions of An ~25, and An ~42-47 were identified with the Michel-Léve method. These compositions are consistent with the peristerite gap (Spear, 1995) and suggest temperatures above ~400 °C. The coexistence of andesine and anorthite (the Voll Gap) was not detected; thus, metamorphic temperatures were likely below ~800 °C. Moreover, hornblende from the representative footwall amphibolite is similar in composition to the typical amphibolite facies composition,

$Na_{0.5}Ca_{1.8}(Fe,Mg)_{3.4}Al_{3.3}Si_{6.3}O_{22}(OH)_2$ (ideal)

$Na_{0.4}Ca_{1.9}(Fe,Mg)_{4.5}Al_{2.3}Si_{6.3}O_{22}(OH)_2$ (observed)

and suggest the Fe-Mg Edenite and Tschermak exchange reactions produced hornblende at the expense of actinolite at the greenschist-amphibolite facies transition (Spear, 1995; Table 1-5). Micas are prevalent (indicating water was present during metamorphism) and the rocks are migmatitic; P-T conditions were likely at or above the wet granite solidus (Fig. 1-29). Furthermore, although K-feldspar is abundant in the Lenoir Quarry migmatite, its absence and the relative abundance of prograde muscovite in the Tallulah Falls Formation metagraywacke indicate footwall metamorphic conditions below the

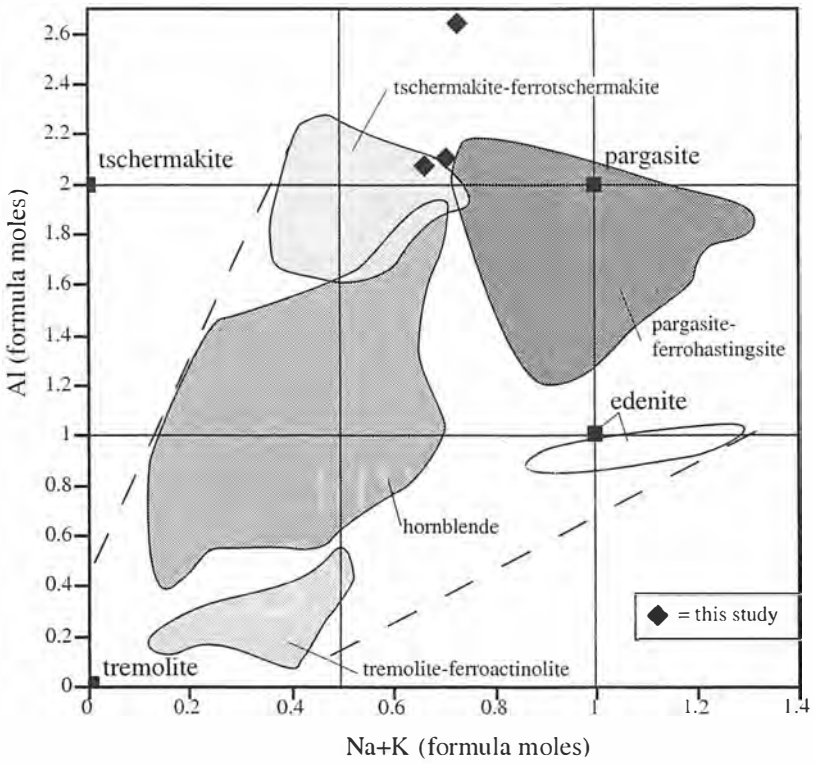

Figure 1-30. Chemical variation diagram for calcium-rich amphibole. Reference fields and filled squares are from Deer et al (1974). Diamonds are data from the present study.

second sillimanite isograd. Peak metamorphic temperatures and pressures in the footwall of the Brindle Creek thrust were likely in the range of 600 to 700 °C, and 3.0 to 7.7 kbar (Fig. 1-29). Muscovite that grew subperpendicular to the foliation in the footwall of the Mill Spring thrust may represent a retrograde overprint (locally generated by thrusting; Part II) of a slightly higher temperature fabric.

Brindle Creek thrust hanging wall

Although mineral compositions from an unaltered sample from the Brindle Creek thrust sheet were not obtained in this study, P-T estimates from adjacent and along-strike areas are available, and are thought to be consistent throughout the Kings Creek quadrangle. P-T estimates by Bier (2001) for garnet metagraywacke-schist were 645 $\pm$ 20 °C and 5.2 $\pm$ 1 kbar. P-T estimates for the Walker Top Granite were 525 to 640 °C and 3.8 $\pm$ 0.8 to 5.4 $\pm$ 0.8 kbar (Bier, 2001). More recent data, presented by Merschat and Kalbas (2002), confirm high grade conditions (585 °C, 2.8 kbar to 710 °C, 4.7 kbar) in the hanging wall of the Brindle Creek thrust in the Ellendale quadrangle. Both Bier (2001) and Merschat and Kalbas (2002) also noted local occurrences of sillimanite II assemblages; no such assemblages were observed in the Kings Creek quadrangle.

Discussion

Timing of metamorphism and deformation

The Brushy Mountains and South Mountains share a Barrovian metamorphic history (Fig. 1-29). The similarity of estimated P-T conditions in the western and eastern IP along the Brindle Creek thrust throughout western North Carolina yields two hypotheses for the timing of thrust emplacement and metamorphism. A simple explanation is that the hanging wall was separated from the western IP at the time of

metamorphism, but was subjected to similar, contemporaneous, high-grade conditions. The two could have been juxtaposed and deformed during a later deformation event. This is not viable however, because no evidence for retrogression was found in either thrust sheet in the study area. Assemblages on either side of the fault were probably subjected to the same Neoacadian amphibolite-facies metamorphic conditions (Fig. 1-29). Faulting is thought to be synmetamorphic, and cannot be attributed to deformation after the earliest Alleghanian (Part II).

Recent contributions to the regional geochronologic database significantly advance our understanding of the timing and conditions of Brindle Creek thrust emplacement. High resolution ion microprobe analyses of zircons from the Walker Top Granite yielded a crystallization age of ~366 Ma (Mapes, 2002). Since the Walker Top Granite crops out exclusively in the Brindle Creek thrust sheet, it can be inferred that the western and eastern IP belts were separated at the time of Walker Top intrusion. Various geochronologic studies (Kish, 1990; Dennis and Wright, 1997; Mirante and Patino-Douce, 2000; Bream et al., 2001a; Carrigan et al., 2001; and Kalbas et al., 2002) indicate a Late Devonian or early Mississippian (latest Neoacadian/earliest Alleghanian) thermal-metamorphic event affected both the western and eastern IP. This event is recognized in the Kings Creek quadrangle by 342 Ma and 330 Ma zircon rims from the Lenoir Quarry migmatite (Part III). Devono-Mississippian rims are thought to represent peak upper amphibolite-facies metamorphism and coeval anatexis. The emplacement age of the Brindle Creek thrust sheet can thus be constrained to an ~24 million year interval between 366 and 342 Ma. $^{40}Ar/^{39}Ar$ plateau ages for similar rocks in the Chauga belt and Walhalla to eastern Six-Mile nappes (southwest of the study area) indicate

postmetamorphic cooling through the hornblende closure temperature of ~550 °C between ~333 and 322 Ma (Dallmeyer, 1988). No pervasive Alleghanian (Hatcher, 2001) retrograde mineral assemblages were discovered in the study area; faulting is attributed to latest Neoacadian or earliest Alleghanian deformation (Part II).

Petrogenesis of the Walker Top Granite

The Walker Top Granite is confined to the hanging wall of the Brindle Creek thrust, but crosscuts contacts of the sillimanite schist and the metagraywacke. It is likely a mid- to lower-crustal intrusive body (Giorgis et al., 2002), but plutonic zoning and contact aureoles are not present and few xenoliths have been found in the unit. Intrusion and cooling of the Walker Top Granite likely took place at 366 ±3 Ma (Mapes, 2002).

Two cooling rates can be inferred from the bimodal grain-size distribution: (1) an early stage of slow cooling promoted phenocryst growth; and (2) a subsequent, faster cooling event promoted the growth of the fine-grained matrix (e.g., Raymond, 1995). Petrographic analyses indicate that some microcline megacrysts are actually aggregates of finer-grained microcline crystals. These may result from rapid nucleation of many grains in segregated regions of the granite rather than slow growth of an individual grain.

Petrogenesis of the Hibriten Orthogneiss

The Hibriten orthogneiss crops out as a narrow belt of orogen-parallel, discontinuous bodies in the hanging wall of the Brindle Creek thrust (Plate 1). The origin of characteristic rounded plagioclase porphyroclasts in the Hibriten orthogneiss and their relationship to the tectonic history of the unit are not completely understood and require further investigation. Specifically, whereas feldspar-rich ortho- and paragneisses

containing matrix plagioclase are common throughout the IP, dominantly rounded plagioclase porphyroclasts in the Hibriten orthogneiss are especially plentiful.

Close proximity of the Hibriten orthogneiss to a large crustal shear zone implies mylonitization of the plagioclase-rich fabric. Rounded porphyroclasts in the Hibriten orthogneiss, however, are not typically flattened or tailed, and do not indicate shear sense. It is possible that a critical matrix-to-clast ratio (for formation of mantled clasts; Hatcher, personal communication) was not satisfied; simple shear was principally recovered in the biotite-rich matrix.

Numerous grains display asymmetric compositional zonation; certain plagioclase grains, in a representative thin section, are engulf biotite crystals in optical continuity with matrix biotite (Fig. 1-18), and may suggest local growth of some plagioclase after peak metamorphism. A model, proposed by Wintsch (1975), working in staurolite-grade Tatnic Hill Formation of eastern Connecticut, describes the reaction kinetics and solution-mineral reactions necessary for metamorphic growth of K-feldspar and/or plagioclase from quartz-mica-rich assemblages similar to those found in the Hibriten orthogneiss matrix. The plagioclase porphyroblasts observed by Wintsch (1975), however, were small relative to those in the Hibriten orthogneiss. Cation exchange reactions (reaction 4; Wintsch, 1975) on mica (muscovite or biotite) surfaces during rapid deformation (grain size reduction) at constant temperatures and pressures shifts K^+/H^+ activity ratios from the mica stability field to the feldspar stability field (feldspathization; Wintsch, 1975).

$$KAl_3Si_3O_{10}(OH)_2 + H^+ = HAl_3Si_3O_{10}(OH)_2 + K^+ \qquad (4)$$

In an open system, muscovite can dissolve to produce K-feldspar (reaction 5; Wintsch, 1975) and/or plagioclase (reaction 6; Hemley and Jones, 1964)

$$KAl_3Si_3O_{10}(OH)_2 + 6SiO_2 + 2K^+ = 3KAlSi_3O_8 + 2H^+ \quad (5)$$

$$KAl_3Si_3O_{10}(OH)_2 + 6SiO_2 + 3Na^+ = 3NaAlSi_3O_8 + K^+ + 2H^+ \quad (6)$$

Whereas some plagioclase grains may be the result of feldspathization during deformation, the high percentage of plagioclase in the unit suggests primary (igneous) crystallization of major components. Furthermore, growth of plagioclase in chemical equilibrium with mica and quartz at fixed temperatures and pressures yields unzoned crystals at middle amphibolite facies or higher-grade conditions (Evans and Guidotti, 1966; Wintsch and Knipe, 1983). If plagioclase grains in the Hibriten orthogneiss were porphyroblasts rather than porphyroclasts, no chemical zonation would be expected. Under cross-polarized light, slight (< 5°) rotations of the stage, while numerous plagioclase crystals from samples KC-494 and KC-536 are near extinction, reveals faint, concentric chemical zonation. Chemical zonation may be the result of rhythmic variations in An content during crystallization (Nord et al., 1978; Wintsch and Knipe, 1983). If zoned porphyroclasts were recrystallized during deformation, changes in P-T conditions and/or chemical disequilibria during crystal regrowth must be assumed.

The Hibriten orthogneiss is a prominent and easily recognizable unit; this study, however, is the first detailed examination of its distribution, mineralogy, and to a lesser degree its petrogenesis. Tentative classification of the unit as an orthogneiss is based on its texture and mineralogy. Bulk geochemical, geochronologic, and thermobarometric studies are necessary to confirm an igneous protolith and better constrain its genetic affinity.

Conclusions

- Three lithotectonic units in the Kings Creek 7.5-minute quadrangle are composed of eight distinctive lithologic units.

- Exposure of the Brindle Creek thrust in the Brushy Mountains suggests it is a significant thrust in southwestern and south-central western North Carolina.

- Amphibolite facies (sillimanite grade) metamorphic assemblages are present throughout the Kings Creek quadrangle. Similar Barrovian metamorphic conditions in the Brushy Mountains and South Mountains are inferred from mineral assemblages and chemical compositions.

- Temporal and P-T data indicate Neoacadian sillimanite grade peak metamorphism on both sides of the Brindle Creek thrust.

- The Walker Top Granite intruded the eastern IP at 366 Ma. Since it is not present in the western IP, thrust emplacement can reasonably be inferred to have occurred after 366 Ma. Both the western and eastern IP were synchronously metamorphosed and deformed at 342 and 330 Ma; Brindle Creek thrust emplacement must have taken place between 366 and 342 Ma.

- No lower-greenschist facies retrograde overprint was observed; no component of thrust movement, therefore, can be attributed to Alleghanian movement along the Brevard fault zone.

References Cited

Adams, G. I., 1933, General geology of the crystalline rocks of Alabama: Journal of Geology, v. 41, p. 159-173.

Bergman, R. G., 1990, Mixing properties of Ca-Fe-Mg-Mn garnets: American Mineralogist, v. 75, p. 328-344.

Bier, S. E., 2001, Geology of the southeastern South Mountains, North Carolina [unpublished M.S. thesis]: Knoxville, University of Tennessee, 162 p.

Bier, S. E., Bream, B. R., Giorgis, S. D., 2002, *in* Hatcher, R. D., Jr., and Bream, B. R., eds., Inner Piedmont tectonics focused mostly on detailed studies in the South Mountains and the southern Brushy Mountains, North Carolina: Carolina Geological Society Guidebook, North Carolina Geological Survey, p. 65-100.

Bier, S. E., Bream, B. R., and Hatcher, R. D., Jr., 2000, Detailed geologic mapping of the western and central Inner Piedmont, North Carolina: Geological Society of America Abstracts with Programs, v. 32, p. A-234.

Bohlen, S. R., Wall, V. J., and Boettcher, A. L., 1983a, Experimental investigation and application of garnet granulite equilibria: Contributions to Mineralogy and Petrology, v. 83, p. 52-61.

Bohlen, S. R., Wall, V. J., and Boettcher, A. L., 1983b, Experimental investigations and geological applications of equilibria in the system FeO-TiO_2-Al_2O_3-SiO_2-H_2O: American Mineralogist, v. 68, p. 1049-1058.

Bream, B. R., 1999, Structure and stratigraphic relationships of ortho- and paragneisses southwest of Marion, North Carolina [unpublished M.S. thesis]: Knoxville, University of Tennessee, 155 p.

Bream, B. R. 2002, The southern Appalachian Inner Piedmont: new perspectives and enduring issues based on recent detailed mapping, isotopic evidence, and geochronology: *in* Hatcher, R. D., Jr., and Bream, B. R., eds., Inner Piedmont tectonics focused mostly on detailed studies in the South Mountains and the southern Brushy Mountains, North Carolina: Carolina Geological Society Guidebook, North Carolina Geological Survey, p. 45-64.

Bream, B. R., and Williams, S. T., 1999, Geologic map of the Glenwood quadrangle: North Carolina Department of Environmental and Natural Resources Open File Report, scale 1:24,000.

Bream, B. R., Hatcher, R. D., Jr., Miller, C. F., Carrigan, C. W., and Fullagar, P. D., 2001a, Provenance and geochemistry of Late Proterozoic southern Appalachian crystalline core paragneisses, NC-SC-GA-TN: Geological Society of America Abstracts with Programs, v. 33, no. 2, p. A-65.

Bream, B. R., Hatcher, R. D., Jr., Miller, C. F., and Fullagar, P. D., 2001b, Geochemistry and provenance of Inner Piedmont paragneisses, NC and SC: Evidence for an internal terrane boundary: Geological Society of America Abstracts with Programs, v. 33, p. A-65.

Brown, P. M., Burt, E. R., III, Carpenter, P. A., III, Enos, R. M., Flynt, B. J., Jr., Gallagher, P. E., Hoffman, C. W., Merschat, C. E., Wilson, W. F., and Parker, J. M., III, 1985, Geologic Map of North Carolina: North Carolina Geological Survey, scale 1:500,000.

Butler, J. R., 1991, Metamorphism, *in* Horton, J. W., Jr., and Zullo, V. A., eds., The geology of the Carolinas, Carolina Geological Society Fiftieth Anniversary Volume: Knoxville, University of Tennessee Press, p. 127-142.

Carrigan, C. W., Bream, B. R., Miller, C. F., and Hatcher, R. D., Jr., 2001, Ion microprobe analyses of zircon rims from the eastern Blue Ridge and Inner Piedmont, NC-SC-GA: Implications for the timing of Paleozoic metamorphism in the southern Appalachians: Geological Society of America Abstracts with Programs, v. 33, p. A42.

Chatterjee, N. D., and Johannes, W., 1974, Thermal stability and standard thermodynamic properties of synthetic 2M1 muscovite, $KAl_2AlSi_3O_{10}(OH)_2$: Contributions to Mineralogy and Petrology, v. 48, p. 89-114.

Dallmeyer, R. D., 1988, Late Paleozoic tectonothermal evolution of the western Piedmont and eastern Blue Ridge, Georgia: Controls on the chronology of terrane accretion and transport in the southern Appalachian orogen: Geological Society of America Bulletin, v. 100, p. 702-713.

Davis, T. L., 1993a, Lithostratigraphy, structure, and metamorphism of a crystalline thrust terrane, western Inner Piedmont, North Carolina [unpublished Ph.D. dissertation]: Knoxville, University of Tennessee, 245 p.

Davis, T. L., 1993b, Geology of the Columbus Promontory, western Piedmont, North Carolina, southern Appalachians, *in* Hatcher, R. D., Jr., and Davis, T. L., eds., Studies of Inner Piedmont geology with a focus on the Columbus Promontory: Carolina Geological Society Field Trip Guidebook, p. 17--44.

Davis, T. L., Hatcher, R. D., Jr., Liu, A., and Tabor, J. R., 1991, Structural development of a progressively deformed crustal-scale shear zone, southern Appalachian Inner Piedmont, U. S. A.: The geometry of deformed rocks: Geological Society of America Abstracts with Programs, v. 23, p. A-138.

Deer, W. A., Howie, R. A., and Zussman, J., 1974, Rock-forming silicates: London, Longman Group LTD, v. 2., 379 p.

Dennis, A. J., and Wright, J. E., 1997, Middle and late Paleozoic monazite U-Pb ages, Inner Piedmont, South Carolina: Geological Society of America Abstracts with Programs, v. 29, p. 12.

Evans, B. W., and Guidotti, C. V., 1966, The sillimanite-potash feldspar isograd in western Maine, U.S.A.: Contributions to Mineralogy and Petrology, v. 12, p. 25-62.

Ferry, J. M., and Spear, F. S., 1978, Experimental calibration of Fe and Mg partitioning between biotite and garnet: Contributions to Mineralogy and Petrology, v. 66, p. 113-117.

Giorgis, S. D., 1999, Inner Piedmont geology of the northwestern South Mountains near Morganton, North Carolina [unpublished M.S. thesis]: Knoxville, University of Tennessee, 191 p.

Giorgis, S. D., and Williams, S. T., 1999, Geologic Map of the Dysartsville quadrangle: North Carolina Department of Environmental and Natural Resources open file report, scale 1:24,000.

Giorgis, S. D., Hatcher, R. D., Jr., and Riedel, J. J., 1998, Evolution of thrust sheets in the western Inner Piedmont, NC: Geological Society of America Abstracts with Programs, v. 30, p. A-124.

Giorgis, S. D., Mapes, R. W., and Bream, B. R., 2002, The Walker Top Granite: Acadian granitoid or eastern Inner Piedmont basement?: *in* Hatcher, R. D., Jr., and Bream, B. R., eds., Inner Piedmont tectonics focused mostly on detailed studies in the South Mountains and the southern Brushy Mountains, North Carolina: Carolina Geological Society Guidebook, North Carolina Geological Survey, p. 33-44.

Goldsmith, R., Milton, D. J., and Horton, J. W., 1988, Geologic map of the Charlotte 1°x 2° quadrangle, North Carolina and South Carolina: U. S. Geological Survey Map I-125-E, scale 1:250,000.

Griffin, V. S., Jr., 1969, Inner Piedmont tectonics in the vicinity of Walhalla, South Carolina: South Carolina Division of Geology, Geologic Notes, v. 13, p. 15–28.

Griffin, V. S., Jr., 1971, The Inner Piedmont belt of the southern crystalline Appalachians: Geological Society of America Bulletin, v. 82, p. 1885–1898.

Griffin, V. S., Jr., 1972, Inner Piedmont belt of the southern crystalline Appalachians: Reply: Geological Society of America Bulletin, v. 83, p. 1897–1900.

Griffin, V.S., Jr., 1974, Analysis of the Piedmont in northwest South Carolina: Geological Society of America Bulletin, v. 85, p. 1123-1138.

Harper, S. B., and Fullagar, P. D., 1981, Rb–Sr ages of granitic gneisses of the Inner Piedmont belt of northwestern North Carolina and southwestern South Carolina: Geological Society of America Bulletin, v. 92, p. 864–872.

Hatcher, R. D., Jr., 1969, Stratigraphy, petrology, and structure of the low rank belt and part of the Blue Ridge of northwesternmost South Carolina: South Carolina Division of Geology, Geologic Notes, v. 13, p. 105-141.

Hatcher, R. D., Jr., 1971, The geology of Rabun and Habersham Counties, Georgia: A reconnaissance study: Geological Survey of Georgia, Department of Mines, Mining, and Geology Bulletin, 48 p.

Hatcher, R. D., Jr., 1972, Developmental model for the southern Appalachians: Geological Society of America Bulletin, v. 83, p. 2735-2760.

Hatcher, R. D., Jr., 1973, Basement versus cover rocks in the Blue Ridge of northeast Georgia, northwestern South Carolina and adjacent North Carolina: American Journal of Science, v. 273, p. 671–685.

Hatcher, R. D., Jr., 1987, Tectonics of the southern and central Appalachian internides: Annual Review of Earth and Planetary Science, v. 15, p. 337-362.

Hatcher, R. D., Jr., 1989, Tectonic synthesis of the U.S. Appalachians, Chapter 14, *in* Hatcher, R. D., Jr., Thomas, W. A., and Viele, G. W., eds., The Appalachian–Ouachita orogen in the United States: Boulder, Colorado, Geological Society of America, The Geology of North America, v. F–2, p. 511–535.

Hatcher, R. D., Jr., 1993, Perspective on the tectonics of the Inner Piedmont, southern Appalachians, *in* Hatcher, R. D., Jr., and Davis, T. L., eds., Studies of Inner Piedmont geology with a focus on the Columbus Promontory: Carolina Geological Society Guidebook North Carolina Geological Survey, p. 1-16.

Hatcher, 2001, Rheological partitioning during multiple reactivation of the Palaeozoic Brevard Fault Zone, Southern Appalachians, USA: *in* Holdsworth, R. E., Strachan, R. A., Magloughlin, J. F., and Knipe, R. J., eds., The nature and tectonic significance of fault zone weakening: Geological Society of London Special Publication 186, p. 255-269.

Hatcher, R. D., Jr., and Acker, L. L., 1984, Geology of the Salem quadrangle, South Carolina: South Carolina Geological Survey, MS–26, 23 p., scale 1:24,000.
Hatcher, R. D., Jr., and Hooper, R. J., 1992, Evolution of crystalline thrust sheets in the internal parts of mountain chains, *in* McClay, K. R., ed., Thrust tectonics: London, Chapman & Hall. p. 217-233.
Hatcher, R. D., Jr., Osberg, P. H., Drake, A. A., Jr., Robinson, P., and Thomas, W. A., 1990, Tectonic map of U.S. Appalachians, *in* Hatcher, R. D., Jr., Thomas, W. A., and Viele, G. W., eds., The Appalachian–Ouachita Orogen in the United States: Boulder, Geological Society of America, The Geology of North America, v. F–2, Plate 1, scale 1:2,000,000.
Hatcher, R. D., Jr., Bream, B. R., Hill, J. C., Giorgis, S. D., and Williams, S. T., 1999, Transect through the Acadian orogen in the Carolinas and northeast Georgia: Geological Society of America Abstracts with Programs, v. 31, p. 19.
Hemley, J. J., and Jones, W. R., 1964, Chemical aspects of hydrothermal alteration with emphasis on hydrogen metasomatism: Economic Geology, v. 59, p. 538-569.
Hill, J. C., 1999, Stratigraphy, structure, and tectonics of part of the southern Appalachian Inner Piedmont, near Marion, North Carolina [unpublished M.S. thesis]: Knoxville, University of Tennessee, 188 p.
Hodges, K. V., and Spear, F. S., 1982, Geothermometry, geobarometry and the Al_2SiO_5 triple point at Mt. Moosilauke, New Hampshire: American Mineralogist, v. 67, p. 1118-1134.
Holdaway, M. J., 1971, Stability of andalusite and the aluminum silicate phase diagram: American Journal of Science, v. 271, p. 97-131.
Holdaway, M. J., Dutrow, B. L., Hinton, R. W., 1988, Devonian and Carboniferous metamorphism in west-central Maine: The muscovite-almandine geobarometer and the staurolite problem revisited: American Mineralogist, v. 73, p. 20-47.
Hopson, J. L., and Hatcher, R. D., Jr., 1988, Structural and stratigraphic setting of the Alto allochthon, northeast Georgia: Geological Society of America Bulletin, v. 100, p. 339-350.
Horton, J. W., Jr., Drake, A. A., Jr., and Rankin, D. W., 1989, Tectonostratigraphic terranes and their Paleozoic boundaries in the central and southern Appalachians, *in* Dallmeyer, R. D., ed., Terranes in the Circum–Atlantic Paleozoic orogens: Geological Society of America Special Paper 230, p. 213–245.
Horton, J. W., Jr., and Dicken, C. L., 2001, Preliminary digital geologic map of the Appalachian Piedmont and Blue Ridge, South Carolina segment: U. S. Geological Survey, Open-file Report 01-298, scale 1:500,000.
Horton, J. W., Jr., and McConnell, K. I., 1991, The western Piedmont, *in* Horton, J. W., Jr., and Zullo, V. A., eds., The Geology of the Carolinas–Carolina Geological Society Fiftieth Anniversary Volume: Knoxville, University of Tennessee Press, p. 36–59.
Kalbas, J. L., Merschat, A. J., Hatcher, R. D., Jr., Bream, B. R., 2001, Detailed geologic mapping of the Brushy Mountains, Inner Piedmont, near Lenoir, North Carolina: Geological Society of America Abstracts with Programs, v. 33, p. A-82.
Kalbas, J. L., Bream, B. R., Hatcher, R. D., Jr., Maybin, A. H., III, 2002, Evidence for mafic Ordovician magmatism and Acadian metamorphism in the Brushy Mountains, Western Inner Piedmont, of North Carolina: Geological Society of America Abstracts with Programs, v. 34, p. A-119.

Keith, A., 1905, Description of the Mount Mitchell quadrangle (North Carolina-Tennessee): U.S. Geological Survey Geologic Atlas, Folio 124, 10 p.
Keith, A., 1907, Description of the Pisgah quadrangle (North Carolina-South Carolina): U.S. Geological Survey Geologic Atlas, Folio 147, 10 p.
Kish, S. A., 1983, A geochronological study of deformation and metamorphism in the Blue Ridge and Piedmont of the Carolinas [unpublished Ph.D. dissertation]: Chapel Hill, University of North Carolina, 220 p.
Kish, S. A., 1990, Timing of middle Paleozoic (Acadian) metamorphism in the southern Appalachians; K-Ar studies in the Talladega Belt, Alabama: Geology, v. 18, p. 650-653.
Kohn, M. J., 2001, Timing and accretion in the southern Appalachians: perspectives from the Laurentian margin: Geological Society of America Abstracts with Programs, v. 33, p. A-262.
Kohn, M. J., and Spear, F. S., 1990, Two new geobarometers for garnet amphibolites, with applications to southeastern Vermont: American Mineralogist, v. 75, p. 89-96.
Lemmon, R. E., 1973, Geology of the Bat Cave and Fruitland quadrangles and the origin of the Henderson Gneiss, western North Carolina [unpublished Ph.D. dissertation]: Chapel Hill, University of North Carolina, 145 p.
Lemmon, R. E., 1982, Evidence for an Acadian tectonic event in the western Inner Piedmont, North Carolina: Geological Society of America Abstracts with Programs, v. 14, p. A-34.
Lemmon, L. E., and Dunn, D. E., 1973a, Geologic map and mineral resources of the Fruitland quadrangle, North Carolina: North Carolina Department of Natural Resources and Community Development GM 202-NW, scale 1:24,000.
Lemmon, L. E., and Dunn, D. E., 1973b, Geologic map and mineral resources of the Bat Cave quadrangle, North Carolina: North Carolina Department of Natural Resources and Community Development GM 203-NW, scale 1:24,000.
Lemmon, R. E., and Dunn, D. E., 1975, Origin and geologic history of the Henderson Gneiss from Bat Cave and Fruitland quadrangles, western North Carolina: Geological Society of America Abstracts with Programs, v. 7, p. A-509.
Lister, G. S., and Snoke, A. W., 1984, S–C mylonites: Journal of Structural Geology, v. 6, p. 617–638.
Liu, A., 1991, Structural geology and deformation history of the Brevard fault zone, Chauga belt, and Inner Piedmont, northwestern South Carolina and adjacent areas [unpublished Ph.D. dissertation]: Knoxville, Tennessee, University of Tennessee, 200 p.
Luth, W. D., Jahns, R. H., and Tuttle, O. F., 1964, The granite system at pressures of 4 to 10 kilobars: Journal of Geophysical Research, v. 69, p. 759-773.
Mapes, R. W., 2002, Geochemistry and geochronology of mid-Paleozoic granitic plutonism in the southern Appalachian Piedmont terrane, North Carolina-South Carolina-Georgia [unpublished M.S. Thesis]: Vanderbilt University, 140 p.
Mapes, R. W., Maybin, A. H., III, Miller, C. F., Fullagar, P. D., and Bream, B. R., 2002, Geochronology and geochemistry of mid Paleozoic granitic magmatism, Central and Eastern Inner Piedmont, NC & SC: Geological Society of America Abstracts with Programs, v. 34, p. A-94.

Merschat, A. J., in progress, Structure and metamorphism of the central Inner Piedmont, Brushy Mountains, North Carolina [unpublished M.S. thesis]: Knoxville, University of Tennessee.

Merschat, A. J., and Kalbas, J. L., 2002, Geology of the southwestern Brushy Mountains, North Carolina Inner Piedmont: A summary and synthesis of recent studies: *in* Hatcher, R. D., Jr., and Bream, B. R., eds., Inner Piedmont tectonics focused mostly on detailed studies in the South Mountains and the southern Brushy Mountains, North Carolina: Carolina Geological Society Guidebook, North Carolina Geological Survey, p. 101-126.

Mirante, D. C., and Patino-Douce, A. E., 2000, Melting and migmatization in the southern Appalachian Inner Piedmont of northeast Georgia; the Athens Gneiss: Geological Society of America Abstracts with Programs, v. 32, p. A-297.

Nelson, A. E., Horton, J. W., Jr., and Clarke, J. W., 1998, Generalized tectonic map of the Greenville 1 ° x 2 ° quadrangle, Georgia, South Carolina, and North Carolina: U. S. Geological Survey Miscellaneous Field Studies Map MF–1898, Scale 1:250,000.

Nesse, W. D., 1991, Introduction to optical mineralogy, second edition: New York, Oxford University Press, 335 p.

Nord, G. L., Hammarstrom, J., and Zen, E., 1978, Zoned plagioclase and peristerite formation in phyllites from southwestern Massachusetts: American Mineralogist, v. 63, p. 947-955.

Odom, A. L., and Fullagar, P. D., 1973, Geochronological and tectonic relationship between the Inner Piedmont, Brevard zone, and Blue Ridge belts, North Carolina: American Journal of Science, v. 273-A, p. 133-149.

Odom, A. L., and Russell, G. S., 1975, The time of regional metamorphism of the Inner Piedmont, North Carolina, and Smith River allochthon: Inference from whole–rock ages: Geological Society of America Abstracts with Programs, v. 7, p. 522–523.

Overstreet, W. C., Yates, R. G., and Griffitts, W. R., 1951, Geologic map of the Shelby 15' quadrangle: U. S. Geological Survey, scale 1:62,500.

Overstreet, W. C., Whitlow, J. W., White, A. M., and Griffitts, W. R., 1963a, Geologic map of the southern part of the Casar Quadrangle, Cleveland, Lincoln, and Burke Counties, North Carolina, showing areas mined for monazite and mica: U.S. Geological Survey Mineral Investigations Field Studies Map MF-257, scale 1:24,000.

Overstreet, W. C., Yates, R. G., and Griffitts, W. R., 1963b, Geology of the Shelby Quadrangle, North Carolina: U. S. Geological Survey Miscellaneous Geologic Investigations Map I–384, 1:62,500.

Passchier, C. W., and Trouw, R. A. J., 1998, Microtectonics: Berlin, Springer-Verlag. 289 p.

Rankin, D. W., Espenshade, G. H., and Neuman, R. B.,1972, Geologic map of the west half of the Winston-Salem quadrangle, North Carolina, Virginia, and Tennessee: U.S. Geological Survey Map I-709-A, scale 1:250,000.

Rankin, D. W., Drake, A. A., Jr., Glover, L., III, Goldsmith, R., Hall, L. M., Murray, D. P., Ratcliff, N. M., Read, J. F., Secor, D. T., and Stanley, R. S., 1989, Pre–orogenic terranes, *in* Hatcher, R. D., Jr., Thomas, W. A., and Viele, G. W., eds., The Appalachian–Ouachita orogen in the United States: Boulder, Geological Society of America, The Geology of North America, v. F–2, p. 7–100.

Raymond, L. A., 1995, Petrology: The study of igneous, sedimentary, and metamorphic rocks: Boston, McGraw-Hill, 742 p.

Reed, J. C., 1964, Geology of the Lenoir quadrangle, North Carolina: U. S. Geological Survey Map I-709-A, scale 1:62,500.

Reed, J. C., and Bryant, B., 1964, Evidence for strike-slip faulting along the Brevard zone in North Carolina: Geological Society of America Bulletin, v. 75. p. 1177-1195.

Shufflebarger, T. E., 1961, Notes on relationships of Piedmont sedimentary rocks with emphasis on the Poor Mountain-Chauga River area, Oconee County, South Carolina: South Carolina Division of Geology, Geologic Notes, v. 5, p. 31-38.

Sinha, A. K., Hund, E. A., and Hogan, J. P., 1989, Paleozoic accretionary history of the North American plate margin (central and southern Appalachians): Constraints from the age, origin, and distribution of granitic rocks, *in* Hillhouse, J., ed., Deep structure and past kinematics of accreted terranes: American Geophysical Union Monograph Series #50, p. 219-238.

Spear, F. S., 1995, Metamorphic phase equilibria and pressure-temperature-time paths: Washington D.C., Mineralogical Society of America, 799 p.

Streckeisen, A. L., 1976, To each plutonic rock its proper name: Earth Science Reviews, v. 12, p. 1-33.

Tabor, J. R., 1990, Geologic map of the Mill Spring quadrangle [unpublished mapping]: Knoxville, University of Tennessee, scale 1:24,000.

Thompson, A. B., 1982, Dehydration melting of pelitic rocks and the generations of H_2O undersaturated liquids: American Journal of Science, v. 282, p. 1567-1595.

Tobi, A. C., and Kroll, H., 1975, Optical determination of the An-content of plagioclase twinned by the Carlsbad-law: A revised chart: American Journal of Science, v. 275, p. 731-726.

Verseput, T. D., 1980, Structure of the South Mountain State Park area, Burke County, North Carolina [unpublished undergraduate thesis]: Carbondale, Southern Illinois University, 61 p.

Vinson, S. B., and Miller, C. F., 1999, Constraints on timing of Inner Piedmont plutonism, N.C.–S.C., from ion microprobe U-Pb zircon analysis: Geological Society of America Abstracts with Programs, v. 31, p. A77.

Whisnant, J. S., 1975, Geology of the southeast quarter of the Marion 15-minute quadrangle, North Carolina [unpublished M.S. thesis]: Chapel Hill, University of North Carolina, 50 p.

Williams, S. T., 2000, Structure, stratigraphy, and migmatization in the southwestern South Mountains, North Carolina [unpublished M.S. thesis]: Knoxville, University of Tennessee, 111 p.

Wintsch, R. P., 1975, Feldspathization as a result of deformation: Geological Society of America Bulletin, v. 86, p. 35-38.

Wintsch, R. P., and Knipe, R. J., 1983, Growth of a zoned plagioclase porphyroblast in a mylonite: Geology, v. 11, p. 360-363.

Yanagihara, G. M., 1994, Structure, stratigraphy, and metamorphism of a part of the Columbus Promontory, western Inner Piedmont, North Carolina [unpublished M.S. thesis]: Knoxville, University of Tennessee, 214 p.

PART II

Structural geology of the Kings Creek quadrangle, North Carolina

Abstract

Rocks of the Kings Creek 7.5-minute quadrangle provide a detailed record of deformation during mid- to late Paleozoic southern Appalachian orogenesis. Structures here are similar to those in other Inner Piedmont (IP) areas mapped in detail; direct evidence reveals six deformation events. The Green Mountain fault (the suspected lateral equivalent of the Mill Spring thrust; Plate 1) crops out in the northwestern corner of the Kings Creek quadrangle. Kinematic indicators show the Green Mountain and Brindle Creek faults accommodated both dip- and strike-slip movement during peak Neoacadian and earliest Alleghanian tectonothermal events.

Two structural domains were identified. Structures in Domain I dominantly trend northeast-southwest and verge to the northwest and southwest; foliations and axial surfaces generally dip southeast. Domain II, located in the southeastern corner of the quadrangle, contains variably oriented fold axes, foliations, and mineral stretching lineations that trend east-west, north-south, and northwest-southeast. The domain boundary is not coincident with the Brindle Creek thrust, a major fault striking N 55°E through the quadrangle. The local change in structural patterns from Domain I to Domain II is consistent with regional map-scale trends. Mineral stretching lineations indicate a component of southwest-directed simple shear with changes from east-west, north-south, and northwest-southeast trends in Domain II to strong northeast-southwest orientations in Domain I.

My structural data support Davis' 1993 oblique convergence model. Northwest-southeast-directed shortening buttressed ductile IP thrust sheets against the primordial Brevard fault zone and produced southwest-directed transpressional flow in the

northwestern IP. Strongly aligned sillimanite and amphibole mineral lineations here indicate a significant component of southwest-directed simple shear in both eastern and western IP rocks; the transpressional flow zone therefore overprints the Brindle Creek thrust in the southwestern Brushy Mountains. In keeping with conclusions of Davis and Tabor, pervasive western IP mylonite northwest of the Green Mountain fault in the southwestern Brushy Mountains were likely part of a Late Devonian to early Mississippian crustal-scale shear zone. Discreet faults and mylonites southeast of the Green Mountain fault, results of a similar latest Neoacadian to earliest Alleghanian stress field, probably mark localized deformation partitioned into high-strain zones. Continued earliest Alleghanian deformation tightly folded the Bindle Creek fault, partially transposed D_2 structures, and produced a crenulation cleavage that mimics orientation changes from Domain I to Domain II. Two later episodes of brittle open folding refolded tight to isoclinal (F_2 and F_3) folds. Joints formed episodically in response to late Alleghanian, Mesozoic, and Cenozoic brittle deformation.

Introduction

The IP contains a structurally complex, polydeformed stack of transpressional west- and southwest-verging crystalline thrust sheets. Decades of detailed and reconnaissance geologic mapping have revealed a regional stratigraphy for the western IP (Part I); macroscopic tectonic trends are therefore more easily deciphered there. Penetratively deformed, superposed fabrics— the result of Paleozoic ductile and semibrittle deformation, coeval metamorphism (Davis, 1993; Hatcher, 1998), and late Paleozoic, Mesozoic, and Cenozoic brittle deformation— are difficult to interpret and seldom display primary (S_0) and secondary (D_1) mesoscopic structures. Detailed

geologic mapping of successive IP thrust nappes supported by detailed, high resolution geochronology and geochemistry, has fostered development of increasingly sophisticated tectonic models (e.g., Bream et al., in review); a comprehensive and unequivocal tectonic history has yet to be presented (and perhaps never will be).

The IP has traditionally been represented (Fig. 2-1) as a contiguous belt of high grade metamorphic rocks that extends from northern North Carolina to eastern Alabama. Recent detailed geologic mapping in the South Mountains and Brushy Mountains (Giorgis, 1999; Williams, 2000; Bier, 2001; Kalbas et al., 2001; Merschat and Kalbas, 2002) has subdivided the IP into western and eastern components. Bream et al. (2001) proposed the Brindle Creek thrust is a terrane boundary separating the two belts (Fig. 2-1). The western IP (eastern Tugaloo terrane; Hatcher, 2001b; Hatcher, 2002) lies between the Brevard fault zone and Brindle Creek thrust. The western IP is characterized by dominantly northeast-southwest-oriented structures; it is composed of successive, thin, shallow to moderately southeast-dipping thrust sheets dominated by early Paleozoic paragneisses and metamorphosed Middle Ordovician sedimentary, volcanic, and intrusive rocks. The eastern IP (Cat Square terrane; Hatcher, 2001b; Hatcher, 2002) extends from the Brindle Creek thrust to the Central Piedmont suture and is composed of Siluro-Devonian paragneisses and metamorphosed Devono-Mississippian granitoids. Eastern IP structural patterns change further southeast to north-south-, northwest-southeast-, and east-west-trending isoclinal-recumbent and open folds (Plates 1, 2; Goldsmith et al., 1988).

The Kings Creek 7.5-minute quadrangle (Fig. 2-1), located in the southwestern Brushy Mountains ~100 km east of Asheville and ~50 km northwest of Hickory, North

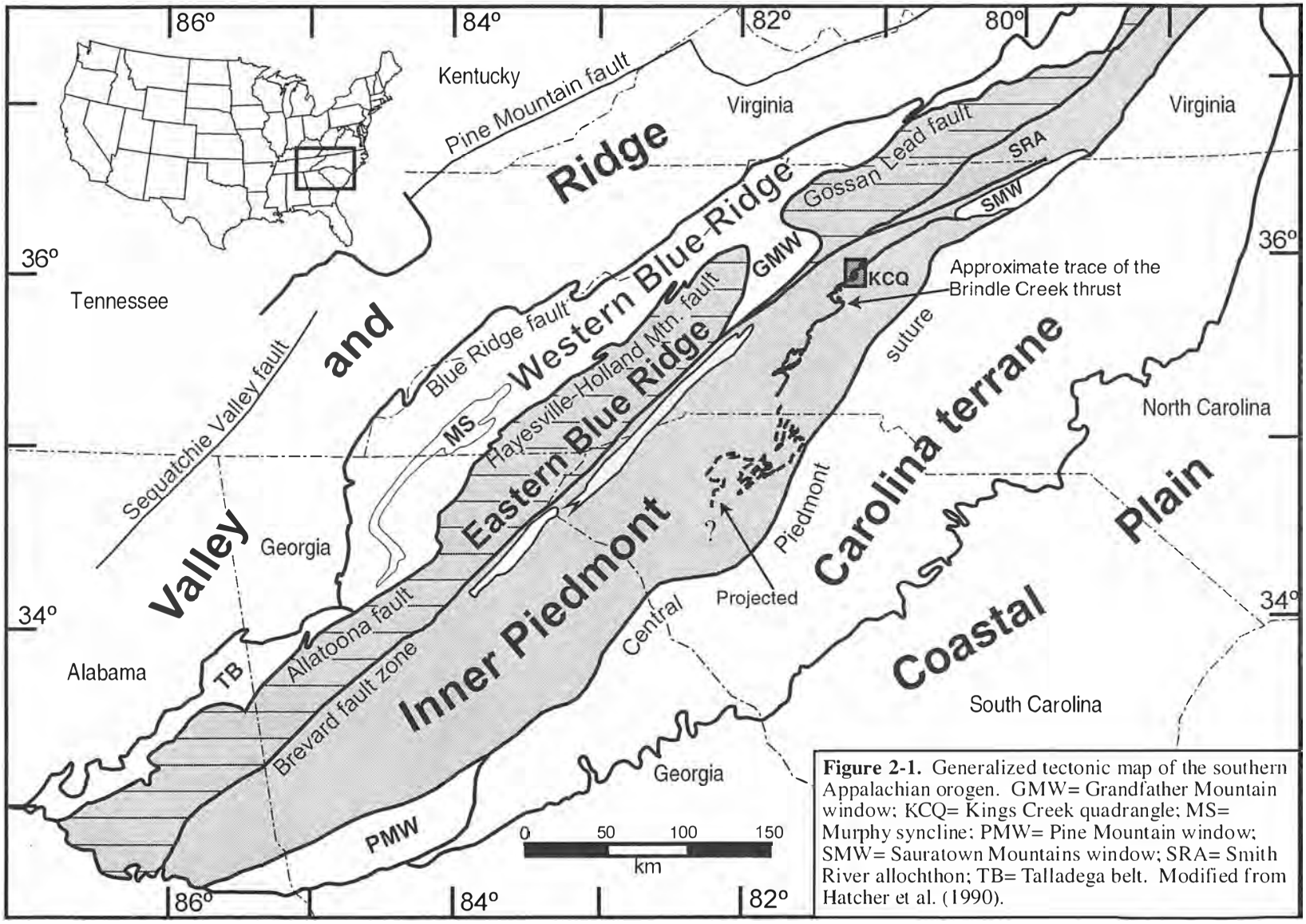

Figure 2-1. Generalized tectonic map of the southern Appalachian orogen. GMW= Grandfather Mountain window; KCQ= Kings Creek quadrangle; MS= Murphy syncline; PMW= Pine Mountain window; SMW= Sauratown Mountains window; SRA= Smith River allochthon; TB= Talladega belt. Modified from Hatcher et al. (1990).

Carolina, is an ideal location for detailed study of IP tectonics. The quadrangle contains a segment of the Brindle Creek thrust and several rock units that are correlative with those in the South Mountains (Goldsmith et al., 1988; Giorgis, 1999; Williams, 2000; Bier, 2001). Moreover, the Brevard fault zone crops out ~2.7 km northwest of the northwestern corner of the quadrangle and the sillimanite-in isograd is located immediately northwest of the study area (Butler, 1991). The outcrop width of the western IP in the southwestern Brushy Mountains is significantly smaller than farther southwest (~10 km vs. ~24 km near Morganton, and ~47 km at the South Carolina-North Carolina border; Fig. 2-1); therefore, multiple fault-bounded sections of both western and eastern IP rocks crop out in close spacial proximity to each other and the Brevard fault zone (Plate 1). The purpose of this paper is to document and interpret micro-, meso-, and macroscopic structures in the Kings Creek quadrangle to better understand the structure and tectonic history of the composite IP.

Methods

Detailed geologic mapping of the Kings Creek quadrangle began in January, 2001, and continued through mid-August, 2001, with additional field work in January, 2002. Standard 1:24,000- and enlarged 1:12,000-scale USGS 7.5-minute topographic maps were used as base maps. Fabric orientations were measured with a Brunton™ pocket transit and recorded at 1872 stations. Fabric diagrams were constructed using the Allmendinger (2001) Stereonet PPC program. Fabric data were contoured using both the traditional (percent per percent area) method and the method developed by Kamb (1959).

Structural and Tectonic Framework

Map Patterns

Three thrust sheets have been recognized in the Kings Creek quadrangle (Fig. 2-2; Plate 2). The northwesternmost is the Marion thrust sheet containing western IP rocks southeast of the Brevard fault zone and northwest of the Green Mountain fault (Merschat and Kalbas, 2002; Plate 1). Previous studies in the Columbus Promontory (Davis, 1993) concluded the Henderson Gneiss in the Marion thrust sheet is bounded by the Tumblebug Creek thrust. Subsequent studies near Marion, North Carolina (Bream, 1999; Hill, 1999) also favored fault emplacement of the Henderson Gneiss. In the Kings Creek quadrangle, the Henderson Gneiss shares a sharp contact with mylonitized upper Tallulah Falls Formation metagraywacke, but limited outcrop length precludes determination of the existence of the Tumblebug Creek thrust. The Henderson Gneiss is therefore grouped with the Tallulah Falls Formation as part of the Marion thrust sheet.

The Green Mountain fault, the northwesternmost fault in the study area overrides the Marion thrust sheet. It is reasonable to link the Green Mountain fault with the Mill Spring thrust of Davis (1993) and Yanagihara (1994) because: (1) a similar stratigraphy is present (migmatitic Poor Mountain Amphibolite and probably Tallulah Falls Formation (Part III) thrust over upper Tallulah Falls Formation metagraywacke and Henderson Gneiss); (2) interpolations (Plate 1) of contacts on detailed and reconnaissance maps (Reed, 1964; Goldsmith et al., 1988) project the Mill Spring thrust into the northwestern corner of the Kings Creek quadrangle; (3) mylonitic metagraywacke crops out in the footwall of the thrust.

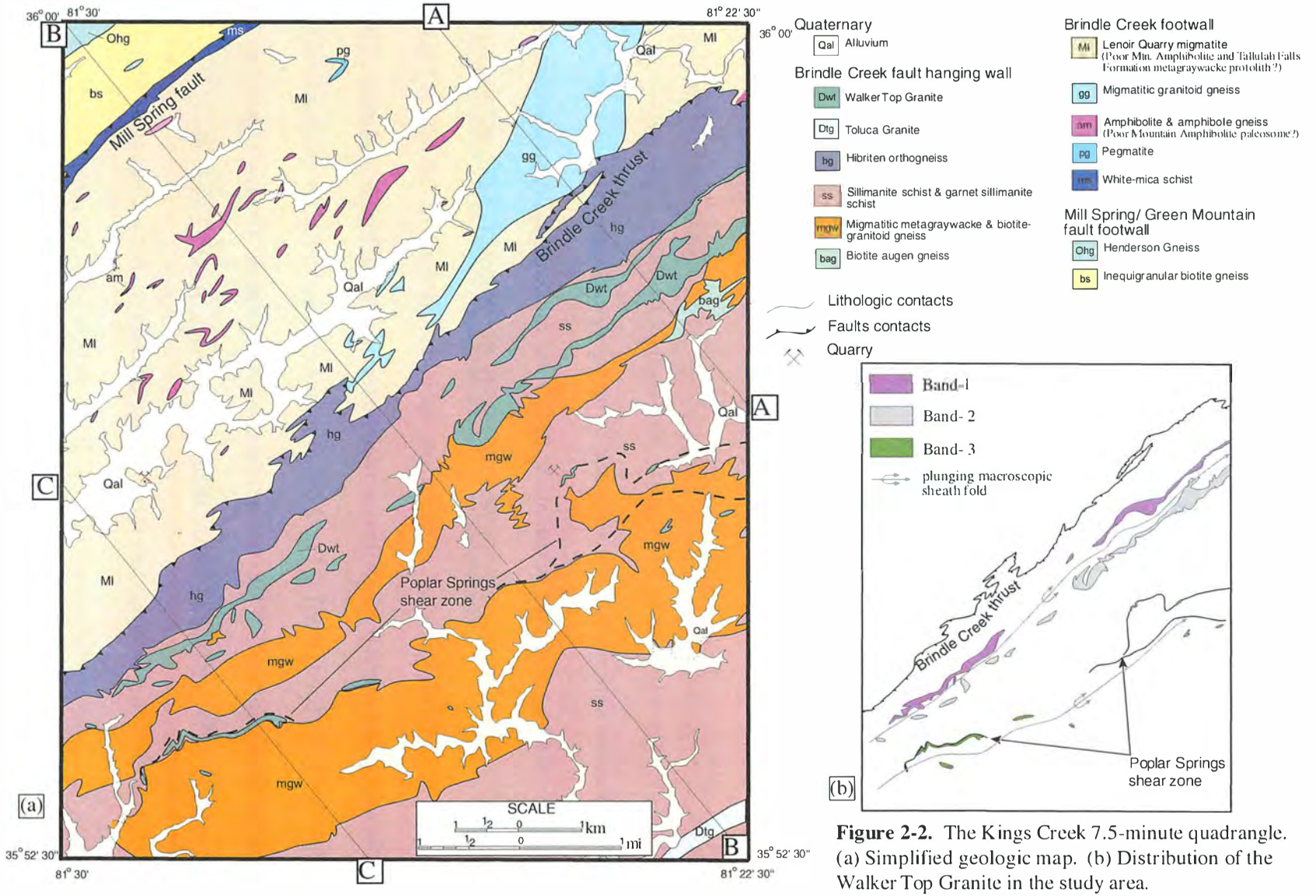

Figure 2-2. The Kings Creek 7.5-minute quadrangle. (a) Simplified geologic map. (b) Distribution of the Walker Top Granite in the study area.

The Green Mountain thrust sheet in the study area is dominated by two units: muscovite schist, and intensely migmatized amphibolite (Lenoir Quarry migmatite) (Fig. 2-2; Plate 2). The intensely migmatitic unit is dominated by amphibolite and biotite-hornblende granodiorite. Folded meso- to macroscale amphibolite boudins, interpreted as paleosome, are also present (Fig. 2-2; Part III). A poorly foliated granitoid also crops out in the Green Mountain thrust sheet. It is truncated by the Brindle Creek thrust. Western IP rock units in the study area (i.e., both the Marion and Green Mountain thrust sheets) are strongly aligned northeast-southwest.

The Brindle Creek thrust juxtaposed migmatitic metagraywacke, pelitic schist, inequigranular quartz-plagioclase-biotite gneiss (Hibriten orthogneiss; Part I), and Walker Top Granite over rocks of the Green Mountain thrust sheet. Three northeast-trending bands of sillimanite schist separated by metagraywacke are exposed in the Brindle Creek thrust sheet; the schists are texturally and mineralogically similar, but a discernable stratigraphy is not represented. Similarly, the Walker Top Granite, named by Giorgis (1999) and Giorgis et al. (2002), crops out in three distinctive, laterally extensive, but disconnected lenticular bands that parallel the regional trend (Fig. 2-2; Plate 2). The northwesternmost band (Band 1; Fig. 2-2b) crops out entirely within the sillimanite schist and is locally in contact with Hibriten orthogneiss. It is dominated by two continuous bodies separated by sillimanite schist. Walker Top Granite Band 2 crops out discontinuously in the southwestern quarter of the quadrangle, but is continuous for ~5.3 km along strike farther northeast (Fig. 2-2). It is mostly in contact with sillimanite schist, but locally is in contact with metagraywacke. Similarly, Walker Top Granite Band 3 (the

southeasternmost band) is bounded by both sillimanite schist and metagraywacke; lenticular macroscopic bodies, however, are smaller and more widely spaced. South of Draco, small isolated Walker Top Granite bodies crop out within sillimanite schist and metagraywacke. Biotite augen gneiss, characterized by smaller K-feldspar augen, crops out as an isolated body near the eastern termination of the quadrangle (Fig. 2-2; Plate 2). Its rounded porphyroclastic texture differs from that of the Walker Top Granite and it does not correlate with other along strike bodies; although it may share a genetic link with the Walker Top Granite, this augen gneiss was mapped as a separate unit. A body of Devonian Toluca Granite crops out in the southeastern corner of the Kings Creek quadrangle within the Brindle Creek thrust sheet and connects with larger bodies in the Ellendale quadrangle (Merschat and Kalbas, 2002).

Structural trends, also recognized by Bryant and Reed (1970) and Goldsmith et al. (1988), permit subdivision of the Kings Creek quadrangle into two foliation domains (Fig. 2-3). Domain I contains the Marion and Green Mountain thrust sheets (western IP) and part of the Brindle Creek thrust sheet (eastern IP), and has a strong northeast-southwest foliation pattern. Domain II includes only rocks of part of the Brindle Creek thrust sheet in the southeasternmost corner of the quadrangle. Northeast-southwest trends near the fault change in the southeastern portion of the quadrangle to variably east-west-, north-south-, and northwest-southeast-trending fabrics.

Deformation Hierarchy

Relative timing of deformation was interpreted by Davis (1993) and has been subsequently modified (Yanagihara, 1994; Bream, 1999; Giorgis, 1999; Hill, 1999; Williams, 2000; Bier, 2001; Merschat and Kalbas, 2002; Table 2-1). Six deformation

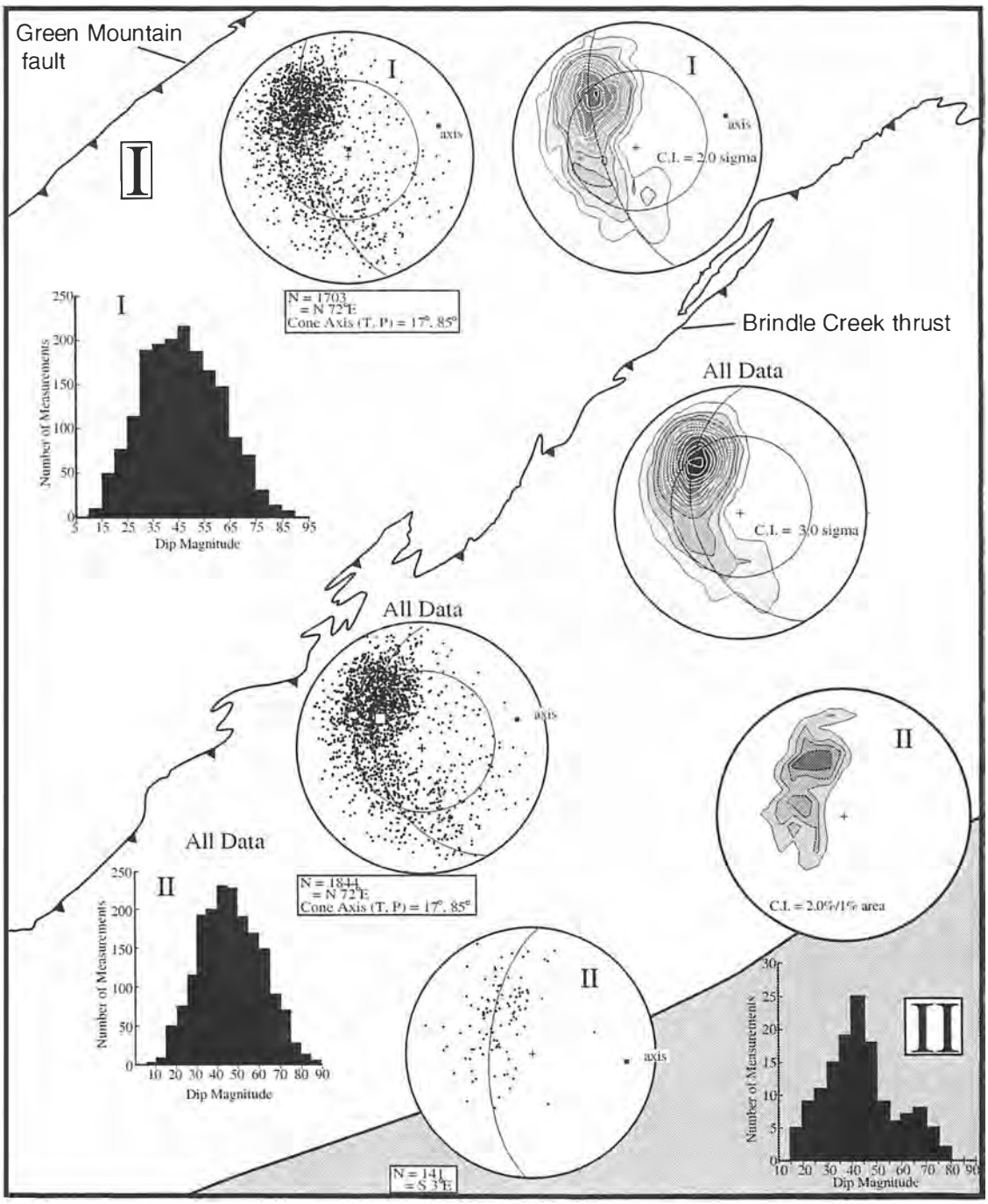

Figure 2-3. Lower hemisphere equal-area scatter plot and contour projections of poles to foliation and dip histograms. Data from 1844 measurements are shown together as "all data" and separated into two structural Domains (I and II). Kamb (1959) and 2 % area contours were used. (T, P) = trend and plunge.

Table 2-1. The relative timing and nature of deformation events in the central and western IP, North Carolina*.

Deformation Events	Structures			Regional Events	Orogenic Event/ Age
	Fabrics	Folds	Faults		
$D_{6...}$	joints	regional broad, open folds (Merschat and Kalbas, 2002)	———	uplift — — —?— — — rifting	Cenozoic — — ?— — — Mesozoic
D_5	joints	F_5 open, upright, trend = northwest	brittle reactivation of the BFZ along the Rosman fault; Hatcher, 2001a	exhumation of the BRP composite thrust sheet	Alleghanian
D_4	joints (in strong layers only; penetrative S-C fabric in the BFZ)	F_4 open, upright, trend = northeast *flexural slip*	lower greenschist facies reactivation of the BFZ (Hatcher, 2001a)	exhumation of the BRP composite thrust sheet	
D_{3b}	L_{3b} = intersection between PSSZ splay and F_3 axial plane	———	semi-brittle splay originating at the PSSZ	———	Earliest Alleghanian
D_{3a}	S_3, L_{3a}	F_3 = tight reclined to upright, and crenulations; trend = northeast; vergence = northwest *flexural flow*	Type-F motion on the PSSZ; folding of the BCT and GMF	Cessation of migmatization and ductile deformation	
D_2	S_2, L_2	F_2 tight to isoclinal, reclined to recumbent, isoclinal and sheath?; trend northeast, southwest, and southeast; *passive to flexural flow*	initial northwest and then southwest deflected motion on the BCT, GMF, SMT, and TCT?	intense migmatization in the footwall of the BCT.	Latest Neoacadian
D_1	S_1	F_1 intrafolial folds (Davis, 1993); macroscopic folding of the Walker Top Granite (?); microscopic layering; *passive flow (?)*	———	———	Pre- or early Neoacadian

*Modified from Davis, 1993; Yanagihara, 1994; Bream, 1999; Hill, 1999; Giorgis, 1999; Williams, 2000; and Bier, 2001). BCT = Brindle Creek thrust; BFZ = Brevard fault zone; BRP = Blue Ridge-Piedmont; GMF = Green Mountain fault; PSSZ = Poplar Springs shear zone; SMT = Sugarloaf Mountain thrust; TCT = Tumblebug Creek thrust.

events were recognized in the IP of southwestern North Carolina. D_1 structures, recognized in the western IP by Davis (1993), consist of rootless intrafolial folds (F_1) and penetrative S_1 axial planar foliations in boudins. D_2 and D_3, respectively, produced penetrative and locally penetrative northeast structural trends in the western IP and variable orientations of structures in the eastern IP. Davis (1993) concluded the S_2 foliation (schistosity, gneissic banding, and compositional layering) is a high temperature fabric formed during peak metamorphism. D_2 and D_3 may, however, represent continuous deformation during a single prograde metamorphic event (Yanagihara, 1994). Pre- and post-metamorphic structures have also been documented throughout the Carolinas IP (Davis, 1993). Davis' interpretation is consistent with structural trends in the Kings Creek quadrangle and therefore will be followed throughout this paper.

Absolute ages from Rb-Sr whole-rock and sensitive high resolution ion microprobe reverse geometry (SHRIMP RG) U-Pb analyses are helpful in constraining the timing of deformation. Rb-Sr analyses of numerous western IP orthogneisses yielded early to middle Paleozoic crystallization ages ranging from 500 to 409 Ma (Fullagar, 1971, 1981; Lemmon, 1973; Odom and Fullagar, 1973; Odom and Russell, 1975; Harper and Fullagar, 1981; McSween et al., 1991; Fullagar et al., 1997; Vinson and Miller, 1999). Acadian and Neoacadian ion microprobe metamorphic ages of zircon rims have also been reported from the western IP of Georgia, South Carolina, and North Carolina (Bream et al., 2001; Carrigan et al., 2001). Conventional U-Pb analyses of monazite by Dennis and Wright (1997) from the South Carolina IP yielded 360 Ma and 330-320 Ma metamorphic ages that, along with significantly younger (than western IP granitoids)

crystallization ages of eastern IP granitoids (375 to 320 Ma; e.g., Mapes et al., 2002), indicate a pervasive Late Devonian to early Mississippian thermal event. The Walker Top Granite crops out exclusively in the eastern IP and has a crystallization age of 366 ±3 Ma (Giorgis et al., 2002; Mapes, 2002). $^{40}Ar/^{39}Ar$ plateau ages for Stumphouse Mountain, Walhalla, and Six Mile nappes in South Carolina indicate post-metamorphic cooling through the hornblende closure temperature of ~550 °C between 333 and 322 Ma (Dallmeyer, 1988).

Zircon rim ages from Lenoir Quarry migmatite in the Brindle Creek thrust footwall (Part III) indicate metamorphism, thrust emplacement, and penetrative deformation likely occurred at 342 Ma (Bream, 2002; Part III). A later tectonothermal event occurred at 330 Ma (Bream, 2002; Part III). Alignment (parallel to the S_3 axial planar foliation and L_2 mineral stretching lineation) of high grade mineral assemblages in the southwestern Brushy Mountains, in the absence of retrograde assemblages, indicates penetrative and partially penetrative fabrics are the result of latest Neoacadian to earliest Alleghanian deformation. Absolute ages and high temperature mineral assemblages delimit the relative order of deformation events and allow categorization of fabrics into pre-Acadian to Neoacadian, Neoacadian and earliest Alleghanian, and post-early Alleghanian timeframes (Table 2-1).

Pre-Acadian to Neoacadian Structures in the Kings Creek Quadrangle

Intrafolial folds and truncated foliations in boudins have been cited as evidence for deformation prior to penetrative syn-peak metamorphic deformation in the southwestern North Carolina western IP (Davis, 1993; Yanagihara, 1994; Bream, 1999; Hill, 1999; Giorgis, 1999; Williams, 2000; Bier, 2001). Davis (1993) documented S_1

gneissic layering in rootless F_1 folds in boudins in the Columbus Promontory. Further evidence for D_1 was observed near Marion, North Carolina, where F_1 macroscopically folded Tallulah Falls Formation rocks are truncated at the Henderson Gneiss contact by the Tumblebug Creek fault (Bream, 1999; Hill, 1999; Plate 1).

Evidence for pre-Acadian to Neoacadian peak deformation in the Kings Creek quadrangle exists in structures at all scales. Microscopic truncations of biotite and quartz splinters (S_1?) against quartz layers in sillimanite schist may be evidence for D_1 particularly since there is no annealed (120° grain boundary) quartz fabric along what would be a required localized microfault (Fig. 2-4). Moreover, Bryant and Reed (1970), working west of Lenoir, North Carolina, documented folds and foliations truncated by an oblique foliation; this fabric likely represents D_1. The outcrop pattern of the Walker Top Granite permits the interpretation of F_1 folds in cross sections (Fig. 2-5; discussed in detail below). Although boudins are common in the study area, internal truncated foliations can be interpreted as either evidence for D_1 deformation or later rotation of paleosome schollen in anatectic melts.

Latest Neoacadian/ Earliest Alleghanian Structures in the Kings Creek Quadrangle

On the basis of field, petrologic, and geochronologic evidence, several workers concluded penetrative deformation accompanied Neoacadian prograde metamorphism and migmatization (Davis, et al., 1991; Davis, 1993; Hatcher et al., 1999; Part III). This event has been characterized by the penetrative axial planar foliation (S_2) and mineral lineation (L_2), recumbent isoclinal (F_2) folds, and inclined to recumbent tight (F_3) folds, F_2 (?) sheath folds, and thrust faults (Table 2-1). Whisnant (1975) concluded isoclinal folds, lineations, and foliations in the western IP formed coevally. In southwestern North

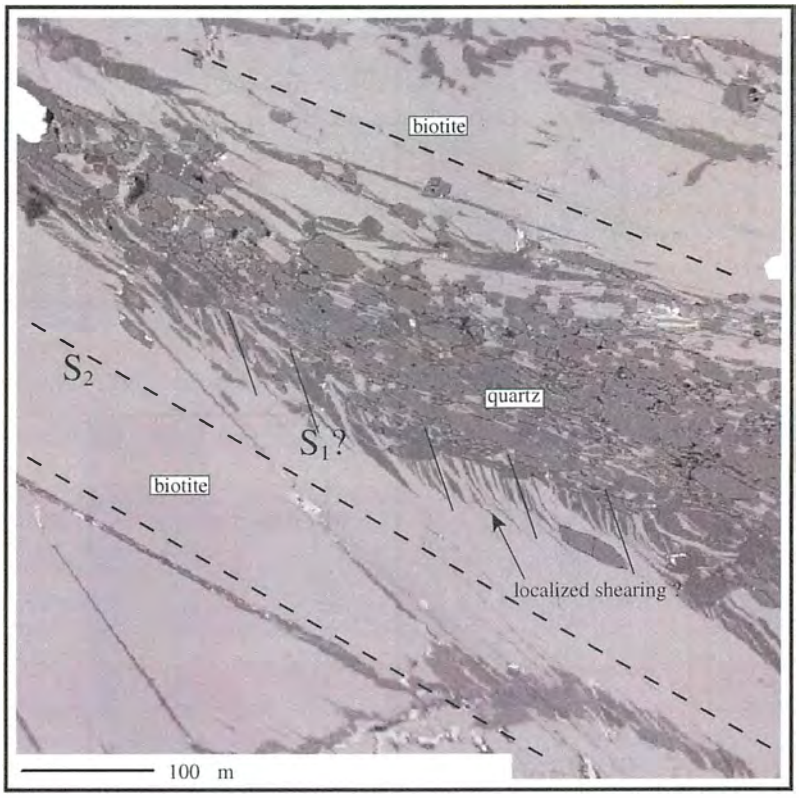

Figure 2-4. Backscatter electron image of localized truncations of biotite into a quartz layer in sillimanite schist. The inclined fabric in biotite and quartz crystals can be interpreted as a remnant S_1 surface, the product of localized simple shear, or the result of a crystallographic effect. Dashed lines indicate the S_2 foliation orientation; solid lines highlight the relict S_1 foliation or D_3 shear planes. If this is an overprint, there is no localized shearing. The sample is from 1.7 km northeast of Draco, North Carolina.

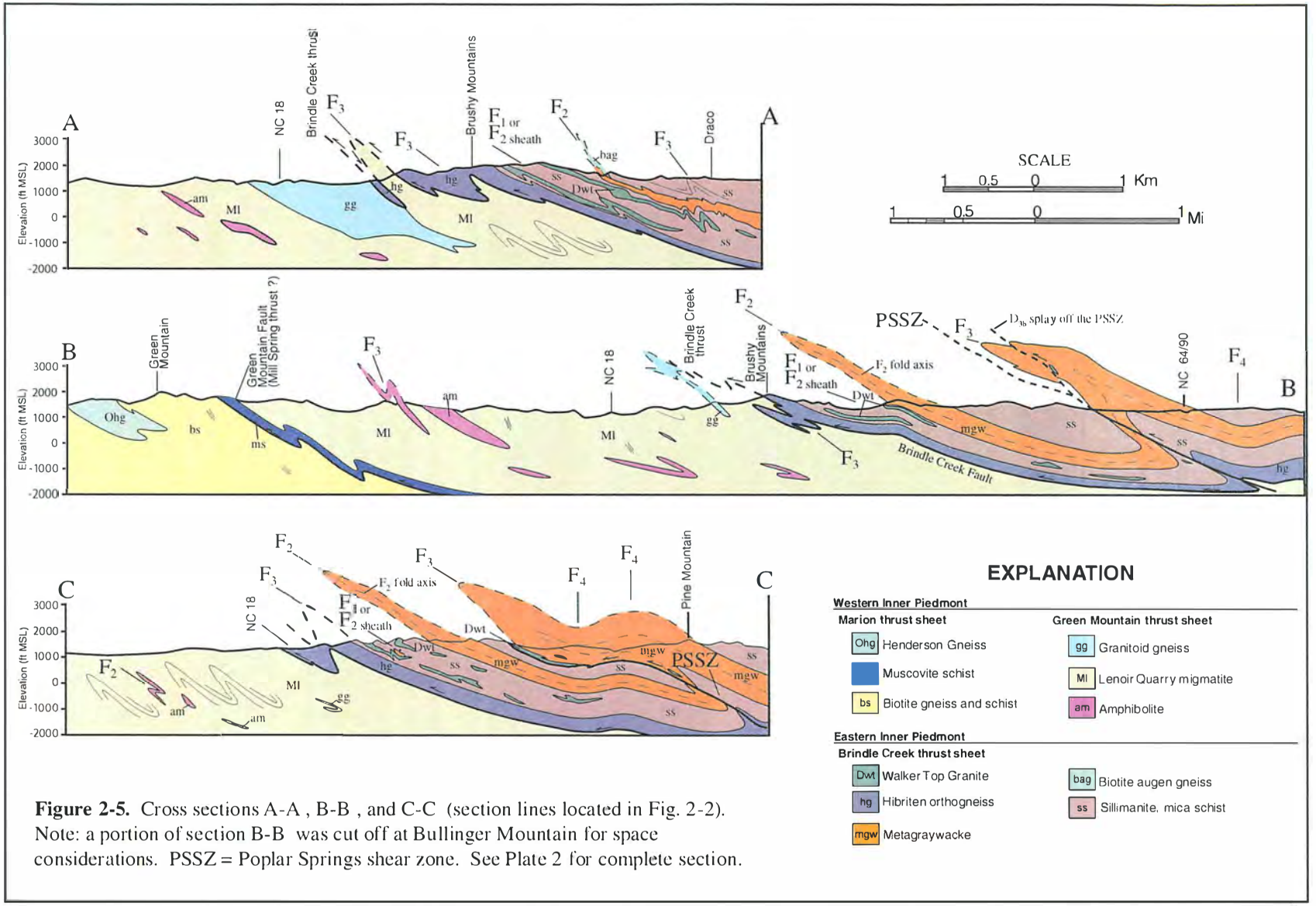

Figure 2-5. Cross sections A-A , B-B , and C-C (section lines located in Fig. 2-2). Note: a portion of section B-B was cut off at Bullinger Mountain for space considerations. PSSZ = Poplar Springs shear zone. See Plate 2 for complete section.

Carolina, D_2 was subdivided into D_{2a} and D_{2b} by Davis (1993), Bream (1999), and Hill (1999) on the basis of the post 490 Ma (= crystallization age of the Henderson Gneiss; Carrigan et al., 2001) truncation of the Tumblebug Creek thrust by the Sugarloaf Mountain thrust (Bream, 1999; Hill, 1999).

The timing of isolated Devono-Mississippian eastern IP magmatism (Giorgis et al., 2002; Mapes, 2002) and the common ages of metamorphism in the composite IP belt indicate Brindle Creek thrusting occurred between 366 and 342 Ma (Parts I and III). Parallel northeast-southwest-striking, southeast-dipping foliations, lineations, and fold axes in Domain I (Figs. 2-3, 2-6, 2-7) indicate penetrative, synmetamorphic D_2 deformation occurred during or immediately following faulting and paralleled dominant western IP structural trends noted by Hatcher (1970), Conley and Drummond (1975), and Davis (1993). In the southwestern Brushy Mountains, the dominant foliation, S_2 (Fig. 2-3), parallels compositional layering (Fig. 2-8). Tight F_3 folds locally developed a weak axial planar S_3 foliation (Fig. 2-8). The average coaxial penetrative mineral lineation (L_2; mean = 37°/ N80°E; Fig. 2-6) is defined by alignment of hornblende, quartz, and less commonly sillimanite. L_{3a} is formed by intersection of the S_2 foliation and S_3 axial planes and weak S_3 foliations. Foliations, mineral lineations, and fold axes in migmatite neosome are consistent with regional D_2 structural trends; migmatization and D_2 deformation were coeval (Part III) and enhanced the S_2 compositional layering. Transposition of the footwall migmatite resulted from pure shear induced by thrust loading of the Brindle Creek thrust sheet.

A distinct change in the orientations of lineations (L_2) and fold axes (F_2, F_3; described below) occurs from Domain I to Domain II (Figs. 2-6, 2-7, 2-9); structures in

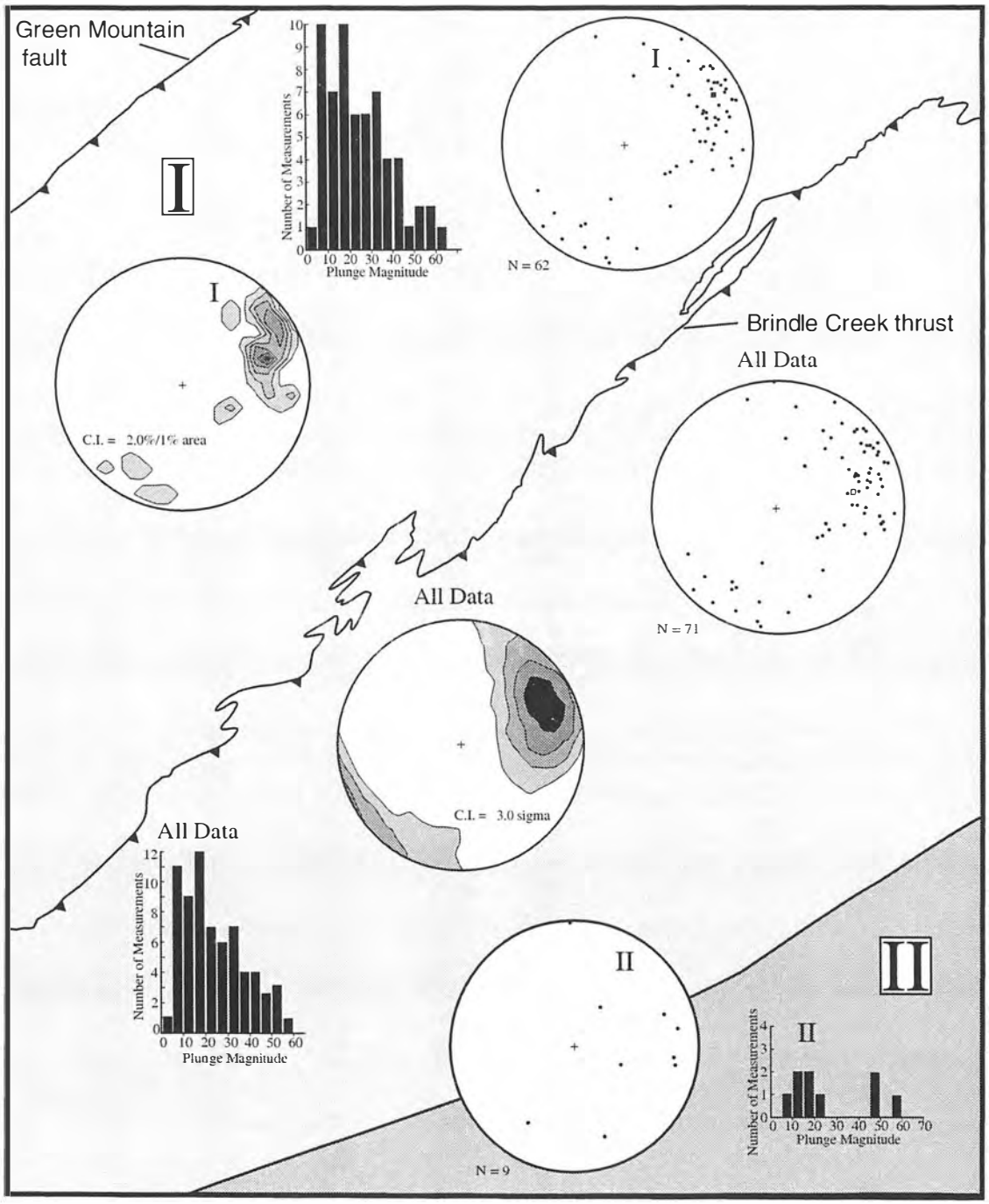

Figure 2-6. Lower hemisphere, equal-area scatter plot and contoured lineation orientations and plunge histograms. Data from 71 measurements are shown together as "all data" and separated into two structural Domains (I and II). Kamb (1959) and 2 % area contours were used.

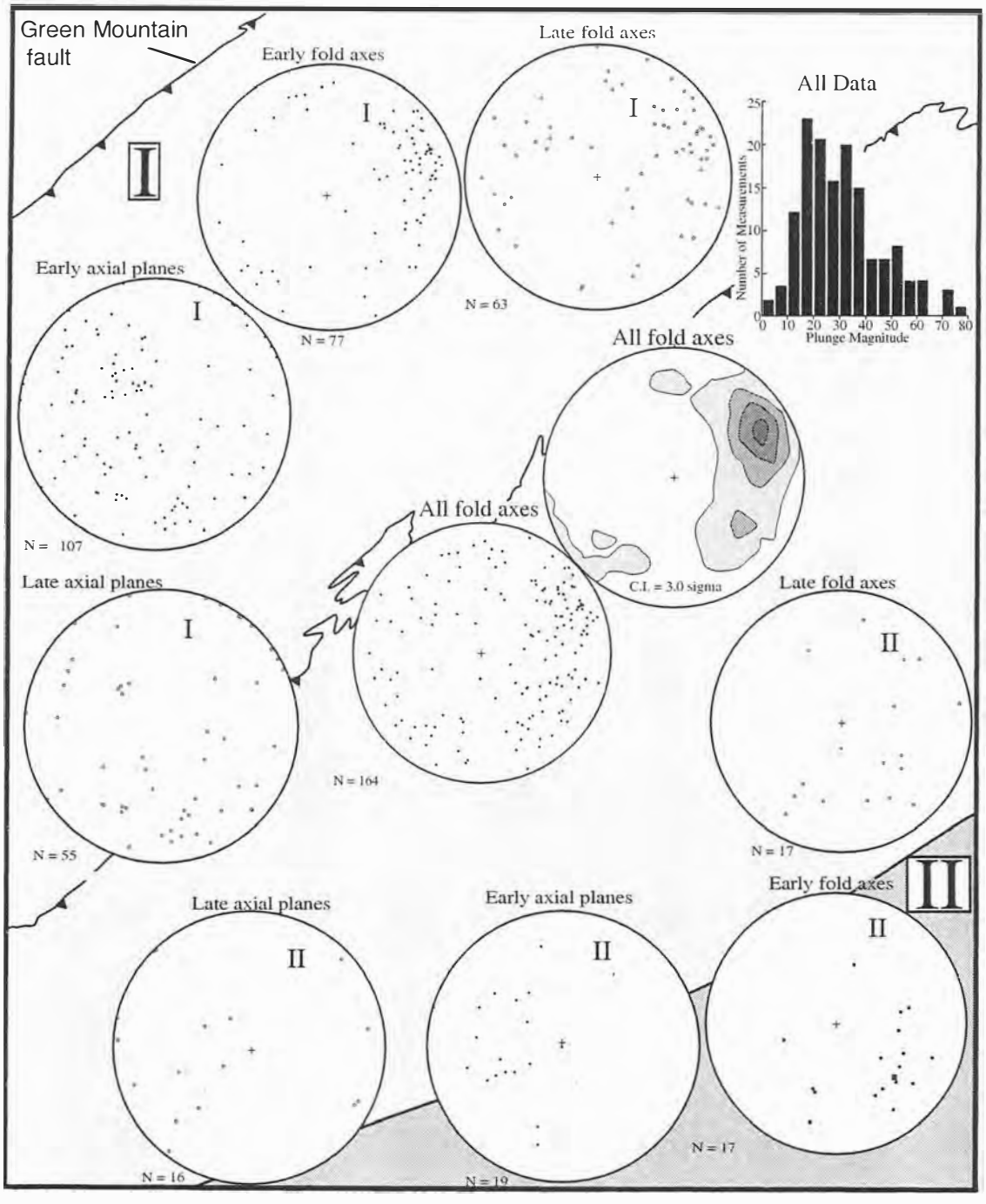

Figure 2-7. Lower hemisphere equal-area scatter plots of fold axis and axial surface orientations. Data from 164 measurements are shown together as "all data" and separated into two structural Domains (I and II). For each domain, the data are divided into early (F_2 and F_3) and late (F_4 and F_5) subsets. Kamb (1959) contours were used. (T, P) = trend and plunge.

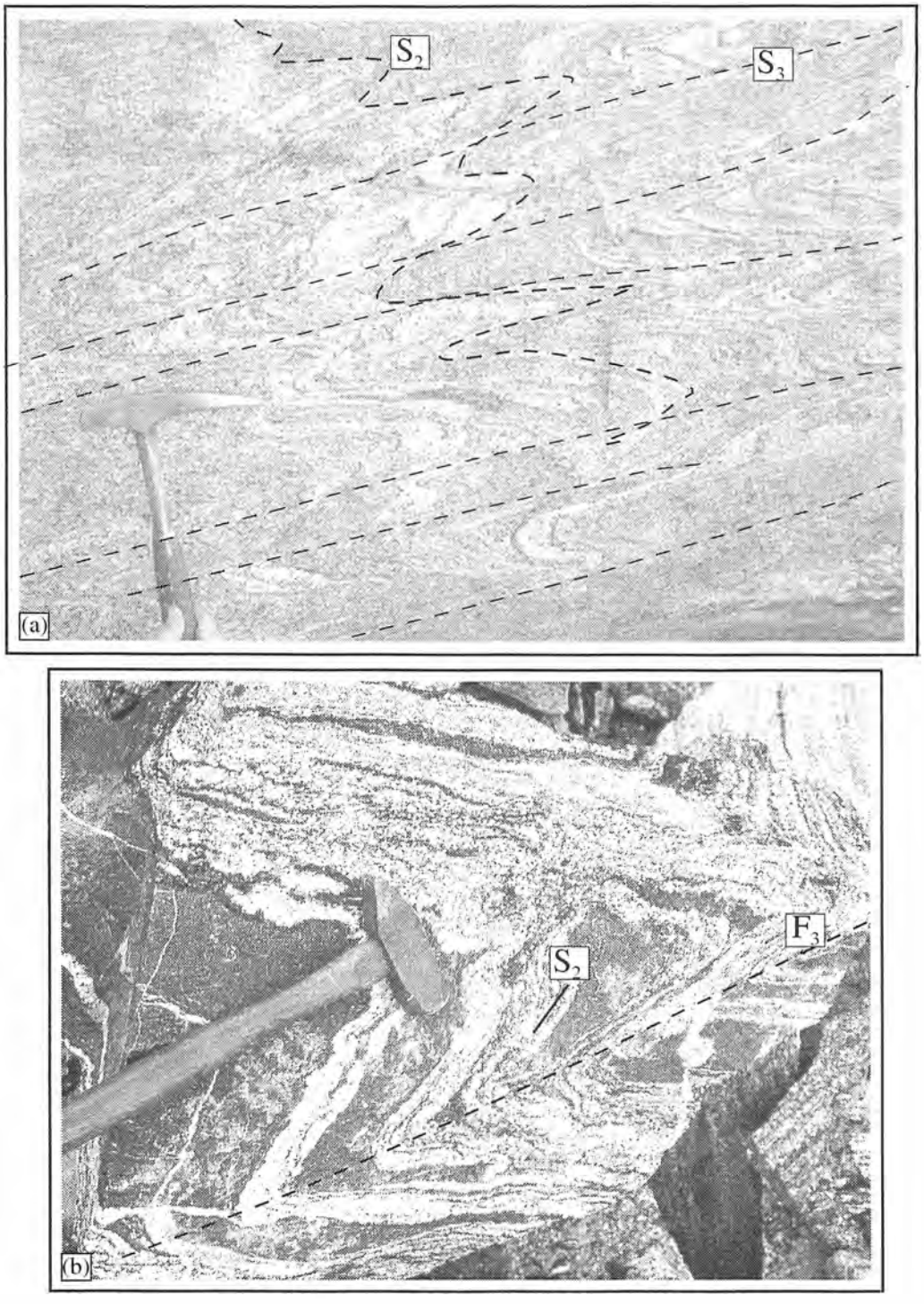

Figure 2-8. Structures in migmatite of the Green Mountain thrust sheet. (a) Folded (F_3), diktyonitic migmatite at the Cedar Rock Country Club 0.42 km south of North Carolina 18. Dashed lines indicate incipient transposition along attenuated limbs of tight to isoclinal folds. (b) Tight folds (F_3) of S_2 in stromatic migmatite at Lenoir Quarry.

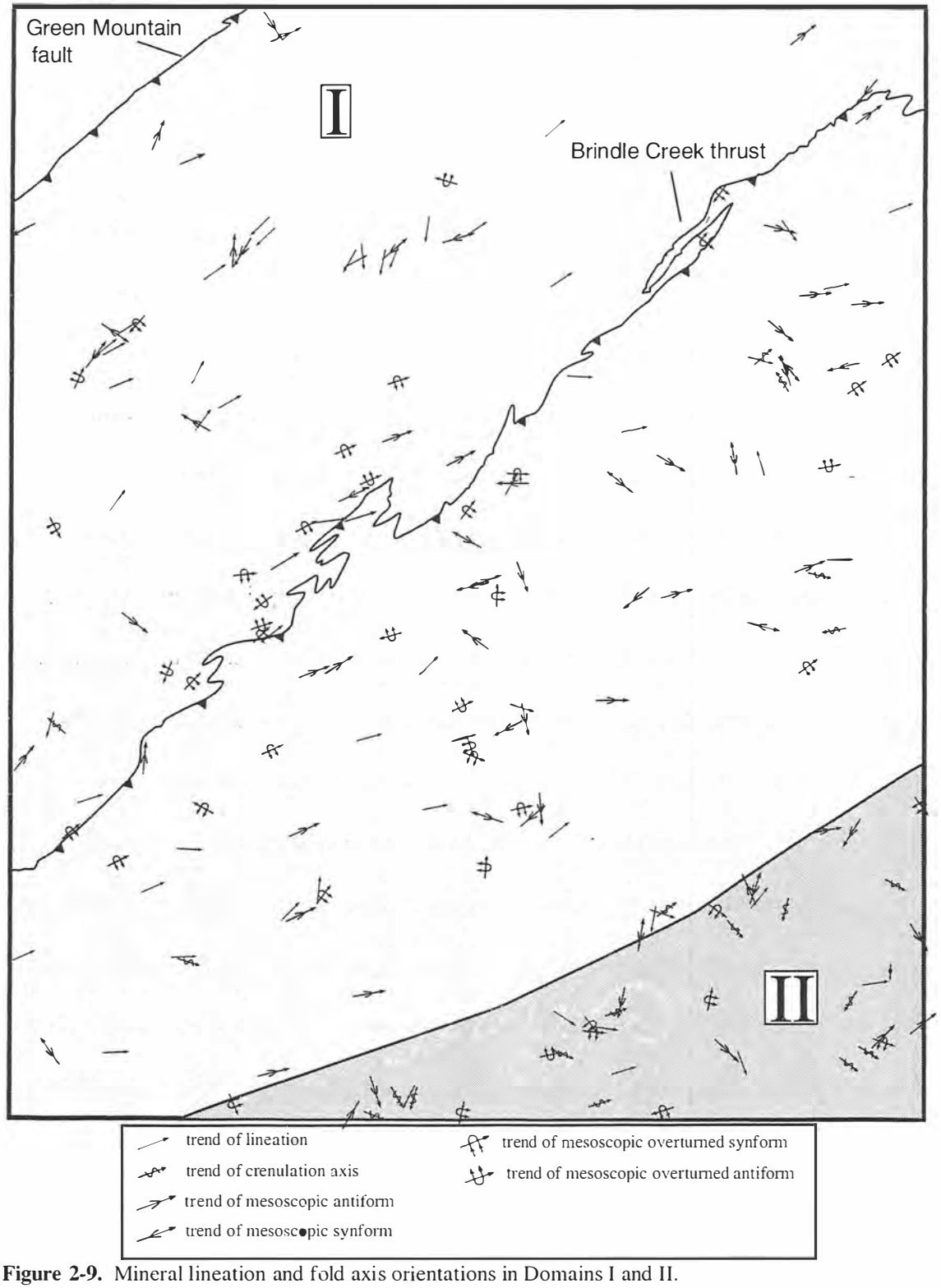

Figure 2-9. Mineral lineation and fold axis orientations in Domains I and II.

Domain I dominantly trend N 60°E to N 80°E, and parallel regional trends. Domain II structural orientations are more variable (mean L_2 = S 72°E; mean F_2 and F_3 = S 48°E). Axial surface orientations also change from Domain I to II; Domain I early axial surfaces strike ~N 50°E whereas Domain II early axial surfaces strike ~N-S (Fig. 2-7). S_2 partially mimics this variation with changes from dominantly orogen-parallel orientations in the northwest to dominantly east-west- and north-south-striking, east- and south-dipping trends in the southeast (Fig. 2-3). No appreciable change in dip occurs across the domain boundary. These patterns are consistent with observations of Goldsmith et al. (1988), Davis (1993), Hatcher (2001a), and Merschat and Kalbas (2002).

Meso- and macroscopic superposed fold patterns in both domains indicate two fold sets dominated by latest Neoacadian and earliest Alleghanian structures (respectively D_2 and D_3; Table 2-1). The earliest preserved regional fold set, F_2, is characterized by reclined to recumbent, dominantly northwest-verging, tight to isoclinal, passive flow folds (early fold axes; Figs. 2-7, 2-9; Plate 2). A northwest-plunging, outcrop-scale F_2 sheath fold crops out at one locality in Domain II, demonstrating a component of heterogeneous simple shear. Systematic L_2 patterns also suggest heterogeneous simple shear. The second early fold set (F_3, D_{3a}) is characterized by upright to reclined, closed to tight folds, that refold S_2 (Fig. 2-8). Though prevalent in the western and eastern IP, F_3 folds, as noted by Davis (1993), are only locally penetrative. Mesoscale attenuation and shearing of F_3 fold limbs in stromatite indicates synmigmatitic (syn-peak metamorphic) ductile deformation and incipient transposition (Fig. 2-8a). Dominantly southeast-oriented (shallowly plunging) crenulations (F_3; Fig. 2-9) are also present and are most

common in sillimanite schist. Microscopic crenulations were noted in a muscovite-quartz-biotite-sillimanite schist sample from the Brindle Creek thrust sheet.

The Green Mountain and Brindle Creek faults are thought to result from initial macroscale shearing along common limbs of F_2 isoclinal folds (Type-F thrusts of Hatcher and Hooper, 1992; Bier, 2001). Isolated mylonitic fabrics in the Walker Top Granite indicate an additional ductile shear zone (Poplar Springs shear zone) within the Brindle Creek thrust sheet. Transposed (flattened and/or sheared layers) and mylonitic fabrics are mostly present in the southeasternmost linear band of Walker Top Granite (Fig. 2-2). Mylonitic fabrics dominate the southwestern body in Band 3 and are also present within bodies surrounded by folded (F_3) metagraywacke along strike to the northeast. Mylonitic rocks are not present, however, in the central Walker Top Granite body in Band 3 (Fig. 2-2). Mylonitic metagraywacke is present near the eastern boundary of the quadrangle, and indicates faulting (with minor displacement) of the F_3 fold in metagraywacke (Fig. 2-5). D_3 is therefore subdivided into two sub events: (1) Type-F faulting of the Poplar Springs shear zone in response to progressive F_3 folding; and (2) D_{3b} truncation of the folded (F_3) metagraywacke by a splay off the shear zone. L_{3a} can therefore be defined as the intersection between the Poplar Springs shear plane and the F_3 axial plane, L_{3b} is the intersection of the splay off the Poplar Springs shear zone and the F_3 axial plane (Fig. 2-5). Two laterally connected bands of mylonitized Walker Top Granite were recognized along strike in the Ellendale quadrangle and denote northeastward continuity of the Poplar Springs shear zone (Merschat and Kalbas, 2002). Orthogonal (northwest-directed) then oblique (northeast-southwest-directed) transport is implied from fault geometry and kinematic indicators (synmetamorphic mineral lineations, inclined isoclinal folds, sheath

folds, and drag folds; Merschat and Kalbas, 2002), proximal to the shear zone (Merschat and Kalbas, 2002); dextral displacement (last movement) is indicated by mantled feldspar porphyroclasts and southwest-verging asymmetric folds. Furthermore, Merschat and Kalbas (2002) documented northeast-southwest-oriented D_2 macroscopic sheath folds in the Brindle Creek thrust hanging wall as evidence for southwest-directed shearing. No greenschist facies retrograde mineral assemblages were found within the Poplar Springs shear zone; thus, the structure is likely late synmetamorphic. Although more sporadic, mylonitic fabrics are also present in the two northwestern bands of Walker Top Granite. Isolated mylonite in various western IP units has been documented by previous workers (e.g., Davis, 1993; Yanagihara, 1994) and may indicate differential strain localization (as documented in 1996 by Worley and Wilson working in the Wenchuan-Maowen Shear Zone, Central Longmen Shan, China) that is impractical to represent at 1:12,000 and 1:24,000 scales.

The Green Mountain fault is a regionally extensive evolved (now Type C) Type-F thrust that, in the southwestern Brushy Mountains, juxtaposed Tallulah Falls Formation, Poor Mountain Formation, and Dysartsville Tonalite over Poor Mountain Formation, Tallulah Falls Formation, and Henderson Gneiss (Plate 1). In the Kings Creek quadrangle, Tallulah Falls Formation metagraywacke in the Green Mountain fault footwall is characterized by a mylonitic, inequigranular texture composed of asymmetric composite plagioclase-quartz and less common quartz porphyroclasts in an annealed fine- to medium-grained biotite-quartz-plagioclase-rich matrix. Muscovite fish (up to 0.3 x 0.1 cm) in several quartz-rich samples define a Type-II S-C mylonitic fabric (Lister and Snoke, 1984) that developed during peak metamorphism (see Fig. 1-28 in Part I).

Asymmetric folds with southeast-dipping axial surfaces, strike-parallel mineral lineations, muscovite fish, and mantled feldspar porphyroclasts in the footwall mylonite reveal components of first dip-slip then dextral strike-slip shearing, probably related to transpression in the zone of constricted flow adjacent to the primordial (Neoacadian/earliest Alleghanian) Brevard fault zone (Hatcher, 2001a). Mylonitized Tallulah Falls Formation metagraywacke in the study area contains annealed amphibolite facies microfabrics that contrast with the lower greenschist facies retrograde assemblage recognized farther west in the Alleghanian Brevard fault zone (Hatcher, 2001a).

Post-early Alleghanian Structures in the Kings Creek Quadrangle

Post-penetrative deformation (post-peak metamorphism; post-Neoacadian/earliest Alleghanian) structures are also well exposed throughout the IP. Previous workers (Davis, 1993; Bream, 1999; Bier, 2001) identified upright open folds oriented subparallel and oblique to D_2 and D_3 fabrics. Refolded macroscopic and mesoscopic fold patterns, dome-and-basin interference patterns, and brittle structures result from D_4, D_5, and D_6 deformation (Plate 1; Table 2-1). Abundant mesoscopic systematic joints are evidence of brittle deformation in the study area. Mesozoic diabase dikes and cataclasites, such as the Pax Mountain fault in South Carolina (Garihan and Ranson, 1992; Garihan et al., 1993), provide abundant evidence of later brittle deformation in the IP, but were not observed in the study area.

Folded fold axes are partly related to post-Neoacadian folding. Two upright open fold sets were identified at both the macro- and mesoscales in the southwestern Brushy Mountains. An orogen-parallel F_4 fold set was refolded by a north-south- and northwest-trending F_5 set (late fold axes; Fig. 2-7).

Five hundred forty-eight joint orientation measurements reveal three dominant joint sets (Fig. 2-10). Set 1 consists of a dominant N 15°W-striking surface and a conjugate (less abundant) N 75°E-striking surface. Set 2 strikes N 10°E and N 80°W; only the dominant surface in set 3 is exposed (strikes ~N 2°W). Most joints in the field area dip steeply (between 75-80 °); the average dip is 71° (Fig. 2-10). Joint sets probably formed during three deformation events (D_4-D_6; Table 2-1). The first accompanied semi-brittle deformation in the Alleghanian Brevard fault zone and is localized in competent layers. Subsequent joint sets (D_5, D_6) developed in response to Alleghanian exhumation of composite crystalline thrust sheets in the Tugaloo terrane, Mesozoic and Cenozoic deformation (e.g., Garihan et al., 1993; Knapp, 2001), and the contemporary stress field (Engelder, 1982).

Structural Interpretation

While cross sections have been labeled ineffective tools for interpreting macroscopic and mesofabric data from polydeformed belts (Ramsay, 1967), the strong parallel orientation of superposed structures in the Kings Creek quadrangle clearly permits their use here. Parallel cross sections A-A′, B-B′, and C-C′ were drawn perpendicular to strike (Fig. 2-5; Plate 2). The sections primarily depict juxtaposition of Brindle Creek thrust hanging wall units atop migmatitic rocks of the Green Mountain thrust sheet. Fold axis and lineation data indicate structures primarily plunge northeast in Domain I.

Section A-A′

Section A-A′ links to a cross section across part of the adjacent Ellendale quadrangle (Merschat and Kalbas, 2002). It depicts isoclinal and tight F_2 and F_3 folds in

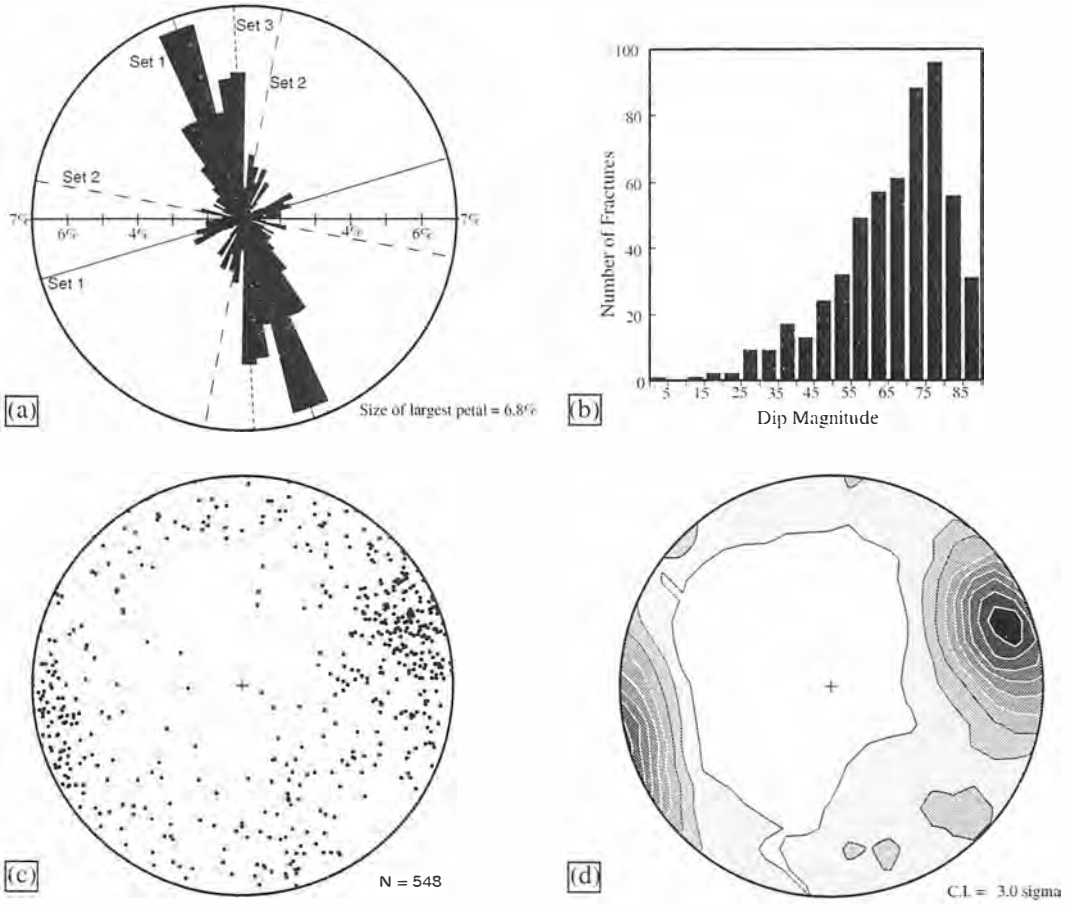

Figure 2-10. Systematic joint orientations in the Kings Creek quadrangle. (a) Rose diagram illustrating the strike of joint planes; major and conjugate (~90° from the dominant) joint pairs are presented as individual sets. (b) Dip magnitude histogram of all joints. (c) Lower hemisphere equal-area scatter plot. (d) Kamb (1959) contour diagram of poles to joints.

hanging wall and footwall units and tight folding of the Brindle Creek thrust trace. Metagraywacke and biotite augen gneisses in the Brindle Creek thrust sheet are shown as conformable, perhaps genetically related units. Sillimanite schist bodies are impossible to differentiate petrologically, and may be in the same stratigraphic position if folded by F_2 isoclinal folds. Walker Top Granite bands are shown as two layer-parallel sills, but could represent one sill on opposite limbs of an F_1 isoclinal fold or an F_2 sheath fold.

Section B-B′

Both the Green Mountain and Brindle Creek faults are crossed by section B-B′. Parasitic (F_3) folds are depicted along both thrust faults and along the limbs of the large antiform in the Brindle Creek thrust sheet (Fig. 2-5). Merschat and Kalbas (2002) proposed initial movement on the Poplar Springs shear zone during D_2; sections B-B′, however, depicts the shear zone crosscutting the Brindle Creek thrust trace. My map data show the D_{3a} axial planar Poplar Springs shear zone originated as a Type-F thrust that produced minor displacement along the northwestern limb of a F_3 fold in metagraywacke. Up-plunge projection of map data (Fig. 2-2) indicates a D_{3b} thrust splay originating at the Poplar Springs shear zone cut the F_3 metagraywacke antiform in the map and above the present erosion surface. Walker Top Granite does not crop out at the present erosion level adjacent to the projected Poplar Springs shear zone and no mylonitic fabrics crop out at section B-B′. All structures were overprinted by open folding. Trends in footwall amphibolite bodies outline F_3 tight upright folds; isoclinal-tight (F_3) and open folds (F_4) also crop occur along the Brindle Creek thrust and in hanging wall units. Granitoid bodies in the Green Mountain thrust sheet can be interpreted as early katazonal melts (perhaps related to the Dysartsville Tonalite). Alternatively, the granitoids may be

crustally derived melts that intruded the migmatite just prior to Brindle Creek thrusting; no contact aureoles are known, however, thus intrusion is thought to have been katazonal. Footwall granitoids were truncated by the Brindle Creek thrust and caught up in D_2 and D_3 deformation. Lenticular outliers of Henderson Gneiss were interpreted by Hatcher (2002) to be either isolated bodies that intruded the Tallulah Falls Formation during Ordovician magmatism or "synformal outliers of sheath fold hinges," a result of Acadian dextral noncoaxial deformation.

Section C-C′

An interesting feature of cross section C-C′ is a northeast-plunging upright antiform-synform pair (F_4) that refolds isoclinal (F_2) and tight (F_3) folds in metasedimentary units of the Brindle Creek thrust sheet (Fig. 2-5). Tight refolding of the Brindle Creek thrust again explains the relatively wide outcrop (~0.85 km) of Hibriten orthogneiss adjacent to the thrust. As in section B-B′, the Poplar Springs shear zone is thought to have minor displacement parallel or subparallel to the common limb of a F_3 fold in metagraywacke, and again demonstrates D_{3a} Type-F shearing of common fold limbs. Tight folds in the Green Mountain thrust sheet are marked at map scale by folded amphibolite bodies.

Brindle Creek Thrust Sheet in the Kings Creek Quadrangle

Complex structural patterns in the Brindle Creek thrust sheet warrant special attention. Several explanations for the macroscopic distribution of Walker Top Granite are plausible. It is possible that emplacement of the Walker Top Granite occurred prior to or during D_1. Bands 1 and 2 (Fig. 2-2) in this model are the same layer that was isoclinally folded along with host rocks during Acadian deformation (F_1). If this is

correct, metagraywacke should be present northwest of the northwesternmost sillimanite schist body. Metagraywacke was not found beyond the schist, however, therefore map patterns in the Kings Creek quadrangle do not support a pre-D_1 intrusion hypothesis.

Alternatively, map patterns and cross sections may reflect post-D_1 emplacement of Walker Top Granite. Two hypotheses deserve consideration; if either is correct, the timing of eastern IP D_1 is constrained between the age of sediment deposition (~400 Ma; Bream, 2002) and Walker Top Granite intrusion (366 Ma; Giorgis et al., 2002; Mapes, 2002). First, the Walker Top Granite may have intruded as a series of lenticular sills. Lower- to midcrustal intrusion of the Walker Top Granite (Giorgis et al., 2002) generally parallel to S_1 may have occurred prior to peak latest Neoacadian and earliest Alleghanian synkinematic metamorphism. Outliers constitute satellite intrusions that were sufficiently insulated to grow the characteristic microcline-dominated porphyritic texture with no chilled margins. This hypothesis presents a thermodynamic problem because no textural or compositional differences between main and satellite bodies was observed. Degrees of chemical differentiation and cooling histories of both small and large Walker Top bodies would be required, in this model, to be identical. Bands 1 and 2 (Fig. 2-2), rather than representing opposite limbs of an F_1 fold, would be separate layer-parallel bodies within the same limb of an F_2 synform (Fig. 2-5). Walker Top Granite Band 3 would also have been intruded as a sill.

A second hypothesis, favored here, states that a single, homogeneous, katazonal Walker Top Granite pluton intruded the country rock and was strongly deformed to its present, disarticulated lenticular geometry during peak Neoacadian deformation. Both northwestern and southeastern Walker Top Granite bands are most simply interpreted as

northeast-plunging macroscopic F_2 sheath folds produced by southwest-directed flow (Fig. 2-2; Merschat and Kalbas, 2002). This interpretation is supported by mesoscopic fabrics (aligned sillimanite and amphibole mineral lineations, foliation-parallel mesoscopic sheath fold axes, and rotated porphyroclasts indicating dextral simple shear in the Brindle Creek thrust sheet). Mesoscopic sheared textures and macroscopic sheath folds are consistent with flow in deep-crustal shear zones (Worley and Wilson, 1996; Alsop and Holdsworth, 1999; Snoke et al., 1999). As discussed below, the sheath fold model is also consistent with the Neoacadian kinematic history of this portion of the IP.

An important question is why the trace of the Poplar Springs shear zone is discontinuous in the southwestern Brushy Mountains. Why did northwest-, then southwest-directed simple shear occur at both ends of the Poplar Springs shear zone in the Kings Creek quadrangle, but not in the center? Alsop and Holdsworth (1999) presented a generic model wherein major and secondary sheath fold culminations are separated by zones of reduced shear strain. Mylonite in the Poplar Springs shear zone may represent macroscopic sheath fold culminations with axes subparallel to cross-section lines A-A′ and C-C′. The nonmylonitic region may be a zone where strain was accommodated by ductile folding without faulting or mylonitization. Another explanation is also plausible. The shear zone is thought to have variable along-strike displacement (compare cross sections B-B′ and C-C′ in Figure 2-5). The discontinuous trace of the Poplar Springs shear zone was suggested by Merschat and Kalbas (2002) to be a result of incipient attenuation of noncylindrical folds.

Textures and crosscutting relationships in the Kings Creek quadrangle provide significant insight into the relative timing and kinematics of latest Neoacadian/earliest

Alleghanian and post-early Alleghanian deformation and certain rheological properties of the deforming rocks. The Brindle Creek and Green Mountain faults are interpreted as Type-C faults that nucleated as Type-F thrusts. Footwall synforms (the result of attenuation and shearing along common limbs of isoclinal folds) were not recognized in the Kings Creek quadrangle, but are well documented in the western IP to the southwest (Plate 1). Passive flow (no layer participation) under high-grade metamorphic conditions (Part I) likely produced penetrative F_2 and F_3 (estimated to be Class 2; Ramsay, 1962, 1963) folds in the study area (Fig. 2-8a). Both F_2 and F_3 flexural flow folds are also abundant in the study area (also F_3; Fig. 2-8b). F_3 crenulations (chevron fold geometries) may indicate at some point during D_3 layer parallel slip was no longer mechanically favorable (Johnson and Ellen, 1974).

As noted by workers in southwestern North Carolina (e.g., Davis, 1993), southwest-oriented L_2 mineral stretching lineations and F_2 fold axes likely represent southwest-directed heterogeneous simple shear and lateral transpressional flow of plastically deforming rocks. If D_3 structures formed after dextral strike-slip motion ceased, no appreciable change in fold axis orientations should be observed across the domain boundary. Trends clearly deflect into a northeast-southwest parallelism in Domain I (Figs. 2-7, 2-9), therefore southwest-directed transpressional flow likely continued during D_3. Slicken surfaces (oriented northwest and east-west) on several late open fold limbs indicate formation of F_4 and F_5 by flexural slip and buckling.

Synthesis

Structural fabrics in the Kings Creek quadrangle record most of the polyphase deformational history of the IP and can be divided into three age groups: pre-Acadian to

Neoacadian, latest Neoacadian/earliest Alleghanian, and post-early Alleghanian. No conclusive evidence for pre-Acadian to Neoacadian deformation (D_1) in the western IP is exposed in the Kings Creek quadrangle. D_1 is represented in the eastern IP of the Kings Creek quadrangle by multiply deformed quartz-mica textures (Fig. 2-4), truncated foliations and rootless folds in boudins, and metasedimentary rocks that may have been deformed prior to Walker Top Granite intrusion. D_2 and D_3 structures are abundant in the Kings Creek quadrangle, and, as concluded in similar studies, can be attributed to deformation during late Neoacadian and earliest Alleghanian tectonothermal events. Parallel and subparallel axial planar foliations (S_2), northwest-verging F_2 passive and flexural flow folds, axial surfaces (S_3) of F_3 passive and flexural flow folds, and coaxial mineral stretching lineations (L_2) may represent continued (if 330 Ma zircon rim growth is a result of influx of hot fluids; Part III) or punctuated deformation during synmetamorphic to slightly post-peak metamorphic tectonic events. Davis (1993) characterized the D_3 event as post-peak metamorphic deformation of still ductile rocks. Curl (1997), working in the South Carolina IP, concluded D_3 was Alleghanian based on overprinted lineations. Symmetric chevron geometries (Johnson and Ellen, 1974) in numerous southwestern Brushy Mountain F_3 folds indicate a cessation of layer-parallel slip between some gneissic layers. Predominance of flexural flow processes supports post-peak metamorphism, earliest Alleghanian D_3. Post-early Alleghanian deformation in the southwestern Brushy Mountains is characterized by upright open folds (F_4 and F_5) and multiple joint sets formed from Alleghanian exhumation of the Tugaloo terrane, Mesozoic extension (e.g., Garihan et al., 1993), Cenozoic uplift and exhumation (e.g., Knapp, 2001), and the current stress field.

Several workers (e.g., Davis, 1993; Hatcher, 2001a; Merschat and Kalbas, 2002) recognized the change in macroscopic trends from east-west and northwest orientations in the "deeper IP" (in this case the eastern IP) to northeast-southwest orientations proximal to the Brevard fault zone (Plate 1). That important structural pattern is clearly manifested in the Kings Creek quadrangle. Overall northwest verging structures in Domain I are the best evidence for initial dip-slip convergence. Synkinematic sillimanite growth "tracks" flow paths (Worley and Wilson, 1996; Merschat and Kalbas, 2002), however, and records deflection of thrust sheets. Southwest-directed flow can be attributed to constricted, internal, dextral (with respect to the eastern Blue Ridge) plastic flow caused by buttressing of thin crystalline thrust sheets against the primordial (Neoacadian to earliest Alleghanian) Brevard fault zone (Hatcher, 2001a). Moreover, Type-II S-C mylonite in the footwall of the Green Mountain fault here can be attributed to the D_2-D_3 event, and, along with mineral stretching lineations, indicate significant southwest-directed flow in the northeast-southwest-trending zone adjacent to the Brevard fault zone. Data from this study support the conclusions of Davis (1993) and subsequent workers; the dominant transpositional deformation event likely occurred in the Neoacadian and had a significant dextral flow component. Data from this study also indicate the flow boundary is not coincident with the Brindle Creek thrust, but is the Domain I-II boundary. Thus, a similar flow regime in both the Green Mountain the Brindle Creek thrust sheets at the time of transpression can be inferred.

Detailed geologic mapping in the southwestern Brushy Mountains allows broad regional comparisons of macroscopic patterns. The outcrop width of the western IP decreases from southwestern North Carolina to the present study area (Plate 1).

Moreover, western IP units and both major thrust faults exposed in the Kings Creek quadrangle dip more steeply (30-50°) than equivalent units and structures in southwestern North Carolina (typically 10-30°). Macroscopic trends may indicate increased contraction along the Brindle Creek thrust in the northeastern portion of the IP. Alternatively, differences in exposure at the current erosional level can be attributed to: (1) thinning of primary sedimentary packages to the northeast; (2) differential erosion; (3) D_4 formation of crustal-scale dome-and-basin structures (a product of refolding; the northeastern IP would reside in a basin); or (4) an increased original thickness of eastern IP sedimentary units in the northeast. The zone of constricted flow overprints the Brindle Creek thrust trace in the southwestern Brushy Mountains. For this reason, it is most likely that either the original sedimentary packages in the northeastern IP were thinner, or more dip-slip displacement occurred in the southwestern Brushy Mountains than in the Columbus Promontory or the South Mountains.

Conclusions

- Structures in the Kings Creek quadrangle are consistent with the conceptual framework for the relative order of events proposed by Davis (1993) and modified by Yanagihara (1994), Bream (1999), Hill (1999), and Bier (2001). Data from this study support a qualitative model for oblique convergence and/or buttressing of plastically deforming units against the primordial (latest Neoacadian/ earliest Alleghanian) Brevard fault zone. Transpression likely resulted in a zone of constricted flow wherein a significant dextral (with respect to the eastern Blue Ridge) simple shear component produced orogen-parallel lineation patterns and strike-slip kinematic indicators.

- Two major northwest- to southwest-verging faults, the Brindle Creek thrust and the Green Mountain fault, strike ~N55°E across the Kings Creek quadrangle and are laterally continuous throughout the North Carolina IP.

- Penetrative structures in the Kings Creek quadrangle developed during the Neoacadian tectonothermal event and are dominantly oriented northeast-southwest. In Domain II, however, structural trends are north-south and east-west.

- The zone of constricted flow overprints the Brindle Creek thrust trace in the southwestern Brushy Mountains.

- Passive and flexural flow fold mechanisms created F_2 and some F_3 structures; more competent S_2 layers deformed by flexural flow during F_3.

- Structures in the Kings Creek quadrangle are crosscut by two younger generations of open folds and three joint sets.

References Cited

Alsop, G. I., and Holdsworth, R. E., 1999, Vergence and facing patterns in large-scale sheath folds: Journal of Structural Geology, v. 21, p. 1335-1349.

Bier, S. E., 2001, Geology of the southeastern South Mountains, North Carolina [unpublished M.S. thesis]: Knoxville, University of Tennessee, 162 p.

Bream, B. R., 1999, Structure and stratigraphic relationships of ortho- and paragneisses southwest of Marion, North Carolina [unpublished M.S. thesis]: Knoxville, University of Tennessee, 155 p.

Bream, B. R. 2002, The southern Appalachian Inner Piedmont: new perspectives and enduring issues based on recent detailed mapping, isotopic evidence, and geochronology: *in* Hatcher, R. D., Jr., and Bream, B. R., eds., Inner Piedmont tectonics focused mostly on detailed studies in the South Mountains and the southern Brushy Mountains, North Carolina: Carolina Geological Society Guidebook, North Carolina Geological Survey, p. 45-64.

Bream, B. R., Hatcher, R. D., Jr., Miller, C. F., and Fullagar, P. D., 2001, Geochemistry and provenance of Inner Piedmont paragneisses, NC and SC: Evidence for an internal terrane boundary: Geological Society of America Abstracts with Programs, v. 33, p. A-65.

Bream, B. R., Hatcher, R. D., Jr., Miller, C. F., and Fullagar, P. D., in review, Detrital zircon ages and Nd isotopic data from the southern Appalachian crystalline core, GA-SC-NC-TN: New provenance constraints for Laurentian margin paragneisses: *in* Tollo, R. P., and Bartholomew, M. J., eds., Proterozoic evolution of the Grenville Orogen in North America: Geological Society of America Special Paper.

Bryant, B., and Reed, J. C., Jr., 1970, Geology of the Grandfather Mountain window and vicinity, North Carolina and Tennessee: U.S. Geological Survey Professional Paper 614, 189 p.

Butler, J. R., 1991, Metamorphism, *in* Horton, J. W., Jr., and Zullo, V. A., eds., The geology of the Carolinas, Carolina Geological Society 50th Anniversary Volume: Knoxville, University of Tennessee Press, p. 127-142.

Carrigan, C. W., Bream, B. R., Miller, C. F., and Hatcher, R. D., Jr., 2001, Ion microprobe analyses of zircon rims from the eastern Blue Ridge and Inner Piedmont, NC-SC-GA: Implications for the timing of Paleozoic metamorphism in the southern Appalachians: Geological Society of America Abstracts with Programs, v. 33, p. A-42.

Conley, J. F., and Drummond, K. M., 1975, The geology of Polk County, North Carolina: North Carolina Geological Survey unpublished map, scale 1:125,000.

Curl, D. C., 1998, Stratigraphy and structure of Wellford and Reidville quadrangles in part of the eastern Inner Piedmont, near Spartanburg, South Carolina [unpublished M.S. thesis]: Knoxville, University of Tennessee, 129 p.

Dallmeyer, R. D., 1988, Late Paleozoic tectonothermal evolution of the western Piedmont and eastern Blue Ridge, Georgia: Controls on the chronology of terrane accretion and transport in the southern Appalachian orogen: Geological Society of America Bulletin, v. 100, p. 702-713.

Davis, T. L., 1993, Lithostratigraphy, structure, and metamorphism of a crystalline thrust terrane, western Inner Piedmont, North Carolina [unpublished Ph.D. dissertation]: Knoxville, University of Tennessee, 245 p.

Davis, T. L., Hatcher, R. D., Liu, A., and Tabor, J. R., 1991, Southern Appalachian western Inner Piedmont: A progressive crustal-scale shear zone: Geological Society of America Abstracts with Programs, v. 23, p. A-138.

Dennis, A. J., and Wright, J. E., 1997, Middle and late Paleozoic monazite U-Pb ages, Inner Piedmont, South Carolina: Geological Society of America Abstracts with Programs, v. 29, p. A-223.

Engelder, T., 1982, Is there a genetic relationship between selected regional joints and contemporary stress within the lithosphere of North America?: Tectonics, v. 1, p. 161-177.

Fullagar, P. D., 1971, Age and origin of plutonic intrusions in the Piedmont of the southeastern Appalachians: Geological Society of America Bulletin, v. 82, p. 2845-2862.

Fullagar, P. D., 1981, Summary of Rb-Sr whole-rock ages for South Carolina: South Carolina Geology, v. 25, p. 29-32.

Fullagar, P. D., Goldberg, S. A., and Butler, J. R., 1997, Nd and Sr isotopic characterization of crystalline rocks from the southern Appalachian Piedmont and Blue Ridge, North and South Carolina, *in* Sinha, A. K., Whalen, J. B., and Hogan, J. P., eds., The nature of magmatism in the Appalachian orogen: Boulder, Colorado, Geological Society of America Memoir 191, p. 165-179.

Garihan, J. M., and Ranson, W. A., 1992, Structure of the Mesozoic Marietta-Tryon graben, South Carolina and adjacent North Carolina, *in* Bartholomew, M. J., Hyndmann, D. W., Mogk, D. W., and Mason, R., eds., Basement tectonics 8: Characterization and comparison of ancient and Mesozoic continental margins, Proceedings of the 8th International Conference on Basement Tectonics: Dordrecht, Germany, Kluwer Academic Publishers, p. 539-555.

Garihan, J. M., Preddy, M. S., and Ranson, W. A., 1993, Summary of mid-Mesozoic brittle faulting in the Inner Piedmont and nearby Charlotte belt of the Carolinas, *in* Hatcher, R. D., Jr., and Davis, T. L., eds., Studies of Inner Piedmont geology with a focus on the Columbus Promontory: Carolina Geological Society Field Trip Guidebook, p. 55-66.

Giorgis, S. D., 1999, Inner Piedmont geology of the northwestern South Mountains near Morganton, North Carolina [unpublished M.S. thesis]: Knoxville, University of Tennessee, 191 p.

Goldsmith, R., Milton, D. J., and Horton, J. W., 1988, Geologic map of the Charlotte 1° x 2° quadrangle, North Carolina and South Carolina: U.S. Geological Survey Map I-125-E, scale 1:250,000.

Giorgis, S. D., Mapes, R. W., and Bream, B. R., 2002, The Walker Top Granite: Acadian granitoid or eastern Inner Piedmont basement?: *in* Hatcher, R. D., Jr., and Bream, B. R., eds., Inner Piedmont tectonics focused mostly on detailed studies in the South Mountains and the southern Brushy Mountains, North Carolina: Carolina Geological Society Guidebook, North Carolina Geological Survey, p. 33-44.

Harper, S. B., and Fullagar, P. D., 1981, Rb-Sr ages of granitic gneisses of the Inner Piedmont belt of northwestern North Carolina and southwestern South Carolina: Geological Society of America Bulletin, v. 92, p. 864-872.

Hatcher, R. D., Jr., 1970, Stratigraphy of the Brevard zone and Poor Mountain area, northwestern South Carolina: Geological Society of America Bulletin, v. 81, p. 933-940.

Hatcher, R. D., Jr., 1998, Structure of the Appalachian Inner Piedmont: Geological Society of America Abstracts with Programs, v. 30, p. A-17.

Hatcher, R. D., Jr., 2001a, Rheological partitioning during multiple reactivation of the Palaeozoic Brevard Fault Zone, Southern Appalachians, USA, *in* Holdsworth, R. E., Strachan, R. A., Magloughlin, J. F., and Knipe, R. J., eds., The nature and tectonic significance of fault zone weakening: Geological Society of London Special Publication 186, p. 255-269.

Hatcher, R. D., Jr., 2001b, Terranes and terrane accretion in the southern Appalachians: An evolved working hypothesis: Geological Society of America Abstracts with Programs, v. 33, P. A-65.

Hatcher, R. D., Jr., 2002, An Inner Piedmont Primer: *in* Hatcher, R. D., Jr., and Bream, B. R., eds., Inner Piedmont tectonics focused mostly on detailed studies in the South Mountains and Brushy Mountains, North Carolina: Carolina Geological Society Guidebook, North Carolina Geological Survey, p. 1-18.

Hatcher, R. D., Jr., and Hooper, R. J., 1992, Evolution of crystalline thrust sheets in the internal parts of mountain chains, *in* McClay, K. R., ed., Thrust tectonics: London, Chapman and Hall, p. 217-234.

Hatcher, R. D., Jr., Bream, B. R., Hill, J. C., Giorgis, S. D., and Williams, S. T., 1999, Transect through the Acadian orogen in the Carolinas and northeast Georgia: Geological Society of America Abstracts with Programs, v. 31, p. A-19.

Hatcher, R. D., Jr., Osberg, P. H., Drake, A. A., Jr., Robinson, P., and Thomas, W. A., 1990, Tectonic map of U.S. Appalachians, *in* Hatcher, R. D., Jr., Thomas, W. A., and Viele, G. W., eds., The Appalachian–Ouachita orogen in the United States: Boulder, Geological Society of America, The geology of North America, v. F–2, Plate 1, scale 1:2,000,000.

Hill, J. C., 1999, Stratigraphy, structure, and tectonics of part of the southern Appalachian Inner Piedmont, near Marion, North Carolina [unpublished M.S. thesis]: Knoxville, University of Tennessee, 188 p.

Johnson, A. M., and Ellen, S. D., 1974, A theory of concentric, kink, and sinusoidal folding and of monoclinal flexuring of compressible, elastic multilayers: Tectonophysics, v. 21, p. 301-339.

Kamb, W. B., 1959, Ice petrofabric observations from Blue Glacier, Washington, in relation to theory and experiment: Journal of Geophysical Research, v. 64, p. 1891-1909.

Kalbas, J. L., Merschat, A. J., Hatcher, R. D., Jr., and Bream, B. R., 2001, Detailed geologic mapping of the Brushy Mountains, Inner Piedmont, near Lenoir, North Carolina: Geological Society of America Abstracts with Programs, v. 33, p. A-82.

Knapp, J. H., 2001, Cenozoic tectonic evolution of southeastern North America: Evidence for passive margin uplift?: Geological Society of America Abstracts with Programs, v. 33, p. A-6.

Lemmon, R. E., 1973, Geology of the Bat Cave and Fruitland quadrangles and the origin of the Henderson Gneiss, western North Carolina [unpublished Ph.D. dissertation]: Chapel Hill, University of North Carolina, 145 p.

Lister, G. S., and Snoke, A. W., 1984, S–C mylonites: Journal of Structural Geology, v. 6, p. 617–638.

Mapes, R. W., 2002, Geochemistry and geochronology of mid-Paleozoic granitic plutonism in the southern Appalachian Piedmont terrane, North Carolina-South Carolina-Georgia [unpublished M.S. thesis]: Vanderbilt University, 140 p.

Mapes, R. W., Maybin, A. H., III, Miller, C. F., Fullagar, P. D., and Bream, B. R., 2002, Geochronology and geochemistry of mid Paleozoic granitic magmatism, central and eastern Inner Piedmont, NC & SC: Geological Society of America Abstracts with Programs, v. 34, p. A-94.

McSween, H. Y., Speer, J. A., and Fullagar, P. D., 1991, Plutonic rocks, *in* Horton, J. W., Jr., and Zullo, V. A., eds., The geology of the Carolinas: Carolina Geological Society 50th Anniversary Volume: Knoxville, University of Tennessee Press, p. 109-126.

Merschat, A. J., and Kalbas, J. L., 2002, Geology of the southern Brushy Mountains, North Carolina Inner Piedmont, *in* Hatcher, R. D., Jr., and Bream, B. R., eds., Inner Piedmont tectonics focused mostly on detailed studies in the South Mountains and Brushy Mountains, North Carolina: Carolina Geological Society Guidebook, North Carolina Geological Survey, p. 101-126.

Odom, A. L., and Fullagar, P. D., 1973, Geochronological and tectonic relationship between the Inner Piedmont, Brevard zone, and Blue Ridge belts, North Carolina: American Journal of Science, v. 273-A, p. 133-149.

Odom, A. L., and Russell, G. S., 1975, The time of regional metamorphism of the Inner Piedmont, North Carolina, and Smith River allochthon: Inference from whole-rock ages: Geological Society of America Abstracts with Programs, v. 7, p. 522-523.

Ramsay, J. G., 1962, The geometry and mechanics of formation of "similar" type folds: Journal of Geology, v. 70, p. 309-327.

Ramsay, J. G., 1963, Structure and metamorphism of the Moine and Lewisian rocks of the northwest Caledonides, *in* Johnson, M. R. W., and Seward, F. H., eds., The British Caledonides: Edinburgh, Oliver and Boyd, Ltd., p. 1434-1475.

Ramsay, J. G., 1967, Folding and fracturing of rocks: London, McGraw-Hill, 568 p.

Reed, J. C., 1964, Geology of the Lenoir quadrangle, North Carolina: U. S. Geological Survey Map I-709-A, scale 1:62,500

Snoke, A. W., Kalakay, T. J., Quick, J. E., and Sinigoi, S., 1999, Development of a deep-crustal shear zone in response to syntectonic intrusion of mafic magma into the lower crust, Ivrea–Verbano zone, Italy: Earth and Planetary Science Letters, v. 166, p. 31-45.

Vinson, S. B., and Miller, C. F., 1999, Constraints on the timing of Inner Piedmont plutonism, N.C.-S.C., from ion microprobe U-Pb zircon analysis: Geological Society of America Abstracts with Programs, v. 31, p. A-77.

Whisnant, J. S., 1975, Geology of the southeast quarter of the Marion 15-minute quadrangle, North Carolina [unpublished M.S. thesis]: Chapel Hill, University of North Carolina, 50 p.

Williams, S. T., 2000, Structure, stratigraphy, and migmatization in the southwestern South Mountains, North Carolina [unpublished M.S. thesis]: Knoxville, University of Tennessee, 111 p.

Worley, B. A., and Wilson, C. J. L., 1996, Deformation partitioning and foliation reactivation during transpressional orogenesis, an example from the Central Longmen Shan, China: Journal of Structural Geology, v. 18, p. 395-411.

Yanagihara, G. M., 1994, Structure, stratigraphy, and metamorphism of a part of the Columbus Promontory, western Inner Piedmont, North Carolina [unpublished M.S. thesis]: Knoxville, University of Tennessee, 214 p.

PART III

Intense migmatization beneath the Brindle Creek thrust separating the eastern and western Inner Piedmont, North Carolina: Distribution, geochronology, geochemistry, and petrogenesis

Abstract

The northeastern extension of the Brindle Creek thrust has recently been documented in the southwestern Brushy Mountains, North Carolina. This fault is a major structural boundary that is continuous throughout central western and southwestern North Carolina. Field, petrologic, and whole-rock chemical data from migmatitic amphibolite and biotite-hornblende granodiorite in the footwall of this thrust confirm like lithologies at several sights mapped in detail and imply lateral continuity of a wide (< 2 to 10 km) zone of intense migmatization for at least 110 km in North Carolina. Mesoscopic structures and whole-rock major and trace element chemistry of one leucosome and numerous melanosome samples indicate pervasive anatectic conditions between 630 and 700 °C produced diatexite. Coaxial folding of migmatite melanosome and leucosome denotes synchronous metamorphic (anatectic) differentiation and deformation during D_2. Synmetamorphic emplacement of the hot Brindle Creek thrust sheet may have affected heat transfer to the footwall near peak metamorphism allowing favorable conditions for creation of the zone of intense migmatization. Trace element concentrations indicate partial melt segregation of impure leucosome from the intermediate or mafic protolith. Localized subsolidus metamorphic differentiation and metasomatism, unlike other petrogenetic processes, cannot be ruled out by rare earth element chemistry in this case.

Geometric, temporal, and geochemical evidence indicates the migmatite protolith likely included the Poor Mountain Amphibolite. Detailed geologic mapping in the Kings Creek quadrangle places the intense migmatite zone structurally above the Tallulah Falls Formation in the stratigraphic position of the Poor Mountain Formation. Synclinal preservation of Poor Mountain Formation rocks occurs immediately below major thrust

faults in the South Mountains to the southwest and may exist in the Brushy Mountains although this structural relationship is unclear here. Intense migmatization has destroyed any primary sedimentological or volcanic features that would unequivocally reveal the migmatite protolith. U-Pb ion microprobe geochronology of zircons from the migmatite zone indicates crystallization of the migmatite protolith at ~450 Ma and subsequent metamorphic pulses at 342 Ma (coeval with latest Neoacadian deformation) and 330 Ma (coeval with earliest Alleghanian deformation). The Poor Mountain Formation (dated here by zircons from the Poor Mountain Quartzite member) and several western Inner Piedmont granitoids have nearly coeval Ordovician crystallization ages and are the most likely candidates, based solely on geochronologic constraints, for the migmatite protolith. Spatial and temporal data strongly favor a Poor Mountain Formation protolith for the migmatite; major and trace element data indicate migmatite adjacent to the Brindle Creek thrust is chemically compatible with the Poor Mountain Amphibolite, but a subset of melanosome samples from a lower position in the thrust sheet have trace element concentrations that consistently have identical rare earth element (REE) fractionation trends and trace element concentrations as Tallulah Falls metagraywacke. It is possible the former are derived from Tallulah Falls Formation rocks, whereas rocks closer to the fault have a Poor Mountain Amphibolite protolith.

Introduction

Renewed attention has recently been focused on the processes and tectonic importance of migmatite formation (e.g., Nabelek et al., 1999; Thompson, 2001). The spatial and temporal coincidence of *in situ* and allochthonous granitic magmatism, migmatization, and deformation zones is also well documented (e.g., Hollister and

Crawford, 1986; Druguet and Hutton, 1998). A sequence of events for a given area, however, can be difficult to differentiate without detailed geologic mapping, geochronology, and geochemical characterization of exposed rocks. The Inner Piedmont has long been recognized as a migmatitic belt composed dominantly of sillimanite grade metamorphic assemblages (King, 1950, Griffin, 1967; Hatcher; 1970; Butler, 1991). Available data, however, have been largely limited to field observations and a small, but growing quantity of geochronologic (e.g., Dennis and Wright, 1997) and geochemical (e.g., Mirante and De La Rosa, 2001) studies addressing the timing and conditions of metamorphism and migmatization.

New detailed geologic mapping in the Kings Creek quadrangle, North Carolina, has revealed a laterally extensive zone of intense migmatization in the immediate footwall of the Brindle Creek thrust, potentially a crustal-scale boundary in southwestern and central western North Carolina (Fig. 3-1; Giorgis et al., 1998; Williams, 2000; Bream et al., 2001b; Kalbas et al., 2001, 2002; Merschat and Kalbas, 2002). Despite the recognition of intensely migmatized rocks by several workers (Reed, 1964; Goldsmith et al., 1988; Giorgis, 1999; Williams, 2000; Merschat and Kalbas, 2002), their temporal, geometric, and kinematic relationships to the Brindle Creek thrust, and their petrogenesis have not previously been investigated. This study compares the macroscopic distribution, petrology, and whole-rock major- and minor-element chemistry of the prominent unit in the footwall migmatite complex to those of possible protoliths (including the favored Poor Mountain Formation). The goal is to acquire an understanding of the distribution, age, and composition of the migmatite, and to infer its

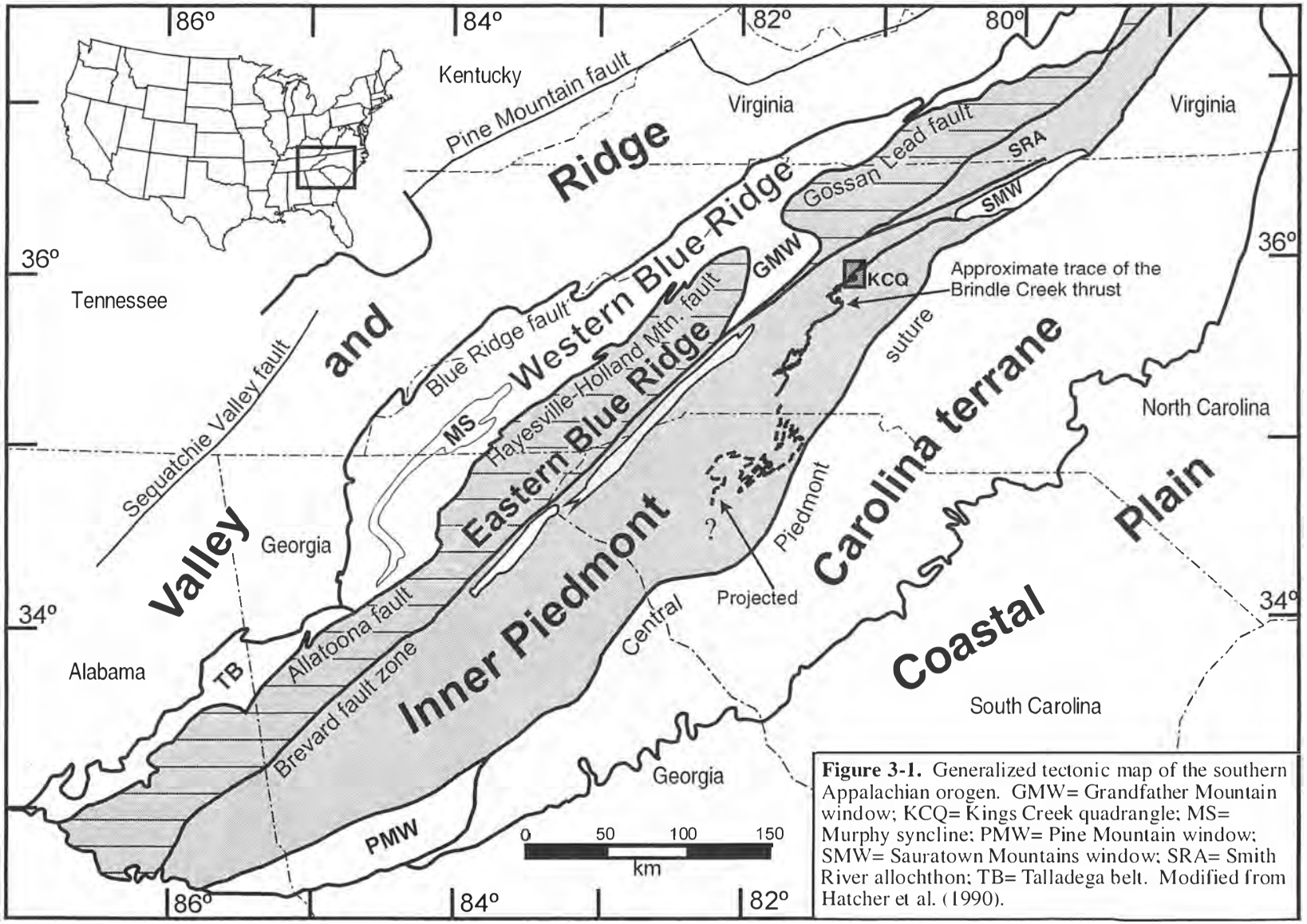

Figure 3-1. Generalized tectonic map of the southern Appalachian orogen. GMW= Grandfather Mountain window; KCQ= Kings Creek quadrangle; MS= Murphy syncline; PMW= Pine Mountain window; SMW= Sauratown Mountains window; SRA= Smith River allochthon; TB= Talladega belt. Modified from Hatcher et al. (1990).

protolith, petrogenesis, and kinematic relationships to middle to late Paleozoic thrust emplacement, deformation, and metamorphism.

Macroscopic Relationships

The Brindle Creek thrust is now recognized as the boundary between the eastern and western Inner Piedmont, and may represent a terrane boundary (Bream et al., 2001a). Evidence for faulting has been documented by Giorgis et al. (1998), Bier et al. (2000), Kalbas et al. (2002), and Merschat and Kalbas (2002), and consists mainly of structural and lithologic truncations and diachronous relationships across the boundary (Bream et al., 2001b). The eastern Inner Piedmont, from the Brindle Creek thrust southeastward to the central Piedmont suture, consists of a series of paragneiss units (mostly aluminous schist and biotite gneiss) and amphibolite, and contains Devonian and Mississippian granitoids. Complex, north-south-, northwest-southeast-, and east-west-trending isoclinal-recumbent and open folds in the southeastern part of the Brindle Creek thrust sheet (Domain II; Part II) contrast with pronounced northeast-trending structures in the western Inner Piedmont and the eastern Inner Piedmont adjacent to the Brindle Creek thrust. The western Inner Piedmont southeast of the Brevard fault zone contains successive thrust stacks of early Paleozoic paragneisses that were intruded by Ordovician plutons (Fig. 3-2; Plate 1). The Brindle Creek thrust, where it has been mapped in detail in southwestern and central western North Carolina, juxtaposes migmatitic biotite gneiss, sillimanite schist, and Devonian orthogneisses over migmatitic amphibolite, quartzite, schistose quartzite, granodiorite, and biotite gneiss. Similar lithotectonic relationships, extrapolated into South Carolina, may indicate the Brindle Creek thrust continues southwestward for a minimum of ~40 km into Greenville County, South Carolina (Fig. 3-

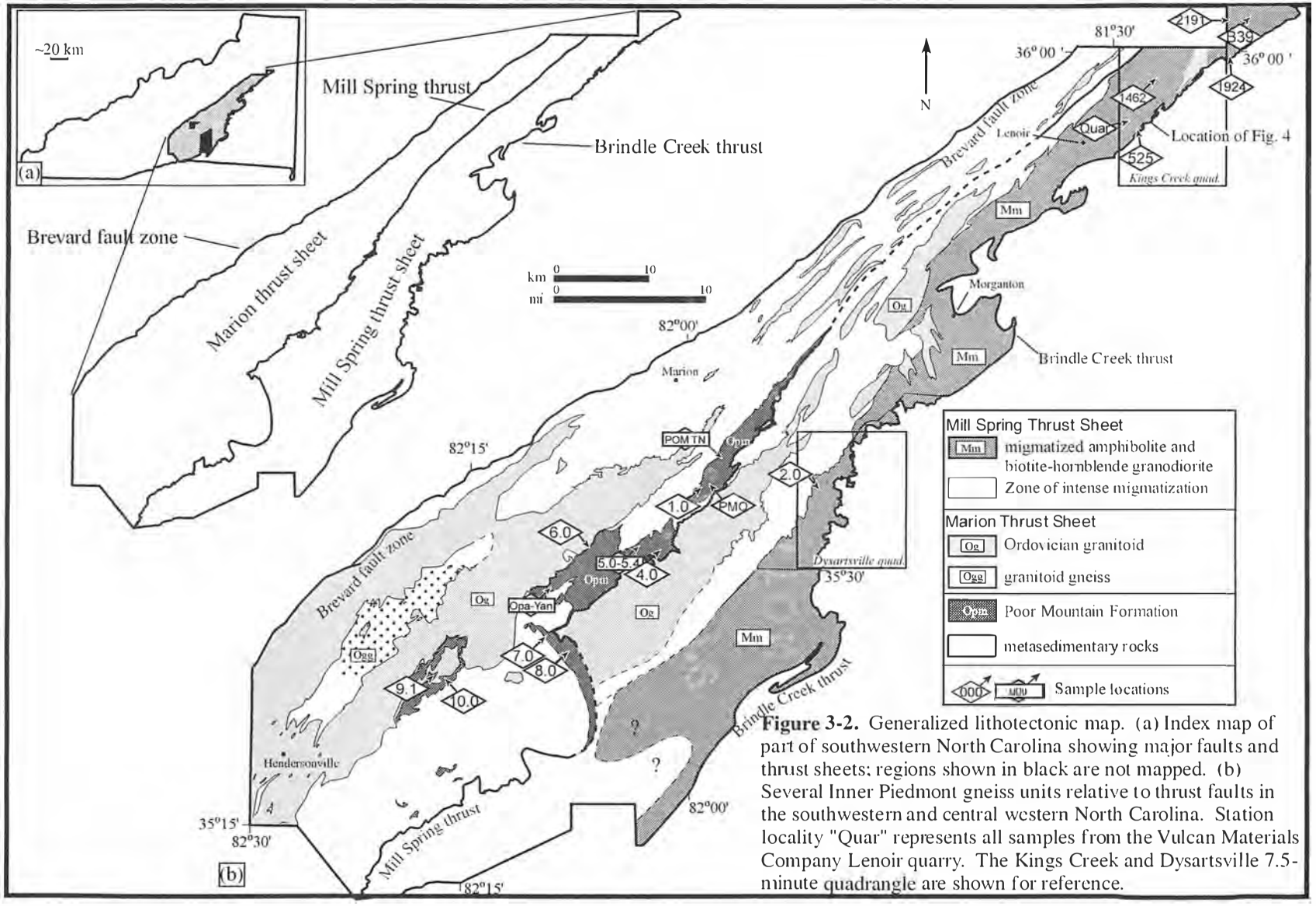

Figure 3-2. Generalized lithotectonic map. (a) Index map of part of southwestern North Carolina showing major faults and thrust sheets; regions shown in black are not mapped. (b) Several Inner Piedmont gneiss units relative to thrust faults in the southwestern and central western North Carolina. Station locality "Quar" represents all samples from the Vulcan Materials Company Lenoir quarry. The Kings Creek and Dysartsville 7.5-minute quadrangle are shown for reference.

1; Nelson et al., 1987; Curl, 1997a, 1997b; Niewendorp et al., 1997; Maybin, 1998; Maclean and Blackwell, 2001).

The Mill Spring thrust is a second large-scale thrust that, in North Carolina, emplaced Tallulah Falls Formation and Dysartsville Tonalite over Poor Mountain Formation and Tallulah Falls Formation (Fig. 3-2; e.g., Davis, 1993b; Yanagihara, 1994). Bream (1999) and Hill (1999), working near Marion, North Carolina, mapped several synclines cored by Poor Mountain Formation rocks that are truncated by the Mill Spring thrust (Plate 1). Interpolation (Plate 1) based on detailed and reconnaissance maps (Goldsmith et al., 1988) projects the Mill Spring thrust into the northwestern corner of the Kings Creek quadrangle. The continuation of the Mill Spring thrust in central western North Carolina is further supported by juxtaposition of migmatitic amphibolite over mylonitic Tallulah Falls Formation metagraywacke and Henderson Gneiss (Part I).

Mapping at several scales has revealed a zone of intense migmatization up to 10 km wide and at least ~110 km long in western North Carolina. Mapping by Reed (1964) and Goldsmith et al. (1988) documented an extensive belt of "migmatitic quartz diorite, granodiorite, and quartz monzonite" containing "frequent septa" and blocks of hornblende amphibolite, biotite gneiss, biotite schist, and metagabbro. This unit and an associated gneiss (biotite granodiorite and hornblende-biotite-quartz diorite) crop out almost continuously along the trace of the Brindle Creek thrust in North Carolina (Fig. 3-2; continuity of units has not been confirmed by detailed mapped). Goldsmith et al. (1988) also recognized a unit composed of interlayered biotite gneiss, hornblende gneiss, and amphibolite and a unit composed of mica schist that irregularly crop out northwest of the migmatite.

Detailed geologic mapping (1:24,000-scale) in the Dysartsville, Glen Alpine, Glenwood, Morganton South, and Sunshine 7.5-minute quadrangles revealed a medium-grained, migmatitic, plagioclase-hornblende-quartz-biotite-muscovite gneiss ("migmatitic Poor Mountain Amphibolite") overlain by medium-grained, feldspar-quartz-muscovite-biotite quartzite ("migmatitic Poor Mountain Quartzite"; Figs. 3-2, 3-3a; Giorgis, 1999; Williams, 2000). Goldsmith et al. (1988) included these subdivisions in their migmatitic granitoid gneiss unit; but, regional structural relationships, based on detailed mapping (Giorgis, 1999; Williams, 2000), demonstrate they are in the same stratigraphic position (above the Tallulah Falls Formation in the Mill Spring thrust sheet) as the Poor Mountain Formation (Sloan, 1908; Shufflebarger, 1961; Hatcher, 1969, 1970). Williams (2000) identified an intensely migmatitic zone in the Brindle Creek footwall where migmatitic features like those described by Mehnert (1968) are abundant. The zone of intense migmatization locally overprints upper Tallulah Falls Formation rocks, but has not been delineated in lower stratigraphic units.

Detailed work in the Kings Creek, Ellendale, and Boomer 7.5-minute quadrangles has identified an extensive migmatite zone that is dominantly composed of amphibolite, hornblende-plagioclase-quartz-biotite gneiss, and quartz-biotite-K-feldspar-plagioclase gneiss (Fig. 3-2; Kalbas et al., 2002; Merschat and Kalbas, 2002). Lithologic descriptions are consistent with those of Goldsmith et al. (1988) and Reed (1964). Macroscopic elliptical amphibolite bodies were mapped within the migmatite and may represent paleosome; mappable, discontinuous granitoids are also present. A single thrust-bounded unit was mapped in the Brushy Mountains (Plate 2); compositional heterogeneity at all scales, however, implies complex metamorphic and deformational

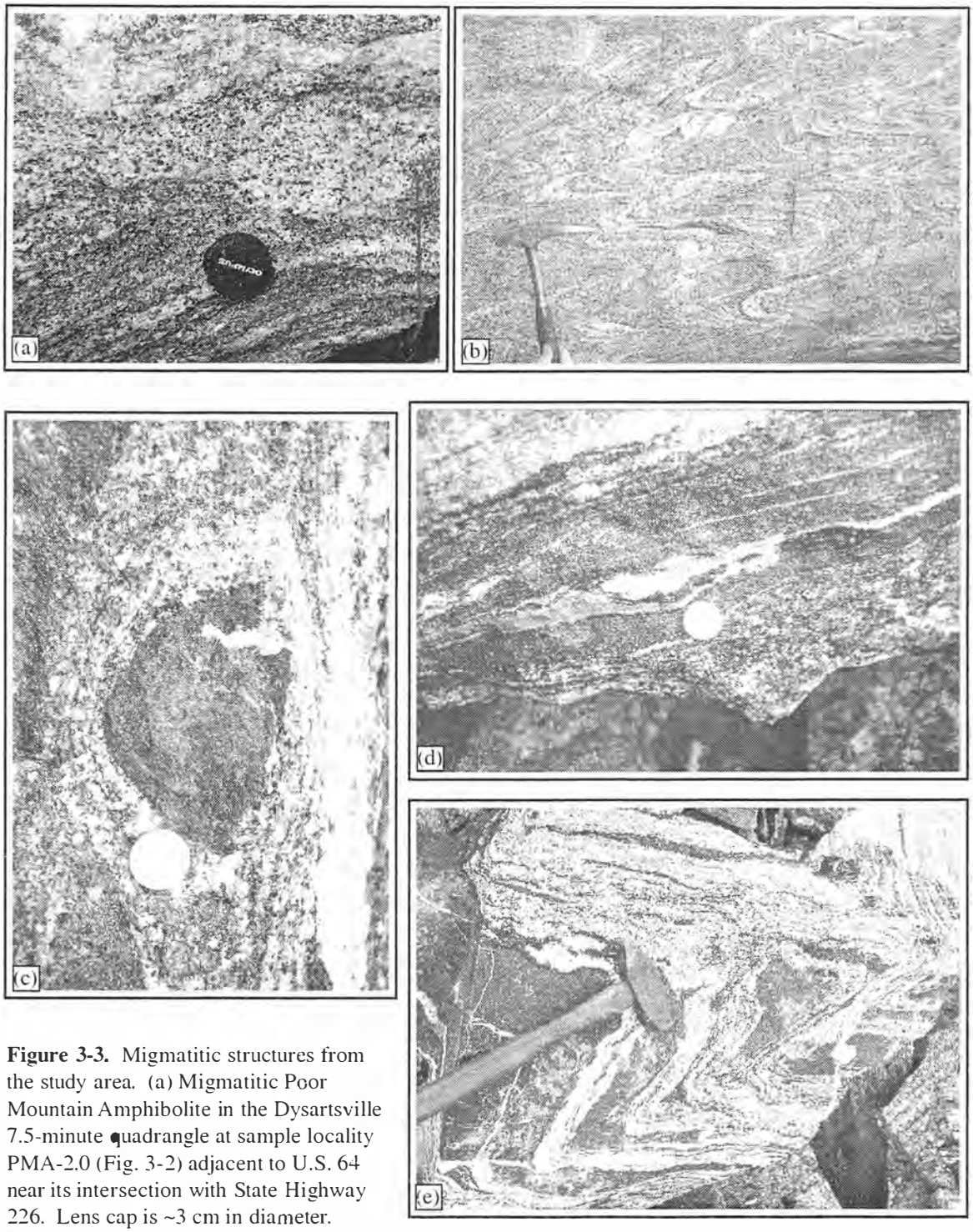

Figure 3-3. Migmatitic structures from the study area. (a) Migmatitic Poor Mountain Amphibolite in the Dysartsville 7.5-minute quadrangle at sample locality PMA-2.0 (Fig. 3-2) adjacent to U.S. 64 near its intersection with State Highway 226. Lens cap is ~3 cm in diameter. (b) Folded (F_3) diktyonitic migmatite at Cedar Rock Country Club 0.35 km south of North Carolina 18. (c) Amphibolite boudin (surreitic structure) surrounded by diatexite neosome at Lenoir Quarry. (d) Stromatic migmatite at Lenoir Quarry composed of amphibolite, biotite-hornblende gneiss, and quartz-plagioclase-K-feldspar gneiss. (e) Tight folds (F_3) in stromatic migmatite at Lenoir Quarry.

interactions may have formed the migmatite from multiple protoliths (including the Poor Mountain Formation; Figs. 3-2, 3-4). Recrystallized amphibolite in the southwestern Brushy Mountains is texturally and mineralogically similar to both Poor Mountain Amphibolite in the footwall of the Mill Spring thrust, and migmatite in the Glen Alpine, Morganton South, Dysartsville, and Sunshine quadrangles. This suggests lateral continuity of the zone of intense migmatization in the Mill Spring thrust sheet, but has not been confirmed by detailed mapping. For clarity, the migmatitic amphibolite and biotite-hornblende granodiorite unit in the Mill Spring thrust sheet (and migmatitic Poor Mountain Formation rocks recognized by Giorgis (1999) and Williams (2000)) are labeled "migmatite" in this paper.

Mesoscopic relationships

The nomenclature used in this paper to describe migmatite follows that of Mehnert (1968) and Henkes and Johannes (1981). Leucosome refers to leucocratic layers usually composed of quartz, plagioclase, and K-feldspar; melanosome refers to dark migmatite layers dominated by mafic minerals; paleosome is parent rock, while newly generated daughter rock is referred to as neosome. Metatexite is anatectic melt that contains only felsic minerals; diatexite is anatectic melt composed of both felsic and mafic minerals. The term mobilizate is used for phases that were formed by thermochemical liberation. Detailed descriptions and analysis of migmatites were presented by Mehnert (1968), and should be consulted for a more comprehensive analysis of features documented here.

Intensely migmatitic gneisses in the immediate Brindle Creek footwall have variable outcrop-scale textures and compositions (Fig. 3-3). Melanosomes occur as thin

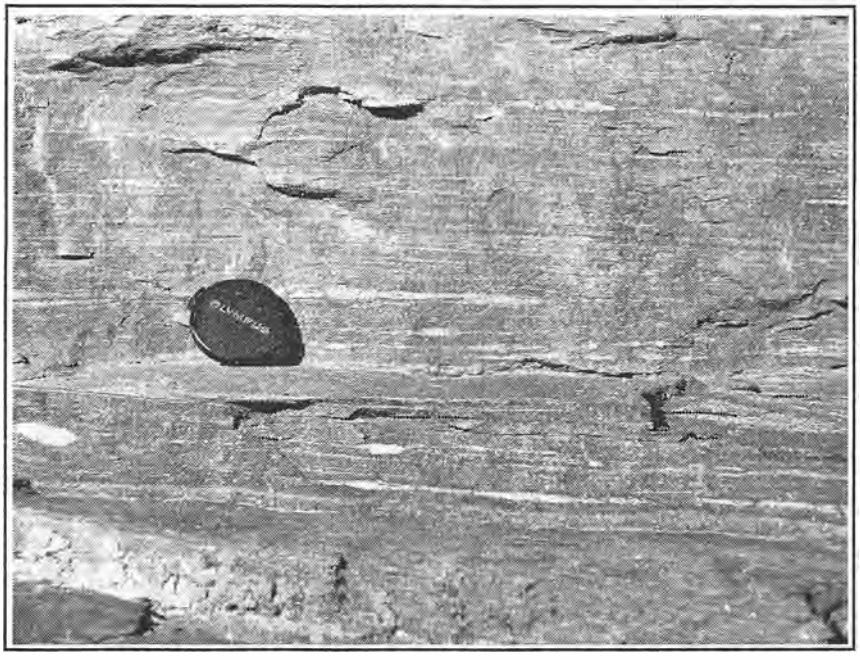

Figure 3-4. Typical Poor Mountain Amphibolite at station PMA-1.0 (Fig. 3-2) located in the Mill Spring thrust footwall ~4 km south of Glenwood on North Carolina 18. Amphibolite is finer grained than melanosomes in the migmatitic amphibolite adjacent to the Brindle Creek thrust. Note the thin layers of fine-grained amphibolite and interlayered quartz-feldspar laminations. Lens cap is ~3 cm in diameter.

(1.5 to 11 cm thick) continuous and discontinuous layers and boudins composed of fine- to medium-grained amphibolite and biotite-hornblende gneiss. Corresponding sympathetic and crosscutting leucosomes are typically coarse grained with granitic and granodioritic compositions. Leucosome layers are folded (F_3) at macro-and mesoscales with layered melanosome. Both metatexitic and diatexitic neosomes are present and indicate differential or fractional partial melting of felsic and mafic constituents. Prominent > 4 mm hornblende and biotite porphyroblasts stand out in leucocratic mobilizates. At several localities outcrops are dominated by foliated granitic and granodioritic leucosome with only minor melanocratic layers.

Migmatite structures are well exposed in the southwestern Brushy Mountains northwest of the Brindle Creek thrust (Fig. 3-3). Folded stromatic (layered) and schollen (raft) structures dominate; phlebitic (vein), and schlieren (flow fabric) structures and boudins are also common (terminology from Mehnert, 1968). Insipient transposition of S_2 surfaces can also be seen in some diktyonitic (reticulated, vein-like structure) migmatite (Fig. 3-3b). Tight and isoclinal fold axial planes are consistently subparallel to foliation in stromatite (Figs. 3-3b, 3-3e). Gradational transitions from stromatic migmatites to more homogeneous granitoids were recognized at several localities; beaded leucosomes surrounded by amphibolite and biotite-hornblende granodiorite grade into lenticular hornblende- and biotite-rich pods engulfed by quartz- and feldspar-rich rock. Sharp contacts between melanosomes and leucosomes were also documented. Schollen, stromatic, agmatitic (breccia-like), and ophthalmitic (rich in feldspar augen) migmatites are exposed in the Dysartsville quadrangle (Williams, 2000), and indicate similar processes affected the immediate Brindle Creek footwall in the South Mountains.

Penetrative northeasterly structural trends (S_2 foliation and F_3 upright to reclined tight folds) dominate western Inner Piedmont thrust sheets and are thought to be the result of Neoacadian deformation (D_2 of Davis, 1993a, and D_3; Part II). Northeast-striking foliations and gently northeast- or southwest-plunging fold axes and coaxial mineral stretching lineations in migmatite neosome are consistent with the regional structural trend and are orogen parallel. Poorly developed foliations in some granodiorite and early pegmatite also parallel the dominant, northeasterly structural trend (Fig. 3-5); Druguet and Hutton (1998) interpreted analogous structures in stromatic migmatite in the eastern Pyrenees as possible evidence for synkinematic migmatization. Similarly, foliations in leucocratic and diatexite neosomes surrounding amphibolite (and less commonly calc-silicate) boudins are typically layer parallel (Fig. 3-3c). At least two generations of granitic pegmatites are also present: an axial planar generation that likely resulted from syndeformational migmatization, and later, less deformed crosscutting pegmatites.

Petrography

Migmatite samples have moderately to well-developed foliations defined by parallel allignment of hornblende and/or biotite. Leucosome consists of medium- to coarse-grained quartz (38-68 %), plagioclase (32-36 %; An_{24-34}), biotite (12-14 %), $\pm$ microcline (< 10 %), hornblende (< 5 %), myrmekite (2-3 %), and epidote/clinozoisite (1-2 %), with trace chlorite, garnet, apatite, zircon, pyrite, and ilmenite. Melanosome is dominantly an assemblage of fine- and medium-grained hornblende (33-99 %), quartz (0-27 %), plagioclase (< 1-27 %; An_{24-44}), biotite (0-12 %), and epidote/clinozoisite (< 1-7 %), with accessory muscovite, sericite, apatite, sphene, and opaque minerals. Both

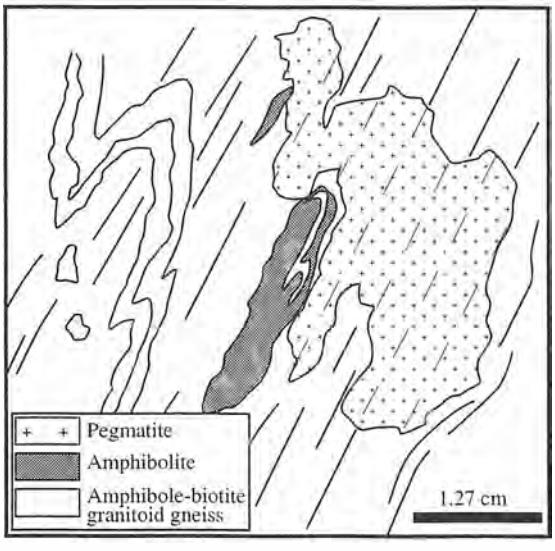

Figure 3-5. Sketch of structures in migmatite adjacent to the Brindle Creek thrust ~2 km east of the Vulcan Materials Company Lenoir Quarry in the Kings Creek quadrangle. Location is shown in Fig. 3-2. The small pegmatite body has an internal fabric that parallels the S_2 foliation and axial planes of the tight folds.

prograde and retrograde epidote/clinozoisite are present in migmatite melanosome. As noted by Davis (1993b) in southwestern North Carolina, prograde epidote in the current sample set consists of coarse, foliation-parallel, tabular crystals; retrograde epidote is identified by randomly oriented, fine-grained hornblende and/or plagioclase replacements. All geochemical samples discussed below have lepidoblastic to nematoblastic foliations defined by the parallel orientation of hornblende, plagioclase, biotite, and quartz.

Sampling and Analytical Methods

Migmatite samples were collected from leucosome and melanosome in the immediate footwall of the Brindle Creek thrust (Fig. 3-2). Melanocratic migmatite was preferentially sampled to obtain assemblages mineralogically similar to Poor Mountain Amphibolite (the most likely candidate for melanosome protolith). Unaltered Poor Mountain Amphibolite and Poor Mountain Quartzite samples from the Sugarloaf Mountain thrust sheet were collected for comparison with the migmatite (Fig. 3-2). Sample LVQ-1, used for U-Pb zircon geochronology, was obtained at the Vulcan Materials Company Lenoir Quarry on North Carolina 18, east of Lenoir in the Kings Creek 7.5-minute quadrangle.

Whole-rock Chemistry

Fresh samples were cut with a diamond bit trim saw; washed with tap and distilled water; rinsed with isopropyl alcohol; dried at ~85 °C; and powdered with an alumina ceramic mill. Multielement whole-rock analyses were performed by Activation Laboratories™ (Ancaster, Ontario) using lithium metaborate/tetraborate fusion inductively coupled plasma emission spectroscopy and inductively coupled plasma mass

spectrometry. Analytical precision was validated by comparisons with 20 natural calibration standards.

Zircon Geochronology

Sensitive high resolution ion microprobe reverse geometry (SHRIMP RG) U-Pb analyses of zircons separated from leucosome material sampled at the Vulcan Materials Company Lenoir Quarry were obtained by B. R. Bream at Stanford University. Typical SHRIMP RG operating conditions and procedures for zircon analyses (e.g., Bacon et al., 2000), summarized below, were used. Zircons were separated using standard techniques, hand picked, mounted with standards in epoxy, polished, and covered with a 10 nm gold coat. Prior to SHRIMP RG analysis, surface and internal features of individual grains were identified from cathodoluminescence (CL) images and photomicrographs (a combination of reflected and transmitted light). A primary $^{16}O_2^-$ ion beam at ~15 nA was focused to produce a beam ~30 to 40 μm in diameter. Analyzed surfaces were rastered (Bacon et al., 2000) for ~4 minutes to remove the gold coat and surface contamination. For each spot, 5 scan cycles were completed for peaks at Zr_2O, ^{204}Pb, ^{206}Pb, ^{207}Pb, ^{208}Pb, ^{238}U, $^{232}Th^{16}O$, and $^{238}U^{16}O$. AS57 (1099 Ma; Paces and Miller, 1993) zircons, analyzed every 4-5 analyses, were used to calibrate counts at mass peaks. Zircon standard SL13 was used to calibrate U concentrations. All data were plotted on standard concordia diagrams, discordia lines were produced for some subsets of the data (see below), and concordia ages (Ludwig, 1998) were determined using Isoplot/Ex software (Ludwig, 1991). Geochronologic errors are 2 sigma unless otherwise noted. Statistical terms used for the reported ages include MSWD (mean square of weighted deviates) and n (number of analyses used for the reported age).

Chemical relationships

Whole-rock major and minor element geochemistry and normative mineralogy for all samples are provided in Tables 3-1 and 3-2. The following arithmetic terms are used to quantify relationships: (1) N subscript designates chondrite-normalized values (for example: La_N/Yb_N = the ratio of chondrite-normalized La to chondrite-normalized Yb); and (2) $Eu/Eu^* = Eu_N/[(Sm_N + Gd_N)/2]$. Values of $Eu/Eu^* < 1$ indicate a negative anomaly and $Eu/Eu^* > 1$ indicate a positive anomaly. Trace element data are divided into, and referred to as, two subsets: (1) trace elements including select REE (= "trace elements"); and (2) REE alone (= "REE").

Chemistry of the Migmatite

Migmatite samples are all hypersthene- or olivine-normative (up to 25 %, and 18 %, respectively); minor amounts of normative nepheline or quartz are also variably present (Table 3-2). Select major oxide and trace element concentrations are shown in element variation diagrams versus Zr and Mg # fractionation indices (Figs. 3-6, 3-7). Zr concentrations are expected to increase with increased fractionation; Mg # is expected to decrease with increased fractionation (Cox et al., 1979; Rollinson, 1998). Discernable trends are apparent with respect to most major oxides and trace elements although variable scatter was detected with respect to each. Migmatite samples have a wide distribution of Zr concentrations, a sign of variable fractionation (terminology from Rollinson [1998]).. Incompatible oxide, element (TiO_2, P_2O_5, Nb, V, etc.), Na_2O, and REE concentrations generally show positive linear trends with increasing fractionation (Fig. 3-6). The distinct linear Hf trend is attributed to substitution for Zr in zircon. Negligible changes were detected in other major oxide concentrations relative to Zr

Table 3-1. Concentrations of major and trace elements in migmatitic amphibolite and biotite-amphibole granodiorite. Det. = detection limits; nd = not detected.

		Migmatite						
	Det.	K525	K1462	B2191	B1924	B39	PMA2.0	LVQ1
wt% SiO_2	0.01	49.64	48.15	57.88	57.55	48.64	46.35	75.08
Al_2O_3	0.01	17.12	12.76	14.91	15.83	17.86	14.67	13.58
Fe_2O_3	0.01	10.42	17.41	8.85	10.79	8.78	11.25	1.83
MnO	0.01	0.20	0.26	0.25	0.19	0.21	0.20	0.03
MgO	0.01	6.95	5.05	3.56	3.23	4.90	9.46	0.79
CaO	0.01	10.89	9.47	8.06	6.95	11.29	12.27	3.31
Na_2O	0.01	2.80	2.59	3.56	2.33	3.89	2.04	3.82
K_2O	0.01	0.96	0.39	0.78	0.97	0.97	0.86	0.99
TiO_2	0.005	0.382	2.855	1.225	0.427	1.608	0.625	0.213
P_2O_5	0.01	0.03	0.23	0.28	0.08	0.59	0.05	0.03
LOI	0.01	0.99	0.82	0.77	1.96	1.31	1.03	0.74
TOTAL		100.38	99.98	100.12	100.31	100.05	98.8	100.44
ppm V	5	253.4	506.8	183.4	216.8	276.1	264.4	nd
Cr	20	nd	37.1	61.0	nd	37.7	50.4	6.0
Co	1	38.7	40.5	17.7	24.7	22.7	50.9	4.5
Ni	15	33.7	79.8	44.1	nd	60.7	71.2	4.0
Cu	10	22.8	52.3	17.6	48.3	13.9	41.1	8.0
Zn	30	75.1	126.5	53.4	93.9	62.3	76.2	26.0
Ga	1	14.7	21.8	21.5	16.1	24.2	13.5	12.0
Ge	1	1.7	1.8	2.3	1.8	2.2	1.5	1.1
As	5	nd	nd	nd	nd	nd	nd	nd
Rb	2	9.0	4.0	5.4	22.7	12.8	8.8	43.0
Sr	2	98.5	83.6	229.8	86.2	349.0	91.8	130.0
Y	1	14.7	56.7	65.9	11.2	31.7	15.9	3.0
Zr	5	23.8	165.6	347.9	36.0	347.7	17.1	98.0
Nb	1	1.9	5.2	8.4	2.2	32.4	0.5	3.2
Mo	2	nd	nd	nd	nd	nd	nd	nd
Ag	0.5	nd	1.0	2.0	nd	nd	nd	nd
In	0.2	nd	nd	nd	nd	nd	nd	nd
Sn	1	nd	1.7	2.5	nd	2.3	nd	2.0
Sb	0.5	nd	nd	nd	nd	nd	nd	nd
Cs	0.5	nd	nd	nd	0.5	0.1	nd	0.8
Ba	3	43.1	71.0	89.0	130.9	41.9	76.5	nd
La	0.1	2.0	8.6	37.2	4.4	63.5	1.8	11.0
Ce	0.2	5.1	22.7	67.7	4.5	132.1	5.0	20.7
Pr	0.05	0.9	3.6	9.9	1.3	16.2	0.8	2.3
Nd	0.1	4.6	18.7	41.4	5.5	64.4	4.5	8.4
Sm	0.1	1.6	6.0	9.9	1.6	11.8	1.6	1.4
Eu	0.05	0.7	2.2	2.6	0.5	2.7	0.7	0.4
Gd	0.1	2.0	8.0	10.6	1.7	9.5	2.1	1.0
Tb	0.1	0.4	1.5	1.8	0.3	1.3	0.4	0.1
Dy	0.1	2.5	9.7	11.6	1.9	6.6	2.7	0.6
Ho	0.1	0.5	2.1	2.4	0.4	1.2	0.6	0.1
Er	0.1	1.7	5.9	7.1	1.3	3.3	1.8	0.3
Tm	0.05	0.3	0.9	1.1	0.2	0.5	0.3	0.0
Yb	0.1	1.8	5.9	7.2	1.4	3.1	1.7	nd
Lu	0.04	0.3	0.9	1.1	0.2	0.5	0.3	0.0
Hf	0.2	0.9	4.8	9.3	1.1	9.7	0.8	2.6
Ta	0.1	0.3	0.4	0.5	0.4	2.1	0.0	0.3
W	0.5	nd	nd	0.8	nd	nd	nd	nd
Tl	0.1	0.1	nd	0.1	0.2	0.1	0.1	0.2
Pb	5	30.3	15.0	18.6	21.3	14.1	8.2	11.0
Bi	0.2	0.5	0.3	1.2	0.4	0.4	nd	nd
Th	0.1	0.4	0.5	7.7	3.2	9.2	0.2	4.5
U	0.1	0.7	0.2	1.9	1.3	5.5	0.1	0.5
La_N/Yb_N	--	0.738	0.977	3.490	2.105	13.629	0.713	25.977
Eu/Eu*	--	1.134	0.982	0.777	0.939	0.758	1.160	0.912
Latitude	°N	35.9273	35.9716	36.0250	35.9933	36.0302	35.5772	35.9308
Longitude	°W	81.4774	81.4542	81.3704	81.3703	81.3458	81.8405	81.4794

Table 3-2. Normative mineralogy. Qtz = quartz; F-spar = feldspar; Plag = plagioclase; K-Spar = K-feldspar.

	Migmatite							
Min. wt. %	K569	K525	K1462	B2191	B1924	B-39	PMA2.0	LVQ-1
Quartz	—	—	0.69	11.09	15.22	—	—	39.95
Corundum	—	—	—	—	—	—	—	0.28
Orthoclase	0.3	5.67	2.3	4.6	5.73	5.73	5.08	5.84
Albite	6.39	23.67	21.89	30.09	19.7	25.27	13.27	32.29
Anorthite	41.73	31.3	22.03	22.39	29.86	28.4	28.32	16.21
Nepheline	1.26	—	—	—	—	4.12	2.15	—
Diopside	41.03	18.51	19.7	13.13	3.44	19.54	26.27	—
Hypersthene	—	2.07	22.01	12.74	20.56	—	—	4.14
Olivine	3.39	14.68	—	—	—	8.98	18.49	
Magnetite	1.83	1.82	3.04	1.54	1.88	1.53	1.96	0.32
Ilmenite	2.54	0.73	5.43	2.33	0.81	3.96	1.19	0.41
Apatite	0.48	0.07	0.5	0.61	0.17	1.29	0.11	0.07
Total	98.95	98.52	97.59	98.52	97.37	98.82	96.84	99.51
F-spar/ Qtz	1.26	0	0.69	11.09	15.22	4.12	2.15	39.95
Plag	16.5	60.6	41.1	51.4	55.3	59.4	46.7	35.4
K-Spar	32	0	5.1	5.7	0	0	0	19

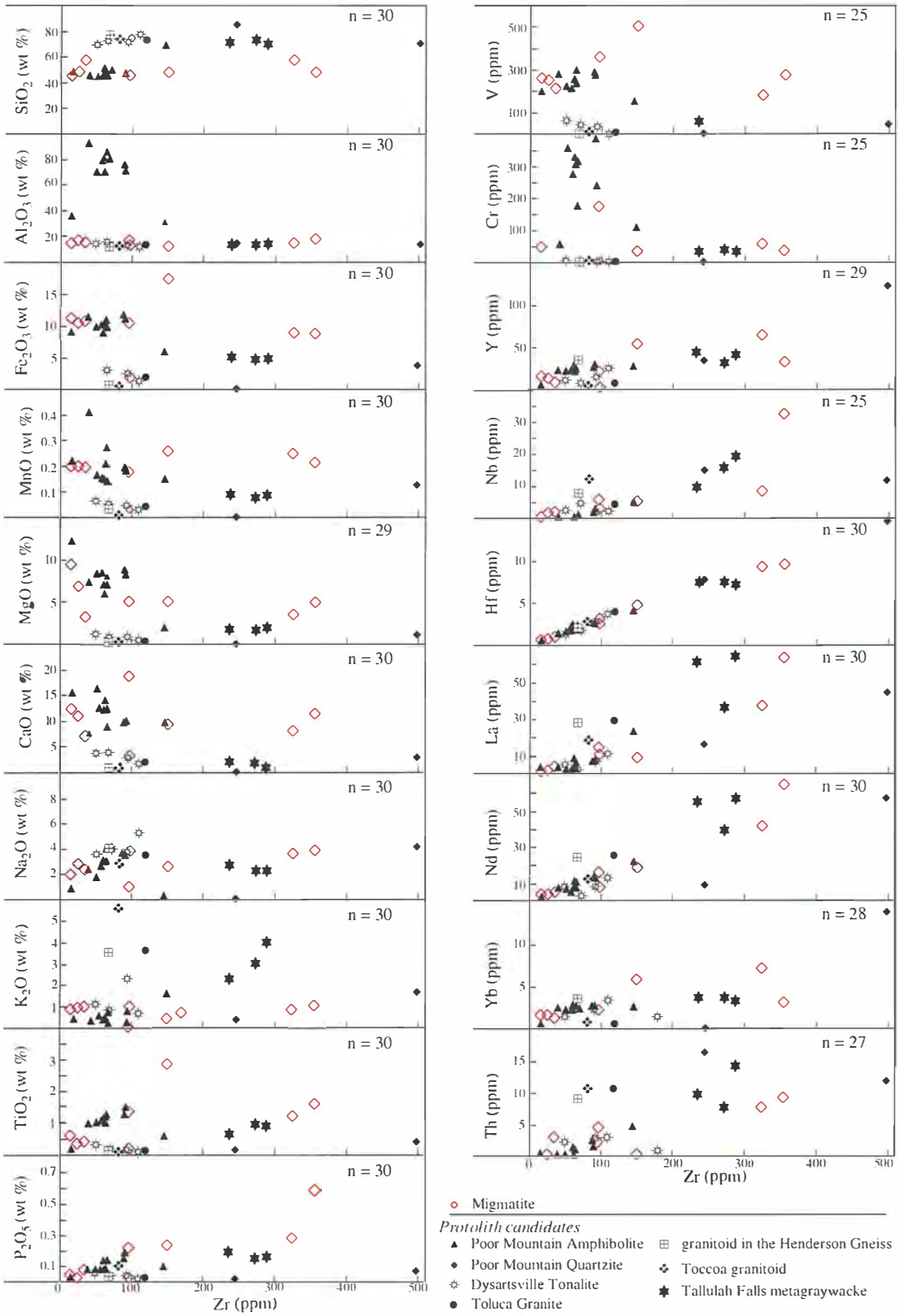

Figure 3-6. Two-element variation diagrams of major oxide and select trace element concentrations vs. Zr.

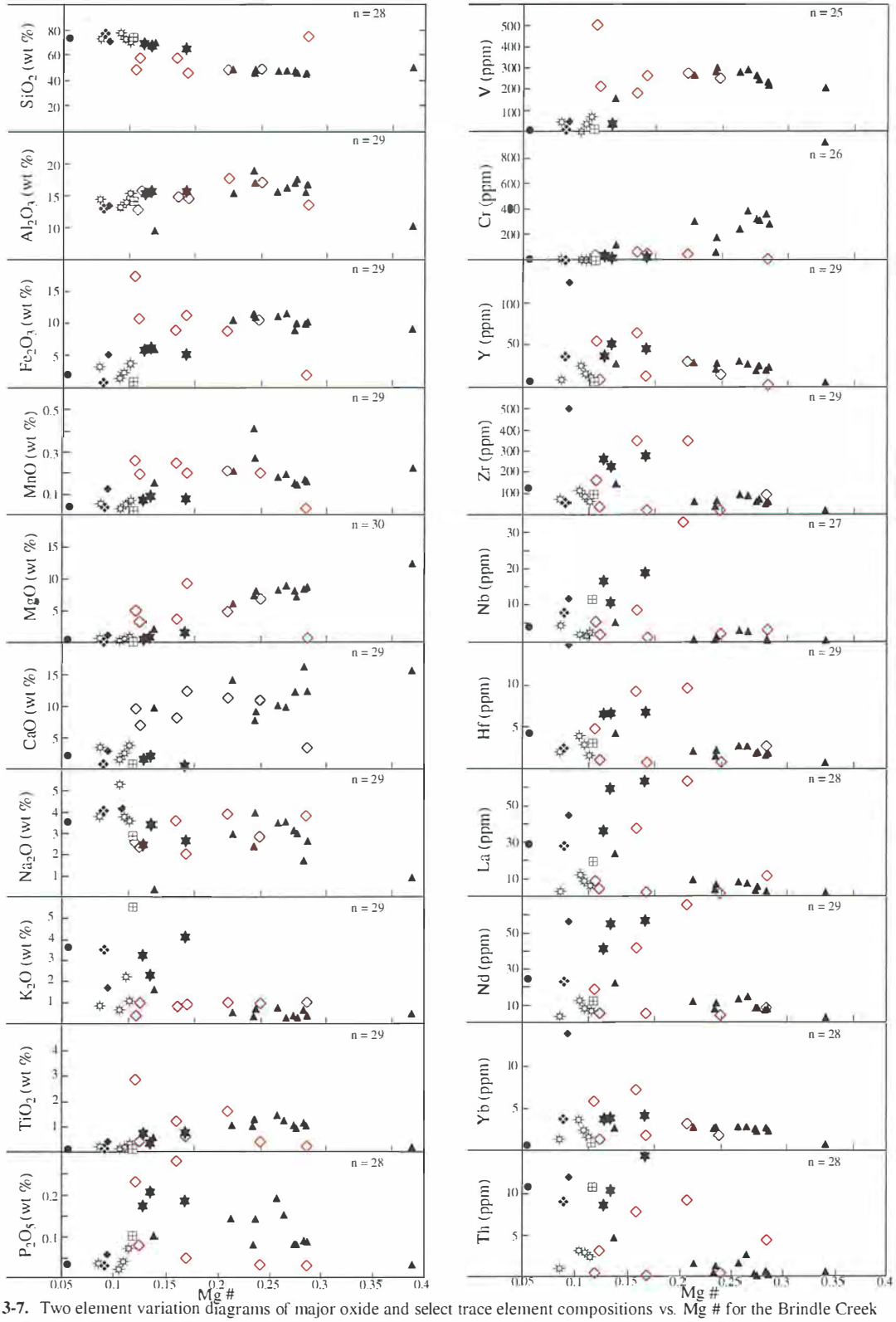

Figure 3-7. Two element variation diagrams of major oxide and select trace element compositions vs. Mg # for the Brindle Creek footwall migmatite, Poor Mountain Amphibolite, Tallulah Falls metagraywacke, Poor Mountain Quartzite, Dysartsville Tonalite, Toluca Granite, granitoid in the Henderson Gneiss, and Toccoa granitoid (refer to Figure 3-6 for symbol descriptions; granitoid concentrations are from Bream, unpublished data). Mg # = [MgO/(FeO + Fe_2O_3 + MgO)]. Weight % oxides were used because all whole-rock FeO analyses were calculated as Fe^{3+}. The oxygen fugacity was approximated; FeO and Fe_2O_3 were calculated using Fe^{2+}/Fe^{3+} = 9/1.

concentration. Trends in data plotted versus the Mg # fractionation index generally mirror the data plotted against Zr, thus linear trends in data can also be attributed to fractionation.

Several other important features are highlighted where the Mg # fractionation index is used (Fig. 3-7). Migmatite concentrations are consistently scattered and have relatively low Mg #. Positive linear trends in Al_2O_3, FeO, MgO, CaO, V, and Cr indicate decreased concentration with increased fractionation. Enrichment of REE with increased fractionation was also observed in melanocratic migmatite (Fig. 3-7).

Trace element concentrations in all migmatite samples (Fig. 3-8) are enriched relative to chondrite. Three trends are distinguishable (Figs. 3-8b, 3-8c, 3-8d); the first and third (leucosome and melanosome group 2) are characterized by low concentrations of low compatibility trace elements (Ba and Rb) and pronounced Sr anomalies (Fig. 3-8b, 3-8d). Migmatite leucosome is disproportionately enriched in Rb and depleted in Tb, Y, Tm, and Yb. The leucosome and melanosome group 2 are generally enriched in other trace elements relative to melanosome group 1 (Fig. 3-8c). Low compatibility trace element concentrations in melanosome group 1 vary considerably, but higher compatibility trace element concentrations are generally lower (< 10).

Three distinct groups are also distinguishable in REE concentration diagrams (Fig. 3-9), and correspond to trace element groups. Leucosome sample LVQ-1 has a distinctive trend; it is enriched in LREE, but is significantly HREE-depleted (La_N/Yb_N = 26.0; Fig. 3-9). REE concentrations remain below those of melanosome groups 1 and 2. Though a positive Eu anomaly is expected for leucosome enriched in plagioclase (Johannes et al., 1995), a slightly negative value (Eu/Eu* = 0.9) was observed in the

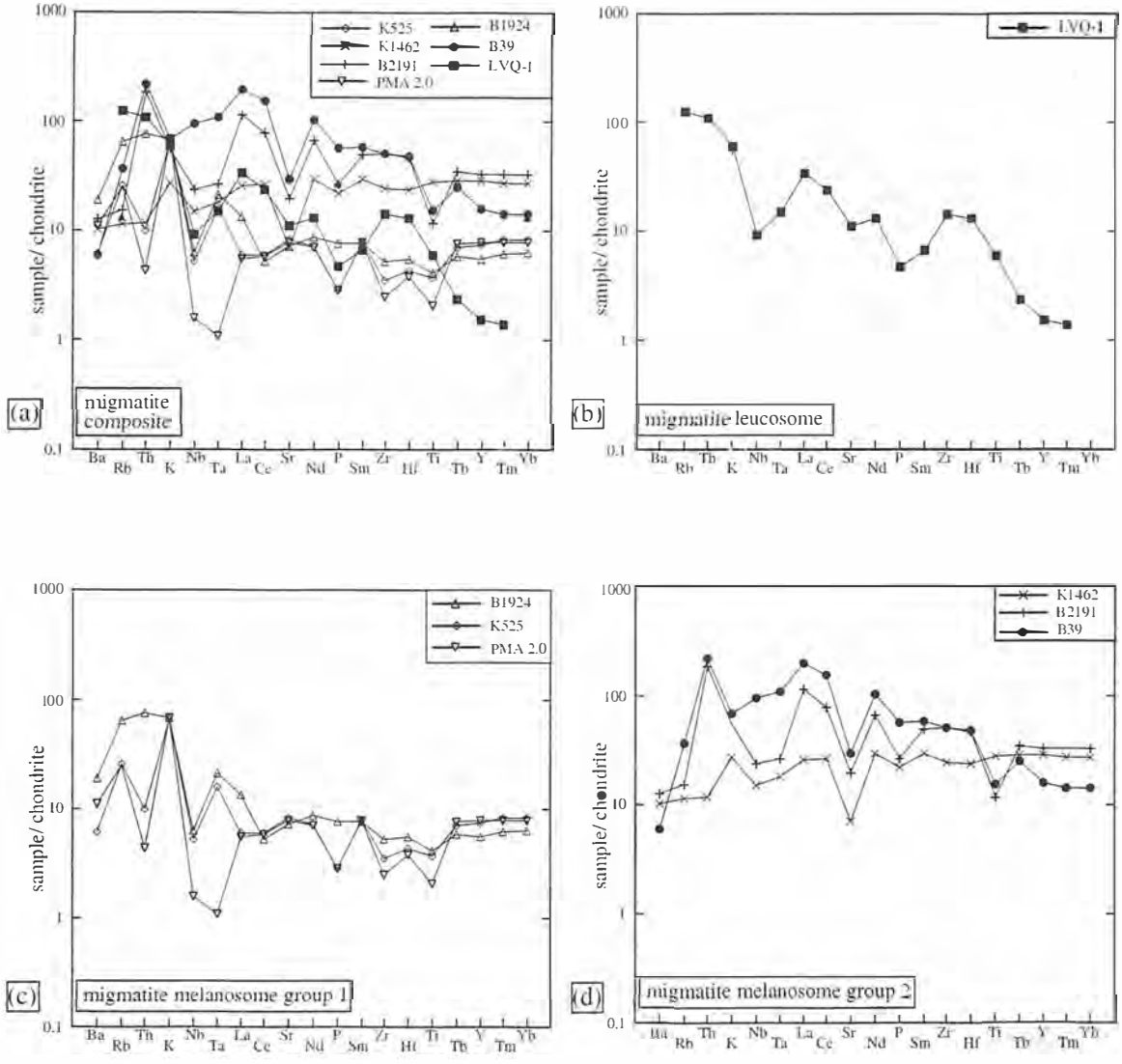

Figure 3-8. Chondrite-normalized trace element concentrations. (a) Concentrations of all samples from the Brindle Creek thrust footwall migmatite. Plots (b), (c), and (d) show select sample groupings extracted from (a) where concentrations and/or patterns are similar. Sample locations are shown in Figure 3-2. Chondrite values are from Thompson (1982).

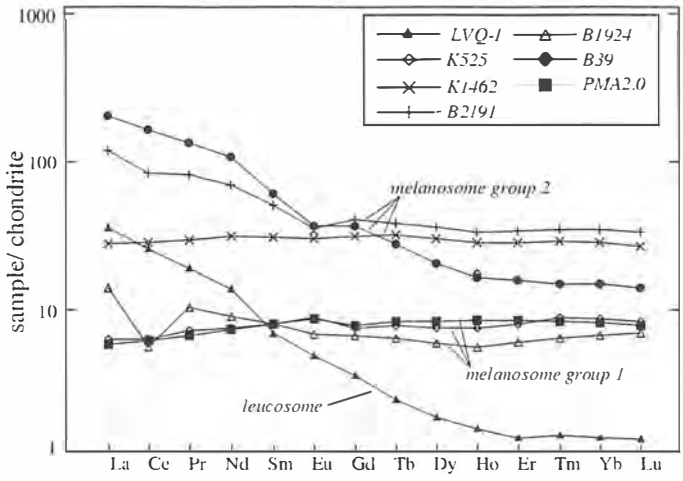

Figure 3-9. Chondrite-normalized REE concentration of Brindle Creek thrust footwall migmatite. Sample locations are shown in Figure 3-2. C1 chondrite values are from Boynton (1984).

leucosome sample. Samples in melanosome group 1 have no fractionation or are slightly enriched in heavy rare earth elements (HREE), La_N/Yb_N = 0.7 to 2.1. Two samples have slightly positive Eu anomalies (Eu/ Eu* = 1.1). Melanosome group 2 is characterized by enrichment in light rare earth elements (LREE) and depletion in HREE; a more pronounced REE fractionation ranges from La_N/Yb_N = 3.5 to 13.6. Only one sample, B-2191, has a negative Eu anomaly (Eu/ Eu* = 0.8). Sample K-1462 is enriched in all REE with respect to melanosome group 1 concentrations, but shows a similar, flat trend (Fig. 3-9).

Tectonic Affinity of the Poor Mountain Amphibolite

Poor Mountain Amphibolite shows distinctive patterns on element variation diagrams (Figs. 3-6, 3-7; Table 3-3). The relatively small range in Zr concentration of Poor Mountain Amphibolite may indicate a small degree of fractionation. Incompatible elements and REE show positive and negative trends in Figures 3-6 and 3-7, respectively, and conform to unusually linear trends in the migmatite. In each plot, Poor Mountain Amphibolite groups near the low fractionation ends of the X-axes; the Poor Mountain Quartzite, however, plots in the moderate and high fractionation segment of Zr-axes and has high fractionation with respect to Mg #. Relatively small concentration ranges occur in most major oxides of Poor Mountain Amphibolite; discernable linear trends, however, are not prevalent. Trace element and REE data are used later in this chapter for comparison to migmatite compositions. A tangential discussion of Poor Mountain Amphibolite tectonic affinity is included here in part to substantiate previous workers' conclusions, and to prompt further work on the petrogenesis of this important western Inner Piedmont unit.

Table 3-3. Concentrations of major and trace elements in Poor Mountain Formation. Det. = detection limits.

		Poor Mtn. Amphibolite											P. M. Quartzite	
	Det.	PMA1.1	PMA4.0	PMA5.0	PMA5.2	PMA5.4	PMA6.0	PMA7.0	PMA8.0	PMA9.1	PMA10	PMA-Y	PMQ	PQMTN
wt% SiO_2	0.01	47.97	49.43	46.26	46.22	47.88	48.82	45.93	48.5	45.2	69.86	47.37	70.71	84.5
Al_2O_3	0.01	15.61	10.24	16.60	17.73	17.06	15.46	18.85	17.08	15.41	9.52	16.29	13.43	14.30
Fe_2O_3	0.01	11.17	9.05	10.04	9.96	8.89	10.50	11.45	10.93	9.92	5.94	11.56	4.86	0.05
MnO	0.01	0.18	0.22	0.16	0.14	0.15	0.21	0.41	0.27	0.16	0.15	0.19	0.12	nd
MgO	0.01	8.17	12.14	8.46	7.95	7.04	6.00	7.39	7.07	8.28	2.00	8.82	1.06	nd
CaO	0.01	10.00	15.4	12.4	12.27	12.19	14.00	7.71	9.00	16.14	9.72	9.81	2.81	0.01
Na_2O	0.01	3.46	0.88	2.55	2.94	3.08	2.90	2.35	3.95	1.71	0.32	3.51	4.15	0.12
K_2O	0.01	0.70	0.40	0.31	0.19	0.33	0.50	0.28	0.68	0.52	1.55	0.22	1.69	0.39
TiO_2	0.005	1.455	0.184	1.063	1.156	1.126	1.037	0.984	1.236	1.002	0.588	1.246	0.399	0.155
P_2O_5	0.01	0.19	0.03	0.08	0.09	0.08	0.14	0.08	0.14	0.08	0.10	0.15	0.06	0.02
LOI	0.01	1.32	1.47	2.18	1.66	2.51	0.64	4.68	1.00	1.41	0.52	0.90	0.97	0.72
TOTAL		100.23	99.44	100.09	100.3	100.32	100.2	100.09	99.87	99.83	100.27	100.07	100.26	100.27
ppm V	5	277.8	199.7	220.7	241.0	255.0	264.4	280.9	302.3	225.9	157.0	289.3	41.0	--
Cr	20	241.0	925.1	285.0	316.9	327.1	306.2	63.5	179.1	356.5	114.8	384.8	nd	nd
Co	1	38.2	44.3	44.3	43.6	52.1	39.3	34.6	39.3	47.3	19.3	46.6	5.9	1.0
Ni	15	143.8	159.6	171.4	122.3	133.1	114.6	41.7	98.8	195.6	40.8	202.2	nd	nd
Cu	10	59.9	142.5	66.5	98.2	93.3	31.4	78.2	72.2	72.0	76.3	41.8	nd	nd
Zn	30	91.4	85.1	66.9	70.6	70.2	68.8	119.2	348.5	76.5	61.8	86.7	109.6	4.0
Ga	1	17.5	10.1	15.4	17.3	16.8	16.5	18.5	17.9	14.9	12.2	18.7	26.3	19.0
Ge	1	1.3	1.2	1.0	1.5	1.1	1.5	2.6	1.2	1.6	1.9	1.6	1.5	2.3
As	5	nd	nd	nd	nd	nd	nd	nd	nd	nd	nd	nd	nd	nd
Rb	2	17.2	7.7	5.7	3.3	3.7	5.7	5.0	14.2	9.0	46.7	1.4	38.8	6.0
Sr	2	165.5	150.5	225.1	226.6	188.0	194.5	141.5	177.3	181.2	188.6	124.0	110.2	4.0
Y	1	28.8	6.1	22.8	24.8	22.5	28.4	22.6	26.0	21.7	27.0	26.6	120.8	35.0
Zr	5	99.3	19.2	60.5	64.8	63.3	65.4	43.6	69.6	52.3	147.8	92.8	506.1	250.0
Nb	1	3.1	0.4	0.3	nd	nd	0.5	0.6	0.9	0.5	5.1	2.6	11.7	14.7
Mo	2	nd	nd	nd	nd	nd	nd	nd	nd	nd	nd	nd	nd	--
Ag	0.5	nd	nd	nd	1.2	1.0	1.2	1.0	1.2	1.0	0.9	1.0	3.8	nd
In	0.2	nd	nd	nd	nd	nd	nd	0.2	nd	nd	nd	nd	0.1	nd
Sn	1	nd	nd	nd	nd	nd	nd	1.4	nd	nd	1.1	1.4	4.9	4.0
Sb	0.5	nd	nd	0.2	nd	nd	nd	nd	nd	nd	nd	nd	nd	0.1
Cs	0.5	0.2	0.1	0.1	nd	nd	0.1	nd	0.1	0.3	0.5	nd	0.5	nd
Ba	3	449.7	69.8	242.9	280.9	123.7	211.0	37.5	87.0	499.4	257.1	56.8	564.4	--
La	0.1	7.9	2.2	2.4	3.0	4.0	8.6	3.8	6.4	2.8	23.4	6.9	44.0	16.1
Ce	0.2	19.5	4.8	7.0	8.0	9.1	14.1	7.1	15.5	8.0	44.0	19.0	98.7	16.5
Pr	0.05	2.8	0.6	1.2	1.4	1.5	2.4	1.6	2.3	1.3	5.4	2.9	12.6	1.8
Nd	0.1	13.3	2.7	6.7	7.8	7.9	11.5	7.9	11.2	6.9	21.9	14.5	55.9	7.5
Sm	0.1	3.7	0.7	2.4	2.6	2.6	3.3	2.6	3.3	2.4	4.7	4.0	14.3	2.6
Eu	0.05	1.4	0.2	1.0	1.2	1.1	1.2	1.0	1.3	1.0	1.3	1.5	2.7	0.7
Gd	0.1	4.2	0.9	3.2	3.6	3.3	4.1	3.4	4.1	3.1	4.9	4.5	16.3	3.0
Tb	0.1	0.7	0.2	0.6	0.7	0.6	0.7	0.6	0.7	0.6	0.8	0.8	3.1	0.7
Dy	0.1	4.9	1	4.0	4.4	4.1	4.7	4.2	4.6	3.9	4.9	4.8	20.3	5.6
Ho	0.1	1.1	0.2	0.9	0.9	0.9	1.0	0.9	1.0	0.8	1.0	1.0	4.4	1.4
Er	0.1	3.0	0.7	2.5	2.8	2.6	3.0	2.6	2.9	2.6	2.8	2.9	13.0	4.8
Tm	0.05	0.4	0.1	0.4	0.4	0.4	0.4	0.4	0.4	0.4	0.4	0.5	2.1	0.8
Yb	0.1	2.8	0.8	2.2	2.5	2.3	2.7	2.6	2.6	2.4	2.7	2.8	13.7	--
Lu	0.04	0.4	0.1	0.3	0.4	0.3	0.4	0.4	0.4	0.3	0.4	0.4	2.0	0.9
Hf	0.2	2.6	0.6	1.8	1.8	1.9	2.1	1.4	2.1	1.6	4.1	2.6	14.6	7.7
Ta	0.1	0.2	0	0.0	0.0	0.0	0.1	0.0	0.1	0.0	0.4	0.1	0.8	1.3
W	0.5	nd	nd	nd	nd	nd	1.2	4.0	3.9	nd	0.9	7.6	5.5	--
Tl	0.1	0.2	0.1	0.1	0.1	0.1	0.1	0.1	0.1	0.1	0.2	nd	0.3	0.1
Pb	5	5.7	13.1	nd	nd	nd	11.6	14.0	26.0	6.4	39.6	14.0	23.6	--
Bi	0.2	nd	0.6	nd	nd	nd	0.3	2.0	0.5	0.7	2.4	0.3	0.2	nd
Th	0.1	1.6	0.5	0.2	0.2	0.3	1.4	0.3	1.1	0.4	4.5	2.4	11.7	16.3
U	0.1	0.3	1.9	0.1	0.1	1.9	0.3	0.3	0.4	0.3	2.7	0.4	2.3	2.7
La_N/Yb_N	--	1.919	1.993	0.713	0.829	1.147	2.131	0.997	1.640	0.779	5.742	1.685	2.162	1.942
Eu/Eu^*	--	1.050	0.885	1.086	1.159	1.116	1.021	1.071	1.085	1.104	0.787	1.056	0.533	0.769
Latitude	°N	35.5770	35.5156	35.5156	35.5156	35.5156	35.5157	35.4341	35.4204	35.3976	35.3927	35.4801	35.5808	35.6051
Long.	°W	81.9796	82.0365	82.0365	82.0365	82.0365	82.1068	82.1579	82.1313	82.3034	82.2761	82.1525	81.975	81.9555

High grade metamorphism and deformation have obliterated all primary (sedimentary/ volcanic) structures (e.g., cross bedding; vesicles) in the Inner Piedmont. Our understanding of the origin of the Poor Mountain Formation is, therefore, incomplete. Earlier workers (e.g., Hatcher, 1969, 1970), on the basis of outcrop occurrence and stratigraphic continuity with neighboring metasedimentary units, proposed sedimentary protoliths for components of the Poor Mountain Formation (marble, quartzite, metasiltstone, and, less likely, the amphibolite). Subsequent whole-rock geochemical analyses, however, confirm a volcanic (basaltic) origin for the Poor Mountain Amphibolite (Davis, 1993b; Yanagihara, 1994; Bream, 1999). Poor Mountain Amphibolite data from this study plot in the igneous field of Leake's (1964) ortho- vs. para-amphibolite ternary diagram (Fig. 3-10).

Tectonic discrimination diagrams (e.g., Pearce and Cann, 1973; Rollinson, 1998) are based on major and minor element analyses of many unaltered (mostly Cenozoic to Holocene), noncumulate basaltic lavas; conclusions based on whole-rock chemical data from metamorphic rocks must therefore be used with caution. Consistent tight grouping of data in several discrimination diagrams, however, permit useful statements to be made about protolith affinity (Figs. 3-11-3-14). Data from this study agree with previous determinations; the Poor Mountain Amphibolite has a noncontinental, probably arc volcanic to MORB origin (Davis, 1993b, Yanagihara, 1994; Bream, 1999). The data, when plotted on the AFM ternary plot (Fig. 11) of Irvine and Baragar (1971) and tectonic discrimination diagrams of Pearce and Cann (1973) and Pearce and Norry (1979),

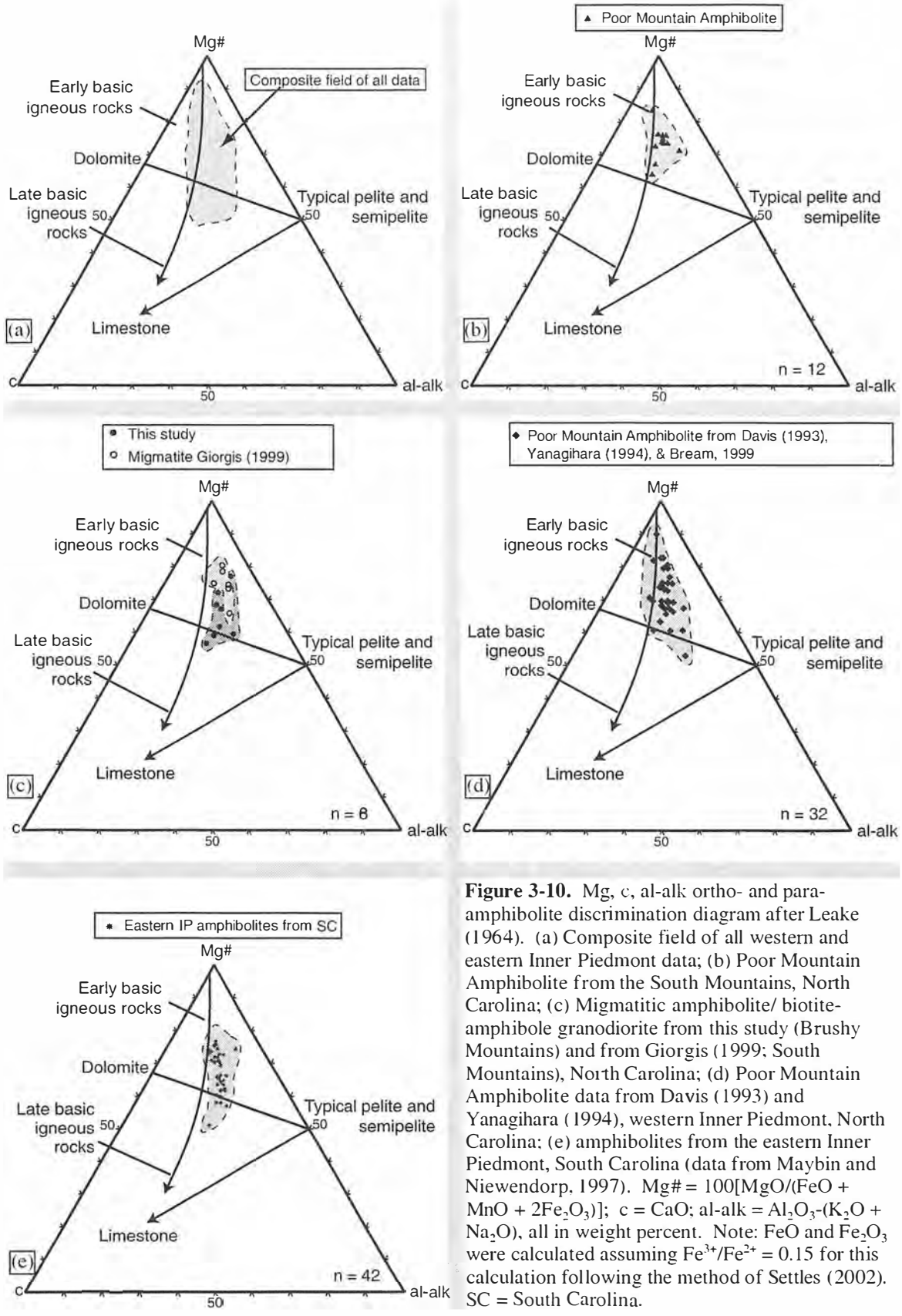

Figure 3-10. Mg, c, al-alk ortho- and para-amphibolite discrimination diagram after Leake (1964). (a) Composite field of all western and eastern Inner Piedmont data; (b) Poor Mountain Amphibolite from the South Mountains, North Carolina; (c) Migmatitic amphibolite/ biotite-amphibole granodiorite from this study (Brushy Mountains) and from Giorgis (1999; South Mountains), North Carolina; (d) Poor Mountain Amphibolite data from Davis (1993) and Yanagihara (1994), western Inner Piedmont, North Carolina; (e) amphibolites from the eastern Inner Piedmont, South Carolina (data from Maybin and Niewendorp, 1997). Mg# = 100[MgO/(FeO + MnO + $2Fe_2O_3$)]; c = CaO; al-alk = Al_2O_3-(K_2O + Na_2O), all in weight percent. Note: FeO and Fe_2O_3 were calculated assuming Fe^{3+}/Fe^{2+} = 0.15 for this calculation following the method of Settles (2002). SC = South Carolina.

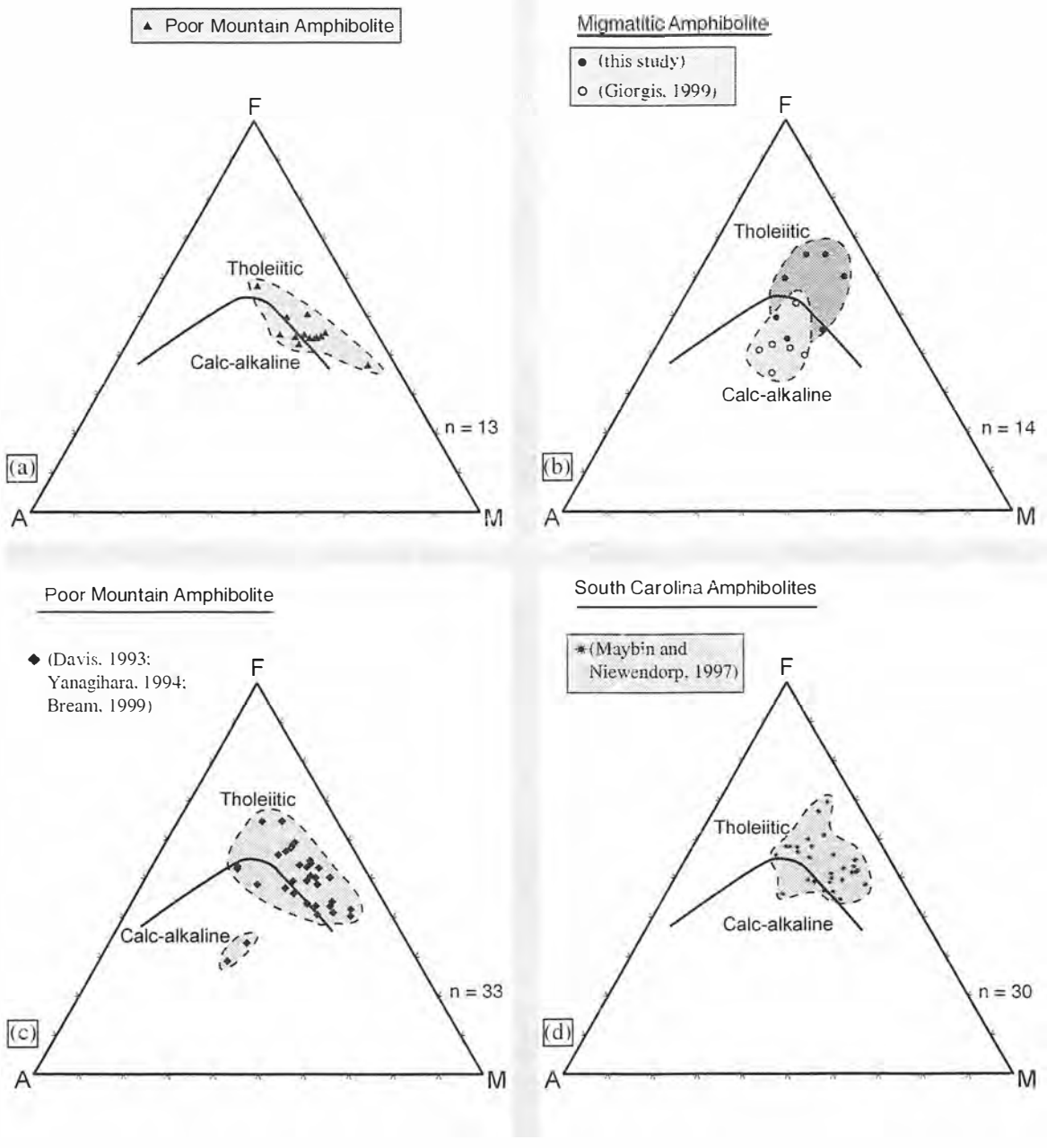

Figure 3-11. AFM ternary diagrams. Comparisons are made between: (a) Poor Mountain Amphibolite from the South Mountains, North Carolina; (b) Migmatitic amphibolite/ biotite-amphibole granodiorite from this study (Brushy Mountains) and from Giorgis (1999; South Mountains), North Carolina; (c) Poor Mountain Amphibolite data from Davis (1993), Yanagihara (1994), and Bream (1999), western Inner Piedmont, North Carolina; and (d) amphibolites from the eastern Inner Piedmont, South Carolina (Maybin and Niewendorp, 1997). Open triangles are data from Davis (1993); addition signs are data from Yanagihara (1994), and open boxes are data from this study. Tholeiitic and calc-alkaline fields were modified from Irvine and Baragar (1971). A = $Na_2O + K_2O$; F = $FeO + 0.8998\ Fe_2O_3$; M = MgO, all in weight percent. Note that FeO and Fe_2O_3 were calculated using $Fe^{3+}/Fe^{2+} = 0.15$ following the method of Settles (2002).

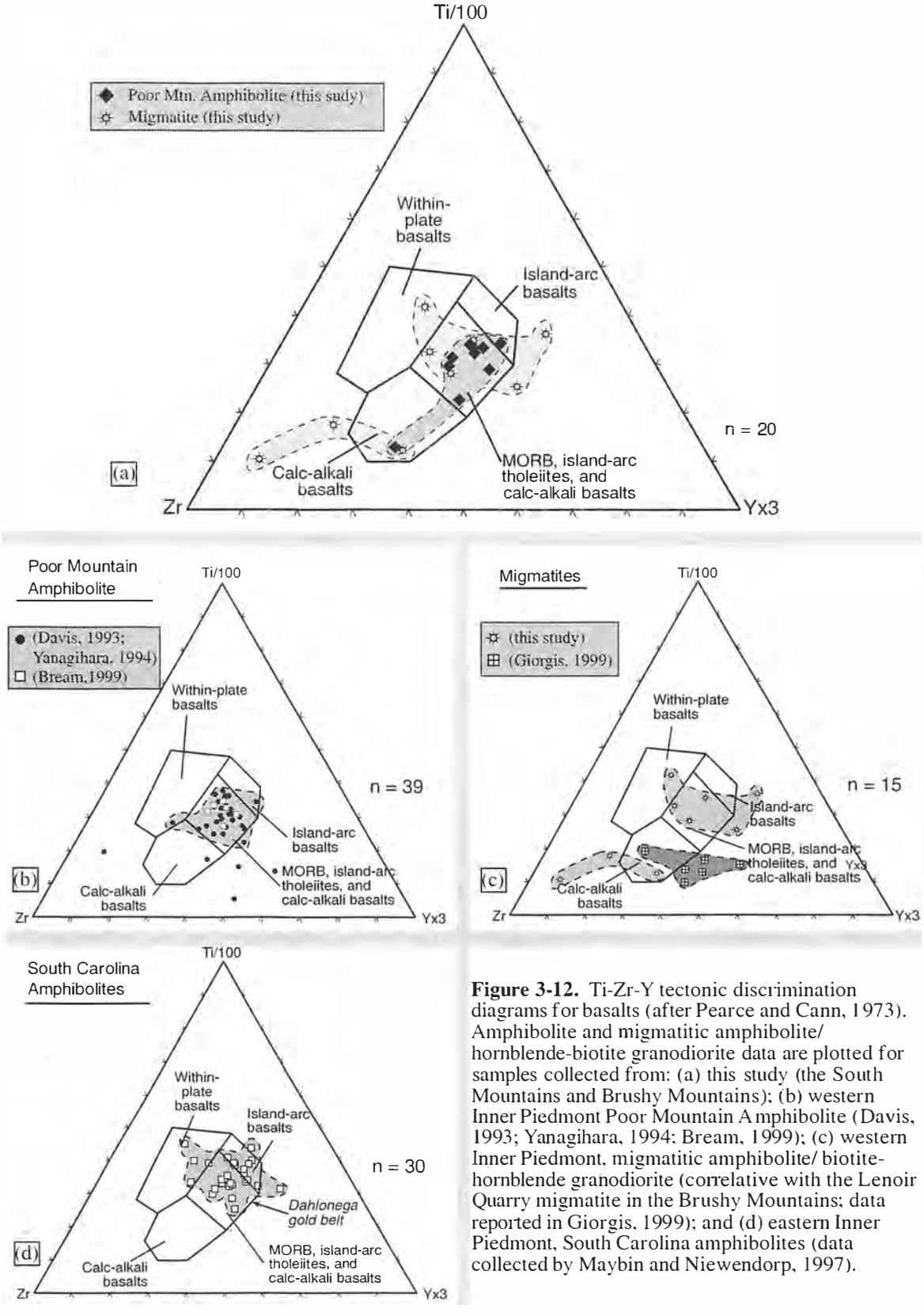

Figure 3-12. Ti-Zr-Y tectonic discrimination diagrams for basalts (after Pearce and Cann, 1973). Amphibolite and migmatitic amphibolite/ hornblende-biotite granodiorite data are plotted for samples collected from: (a) this study (the South Mountains and Brushy Mountains); (b) western Inner Piedmont Poor Mountain Amphibolite (Davis, 1993; Yanagihara, 1994; Bream, 1999); (c) western Inner Piedmont, migmatitic amphibolite/ biotite-hornblende granodiorite (correlative with the Lenoir Quarry migmatite in the Brushy Mountains; data reported in Giorgis, 1999); and (d) eastern Inner Piedmont, South Carolina amphibolites (data collected by Maybin and Niewendorp, 1997).

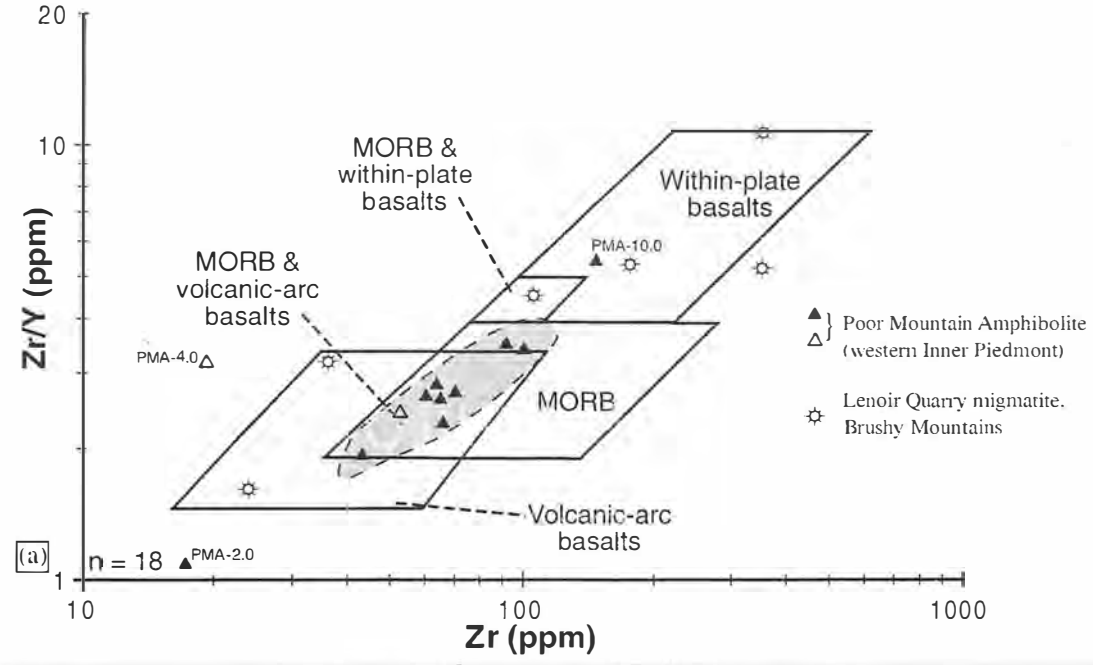

Poor Mountain Amphibolite data from Davis (1993), Yanagihara (1994), and Bream (1999).

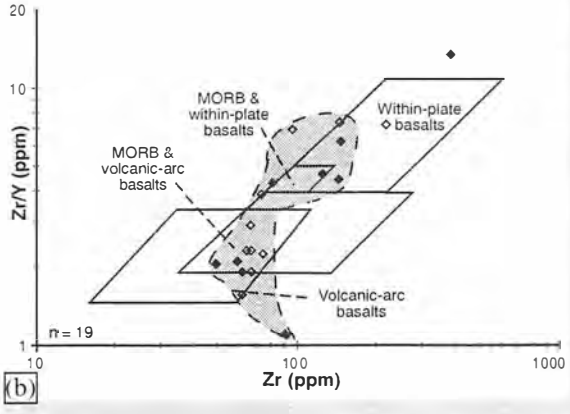

Eastern Inner Piedmont, South Carolina; Maybin and Niewendorp, 1997

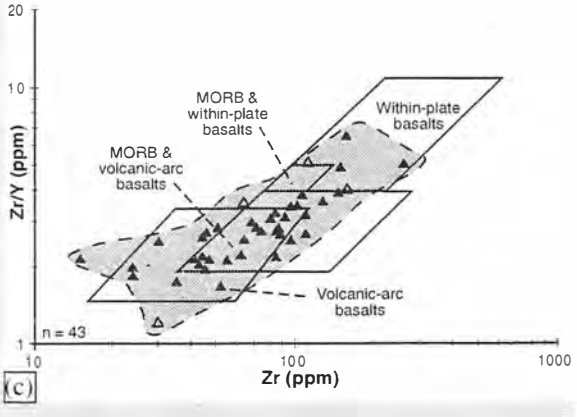

Migmatitic amphibolite data from Giorgis (1999).

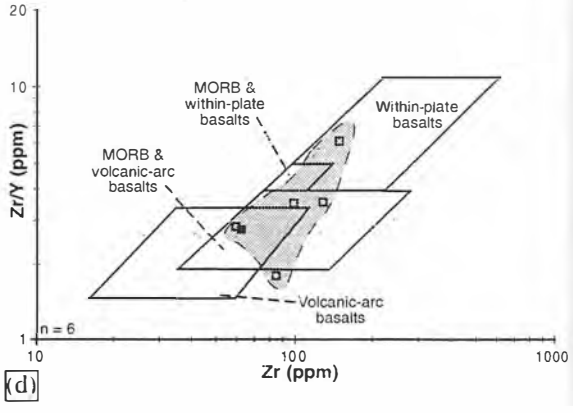

Figure 3-13. Zr/Y-Zr tectonic discrimination diagrams for basalts (after Pearce and Norry, 1979). Amphibolite and migmatite data are plotted for samples collected from: (a) this study (the South Mountains and Brushy Mountains); (b) western Inner Piedmont Poor Mountain Amphibolite (Davis, 1993; Yanagihara,1994; Bream, 1999); (c) eastern Inner Piedmont, South Carolina amphibolites (data reported in Maybin and Niewendorp, 1997); and (d) western Inner Piedmont, migmatitic amphibolite and biotite-amphibole granodiorite (data reported in Giorgis, 1999). Closed blocks, diamonds, and triangles indicate samples with CaO + MgO values between 12-20%. Open blocks indicate samples with CaO + MgO values greater than or less than 12-20%.

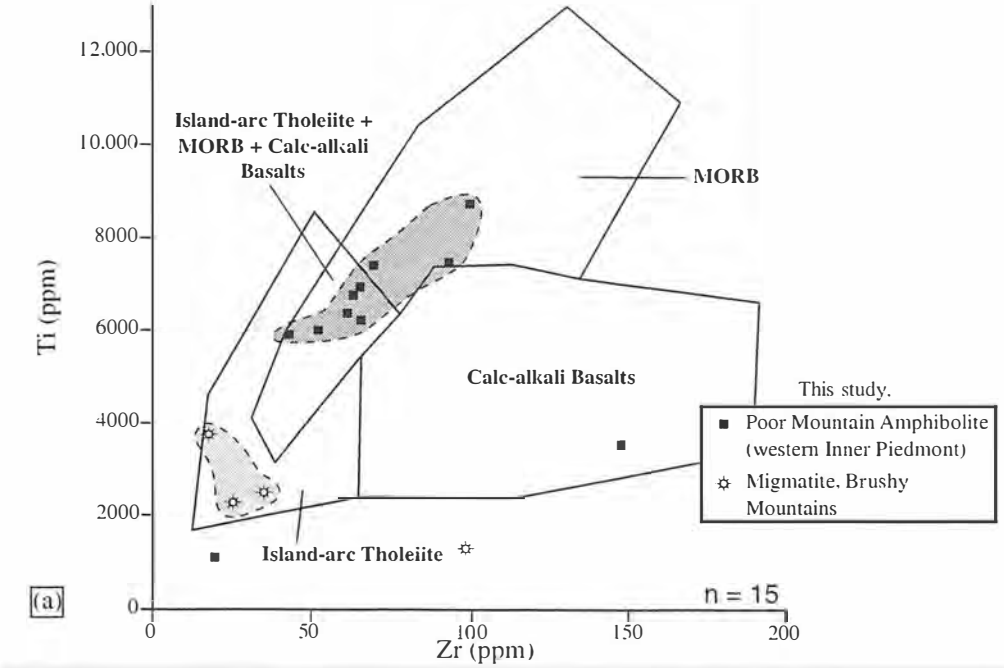

Poor Mountain Amphibolite data from Davis (1993), Yanagihara (1994), and Bream (1999).

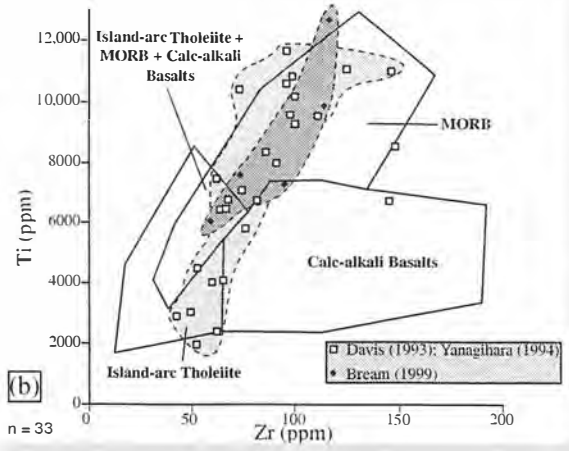

Migmatitic amphibolite/ hornblende-biotite granodiorite: this study and Giorgis (1999).

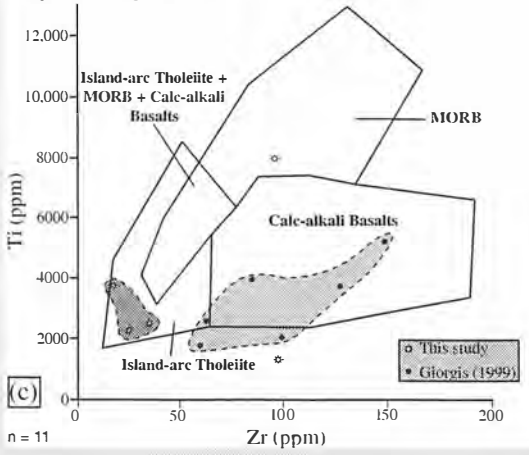

Eastern Inner Piedmont, South Carolina.

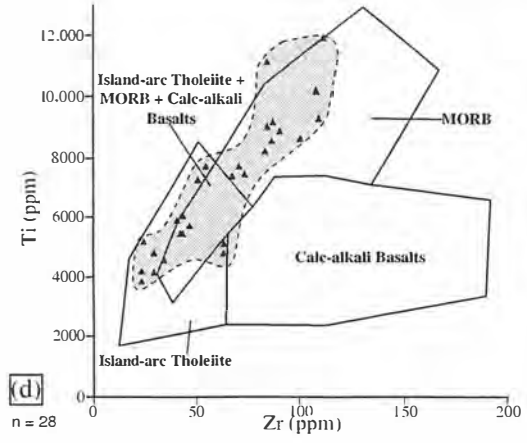

Figure 3-14. Ti/Zr tectonic discrimination diagrams for basalts (after Pearce and Cann, 1973). Amphibolite and migmatite composition data are plotted for samples collected from: (a) this study; (b) western Inner Piedmont Poor Mountain Amphibolite (Davis, 1993; Yanigahara, 1994; Bream, 1999); (c) western Inner Piedmont, migmatitic amphibolite and biotite-amphibole granodiorite (data reported in Giorgis, 1999); and (d) eastern Inner Piedmont, South Carolina amphibolites (data collected by Maybin and Niewendorp, 1997).

indicate the Poor Mountain Amphibolite was probably derived from tholeiitic, mid-ocean-ridge basalt (MORB) or, less likely volcanic-arc basalt (Figs. 3-12-3-14).

A detailed discussion of the origin of the Poor Mountain Formation is not in the scope of this treatment; geochemical data from the Poor Mountain Amphibolite, however, agree with contributions from numerous workers (Davis, 1993b; Yanagihara, 1994; Bream, 1999). A MORB affinity is implied from chemical tectonic discrimination. There is a nearly 1:1 correlation on incompatible element diagrams between concentrations of Sr, Ce, P_2O_5, Zr, Hf, Sm, TiO_2, Y, Yb, Sc, and Cr in the Poor Mountain Amphibolite and MORB concentrations of Pearce (1983). This lends further credibility to an island-arc tholeiite, calc-alkaline basalt, or MORB protolith. Enrichment of mobile trace elements in the Poor Mountain Amphibolite relative to idealized MORB concentrations may indicate post-depositional (diagenetic, metamorphic, metasomatic, or hydrothermal) alteration.

Geochronology

Most zircons from the leucosome sample have inherited magmatic cores with overgrowths (Fig. 3-15). Based on the distinct low fluorescence (in CL) of the overgrowths, several grains appear to have completely crystallized during a later event. The overgrowths have much lower (~0.03) Th/U ratios than inherited cores (up to 0.9; Table 3-4), typical of "metamorphic" zircons. Most grains are small (~100 μm) but several are significantly larger (up to 100's of μms). Inherited core $^{238}U/^{206}Pb$ ages range from 414 Ma to 527 Ma and show a modest tendency toward reverse discordance. Removal of two older and reversely discordant analyses and two younger (possibly core and overgrowth overlap) analyses yields a pooled $^{238}U/^{206}Pb$ age of 450 ± 6 Ma (MSWD

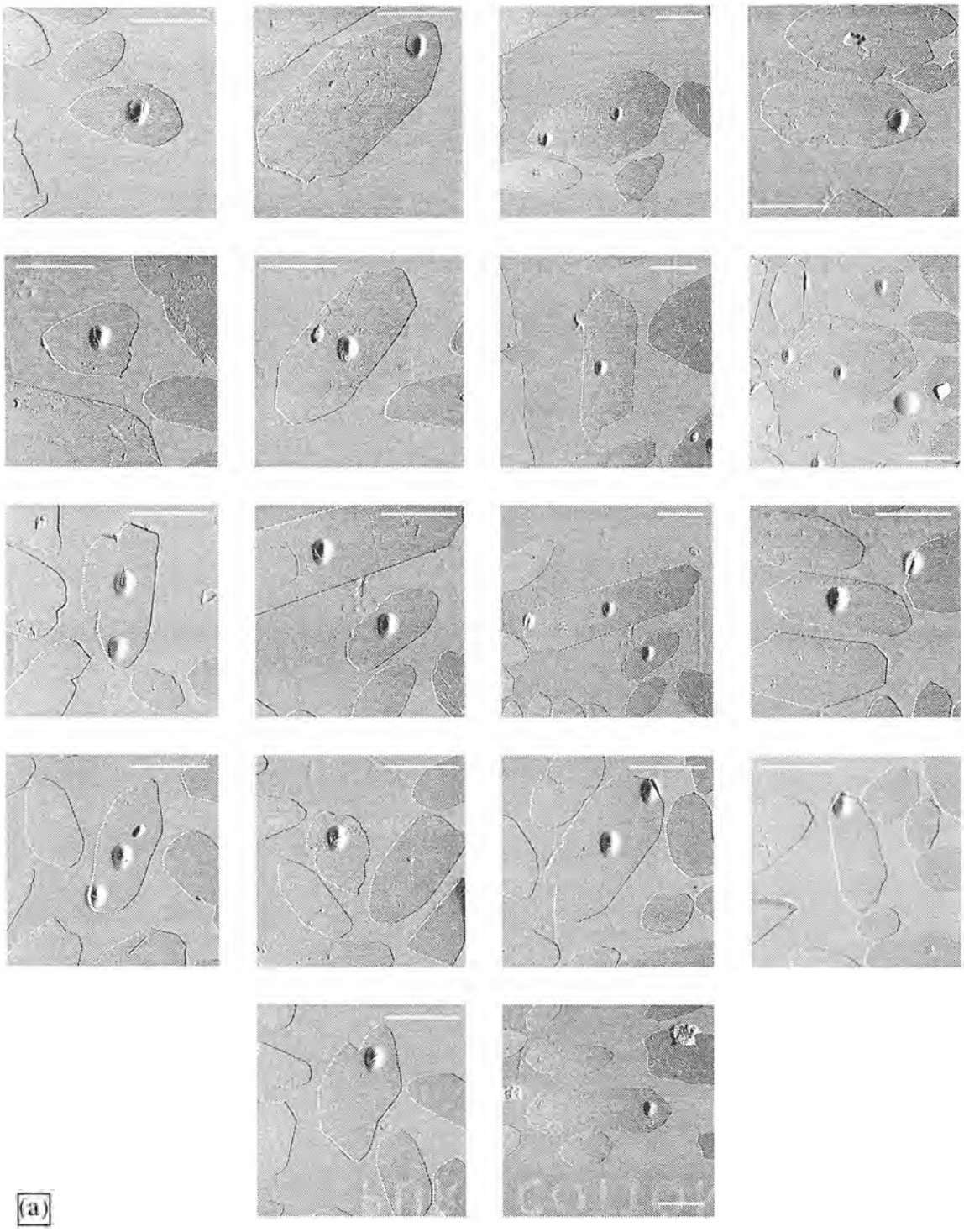

Figure 3-15. Backscattered electron (a) and cathodoluminescence (b) images of zircons from the migmatite leucosome. Zircons were imaged at the University of Tennessee-Knoxville using a Cameca SX-50 electron microprobe. Note that scale bar in each image is 100 m. Values in (b) are $^{206}Pb/^{238}U$ ages reported in Ma with 2 errors.

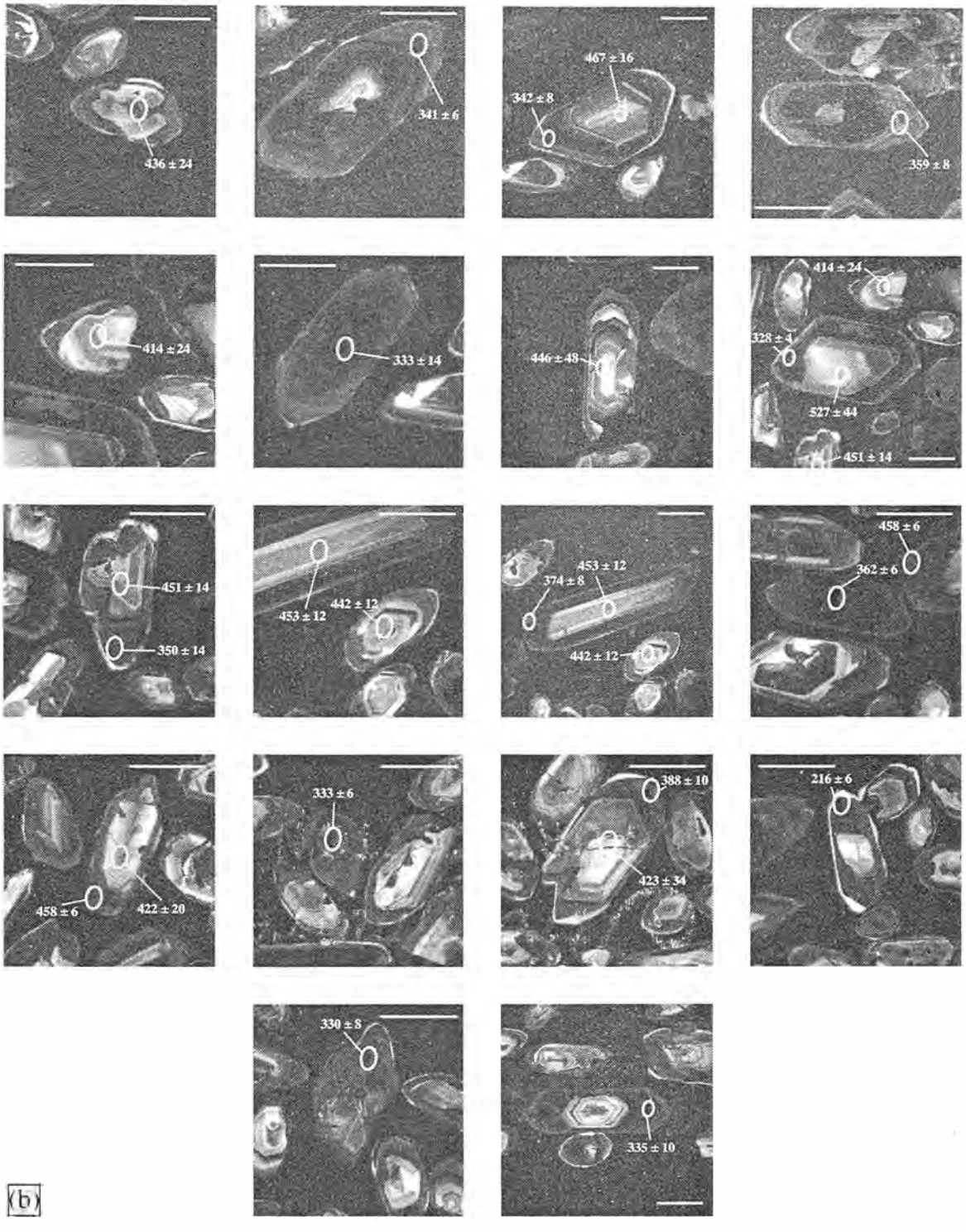

Figure 3-15. (continued)

Table 3-4: Ion microprobe (SHRIMP RG) data for zircons from the Vulcan Materials Company Lenoir Quarry (sample LVQ1).

Analysis		(in ppm)						Total							
					$^{204}Pb/$			$^{238}U/$		$^{207}Pb/$		$^{207}Pb/$		$^{206}Pb/$	
Label	Zone	U	Th	Th/U	^{206}Pb	±1	f206%[2]	^{206}Pb	±1	^{206}Pb	±1	^{235}U	±1	^{238}U	±1
LVQ1-1.1	IC	604	381	0.63	0.000181	0.000056	0.0033	14.25	0.42	0.0575	0.0014	0.556	0.022	0.070	0.002
LVQ1-2.1	M	1544	53	0.03	0.000010	0.000000	0.0002	18.40	0.14	0.0524	0.0008	0.393	0.007	0.054	0.000
LVQ1-3.1	IC	205	97	0.48	0.000160	0.000106	0.0029	13.28	0.25	0.0573	0.0030	0.595	0.035	0.075	0.001
LVQ1-3.2	M	1713	66	0.04	0.000033	0.000025	0.0006	18.36	0.23	0.0531	0.0008	0.399	0.008	0.054	0.001
LVQ1-4.1	M	893	30	0.03	0.000087	0.000043	0.0016	17.46	0.19	0.0520	0.0013	0.411	0.011	0.057	0.001
LVQ1-5.1	M	3523	192	0.05	0.000018	0.000014	0.0003	18.87	0.39	0.0522	0.0006	0.382	0.010	0.053	0.001
LVQ1-6.1	IC	139	62	0.44	0.000413	0.000227	0.0075	13.87	0.77	0.0567	0.0030	0.564	0.046	0.072	0.004
LVQ1-7.1	IC	301	264	0.88	0.000010	0.000000	0.0002	15.07	0.44	0.0559	0.0025	0.511	0.029	0.066	0.002
LVQ1-10.1	IC	211	89	0.42	<0.000001	--	<0.0001	11.74	0.51	0.0497	0.0022	0.584	0.039	0.085	0.004
LVQ1-10.2	M	2345	44	0.02	0.000009	0.000008	0.0002	19.14	0.13	0.0524	0.0004	0.378	0.004	0.052	0.000
LVQ1-11.1	IC	247	106	0.43	0.000095	0.000106	0.0017	13.77	0.21	0.0585	0.0011	0.585	0.015	0.073	0.001
LVQ1-11.2	M	1324	55	0.04	<0.000001	--	<0.0001	17.93	0.38	0.0526	0.0006	0.404	0.010	0.056	0.001
LVQ1-12.1	IC	217	159	0.73	0.000074	0.000068	0.0013	14.08	0.21	0.0561	0.0012	0.549	0.015	0.071	0.001
LVQ1-13.1	IC	256	159	0.62	0.000080	0.000211	0.0014	13.72	0.17	0.0543	0.0022	0.546	0.024	0.073	0.001
LVQ1-13.2	M	857	22	0.03	0.000041	0.000048	0.0008	16.72	0.16	0.0536	0.0009	0.442	0.009	0.060	0.001
LVQ1-14.1	M	12298	335	0.03	0.000005	0.000008	0.0001	17.30	0.17	0.0525	0.0003	0.418	0.005	0.058	0.001
LVQ1-15.1	IC	253	96	0.38	0.000010	0.000000	0.0002	14.78	0.38	0.0527	0.0023	0.491	0.026	0.068	0.002
LVQ1-15.2	M	834	425	0.51	0.000178	0.000052	0.0032	13.54	0.09	0.0553	0.0014	0.563	0.015	0.074	0.001
LVQ1-16.1	M	1547	158	0.10	0.000046	0.000044	0.0008	18.84	0.16	0.0547	0.0008	0.401	0.007	0.053	0.000
LVQ1-17.1	IC	287	142	0.50	0.000081	0.000092	0.0015	13.25	0.17	0.0543	0.0018	0.565	0.020	0.075	0.001
LVQ1-18.1	M	701	20	0.03	0.000070	0.000112	0.0013	16.11	0.20	0.0528	0.0007	0.452	0.009	0.062	0.001
LVQ1-18.2	IC	188	56	0.30	0.000046	0.000092	0.0008	14.74	0.62	0.0538	0.0015	0.504	0.027	0.068	0.003
LVQ1-19.1	M?	1093	721	0.66	0.000145	0.000049	0.0027	29.23	0.42	0.0535	0.0009	0.252	0.006	0.034	0.000
LVQ1-20.1	M	859	34	0.04	0.000010	0.000000	0.0002	19.05	0.23	0.0528	0.0012	0.382	0.010	0.052	0.001
LVQ1-21.1	M	3828	373	0.10	0.000012	0.000007	0.0002	18.75	0.28	0.0526	0.0004	0.387	0.007	0.053	0.001

Notes: (1) Common Pb corrected using measured ^{204}Pb.
(2) f206% denotes the percentage of ^{206}Pb that is common Pb.

= 1.7) and a concordia age of 450 ± 6 Ma (error includes decay constant errors, MSWD of concordance = 1.5, probability of concordance = 0.2). A discordia line, produced for the pooled inherited core analyses, has a lower intercept at 465 Ma and suggests that the actual age of the cores (if equivalent) could be slightly older than the pooled $^{238}U/^{206}Pb$ age (Fig. 3-16). Fourteen zircon overgrowth $^{238}U/^{206}Pb$ ages range from 216 Ma to 458 Ma and have very small errors (all are less than 7 Ma). Removal of the oldest (and extremely reverse discordant) analysis and a younger analysis produces ages ranging from 328 Ma to 388 Ma (n = 12) and yields a pooled age of 344 ± 2 Ma with a large MSWD of 26. Pooling subsets of younger and older analyses yields ages of 330 ± 3 (MSWD = 0.8, n =5) and 342 ± 5 (MSWD = 0.7, n = 3).

Discussion

Intensely migmatized amphibolite and biotite-hornblende granodiorite consistently crop out in the immediate footwall of the Brindle Creek thrust. This migmatite is traceable (with detailed and reconnaissance mapping) throughout most of western North Carolina from the South Carolina border, east of Hendersonville, through the southwestern Brushy Mountains (Fig. 3-2). The fault and the zone of intense migmatization probably continue into South Carolina (Fig. 1 in Hatcher, 2002), and thus are probably continuous along strike for > 110 km.

Petrogenesis

Peak thermobarometric conditions are well constrained in the Brindle Creek thrust hanging wall, and are inferred from footwall migmatite mineral assemblages (Part I). The most recent workers, Merschat and Kalbas (2002), report high grade conditions (585 °C, 2.8 kbar to 710 °C, 4.7 kbar) and local second sillimanite zone rocks in the Brindle

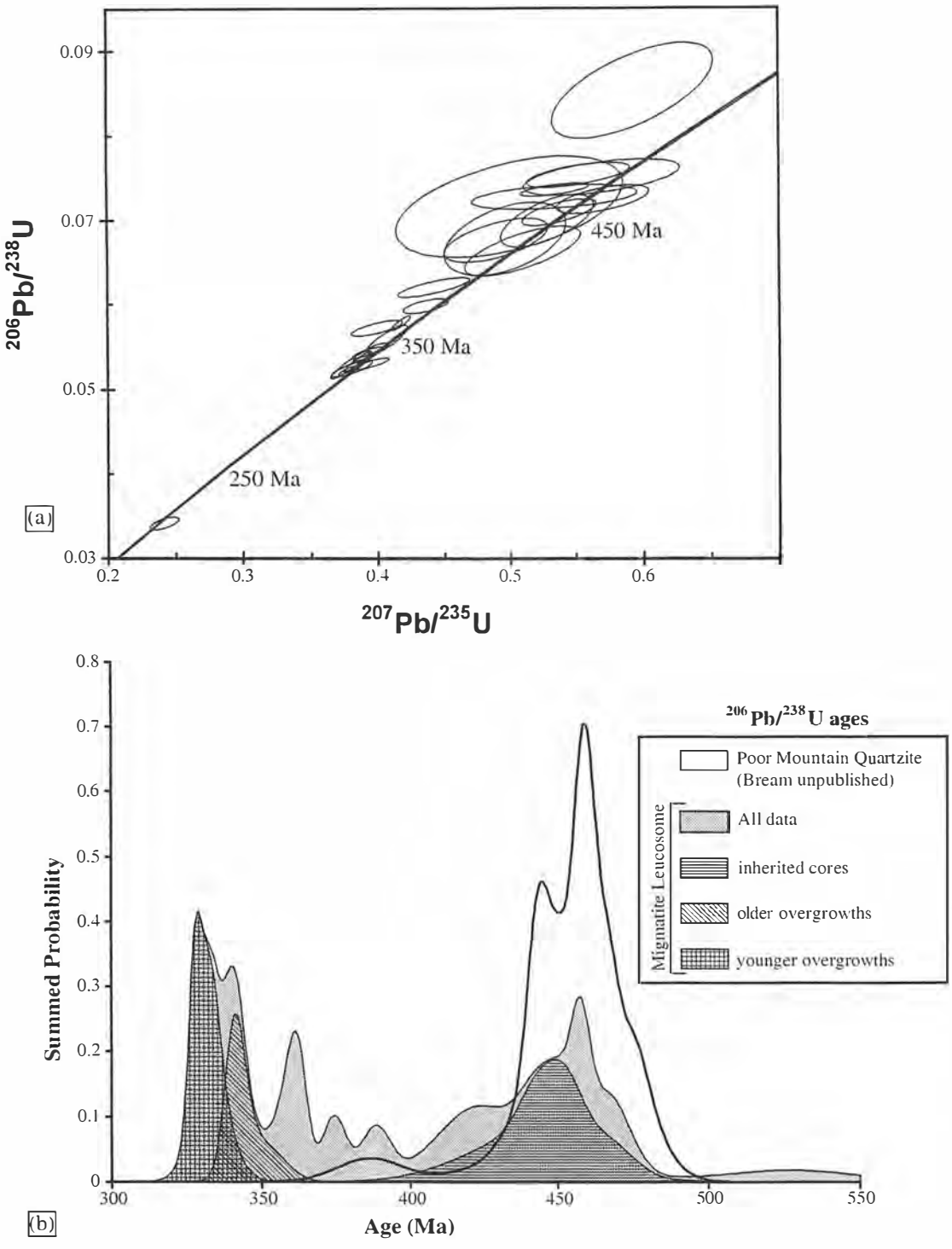

Figure 3-16. Concordia and summed probability plot of SHRIMP RG data. (a) Concordia diagram showing all data from the migmatite leucosome. Ellipses are plotted at 68.3 % confidence level. (b) Summed probability diagram showing all data (and subsets) from the migmatite leucosome with the age of the Poor Mountain Quartzite (Bream, unpublished data) for reference.

Creek thrust sheet in the Ellendale quadrangle. These values are consistent with previously reported Inner Piedmont values. Davis (1993a) reported temperatures from 535 to 690 °C and pressures from 3 to 5 kbar. Charnockite has also been reported in the eastern Inner Piedmont and indicates local granulite facies conditions (Kish, 1997). Higher temperatures were reported for Athens gneiss migmatite in the Inner Piedmont in northeastern Georgia (Mirante and Patino-Douce, 2000).

Several models have been proposed for migmatite formation: (1) subsolidus metamorphic differentiation (Robin, 1979; Ashworth and McLellan, 1985; Chavagnac et al., 1999); (2) subsolidus or hypersolidus metasomatism (e.g., Misch, 1968; Johannes et al., 1995); (3) layer-parallel injection of foreign magmas (e.g., Sederholm, 1934); (4) anatexis (e.g., Holmquist, 1921; Mehnert, 1968); and (5) layer-by-layer transformation (Henkes and Johannes, 1981; Johannes and Gupta, 1982; Johannes et al., 1995). Mesoscopic migmatite features denote intermittent partial melting in the migmatite zone. The presence of deformed metatexite and diatexite indicates partial melt conditions with metamorphic temperatures above 630 °C (Sawyer, 1999) persisted during penetrative deformation. This is consistent with estimated temperatures from mineral assemblages and compositions. Moreover, schlieren imply some melt fractions were at or above the melt escape threshold (Sawyer, 1999). Any plausible model for migmatization must account for at least local anatexis and melt migration.

Bulk major and trace element data are valuable in evaluating genetic models for migmatite formation. REE-bearing accessory phases (monazite, epidote, allanite, zircon, sphene, apatite, and garnet) control the distribution of REE in anatexites (McCarthy and Kable, 1978) and are commonly segregated between leucosome and melanosome

(Johannes et al., 1995); leucosome is usually depleted with respect to each phase except for garnet. Like previous studies (e.g., Johannes et al., 1995), positive linear correlations between Ce and Fe_{total} demonstrate REE are preferentially concentrated in mafic minerals of melanosome. Trace elements generally do not track open system melting, but evidence for melt mobility is not ubiquitous throughout the migmatite zone. My data patterns can thus be attributed to chemical differentiation within a partially closed system.

Complementary REE trends suggest a genetic relationship between some representative melanosome and leucosome sampled in this study (Fig. 3-9). REE sequestration into leucosomes is usually low because of diminished solubility of REE in hot felsic liquids (e.g., Watson, 1979; Harrison and Watson, 1984; Johannes et al., 1995). Leucosome here is strongly fractionated and systematically depleted in HREE relative to all melanosome samples, and depleted in LREE relative to melanosome group 2 (Fig. 9). As noted by Holtz (1989; his work in Portugal), complementary trends in REE data from migmatite samples collected from the Brushy and South Mountains may represent metamorphic segregation or partial melting. Metamorphic segregation at subsolidus conditions, however, typically produces leucosome with marked positive Eu anomalies (Sawyer and Barnes, 1988; Barbey et al., 1989). This was not observed here; therefore, subsolidus metamorphic segregation is not supported by the chemical data or by textures noted above. Supercritical hydrous fluids do not readily dissolve REE (Flynn and Burnham, 1978; Johannes et al., 1995); metasomatism likely had little effect on the immobile trace element chemistry of the migmatite. Likewise, consistent chemical

relationships between all eight migmatite samples rule out the large-scale intrusion of foreign magma.

Timing of Migmatization

Zircon growth can be attributed to a variety of processes related to either the prograde or retrograde portions of P-T-t paths (Connelly, 2001), although discrete overgrowths can be used to date specific thermal and/or fluid influx event(s). The youngest age (325 ma) determined for overgrowth in zircons from the migmatite leucosome is similar to a subset of metamorphic ages reported by several workers (e.g. Kish, 1990; Dennis and Wright, 1997; Mirante and Patino-Douce, 2000; Carrigan et al., 2001) and the 325 Ma age of Inner Piedmont pegmatite located at Zirconia, North Carolina (Callahan et al., 2002; Bream, unpublished data). The older overgrowth age (Fig. 3-16) is slightly younger (by ~10 Ma) than the 350 Ma age most commonly reported for "Neoacadian" monazite (Dennis and Wright, 1997; Mirante and Patino-Douce, 2000) and zircon rim growth (Bream et al., 2001b; Carrigan et al., 2001) within the southern Appalachian crystalline core. I propose that the intense zone of migmatization developed coeval with, or immediately following, a peak 350 Ma regional thermal event as a result of emplacement of the hot Brindle Creek thrust sheet. Following thrust movement, most of the southern Appalachian crystalline core was affected by a regional ~325 Ma metamorphic, pegmatite generation, and/or fluid migration event (Fig. 3-16).

Migmatite Protolith

In areas of detailed mapping, the migmatite conspicuously crops out in the same tectonostratigraphic position as the Poor Mountain Formation, above the Tallulah Falls

Formation. The former is commonly preserved in doubly plunging synclines in the immediate footwall of the Mill Spring thrust. Tallulah Falls rocks are also exposed in the immediate footwall of the Mill Spring thrust. Synclinal preservation of amphibolite overlain by feldspathic quartzite was also observed in migmatite of the Mill Spring thrust sheet in southwestern North Carolina (Giorgis, 1999; Williams, 2000; Plate 1); the repetitious tectonic pattern strongly supports a Poor Mountain Formation protolith for those rocks. It is therefore reasonable to also suspect the presence of the Poor Mountain Formation along strike (in the Brushy Mountains) in the Mill Spring thrust sheet.

The Poor Mountain stratigraphy, however, was not recognized in the Brushy Mountains. Moreover, the areal exposure of the migmatite in the southwestern Brushy Mountains is significantly greater than Poor Mountain Formation within lower thrust sheets (Plate 1). Contribution of an unrecognized migmatite source remains possible, but is more likely for the felsic component than the mafic component. Specifically, while mafic migmatite in the area is thought to be derived from Poor Mountain Amphibolite, qualitative volumetric estimates indicate there is too much leucosome for the migmatite to be derived solely from the Poor Mountain Amphibolite. Therefore, an additional source of leucocratic component, perhaps from adjacent quartzofeldspathic metagraywacke (Tallulah Falls Formation) or granitoids is plausible (Figs. 3-17, 3-18). Furthermore, several granitoid bodies were mapped within the unit in the Kings Creek quadrangle.

The question remains: can the composite migmatite be related to the Poor Mountain Amphibolite? Geochronologic evidence strongly supports a Late Ordovician igneous protolith. Ordovician core ages of migmatite zircons are nearly coeval with Poor

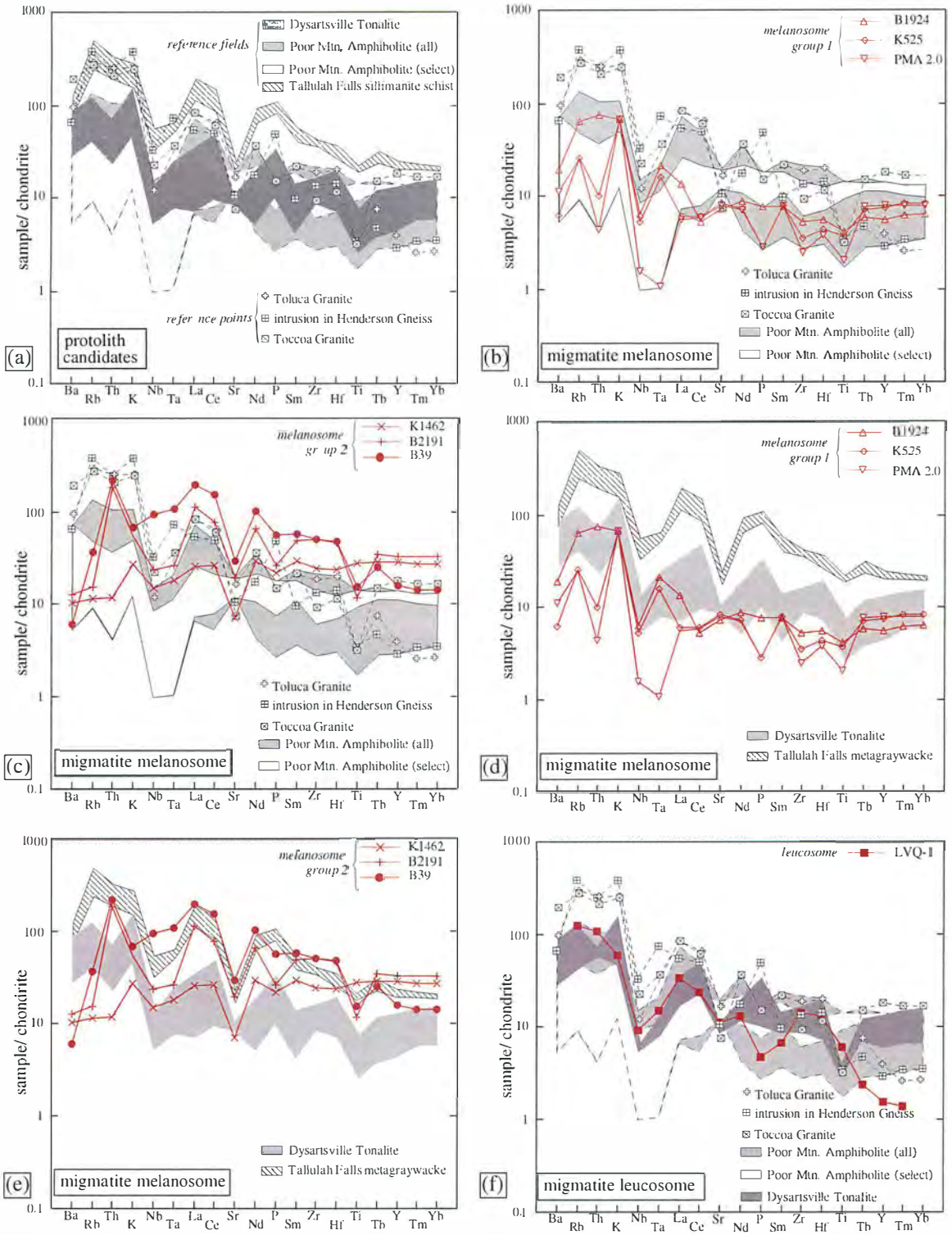

Figure 3-17. Chondrite-normalized trace element concentrations of migmatite sample groups compared with concentration reference points and fields from Poor Mountain Amphibolite and select eastern and western Inner Piedmont orthogneisses. Two reference fields are shown for Poor Mountain Amphibolite: (1) dark field = all data; (2) light field = data minus samples PMA-4.0 and PMA-10.0, which have inconsistent compositions. Trace element concentrations were obtained for Tallulah Falls metagraywacke, Toluca Granite, intrusive granitoid in the Henderson Gneiss, Toccoa granitoid, and Dysartsville Tonalite from Bream (unpublished data). Sample locations for migmatite samples are shown in Figure 2; sample groupings are the same as in Fig. 6. Chondrite values are from Thompson (1982).

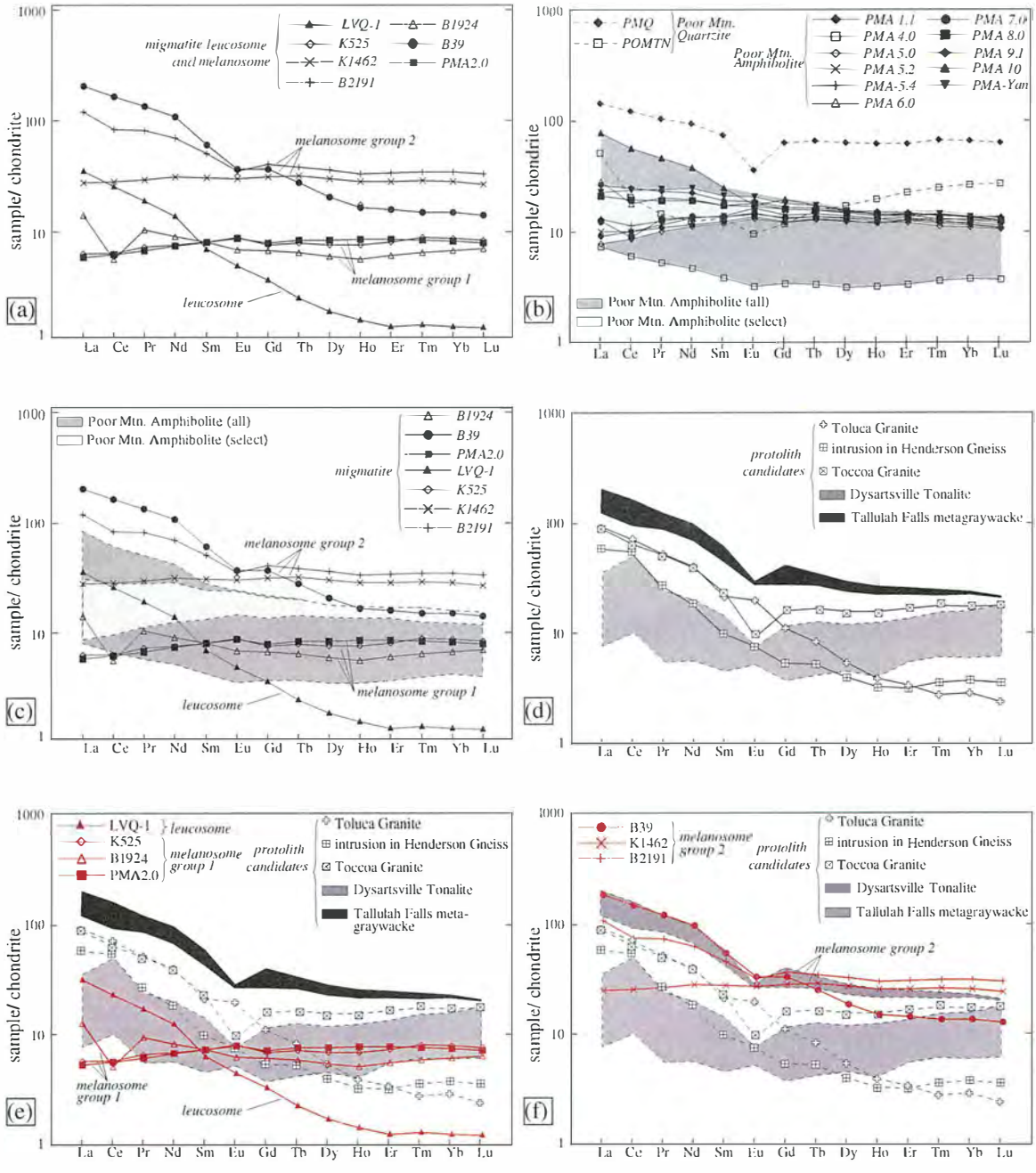

Figure 3-18. Chondrite-normalized REE concentrations. (a) Concentrations of Brindle Creek thrust footwall migmatite. (b) Concentrations of Poor Mountain Amphibolite and Quartzite. Two reference fields are shown for Poor Mountain Amphibolite: (1) dark field = all data; (2) a light field = data minus samples PMA-4.0 and PMA-10.0, which have inconsistent compositions. (c) Comparison of migmatite concentrations vs. Poor Mountain Amphibolite concentrations from (b). (d) REE concentrations of select Inner Piedmont granitoids. (e) Comparison of leucosome and melanosome group 1 concentrations vs. granitoid concentrations from (d). (f) Comparison of melanosome group 2 concentrations vs. granitoid concentrations from (d). Sample locations are shown in Figure 3-2. C1 chondrite values are from Boynton (1984).

Mountain Quartzite felsic tuff crystallization ages (Fig. 3-16) and rule out significant contributions from adjacent amphibolite-bearing metasedimentary units for these samples due to the presence of abundant Proterozoic detrital zircons in western Inner Piedmont metasedimentary samples (Bream, 2002). Contributions from numerous western Inner Piedmont Ordovician granitoids (Vinson and Miller, 1999; Bream, unpublished data) cannot be ruled out on the basis of geochronology.

Geochemical evidence further supports a potentially significant contribution from Poor Mountain Formation. Large variations in Zr concentration and Mg # of the migmatite indicate a substantial degree of fractionation relative to the Poor Mountain Amphibolite (Figs. 3-6, 3-7). Distinctive linear trends on variation diagrams for incompatible element and REE concentrations may represent differentiation of the Poor Mountain Amphibolite to produce the intermediate compositions of the migmatite (Figs. 3-6, 3-7), but do not preclude contributions from other sources. Tallulah Falls metagraywacke most notably plots in general linearity with the migmatite trend at the intermediate to high fractionation (terminology of Rollinson [1998]) sections of both variation diagrams and may have contributed to the composition of the composite migmatite.

Trace element and REE trends in three migmatite groups (melanosome group 1, melanosome group 2, and leucosome; Figs. 8, 9) are discussed here in turn with respect to reference fields and traces of protolith candidates from the western and eastern Inner Piedmont (Figs. 3-17, 3-18). Migmatite melanosome group 1 overlaps the Poor Mountain Amphibolite composite field and low compatibility trace element concentrations in the Poor Mountain Amphibolite select field, but is systematically

depleted in all trace elements with respect to reference granitoids (Fig. 3-17b). The same group is slightly depleted in higher compatibility trace elements with respect to the Poor Mountain Amphibolite select field. Trace element concentration trends in melanosome group 1 are similar to Dysartsville Tonalite and Tallulah Falls metagraywacke, but the migmatite is depleted (especially in low compatibility trace elements) with respect to both. If the Poor Mountain Amphibolite is the protolith for melanosome group 1, depletion in higher-compatibility trace elements in melanosome is consistent with chemical differentiation. Melanosome group 1 REE trends are not in agreement with trends of reference granitoids, Dysartsville Tonalite, or Tallulah Falls metagraywacke (Fig. 3-18e). Figure 3-18c, however, shows melanosome group 1 concentrations overlap the Poor Mountain Amphibolite composite field and patterns mimic the Poor Mountain Amphibolite select field. The melanosome has only minor fractionation with slight HREE enrichment and is depleted in REE relative to average Poor Mountain Amphibolite (Fig. 3-18c). Their REE trends are similar to the partition coefficient of hornblende in basalt (Arth, 1976; Green and Pearson, 1985) and concentrations from Scourian Complex mafic to intermediate gneisses in Scotland reported by Pride and Muecke (1981). These samples may thus represent partially modified (slightly enriched in felsic minerals) Poor Mountain Amphibolite. The data, however, do not distinguish between subsolidus metamorphic differentiation and anatexis. Trends can also be explained by metasomatic influx of felsic minerals, and dilution of the bulk composition with respect to REE.

Melanosome group 2 overlaps the Poor Mountain Amphibolite fields in low compatibility trace elements, but has a dissimilar pattern in higher compatibility trace elements characterized by minor fractionation and enrichment relative to Poor Mountain

Amphibolite and reference granitoids (Fig. 3-17c). Interestingly, the same migmatite group has a nearly identical trend and trace element concentrations as three Tallulah Falls metagraywacke samples (Fig. 3-17c). A similar relationship is seen in REE spider diagrams (Fig. 3-18f) where two of three highly fractionated melanosome group 2 sample trends closely match Tallulah Falls metagraywacke concentrations. Melanosome group 2 samples were collected at the greatest distance (to the northwest) from the fault; it is possible their chemistry reflects a contribution of Tallulah Falls Formation to the migmatite melanosome.

Trends in leucosome concentrations follow the trends of the reference granitoids; the leucosome is, however, depleted in all trace elements with respect to the granitoids (Fig. 3-17f). A similar relationship is seen in REE; the highly fractionated leucosome (enriched in LREE and depleted in HREE) follows the fractionation trend of reference granitoids, but is depleted with respect to each REE. Leucosome trace element and REE patterns are not similar to those of Dysartsville Tonalite. Enrichment, in the leucosome, of low compatibility trace elements and depletion of higher compatibility trace elements relative to average Poor Mountain Amphibolite concentrations strongly suggests it represents a melt fraction derived from the amphibolite (Fig. 3-17f).

Tectonic Implications of Fault-related Anatexis in the IP

Geochronologic evidence indicates diachronous relationships in the eastern and western Inner Piedmont and Neoacadian emplacement of the Brindle Creek thrust sheet. Specifically, western Inner Piedmont thrust sheets contain primarily Ordovician-age granitoids (Vinson and Miller, 1999; Bream, unpublished data). Eastern Inner Piedmont orthogneisses have Late Devonian and early Mississippian crystallization ages (Mapes,

2002); therefore, it is likely that the eastern and western Inner Piedmont remained separated during early and middle to late Paleozoic granitoid intrusion. If Acadian and Neoacadian plutonic suites are restricted to the Brindle Creek thrust sheet and zircon overgrowths date migmatization, the timing of thrust emplacement is confined to an ~30 m.y. interval between the crystallization age of the Walker Top Granite and Toluca Granite and the oldest metamorphic overgrowth in the migmatite (Fig. 3-16).

A paradigm, summarized by Druguet and Hutton (1998), states that deformation has a significant effect on the ascent and emplacement of anatectic melts, but also affects their original formation. The feedback mechanism between partial melting and strain localization (Hollister and Crawford, 1986; Raia and Spera, 1997; Brown and Solar, 1998; Kisters et al., 1998) may have promoted localized shear development near or along the Brindle Creek thrust. The zone of intense migmatization, however, is confined to the footwall of the thrust, and may represent a localized increase in heat transfer caused by the hot emplacement of the thrust sheet. Moreover, as suggested by Vernon and Paterson (2001, in north Queensland, Australia), the presence of leucosome interlayered and coaxially folded (F_2) with melanocratic layers and the regional S_2 structural trend indicates synchronous metamorphic (migmatitic) segregation and deformation.

This study is the first analysis of the petrogenesis of the zone of intense migmatization adjacent to the Brindle Creek thrust in North Carolina. Additional detailed geologic mapping along this boundary is required to better understand the macroscopic distribution of the zone of intense migmatization. U-Pb age dating of zircons from melanosome group 2 samples would help clarify if they are more closely related to Tallulah Falls Formation. Furthermore, the activity of H_2O-rich metasomatic

fluids, while having minimal effect on the distribution of REE (e.g., Brookins, 1989), likely influenced the conditions of migmatization and anatexis in the southern Appalachian Inner Piedmont (Mirante and De La Rosa, 2001).

Conclusions

- The Brindle Creek thrust is an orogen-scale fault that can be traced for at least 110 km in southwestern and central western North Carolina.

- A zone of intense migmatization crops out in the footwall of the Brindle Creek thrust.

- The dominant unit in the migmatite zone consists of amphibolite, biotite gneiss, and biotite-hornblende granodiorite.

- My work supports that of previous workers; the Poor Mountain Amphibolite likely has an oceanic origin and may be derived from tholeiitic MORB or volcanic arc basalt.

- Trace element and REE patterns in stromatic migmatite from the study area are in part the result of partial melt segregation of impure leucosome. Localized subsolidus metamorphic differentiation and metasomatism, unlike other petrogenetic models, cannot be ruled out by trace element data.

- The presence of diatexites indicates partial melting occurred; peak metamorphic temperatures in the footwall of the Brindle Creek thrust were likely 630 to 700 °C, and are compatible with P-T estimates of Merschat and Kalbas (2002).

- Geometric, geochronologic, and geochemical data indicate the migmatite may be partially derived from the Poor Mountain Amphibolite.

- In areas where it was mapped at the 1:24,000 or larger scale, the migmatitic amphibolite and biotite-hornblende granodiorite are in the same tectonostratigraphic position as the Poor Mountain Formation.

- Poor Mountain Quartzite and migmatite leucosome inherited cores have the same Ordovician (450 Ma) age. Subsequent metamorphic/migmatitic rim growth of migmatite zircons occurred at 342 Ma (latest Neoacadian) and 330 Ma (earliest Alleghanian).

- Chemical data indicate the bulk chemistry of one migmatite melanosome group (= three samples) correlates with Poor Mountain Amphibolite compositions. A second migmatite melanosome group has trace-element concentrations that coincide with those of Tallulah Falls metagraywacke, suggesting a genetic relationship. Other Inner Piedmont units (Dysartsville Tonalite, Toluca Granite, Toccoa granitoid, and intrusive rocks in the Henderson Gneiss) are not favored as migmatite protoliths by the chemical data.

- The spatial and temporal coincidence of the zone of intense migmatization and the Brindle Creek thrust indicates Neoacadian/earliest Alleghanian thrust emplacement and migmatization are related.

Acknowledgments

SHRIMP RG analyses, and geochemical analyses were financed by the National Science Foundation (EAR-9814800 awarded to RDH). BRB acknowledges J. Wooden and C. Miller for assistance with SHRIMP RG analyses. Helpful comments were provided by K. Misra and L. Taylor. I gratefully acknowledge the Vulcan Materials Company for unlimited access to the Lenoir quarry. This study benefited from discussions with and/or field assistance by A. Merschat (University of Tennessee), E.

Kalbas, K. Ridgway, D. Granger (Purdue University), C. Merschat, L. Weiner, and M. Carter (North Carolina Geologic Survey). Technical support was provided by my colleagues at Purdue University E. Farmer, M. Lesch, and B. Hampton. This study would not have been possible without access to private property; I therefore sincerely thank the many land owners in Caldwell County, North Carolina, especially B. Bush.

References Cited

Arth, J. G., 1976, Behavior of trace elements during magmatic processes: A summary of theoretical models and their applications: Journal of Research of the U. S. Geological Survey, v. 4, p. 41-47.

Ashworth, J. R., and McLellan, E. L., 1985, Textures: *in* Ashworth, J. R., ed., Migmatites: Glasgow, Blackie, p. 180-203.

Bacon, C. R., Persing, H. M., Wooden, J. L., and Ireland, T. R., 2000, Late Pleistocene granodiorite beneath the Crater Lake caldera, Oregon, dated by ion microprobe: Geology, v. 28, p. 467-470.

Barbey, P., Bertrand, J. M., Angoua, S., and Dautel, D., 1989, Petrology and U/Pb geochronology of the Telohat migmatites, Aleksod, Central Hoggar, Algeria: Contributions to Mineralogy and Petrology, v. 101, p. 207-219.

Bier, S. E., Bream, B. R., and Hatcher, R. D., Jr., 2000, Detailed geologic mapping of the western and central Inner Piedmont, North Carolina: Geological Society of America, Abstracts with Programs, v. 32, p. A-234.

Boynton, W. V., 1984, Geochemistry of the rare earth elements: Meteorite studies, *in* Henderson, P., ed., Rare earth element geochemistry: Amsterdam, Elsevier, p. 63-114.

Bream, B. R., 1999, Structure and stratigraphic relationships of ortho- and paragneisses southwest of Marion, North Carolina [M.S. thesis]: Knoxville, University of Tennessee, 155 p.

Bream, B. R. 2002, The southern Appalachian Inner Piedmont: new perspectives and enduring issues based on recent detailed mapping, isotopic evidence, and geochronology, *in* Hatcher, R. D., Jr., and Bream, B. R., eds., Inner Piedmont tectonics focused mostly on detailed studies in the South Mountains and the southern Brushy Mountains, North Carolina: Carolina Geological Society Guidebook, North Carolina Geological Survey, p. 45-64.

Bream, B. R., Hatcher, R. D., Jr., Miller, C. F., Carrigan, C. W., and Fullagar, P. D., 2001a, Provenance and geochemistry of Late Proterozoic southern Appalachian crystalline core paragneisses, NC-SC-GA-TN: Geological Society of America Abstracts with Programs, v. 33, p. A-65.

Bream, B. R., Hatcher, R. D., Jr., Miller, C. F., and Fullagar, P. D., 2001b, Geochemistry and provenance of Inner Piedmont paragneisses, NC and SC: Evidence for an internal terrane boundary: Geological Society of America Abstracts with Programs, v. 33, p. A-65.

Brookins, D. G., 1989, Aqueous geochemistry of rare earth elements: Geochemistry and mineralogy of the rare earth elements, *in* Lipin, B. R. and McKay, G. A., eds., Mineralogical Society of America, Reviews in Mineralogy , v. 21, p. 201-226.

Brown, M., and Solar, G. S., 1998, Shear-zone systems and melts: Feedback relations and self-organization in orogenic belts: Journal of Structural Geology, v. 20, p. 211-227.

Butler, J. R., 1991, Metamorphism, *in* Horton, J. W., Jr., and Zullo, V. A., eds., The geology of the Carolinas, Carolina Geological Society Fiftieth Anniversary Volume: Knoxville, University of Tennessee Press, p. 127-142.

Callahan, J. E., Stepp, J. D., Johnson, N. E., and Bream, B. R., 2002, Fluorescence and lack thereof in zircons from the Freeman zircon mine, Zirconia District, North Carolina: Geological Society of America Abstracts with Programs, v. 34, p. A-22.

Carrigan, C. W., Bream, B. R., Miller, C. F., and Hatcher, R. D., Jr., 2001, Ion microprobe analyses of zircon rims from the eastern Blue Ridge and Inner Piedmont, NC-SC-GA: Implications for the timing of Paleozoic metamorphism in the southern Appalachians: Geological Society of America Abstracts with Programs, v. 33, p. A-42.

Chavagnac, V., Nagler, T. F., and Kramers, J. D., 1999, Migmatization by metamorphic segregation at subsolidus conditions: Implications for Nd-Pb isotope exchange: Lithos, v. 46, p. 275-298.

Connelly, J. N., 2001, Constraining the timing of metamorphism: U-Pb and Sm-Nd ages from a transect across the northern Torngat Orogen, Labrador, Canada: Journal of Geology, v. 109, p. 57-77.

Cox, K. G., Bell, J. D., and Pankhurst, R. J., 1979, The interpretation of igneous rocks: London, Allen and Unwin, 450 p.

Curl, D. C., 1997a, Bedrock geologic map of the Reidville 7.5 minute quadrangle, Spartanburg and Laurens Counties, South Carolina: South Carolina Geological Survey Open File Report 94, scale 1:24,000.

Curl, D. C., 1997b, Bedrock geologic map of the Welford 7.5 minute quadrangle, Spartanburg County, South Carolina: South Carolina Geological Survey Open File Report 95, scale 1:24,000.

Davis, T. L., 1993a, Geology of the Columbus Promontory, western Piedmont, North Carolina, southern Appalachians, *in* Hatcher, R. D., Jr., and Davis, T. L., eds., Studies of Inner Piedmont geology with a focus on the Columbus Promontory: Carolina Geological Society Field Trip Guidebook, p. 17–44.

Davis, T. L., 1993b, Lithostratigraphy, structure, and metamorphism of a crystalline thrust terrane, western Inner Piedmont, North Carolina [unpublished Ph.D. dissertation]: Knoxville, University of Tennessee, 245 p.

Dennis, A. J., and Wright, J. E., 1997, Middle and late Paleozoic monazite U-Pb ages, Inner Piedmont, South Carolina: Geological Society of America Abstracts with Programs, v. 29, p. A-223.

Druguet, E., and Hutton, D. H. W., 1998, Syntectonic anatexis and magmatism in a mid-crustal transpressional shear zone: An example from the Hercynian rocks of the eastern Pyrenees: Journal of Structural Geology, v. 20, p. 905-916.

Flynn, R. T., and Burnham, C. W., 1978, An experimental determination of rare earth partition coefficients between chloride-containing vapor phase and silicate melts: Geochimica et Cosmochimica Acta, v. 42, p. 685-701.

Giorgis, S. D., 1999, Inner Piedmont geology of the northwestern South Mountains near Morganton, North Carolina [M.S. thesis]: Knoxville, University of Tennessee, 191 p.

Giorgis, S. D., Hatcher, R. D., Jr., and Riedel, J. J., 1998, Evolution of thrust sheets in the western Inner Piedmont, NC: Geological Society of America Abstracts with Programs, v. 30, p. A-124.

Giorgis, S. D., Mapes, R. W., and Bream, B. R., 2002, The Walker Top Granite: Acadian granitoid or eastern Inner Piedmont basement?: *in* Hatcher, R. D., Jr., and Bream, B. R., eds., Inner Piedmont tectonics focused mostly on detailed studies in the South Mountains and the southern Brushy Mountains, North Carolina: Carolina Geological Society Guidebook, North Carolina Geological Survey, p. 33-44.

Goldsmith, R., Milton, D. J., and Horton, J. W., 1988, Geologic map of the Charlotte 1° x 2° quadrangle, North Carolina and South Carolina: U.S. Geological Survey Map I-125-E, scale 1:250,000.

Green, T. H., and Pearson, N. J., 1985, Experimental determination of REE partition coefficients between amphibole and basaltic liquids at high pressure: Geochimica et Cosmochimica Acta, v. 49, p. 1465-1468.

Griffin, V. S., 1967, Geology of the Six Mile quadrangle, South Carolina: South Carolina Division of Geology MS-14, scale 1:24,000.

Harrison, T. M., and Watson, E. B., 1984, The behavior of apatite during crustal anatexis: Equilibrium and kinetic considerations: Geochimica et Cosmochimica Acta, v. 48, p. 1467-1477.

Hatcher, R. D., Jr., 1969, Stratigraphy, petrology, and structure of the low rank belt and part of the Blue Ridge of northwesternmost South Carolina: South Carolina Division of Geology, Geologic Notes, v. 13, p. 105-141.

Hatcher, R. D., Jr., 1970, Stratigraphy of the Brevard zone and Poor Mountain area, northwestern South Carolina: Geological Society of America Bulletin, v. 81, p. 933-940.

Hatcher, R. D., Jr., 2002, An Inner Piedmont primmer, *in* Hatcher, R. D., Jr., and Bream, B. R., eds., Inner Piedmont tectonics focused mostly on detailed studies in the South Mountains and the southern Brushy Mountains, North Carolina: Carolina Geological Society Guidebook, North Carolina Geological Survey, p. 1-18.

Hatcher, R. D., Jr., Bream, B. R., Hill, J. C., Giorgis, S. D., and Williams, S. T., 1999, Transect through the Acadian orogen in the Carolinas and northeast Georgia: Geological Society of America Abstracts with Programs, v. 31, p. A-19.

Hatcher, R. D., Jr., Osberg, P. H., Drake, A. A., Jr., Robinson, P., and Thomas, W. A., 1990, Tectonic map of U.S. Appalachians, *in* Hatcher, R. D., Jr., Thomas, W. A., and Viele, G. W., eds., The Appalachian–Ouachita orogen in the United States: Boulder, Geological Society of America, The Geology of North America, v. F–2, Plate 1, scale 1:2,000,000.

Henkes, J. and Johannes, W., 1981, The petrology of a migmatite (Arvika Varmland, western Sweden): Neues Jahrbuch fuer Mineralogie, v. 141, p. 113-133.

Hollister, L. S., and Crawford, M. L., 1986, Melt-enhanced deformation: A major tectonic process: Geology, v. 14, p. 558-561.

Holmquist, P. J., 1921, Typen and Nomenklatur der Adergesteine: Geologiska Foereningen i Stockholm Foerhandlinger, v. 43, p. 613-631.

Holtz, F., 1989, Importance of melt fraction and source rock composition in crustal granitoid genesis: The example of two granitic suites north of Portugal: Lithos, v. 24, p. 21-35.

Irvine, T. N., and Baragar, W. R. A., 1971, A guide to the chemical classification of common rocks: Canadian Journal of Earth Science, v. 8, p. 523-548.

Jayne, C. C., 1991, Geologic map of part of the Lake Lure quadrangle, North Carolina (unpublished mapping): Knoxville, University of Tennessee, scale 1:24,000.
Johannes, W., and Gupta, L. N., 1982, Origin and evolution of a migmatite: Contributions to Mineralogy and Petrology, v. 79, p. 14-23.
Johannes, W., Holtz, F., and Möller, P., 1995, REE distribution in some layered migmatites: Constraints on their petrogenesis: Lithos, v. 35, p. 139-152.
Kalbas, J. L., Bream, B. R., Hatcher, R. D., Jr., and Maybin, A. H., III, 2002, Evidence for mafic Ordovician magmatism and Acadian metamorphism in the Brushy Mountains, Western Inner Piedmont of North Carolina: Geological Society of America Abstracts with Programs, v. 34, A-119.
Kalbas, J. L., Merschat, A. J., Hatcher, R. D., Jr., and Bream, B. R., 2001, Detailed geologic mapping of the Brushy Mountains, Inner Piedmont, near Lenoir, North Carolina: Geological Society of America, Abstracts with Programs, v. 33, p. A-82.
King, P. B., 1950, Tectonic framework of southeastern United States: Bulletin of American Association of Petroleum Geologists, v. 14, p. 635-671.
Kish, S. A., 1990, Timing of middle Paleozoic (Acadian) metamorphism in the southern Appalachians; K-Ar studies in the Talladega Belt, Alabama: Geology, v. 18, p. 650-653.
Kish, S. A., 1997, The Cat Square charnockite; a Paleozoic charnockite in the Inner Piedmont of North Carolina: Geological Society of America Abstracts with Programs, v. 29, p. A-28.
Kisters, A. F. M., Gibson, R. L., Charlesworth, E. G., and Anhaeusser, C. R., 1998, The role of strain localization in the segregation and ascent of anatectic melts, Namaqualand, South Africa: Journal of Structural Geology, v. 20, p. 229-242.
Leake, B. E., 1964, The chemical distinction between ortho- and para-amphibolites: Journal of Petrology, v. 5, p. 238-254.
Ludwig, K. R., 1991, ISOPLOT: A plotting and regression program for radiogenic-isotope data: OF 91-0445, U.S. Geological Survey, Reston.
Ludwig, K. R., 1998, On the treatment of concordant uranium-lead ages: Geochemica et Cosmochemica Acta, v. 62, p. 665-676.
Maclean, J. S., and Blackwell, S. S., 2001, Paris Mountain Project: Part 1, Geology of the Taylors 7.5 minute quadrangle, Greenville County, South Carolina, *in* Garihan, J. M., Ranson, W. A., and Clendenin, C. W., eds., South Carolina Geology: South Carolina Department of Natural Resources, v. 43, p. 25-35.
Mapes, R. W., 2002, Geochemistry and geochronology of mid-Paleozoic granitic plutonism in the southern Appalachian Piedmont terrane, North Carolina-South Carolina-Georgia [M.S. Thesis]: Vanderbilt University, 140 p.
Mapes, R. W., Maybin, A. H., III, Miller, C. F., Fullagar, P. D., and Bream, B. R., 2002, Geochronology and geochemistry of mid Paleozoic granitic magmatism, central and eastern Inner Piedmont, NC & SC: Geological Society of America Abstracts with Programs, v. 34, p. A-94.
Maybin, A. H., III, 1998, Bedrock geologic map of the Greer 7.5 minute quadrangle, Greenville and Spartanburg Counties, South Carolina: South Carolina Geological Survey Open File Report 113, scale 1:24,000.

Maybin, A. H., III, and Niewendorp, C. A., 1997, Whole-rock geochemical analysis of samples from Abbeville, Greenville, Greenwood, Laurens, Newberry, Saluda, Spartanburg, and Union counties, South Carolina: South Carolina Department of Natural Resources, Geological Survey Open File Report 98, 4 p.

McCarthy, T. S., and Kable, E. J. D., 1978, On the behavior of rare earth elements during partial melting of granitic rocks: Chemical Geology, v. 22, p. 21-29.

Mehnert, K. R., 1968, Migmatites and the origin of granitic rocks: Amsterdam. Elsevier. 393 p.

Merschat, A. J., and Kalbas, J. L., 2002, Geology of the southern Brushy Mountains, North Carolina Inner Piedmont: A summary and synthesis of recent studies: *in* Hatcher, R. D., Jr., and Bream, B. R., eds., Inner Piedmont tectonics focused mostly on detailed studies in the South Mountains and the southern Brushy Mountains, North Carolina: Carolina Geological Society Guidebook, North Carolina Geological Survey, p. 101-126

Mirante, D. C., 2001, Monazite ages from the southern Appalachian Inner Piedmont: The Athens gneiss: Geological Society of America Abstracts with Programs, v. 33, p. A-30.

Mirante, D. C., and De La Rosa, J., 2001, Geochemistry of migmatites from northeastern Georgia: The Athens gneiss: Geological Society of America Abstracts with Programs, v. 33, p. A-30.

Mirante, D. C., and Patino-Douce, A. E., 2000, Melting and migmatization in the southern Appalachian Inner Piedmont of northeast Georgia; the Athens Gneiss: Geological Society of America Abstracts with Programs, v. 32, p. A-297.

Misch, P., 1968, Plagioclase composition and nonanatectic origin of migmatitic gneisses in northern Cascade Mountains of Washington State: Contributions to Mineralogy and Petrology, v. 17, p. 1-70.

Nabelek, P. I., Bartlett, C., and Glascock, M., 1999, Can trace element distribution in migmatites be used as analogues in understanding petrogenesis of anatectic granites?: Physics and Chemistry of the Earth, Part A, v. 24, p. 295-298.

Nelson, A. E., Horton, J. W., Jr., and Clarke, J. W., 1998, Generalized tectonic map of the Greenville 1° x 2° quadrangle, Georgia, South Carolina, and North Carolina: U. S. Geological Survey Miscellaneous Field Studies Map I-2175, Scale 1:250,000.

Niewendorp, C. A., Clendenin, C. W., Dorr, W. R., III, and Maybin, A. H., III, 1997, Geologic map of the Paris Mountain 7.5 minute quadrangle: South Carolina Geological Survey Open–File Report 99, scale 1:24,000.

Paces, J. B., and Miller, J. D., 1993, U-Pb ages of Duluth complex and related mafic intrusions, northeastern Minnesota: Geochronological insights into physical, petrogenetic, paleomagnetic, and tectonomagmatic processes associated with the 1.1 Ga mid-continent rift system: Journal of Geophysical Research, v. 98, p. 13,997-14,013.

Pearce, J. A., and Cann, J. R., 1973, Tectonic setting of basic volcanic rocks determined using trace element analysis: Earth and Planetary Science Letters, v. 19, p. 956-983.

Pearce, J. A., and Norry, M. J., 1979, Petrogenetic implications of Ti, Zr, Y, and Nb, variations in volcanic rocks: Contributions to Mineralogy and Petrology, v. 69, p. 33-37.

Pride, C., and Muecke, G. K., 1981, Rare earth element distributions among coexisting granulite facies minerals, Scourrian complex, NW Scotland: Contributions to Mineralogy and Petrology, v. 76, p. 463-471.
Raia, F., and Spera, F. J., 1997, Simulations of crustal anatexis: Implications for the growth and differentiation of the continental crust: Journal of Geophysical Research, v. 102, p. 22,629-22,648.
Reed, J. C., 1964, Geology of the Lenoir quadrangle, North Carolina: U. S. Geological Survey Map I-709-A, scale 1:62,500.
Robin, P. Y., 1979, Theory of metamorphic segregation and related processes: Geochimica et Cosmochimica Acta, v. 43, p. 1,587-1,600.
Rollinson, H. R., 1998, Using geochemical data: Evaluation, presentation, and interpretation: England, Longman, 352 p.
Sawyer, E. W., 1999, Criteria for the recognition of partial melting: Physics and Chemistry of the Earth, v. 24, p. 269-279.
Sawyer, E. W., and Barnes, S. J., 1988, Temporal and compositional differences between subsolidus and anatectic migmatite leucosomes from the Quetico metasedimentary belt, Canada: Journal of Metamorphic Geology, v. 6, p. 437-450.
Sederholm, J., 1934, On migmatites and associated Precambrian rocks of southwestern Finland; Part 3, the Aland islands: Bulletin de la Commission Géologique de Finlande, v. 107, p. 1-68.
Shufflebarger, T. E., 1961, Notes on relationships of Piedmont sedimentary rocks with emphasis on the Poor Mountain-Chauga River area, Oconee County, South Carolina: South Carolina Division of Geology, Geologic Notes, v. 5, p. 31-38.
Sloan, E., 1908, Catalogue of the mineral localities of South Carolina: South Carolina Geologic Survey, 505 p.
Spear, F. S., 1995, Metamorphic phase equilibria and pressure-temperature-time paths: Washington D.C., Mineralogical Society of America, 799 p.
Thompson, A. B., 2001, Clockwise P-T paths for crustal melting and H_2O recycling in granite source regions and migmatite terrains: Lithos, v. 56, p. 33-45.
Thompson, R. D., 1982, British Tertiary volcanic province: Scottish Journal of Geology, v. 18, p. 49-107.
Vernon, R. H., and Paterson, S. R., 2001, Axial-surface leucosomes in anatectic migmatites: Tectonophysics, v. 335, p. 183-192.
Vinson, S. B., and Miller, C. F., 1999, Constraints on the timing of Inner Piedmont plutonism, N.C.–S.C., from ion microprobe U-Pb zircon analysis: Geological Society of America Abstracts with Programs, v. 31, p. A-77.
Watson, E. B., 1979, Zircon saturation in felsic liquids: Experimental results and application to trace element geochemistry: Contributions to Mineralogy and Petrology, v. 70, p. 407-418.
Williams, S. T., 2000, Structure, stratigraphy, and migmatization in the southwestern South Mountains, North Carolina [M.S. thesis]: Knoxville, University of Tennessee, 111 p.
Wood, D. A., 1980, The application of a Th-Hf-Ta diagram to problems of tectonomagmatic classification and to establishing the nature of crustal contamination of basaltic lavas of the British Teritory volcanic province: Earth and Planetary Science Letters, v. 50, p. 11-30.

Yanagihara, G. M., 1994, Structure, stratigraphy, and metamorphism of a part of the Columbus Promontory, western Inner Piedmont, North Carolina [unpublished M.S. thesis]: Knoxville, University of Tennessee, 214 p.

Appendices

Appendix A

Structural and rock type data for the Kings Creek quadrangle

Note: Stations correspond to locations shown in Plate III. Lithologic descriptors are notations made in field shorthand and do not correspond to specific units.

ABBREVIATIONS:

Lithologic descriptors:

Gss – garnet sillimanite schist

Bgn – biotite gneiss

GG – granitoid gneiss

MGW – metagraywacke

Peg – pegmatite

SS – sillimanite schist

Mig – migmatite

Qz – quartzite

Sap – saprolite

W.T. – Walker Top Granite

Leuco – leucocratic rock

Melano – melanocratic rock

Meso – mesocratic rock

Musc – muscovite

Phyl – phyllite

Calc sil – calc silicate rock

R E bgn – inequigranular gneiss

Amph – amphibole

Mylon – mylonite

CI – color index

TG – granodiorite

Map Unit

SS – sillimanite schist

Bgn – metagraywacke

WT – Walker Top Granite

RE – Hibriten orthogneiss

TG – Migmatitic amphibolite granodiorite

OG – Tallulah Falls metagraywacke

Musc-Sch – muscovite schist

Hen – Henderson Gneiss

Gran – granitoid

Bag – biotite augen gneiss

		Foliation		Lineation		Fold Axis		Axial Surface		IL	Amp.	Fold	Joint		Map
Station	Lithology	Strike	Dip	Plunge	Bearing	Plunge	Bearing	Strike	Dip	Angle	(m)	Verg.	Strike	Dip	Unit
KC-3	BGN/GG	N 30 E	48 SE												TG
KC-4	BGN/GG	N 40 E	65 SE												TG
KC-5	BGN/GG	N 47 E	40 SE										N 22 W	82 SW	RE
KC-6	BGN/GG	N 52 E	34 SE										N 10 W	80 SW	RE
KC-7	BGN	N 55 E	48 SE												RE
KC-8	"	N 55 E	65 SE			32	N 54 E	N 55 E	65 SE						RE
KC-9	BGN/GG	N 60 E	49 SE												RE
KC-10	GG-SAP	N 28 W	50 NE												SS
KC-11	SS	N 55 E	18 NW												SS
KC-12	SS	N 80 W	37 NE			27	S 75 E	N 65 W	60 NE	110			N 23 W	80 SW	SS
						27	S 25 E	N 65 W	60 NE	110					SS
KC-13	SS/G-SAP	N 15 E	35 SE												SS
KC-14	SS/G-SAP	N 13 W	23 NE												SS
KC-15	SS-MIG														SS
KC-16	SS	N 30 E	33 SE												SS
KC-17	SS	N 45 E	18 SE												SS
KC-18	SS	N 31 E	50 SE												SS
KC-19	SS	N 80 E	44 SE										N 45 W	90	SS
KC-20	BAGN	N 58 E	31 SE												WT
KC-21	SS/BGN	N 55 E	27 NW										N 18 W	84 SW	SS
KC 22	SS	N 39 W	70 NE												SS
KC-23	SS	N 60 W	54 NE												SS
KC-24	SS/Musc	N 34 E	40 SE	31	N 90 E								N 10 W	76 SW	SS
	INTRAFOLIAL-->	N 34 W	34 NE												SS
KC-25	SS	N 57 E	41 SE												SS
KC-26	SS	N 90 E	73 S												SS
KC-27	SS	N 25 E	75 SE												SS
KC-28	BGN/GG-MIG	N 77 E	40 SE			37	S 37 E	N 58 E	39 SE	100					BGN
		N 73 E	31 SE			20	S 35 E	N 45 E	40 SE						
KC-29	BGN/GG/SS					33	S 32 W	N 26 E	79 NW						SS
KC-30	SS	N 50 W	21 NE										N 3 W	85 SW	SS
		N 29 W	30 NE												
KC-31	SS	N 74 E	45 SE												SS
KC-32	SS/PEG-GAR	N 20 E	26 SE			46	S 61 E			100					SS
		N 84 E	43 SE												
		N 5 E	60 SE												
		N 23 E	34 SE												
KC-33	GSS	N 36 E	41 SE			31	S 32 E	N 19 W	46 NE	110					SS
KC-34	GSS	N 44 E	44 SE										N 62 E	80 NW	SS
KC-35	GSS-MIG	N 83 W	90 NE												SS
KC-36	MGW	N 60 W	23 NE												BGN
KC-37	MGW-MIG	N 72 E	37 NW												BGN
KC-38	MGW-MIG														BGN
KC-39	GSS/CALC-SIL	N22 E	56 SE												SS
		N 40 E	58 SE												
KC-40	SS-MIG	N 71 E	33 SE												SS
KC-41	BGN	N 44 W	64 NE												SS
	GG/PEG	N 81 E	76 NE												SS
KC-42		N 55 E	49 SE												SS
KC-43	SS	N 42 W	27 NE												SS
KC-44	GSS	N 63 E	60 SE												SS
KC-45	SS-MIG	N 26 E	18 SE												SS
KC-46	SS	N 31 E	33 SE												SS
KC-47	SS	N 69 W	60 NE												SS
KC-48	SS/MGW	N 40 E	57 SE												SS
KC-49	QZ	N 47 E	21SE										N 24 E	75 NW	SS
KC-50	SS/MGW	N 35 W	17 NE												SS
KC-51	QZ	N 78 W	16 NE												
KC-52	SS/GG	N 56 E	52 SE												SS
KC-53	GG												N 11 E	57 NW	BGN/GG
KC-54	SS	N 5 W	24 NE												SS
KC-55	MGW/GG	N 56 E	16 SE										N 20 W	89 SW	BGN/GG
KC-56	GSS/MGW	N 80 E	48 SE												SS
		N 70 E	48 SE												
KC-57	GSS-MGW	N85 W	73 NE										N 14 W	80 SW	SS
		N 85 E	86 SE												
KC-58	GSS	N 35 W	42 NE												SS
KC-59	GG														BGN/GG
KC-60	BGG	N 90 E	9 NW												SS
KC-61	BGN/MGW														BGN/GG
KC-62	GSS														SS
KC-63	GSS														SS
KC-64	BGN/PEG-GAR	N 78 W	57 NE			13	N 54 E	N 71 E	20 SE	70					SS
KC-65	GSS	N 55E	46 SE												SS
KC-66	SS	N 68 E	58 SE												SS
KC-67	SS/MGW														SS
KC-68	SS/MGW	N 42 E	54 SE												SS
KC-69	BAGN-WT????	N 50 E	40 SE												BGN/GG
KC-70	GG	N 14 E	33 SE												BGN/GG
KC-71	SS	N 72 E	42 NW												SS
KC-72	GG	N 7 W	31 NE												BGN/GG
KC-73	SS/MGW														BGN/GG
KC-74	CALC-SIL														CONTACT
KC-75	SS	N 52 E	34 SE												SS

		Foliation		Lineation		Fold Axis		Axial Surface		IL	Amp.	Fold	Joint		Map
Station	Lithology	Strike	Dip	Plunge	Bearing	Plunge	Bearing	Strike	Dip	Angle	(m)	Verg.	Strike	Dip	Unit
KC-76	SS	N 54 E	34 NW												SS
KC-77	MGW	N 28 W	40 NE												SS
		N 40 E	48 SE												SS
KC-78	GG-SAP	N 29 E	23 SE												SS
KC-79	SS/GG-SAP	N 5 E	57 SE												SS
KC-80	SS	N 79 W	22 NE										N 22 W	76 SW	SS
		N 61 E	24 NW												
KC-81	GSS	N 83 W	34 NE										N 42 E	75 SE	SS
KC-82	GSS	N 58 E	47 SE												SS
KC-83	GSS	N 70 E	32 NW										N 7 W	87 NE	SS
KC-84	MGW/GSS	N 57 E	19 SE										N 10 W	78 NE	SS
KC-87	GSS	N 21 E	22 SE										N 22 W	84 NE	SS
KC-88	GSS-MIG	N 48 W	41 NE										N 22 W	88 SW	SS
		N 9 W	44 NE										N 42 E	68 NW	
KC-89	GSS-MIG	N 6 W	21 NE										N 23 W	76 SW	SS
KC-90	GSS-MIG	N 68 W	34 NE												SS
KC-91	GG/SS	N 53 E	44 SE										N 7 W	90 NE	SS
KC-92	SS-MIG	N 50 E	59 SE										N 15 W	88 SW	SS
KC-93	GSS-MGW-MIG	N 53 W	57 NE												SS
KC-94	GSS/MUSC-S-MIG	N 11 E	26 SE			6	S 76 E	N 67 W	56 NE	160			N 8 W	75 SW	SS
		N 58 E	41 SE			22	S 63 E	N 44 W	44 NE	15			N 10 E	80 NW	SS
		N 29 W	37 NE			36	S 68 E			~120					SS
		N 58 W	51 NE												SS
KC-95	GSS-MIG	N 23 W	22 NE			60	S 18 E	N 45 E	35 SE	20		W	N 14 E	82 NW	SS
		N 41 W	25 SE												
KC-96	GG	N 20 W	30 NE												SS
KC-97	SS	N 49 W	52 NE	16	N 75 E										SS
		N 62 E	42 SE												SS
KC-98	GG/MGW														SS
KC-99	MGW	N 59 E	20 SE												MGW-MIG
KC-100	MGW/CALC-SIL-MIG	N 60 W	11 SE			14	N 64 E	N 78 E	60 NW	90					MGW-MIG
		N 7 W	49 NE												MGW-MIG
KC-101	GG/MGW	N 78 E	29 NW												MGW-MIG
KC-102	GG	N 15 E	48 NW												MGW-MIG
KC-103	GG	N 84 W	39 NE												MGW-MIG
		N 43 W	43 NE												MGW-MIG
KC-104	GG														MGW-MIG
KC-105	MGW/PEG	N 51 E	43 SE												MGW-MIG
KC-106	MGW/GG	N 52 E	60 SE												MGW-MIG
	MGW/SCHIST	N 21 W	22 NE												
KC-107	SS	N 26 E	35 SE												SS
KC-108	MGW	N 70 W	23 NE												SS
KC-109	WT	N 73 E	31 SE												WT
KC-110	WT	N 23 E	56 SE			32	N 52 W	N 54 W	90 SW	140			N 27 W	63 SW	WT
		N 20 W	15 NE												WT
KC-111	WT	N 70 E	76 NW												WT
KC-112	WT	N 10 E	25 SE										N 69 W	60 SW	WT
		N 24 W	29 NE												WT
KC-113	SS/MGW	N 65 W	26 NE										N 27 E	63 NW	SS
KC-114	MUSC-GAR-SS	N 37 W	62 NE										N 36 E	60 NW	SS
KC-115	SS	N 50 W	47 NE												SS
KC-116	G-SAP														
KC-117	MGW/SS	N 19 E	49 SE												SS
KC-118	LEUCO-SAP	N 74 E	28 NW												SS
KC-119	MGW/SS	N 6 E	46 NW												SS
KC-120	SS/MGW	N 16 W	22 NE												SS
		N 35 E	62 SE												
KC-121	WT	N 46 E	26 SE												WT
KC-122	SS	N 37 E	52 SE												SS
KC-123	SS														SS
KC-124	SS/MGW	N 0 E	43 SE												SS
KC-125	MGW	N 20 E	55 NW												SS
KC-126	SS	N 9 E	25 SE												SS
KC-127	SS/GG-SAP														SS
KC-128	SS/GG-SAP	N 87 E	76 SE												SS
KC-129	SS	N 52 E	44 SE												SS
KC-130	SS	N 23 W	37 NE												SS
KC-131	SS-MIG	N 57 W	29 NE										N 8 W	65 SW	SS
		N 42 W	19 NE												
KC-132	G-PHYL-SCH														SS
KC-133	SS-MIG														SS
KC-134	SS														SS
KC-135	SS	N 84 E	38 SE												SS
KC-136	SS	N 72 E	56 SE												SS
KC-137	SS/MGW	N 53 E	55 SE												SS
KC-138	G-MUSC-SS/MGW	N 48 W	50 NE												SS
KC-139	SS/MGW	N 87 E	52 SE												SS
KC-140	GG/SS	N 41 E	64 SE												SS
KC-141	MGW	N 1 E	30 SE												MGW-MIG
KC-142	MGW/BGN	N 30 W	34 NE												MGW-MIG
		N 80 W	66 NE												MGW-MIG
KC-143	BGN/GG	N 13 W	45 NE												MGW-MIG
KC-144	WT (?)	N 83 W	50 NE												WT
KC-145	WT (?)														WT

		Foliation		Lineation		Fold Axis		Axial Surface		IL	Amp.	Fold	Joint		Map
Station	Lithology	Strike	Dip	Plunge	Bearing	Plunge	Bearing	Strike	Dip	Angle	(m)	Verg.	Strike	Dip	Unit
KC-146	WT	N 6 W	40 NE												WT
KC-147	MGW/GG	N 11 E	31 SE												MGW-MIG
KC-148	WT	N 56 W	49 NE												WT
KC-149	SS	N 52 W	47 NE												SS
KC-150	MGW	N 3 E	18 SE												SS
KC-151	SS	N 62 E	32 NW										N 26 E	88 SE	SS
KC-152	WT	N 68 E	52 SE												
KC-153	BGN/GSS-MIG	N5 E	26 E										N 22 W	83 NE	SS
													N 18 W	78 NE	SS
KC-154	SS/BIO/MGW	N 16 W	32 NE												SS
KC-155	MUSC-SS	N 30 E	22 NW												SS
KC-156	GBIO-SCH	N 67 W	20 SW												SS
KC-157	MGW	N 81 E	39 SE												SS
KC-158	BIO-QZ-SCH	N 68 E	30 NW												SS
KC-159	SS/MGW	N 27 E	4 0SE	29	S73E										SS
KC-160	GSS	N 16 E	24 SE										N 8 W	83 NE	SS
KC-161	PHYL-SCH					16	S 62 W	N 81 E	19 NW	160		UPRT			SS
KC-162	N 33 E	N 33 E	17 SE												SS
KC-163	GSS	N 21 W	60 NE										N 24 W	64 SW	SS
													N 33 W	83 SW	SS
KC-164	GG/SS	N 18 E	56 SE												SS
KC-165	GG/MGW	N 31 W	39 NE												MGW-MIG
KC-166	SS														SS
KC-167	GG/MIG														BGN/GG
KC-168	SS/GG	N 86 W	62 NE										N 17 W	63 SW	SS
KC-169	SS/MGW	N 84 E	86 NW			27	N 90 E	N 71 W	56 NE						SS
KC-170	MUSC-SS	N 0 E	34 SE										N 33 E	53 NW	SS
KC-171	GSS	N 53 E	47 SE												SS
KC-172	GSS	N 26 E	35 SE												SS
KC-173	GG/SS	N 22 E	34 SE												SS
KC-174	CALC-SIL														CONTACT
KC-175	SS														
KC-176	GG														MGW-MIG
KC-177	GG/PEG	N 54 E	34 SE												SS
KC-178	SS	N 48 E	37 S E												SS
KC-179	MGW/SS	N 72 E	46 E										N 23 W	64 SW	SS
KC-180	GG	N 57 E	35 SE												MGW-MIG
KC-181	GG	N 73 E	34 SE												MGW-MIG
KC-182	GG	N 61 E	69 SE										N 11 E	71 NW	MGW-MIG
KC-183	MGW	N 78 E	60 SE												MGW-MIG
KC-184	MGW	N 70 E	45 SE												MGW-MIG
KC-185	BGN/MGW/PEG	N 44 E	47 SE												MGW-MIG
KC-186	MGW	N 81 E	70 NW										N 22 W	68 SW	MGW-MIG
KC-187	SS	N 35 E	26 SE												SS
KC-188	SS	N 50 E	49 SE												SS
KC-189	SS-MIG/ CALC-SIL	N 23 E	35 SE												SS
KC-190	SS	N 30 W	27 NE												SS
KC-191	GSS	N 82 W	29 NE												SS
KC-192	GSS	N 62 E	73 SE												SS
K -193	MGW	N 48 E	50 NW										N 59 W	68 SW	SS
K -19	SS	N 69 E	50 NW												SS
K 195	GSS	N 72 E	65 NW										N 28 W	56 SW	SS
K - 19	MGW	N 80 E	37 NW												SS
KC-197	SS	N 24 W	51 NE												SS
KC-198	GG/MGW	N 13 E	34 SE												SS
KC-199	GSS/MGW	N 28 E	43 SE										N 17 W	82 SW	SS
KC-200	MGW	N 14 E	60 SE												SS
KC-201	SS	N 7 W	61 NE												SS
KC-202	SS	N 76 E	46 NW												SS
KC-203	SS	N 63 E	44 SE												SS
KC-204	SS	N 58 E	71 SE												SS
KC-205	SS	N 84 E	70 SE												SS
KC-206	SS/GG	N 76 E	62 NW												SS
KC-207	SS	N 72 E	78 SE												SS
KC-208	SS/MGW	N 45 E	54 SE												SS
KC-209	SS	N 67 E	50 NW												SS
KC-210	SS/MGW	N 78 E	42 SE												SS
KC-211	N 22 E	N 22 E	29 NW										N 17 W	90 NE	SS
KC-212	GSS	N 5 E	40 SE												SS
KC-213	Augen-SS	N 74 E	35 NW										N 15 W	78 SW	SS
KC-214	SS	N 72 E	71 SE												SS
KC-215	SS	N 63 E	90 SE										N 19 W	69 SW	SS
KC-216	MGW/SS	N 42 E	33 SE										N 2 W	63 SW	SS
KC-217	SS/GG	N 62 E	73 NW												SS
KC-218	SS	N 83 E	54 NW												SS
KC-219	SS														SS
KC-220	MGW	N 44 E	78 SE												MGW-MIG
KC-221	GG	N 25 E	60 SE												MGW-MIG
KC-222	granodiorite														MGW-MIG
KC-223	SS-SAP	N 63 E	29 NW												SS
KC-224	WT (?)														WT
KC-225	GSS	N 8 E	43 NW												SS
KC-226	SS	N 87 E	46 SE												SS
KC-227	SS	N 82 W	37 SW												SS

		Foliation		Lineation		Fold Axis		Axial Surface		IL	Amp.	Fold	Joint		Map
Station	Lithology	Strike	Dip	Plunge	Bearing	Plunge	Bearing	Strike	Dip	Angle	(m)	Verg.	Strike	Dip	Unit
KC-228	SS-MIG	N 80 E	36 SE												SS
KC-229	SS	N 65 E	59 SE												SS
KC-230	MGW/SS	N 76 E	63 NW												SS
KC-231	GSS	N 33 E	48 SE												SS
KC-232	SS	N 42 E	49 SE												SS
KC-233	WT														WT
KC-234	GSS	N 52 W	37 SW												SS
KC-235	MGW	N 62 E	39 SE												SS
KC-236															SS
KC-237	GSS-MIG	N 13 E	50 SE												SS
KC-238	MGW/SS	N 82 W	47 SW												SS
KC-239	SS	N 62 E	90 SE												SS
KC-240	SS	N 72 E	36 SE										N 70 E	71 NW	SS
KC-241	MGW/SS	N 85 E	44 SE			20	S 50 W	N 38 E	62 NW	OPEN	>1INCH		N 30 W	85 NE	SS
KC-242	MGW/SS	N 46 W	49 SW												SS
KC-243	SS	N 90 W	54 NE			27	N 75 E	N 90 W	70 NE	OPEN					SS
KC-244	SS	N 72 E	30 SE												SS
KC-245	SS-MIG	N 35 E	51 SE												SS
KC-246	SS/QZ	N 25 W	65 NE												SS
KC-247	SS/MGW	N 14 E	30 SE												SS
KC-248	BAG/WT	N 66 E	24 NW										N 42 E	66 SE	WT
KC-249	BAG/WT	N 34 E	23 SE												WT
KC-250	GG/BGN/PEG	N 14 W	24 NE												BGN/GG
KC-251	BGN/MGW					25	N 53 E	N 67 E	37 NW	120	5FT	NW(?)			BGN/GG
KC-252	BGN	N 37 W	59 NE												BGN/GG
KC-253	BGN	N 12 E	25 SE												BGN/GG
KC-254	GG	N 42 W	39 SW												BGN/GG
KC-255	BGN	N 12 W	15 SW												BGN/GG
		N 56 E	58 NW												BGN/GG
KC-256	BGN	N 70 W	27 SW												BGN/GG
KC-257	BGN	N 37 W	16 SW			22	S 81 W	N 67 E	83 NW	110					BGN/GG
KC-258	BGN/WT (?)	N 55 W	40 NE												BGN/GG
KC-259	BGN	N 67 E	77 SE												BGN/GG
KC-260	BGN	N 80 E	22 SE												BGN/GG
KC-261	GG/BGN	N 76 E	41 NW										N 5 W	84 SW	BGN/GG
KC-262	LEU-GG	N 76 E	39 SE												BGN/GG
KC-263	LEU-GG														BGN/GG
KC-264	GBGN	N 38 E	24 NW												BGN/GG
KC-265	BAGN/BGN	N 74 E	20 NW												WT
KC-266	BGN	N 50 W	21 SW												BGN/GG
KC-267	GG														
KC-268	SS/MGW	N 17 E	39 SE			30	S 76 E			140			N 21 W	73 SW	SS
KC-269	GG/BAG	N 2 W	33 NE			26	N 70 E			100?					SS
KC-270	SS	N 70 E	34 SE										N 31 E	52 NW	SS
KC-271	SS	N 84 E	23 SE												SS
KC-272	SS/MGW	N 77 E	70 SE												SS
KC-273	SS/MGW	N 46 E	53 SE												SS
KC-274	GSS														SS
KC-275	G-AMPH-SS														SS
KC-276	SS	N 46 E	38 SE												SS
KC-277	SS-MIG	N 54 E	43 NW												SS
KC-278	SS-MIG	N 56 E	64 SE										N 30 W	90 SW	SS
KC-279	SS-MIG	N 68 E	45 SE												SS
KC-280	SS	N 83 E	31 NW												SS
KC-281	SS	N 54 E	54 SE												SS
KC-282	SS	N 53 E	59 SE												SS
KC-283	SS/MGW	N 17 E	25 SE												SS
KC-284	SS/MGW	N 57 E	42 SE												SS
KC-285	QZ-MICA-SCH	N 90 E	40 NW												SS
KC-286	CALC-SIL														SS
KC-287	SS-MIG/MGW	N 74 E	35 NW	11	N 16 W								N 45 E	84 SE	SS
KC-288	SS	N 54 E	64 SE												SS
KC-289	BGN/MGW	N 57 E	58 SE												BGN
KC-290	GG/BGN	N 18 W	43 NE												BGN
KC-291	BIO-GG	N 49 E	40 SE												BGN
KC-292	MUSC-SCH/MGW	N 18 E	48 SE												BGN
KC-293	MGW	N 12 W	9 NE												SS
KC-294	LEU-GG/BGN	N 5 E	40 SE										N 90 E	63 SE	BGN
KC-295	MGW/BGN	N 61 E	30 SE												BGN
KC-296	BIO-GG	N 53 E	24 SE												BGN
KC-297	MGW/SS	N 53 E	37 NW												SS
KC-298	BGN/SS	N 73 E	28 SE										N 21 W	90 SW	SS
													N 75 E	90 NW	SS
KC-299	SS-MIG	N 46 E	21 NW												SS
KC-300	BGN	N 36 W	22 SW												SS
KC-301	SS/MGW	N 6 W	61 NE												SS
KC-302	MGW	N 21 W	55 NE												SS
KC-303	SS-MIG	N 39 E	18 SE												SS
KC-304	PEG	N 23 E	40 SE										N 3 W	72 SW	SS
KC-305	SS-MIG	N 28 E	31 SE			46	N 80 E	N 6 E	54 SE	10		W/NW			SS
KC-306	SS/MGW	N 47 E	60 SE												SS
KC-307	SS/MGW	N 48 W	36 NE												SS
KC-308	SIL-MICA-SCH-MIG														SS
KC-309	SS-MIG	N 75 E	66 SE												SS

		Foliation		Lineation		Fold Axis		Axial Surface		IL	Amp.	Fold	Joint		Map
Station	Lithology	Strike	Dip	Plunge	Bearing	Plunge	Bearing	Strike	Dip	Angle	(m)	Verg.	Strike	Dip	Unit
KC-310	BAG W.T.(?)	N 75 E	39 SE												BAG
KC-311	GBGN/MGW	N 69 E	56 NW												BGN
KC-312	MGW	N 37 E	28 SE												BGN
KC-313	MGW-SAP	N 43 E	52 SE												BGN
KC-314	BGN/MGW	N 68 E	23 SE												SS
KC-315	SS/MGW	N 30 E	38 SE										N 28 W	68 SW	SS
KC-316	GSS/MGW														SS
KC-317	GSS/MGW	N 8 E	61 SE												SS
KC-318	MGW	N 74 W	65 SW												SS
KC-319	MGW	N 51 E	49 SE												SS
KC-320	SS/MGW	N 50 W	56 NE												SS
KC-321	GBGN/MGW					61	N 32 W	N 33 W	77 NE	120					SS
KC-322	MICA-SCH	N 51 W	51 NE												SS
KC-323	W.T.	N 77 E	53 SE												WT
KC-324	W.T.	N 27 W	43 NE										N 76 W	75 SW	WT
KC-325	W.T. & SS	N 80 W	48 NE			20	N 18 W	N 79 E	23 NW						WT
		N 13 W	53 NE												WT
KC-326	W.T. & SS	N 81 E	37 NW			37	S 40 E						N 6 W	90 SW	WT
		N 70 W	50 NE												WT
KC-327	W.T.	N 24 W	40 NE												WT
KC-328	W.T.	N 5 W	44 NE												WT
KC-329	W.T.	N 40 W	26 NE												WT
KC-330	SS	N 41 E	76 SE												SS
KC-331	SS	N 42 E	46 SE												SS
KC-332	SS/MGW	N 32 E	63 SE												SS
KC-333	SS	N 54 E	66 NW												SS
KC-334	SS	N 66 E	64 NW												SS
KC-335	MGW-MIG/SS														SS
KC-336	MGW	N 73 E	72 SE												SS
KC-337	MGW-MIG/SS	N 72 W	50 NE										N 2 W	75 SW	SS
KC-338	SS	N 88 E	72 SE												SS
KC-339	SS	N 81 W	47 NE												SS
KC-340	SS	N 90 E	67 NW												SS
KC-341	SS	N 68 E	61 NW												SS
KC-342	BAG	N 76 E	67 SE												BAG
KC-343	BAG/BGN	N 64 E	39 SE												BAG
KC-344	SS/MGW	N 21 E	45 SE										N 17 W	73 SW	SS
KC-345	SS	N 5 W	47 NE										N 32 W	71 SW	SS
KC-346	GSS	N 78 E	57 NW												SS
KC-347	GSS	N 2 E	53 SE												SS
KC-348	GSS.MGW	N 22 E	32 SE												SS
KC-349	SS-MIG	N 60 W	71 NE												SS
KC-350	GMGW	N 64 E	83 SE												SS
KC-351	SS	N 17 E	49 SE			56	N 58 E	N 80 E	62 NW						SS
						22	N 55 E								SS
KC-352	BGN	N 12 W	41 NE												BAG
KC-353	BGN	N 60 W	48 NE										N 7 E	56 NW	BAG
KC-354	SS	N 79 E	57 SE										N 90 E	56 NW	SS
KC-355	SS/MGW	N 64 E	54 SE												SS
KC-356	MGW	N 23 E	67 SE												SS
KC-357	SS/MGW	N 56 E	36 SE												SS
KC-358	BAG	N 22 E	54 SE												BAG
KC-359	SS-MIG	N 90 E	45 NW												SS
KC-360	SS	N 29 W	34 NE										N 17 W	77 SW	SS
KC-361	W.T.	N 33 W	47 NE												WT
KC-362	W.T.	N 47 E	60 SE												WT
KC-363	W.T.	N 77 E	50 SE												WT
KC-364	W.T.	N 86 E	40 SE												WT
KC-365	W.T.	N 84 E	44 SE												WT
KC-366	W.T.	N 77 E	34 SE												WT
KC-367	W.T./BGN	N 42 E	79 SE												WT
KC-368	W.T.	N 10 E	39 NW												WT
KC-369	W.T.	N 7 W	63 NE												WT
KC-370	W.T.	N 9 W	28 NE										N 38 W	64 SW	WT
KC-371	W.T.	N 41 E	39 SE										N 10 W	73 SW	WT
KC-372	BAG	N 5 E	30 SE												BAG
KC-373	W.T.	N 76 W	47 NE												WT
KC-374	W.T.	N 67 W	55 SW												WT
KC-375	SS/BGN	N 45 E	23 SE												SS
KC-376	W.T./BGN/GG	N 25 E	36 SE												WT
KC-377	BAG	N 3 E	31 SE												WT
KC-378	W.T.	N 42 E	69 SE												WT
KC-379	GBAG	N 66 E	53 SE												BAG
KC-380	SS/MGW	N 68 E	52 SE										N 22 W	90 SW	SS
KC-381	MGW	N 90 W	72 SW												BGN
KC-382	MGW	N 5 E	54 SE												BGN
KC-383	MGW	N 57 E	31 SE												BGN
KC-384	BGN/MGW	N 42 E	48 SE			15	S 77 W								BGN
KC-385	MGW/BGN	N 41 E	42 SE												BGN
KC-386	MGW/GG	N 62 E	45 SE												BGN
KC-387	SS	N 28 E	52 SE												SS
KC-388	BGN/MGW	N 48 E	48 SE	58	S 52 E										BAG
KC-389	BAG	N 44E	37 NW												BAG
KC-390	BMGW	N 44 E	60 SE												BGN

		Foliation		Lineation		Fold Axis		Axial Surface		IL	Amp.	Fold	Joint		Map
Station	Lithology	Strike	Dip	Plunge	Bearing	Plunge	Bearing	Strike	Dip	Angle	(m)	Verg.	Strike	Dip	Unit
KC-391	MGW/MICA-SCH	N 14 E	40 SE												BGN
KC-392	BAG/GG	N 46 E	54 SE			12	N 55 E						N 43 W	45 NE	BAG
		N 30 W	47 NE												BAG
KC-393	BGN/MGW	N 23 W	41 NE										N 77 W	90 SW	BGN
KC-394	SS	N 54 W	37 NE										N 13 W	64 SW	BGN
KC-395	BGN	N 87 W	40 NE												BGN
KC-396	BAG	N 7 E	54 SE												BAG
KC-397	BGN~50%	N 53 W	38 NE												BAG
KC-398	BAG	N 77 W	62 NE												BAG
KC-399	BGN	N 70 E	33 SE												BAG
KC-400	BGN	N 33 E	62 SE												BGN
KC-401	BGN	N 23 E	36 SE												BGN
KC-402	BGN	N 20 W	50 NE												BGN
KC-403	WT	N 49 E	72 SE										N 24 W	77 SW	WT
KC-404	SS	N 12 E	34 SE			22	N 86 E	N 59 W	22 NE	160			N 24 W	62 SW	SS
KC-405	GG-SAP	N 77 E	72 SE												SS
KC-406	SS	N 29 E	49 SE												SS
KC-407	SS	N 50 W	44 SW												SS
KC-408	WT (?)	N 57 E	74 SE												SS
KC-409	BAG	N 75 W	44 NE												SS
KC-410	SS	N 36 E	35 SE												SS
KC-411	BGNGG														SS
KC-412	SS	N 59 E	28 SE										N 18 E	86 NW	SS
KC-413	WT	N 28 W	72 NE												WT
KC-414	WT	N 3 E	72 NW										N 48 W	67 NE	WT
KC-415	WT	N 6 W	58 NE												WT
KC-416	WT	N 12 E	70 SE												WT
KC-417	WT	N 32 E	59 SE												WT
KC-418	WT	N 48 E	53 SE												WT
KC-419	BGN	N 64 E	65 SE												BGN
KC-420	MGW	N 85 W	26 SW												BGN
KC-421	BAG	N 52 E	29 SE												BAG
KC-422	MGW(?)	N 41 E	33 SE										N 47 W	86 SW	BGN
KC-423	BAG/GMGW/SS-MIG	N 50 E	69 SE												MGW-MIG
KC-424	SS/MGW	N 77 W	63 NE												SS
KC-425	SS-MIG	N 48 E	47 SE												SS
KC-426	WT	N 77 E	77 NW												WT
KC-427	WT	N 39 E	57 SE												WT
KC-428	SS/MICA-SCH/WT	N 39 E	19 SE										N 34 W	81 NE	SS
KC-429	SS-MGW	N 73 W	70 SW												SS
KC-430	SS/MGW	N 4 W	52 SW												SS
		N 37 W	35 SW												SS
KC-431	WT	N 25 W	25 SW												WT
KC-432	WT	N 62 W	73 NE												WT
KC-433	SS	N 50 W	55 NE										N 26 W	60 SW	SS
KC-434	MGW-MIG	N 52 E	60 SE										N 76 E	65 NW	MGW-MIG
KC-435	BMGW	N 43 E	52 SE												MGW-MIG
KC-436	BAG	N 54 W	19 SW										N 7 W	85 NE	MGW-MIG
													N 68 W	83 SW	MGW-MIG
KC-437	BGN/MGW	N 57 W	70 NE												MGW-MIG
KC-438	G-SILL-BGN	N 84 W	28 NE												MGW-MIG
KC-439	SILL/BGN/MGW	N 19 E	33 NW												MGW-MIG
KC-440	GSS-MIG	N 30 E	43 SE												SS
KC-441	GSS/MGW	N 22 E	46 SE			52	N 50 W	N 48 W	90 SW				N 10 E	71 NW	SS
													N 59 W	56 NE	SS
KC-442	WT	N 25 E	35 SE												WT
KC-443	MGW/BGN	N 90 E	55 SE												SS
KC-444	MGW/BGN	N 90 W	50 SW												SS
KC-445	MGW/BGN	N 53 W	64 SW												SS
KC-446	MGW/BGN	N 83 W	46 SW												SS
KC-447	SS	N 78 E	64 NW												SS
KC-448	MGW	N 48 E	64 SE												SS
KC-449	MGW/SS	N 74 W	53 SW												SS
KC-450	MGW	N 33 E	71 SE												SS
KC-451	WT	N 68 E	53 SE												WT
KC-452	MGW	N 37 E	71 SE												SS
KC-453	MGW~50%	N 64 W	43 NE												SS
KC-454	BMGW	N 30 E	58 NW												SS
KC-455	BGN														BGN
KC-456	SS	N 17 E	32 SE												SS
KC-457	SS	N 65 E	67 SE												SS
KC-458	SS	N 37 E	55 SE												SS
KC-459	BGN-MIG	N 44 E	66 SE												SS
KC-460	SS	N 73 E	57 SE												SS
KC-461	BGN-MGW	N 57 E	45 SE			71	N 10 W	N 33 W	90 NE	120					BGN
KC-462	MGW	N 33 W	37 NE												SS
KC-463	WT	N 78 E	80 NW												WT
KC-464	WT	N 64 E	86 NW												WT
KC-465	SS	N 32 E	63 SE			70	S 69 E	N 30 W	90 SW	120					SS
KC-466	MGW-MIG~70 %	N 90 E	50 SE												SS
KC-467	WT	N 55 E	64 NW												WT
KC-468	WT	N 78 E	58 SE												WT
KC-469	SS	N 61 E	66 SE												SS
KC-470	PHY-SCH	N 59 E	41 SE										N 24 W	85 NE	SS

		Foliation		Lineation		Fold Axis		Axial Surface		IL	Amp.	Fold	Joint		Map
Station	Lithology	Strike	Dip	Plunge	Bearing	Plunge	Bearing	Strike	Dip	Angle	(m)	Verg.	Strike	Dip	Unit
KC-471	PHY-SSCH	N 51 E	44 SE										N 13 W	68 SW	SS
KC-472	WT	N 83 W	43 NE												WT
KC-473	SS	N 87 W	84 SW												SS
KC-474	G-S-BGN/MGW	N 49 E	66 SE										N 56 W	66 NE	MGW-MIG
KC-475	MGW-MIG	N 30 E	40 SE												MGW-MIG
KC-476	MGW/BGN	N 43 E	27 SE												MGW-MIG
KC-477	BAG	N 28 E	48 SE										N 27 W	85 NE	BGN
KC-478	BGN/MGW	N 57 E	24 SE												BGN
KC-479	BGN-MGW	N 33 E	61 SE												BGN
KC-480	SS-MIG	N 15 W	32 NE												SS
KC-481	WT	N 66 E	25 NW												WT
KC-482	WT	N 69 E	44 SE										N 20 W	68 SW	WT
KC-483	GG	N 4 W	52 NE												SS
KC-484	BAG/WT(?)	N 45 E	47 SE												WT
KC-485	WT/SS-CONTACT	N 2 E	34 SE										N 32 W	60 SW	WT
		N 32 E	34 SE										N 30 W	82 SW	WT
		N 41 E	31 SE										N 54 E	36 NW	WT
		N 64 E	61 SE												WT
KC-486	BGN/SS					15	N 65 E	N 54 E	23 SE	20		SE(?)	N 36 W	71 SW	WT
KC-487	WT	N 12 E	30 SE										N 44 E	50 NW	WT
													N 64 W	74 SW	
KC-488	BAG	N 50 W	25 NE												RE
KC-489	BAG-C G	N 0 E	52 NW												RE
KC-490	SS	N 72 W	17 NE												RE
KC-491	R-E-BGN	N 42 E	33 SE												RE
KC-492	SCH-SAP														RE
KC-493	R-E-BGN	N 58 E	90 SE												RE
KC-494	GG/BGN~65%	N 33 W	21 NE												RE
KC-495	BAG	N 19 W	45 NE												RE
		N 60 W	31 NE												RE
KC-496	MGW/SCH	N 15 E	34 NW			20	N 6 E	N 6 E	90 SE						RE
		N 30 W	22 NE												RE
KC-515	R-E-BGN	N 2 E	22 SE												RE
KC-516	BGN-C G	N 13 E	38 SE										N 75 E	54 NW	RE
KC-517	R-E-BGN/AMPH	N 24 E	47 SE												RE
KC-518	BGN-C G /AMPH	N 16 E	50 SE												RE
KC-529	BGG	N 51 E	56 SE												TG
		N 11 W	49 NE												RE
KC-530	BGN-SAP	N 23 W	28 NE												RE
KC-531	BGN-SAP	N 58 W	30 NE												RE
KC-532	B-AMPH-GN	N 43 E	48 SE												RE
KC-533	R-E-BGN	N 17 E	49 SE												RE
KC-534	R-E-BGN	N 28 E	38 SE												RE
KC-535	R-E-BGN	N 72 E	39 SE												RE
KC-536	R-E-BGN	N 29 E	60 SE												RE
KC-537	MGW-SCH-SAP	N 73 E	45 SE												RE
KC-538	R-E-BGN	N 63 E	41 SE												RE
KC-539	RE	N 38 E	60 SE												RE
KC-544	R-E-BGN	N 59 E	44 SE												RE
KC-545	R-E-BGN	N 44 E	36 SE												RE
KC-546	B-AMPH-GN	N 19 W	43 NE												RE
KC-547	B-AMPH-GN/AMPH	N 28 E	56 SE												RE
KC-548	B-AMPH-GN	N 10 E	44 SE												RE
KC-549	B-AMPH-GN	N 26 E	42 SE			5	N 46 E	N 54 E	62 SE	10					RE
KC-554	R-E-BGN	N 33 E	28 SE												RE
KC-555	R-E-BGN	N 48 E	36 SE												RE
KC-556	R-E-BGN	N 53 E	46 SE												RE
KC-557	R-E-BGN	N 32 E	52 SE												RE
KC-558	R-E-BGN	N 55 E	32 SE												RE
KC-559	SS-SAP	N 38 E	36 NW												SS
KC-560	WT	N 60 E	53 SE												WT
KC-561	WT	N 36 E	49 SE												WT
KC-562	BGG	N 40 W	44 NE												WT
KC-563	WT	N 44 E	49 SE										N 25 W	90 SW	WT
		N 68 E	85 SE												WT
KC-564	WT-MYLON	N 60 E	73 SE												WT
KC-565	SS/MGW	N 23 E	55 SE			23	N 58 E								SS
KC-566	SS/MGW	N 7 E	38 SE												SS
KC-567	MGW/BAG-MYLON	N 17 E	51 SE			56	N 70 E	N 17 E	51 SE	15		NW	N 5 W	76 SW	SS
KC-568	MGW														RE
KC-569	R-E-BGN-MIG	N 55 E	50 SE												RE
KC-570	R-E-BGN	N 28 E	61 NW												SS
KC-571	MGW/SCH	N 40 E	64 SE												SS
KC-572	SS	N 61 E	58 SE										N 43 E	90 SE	SS
KC-573	MGW/SCH	N 42 E	61 SE												SS
KC-574	MGW	N 45 E	28 SE			27	S 74 W	N 6 E	28 NW	OPEN		SE			SS
KC-575	BGN	N 52 E	74 SE												SS
KC-576	R-E-BGN	N 63 E	48 SE												RE
KC-577	R-E-BGN	N 11 E	42 SE												RE
KC-578	R-E-BGN	N 53 E	71 SE												RE
KC-579	R-E-BGN	N 24 E	57 SE												RE
KC-580	R-E-BGN	N 17 E	60 SE												RE
KC-581	R-E-BGN	N 61 W	33 SW												RE
KC-582	R-E-BGN	N 43 W	41 NE												RE

		Foliation		Lineation		Fold Axis		Axial Surface		IL	Amp.	Fold	Joint		Map
Station	Lithology	Strike	Dip	Plunge	Bearing	Plunge	Bearing	Strike	Dip	Angle	(m)	Verg.	Strike	Dip	Unit
KC-583	R-E-BGN	N 45 E	53 SE												RE
KC-584	R-E-BGN	N 43 W	26 NE												RE
KC-585	BGN/MGW	N 20 W	38 NE												RE
KC-586	MGW/BGN	N 2 E	41 SE												RE
KC-587	R-E-BGN	N 37 E	28 SE												RE
KC-588	R-E-BGN	N 20 W	56 NE												RE
KC-589	MGW-F G	N 11 W	38 NE												RE
KC-590	ICA-SCH/BGN-MG	N 34 W	37 NE												RE
KC-591	R-E-BGN	N 60 W	34 NE												RE
KC-592	BGN/MGW	N 16 E	45 SE												RE
KC-608	R-E-BGN	N 15 E	62 NW												RE
KC-609	R-E-BGN	N 4 E	55 SE										N 86 E	37 NW	RE
KC-610	R-E-BGN	N 10 E	25 NW										N 83 W	67 SW	RE
KC-611	R-E-BGN	N 41 E	39 SE												RE
KC-612	R-E-BGN	N 19 E	48 SE												RE
KC-613	R-E-BGN	N 48 E	61 SE										N 38 W	88 SW	RE
KC-614	SS/MGW	N 72 W	36 SW										N 38 W	88 SW	SS
KC-615	R-E-BGN	N 12 E	61 SE												RE
KC-616	R-E-BGN	N 33 E	54 SE												RE
KC-617	R-E-BGN	N 72 E	29 SE												RE
KC-618	R-E-BGN	N 39 E	35 SE												RE
KC-619	R-E-BGN	N 40 E	42 SE										N 30 E	57 NW	RE
KC-620	R-E-BGN	N 50 E	40 SE												RE
KC-621	R-E-BGN	N 36 E	70 SE												RE
KC-622	BGN/GG	N 29 E	45 SE										N 50 W	70 NE	TG
KC-627	BGN-AMPH	N 36 E	40 SE										N 15 W	80 NE	RE
KC-628	BGN	N 44 E	30 SE												RE
KC-630	BGN&R-E-BGN	N 46 E	38 SE												RE
KC-634	BGN	N 42 E	46 SE												RE
KC-637	R-E-BGN	N 28 E	67 SE												RE
KC-638	R-E-BGN	N 36 E	48 SE										N 64 E	42 NW	RE
													N 42 W	83 SW	RE
KC-639	G-R-E-BGN	N 14 E	37 SE										N 10 W	71 NE	RE
KC-640	MGW/R-E-BGN	N 22 E	62 SE												RE
KC-641	MGW/R-E-BGN	N 63 E	63 SE												RE
KC-642	GSS	N 32 W	31 NE												SS
KC-643	AMPH-weathered														SS
KC-644	SCH/GG	N 48 E	38 SE												SS
KC-645	AMPH-weathered	N 57 W	40 NE										N 45 W	50 SW	SS
KC-646	MGW/SCH	N 9 E	55 SE												SS
KC-647	GSS	N 12 E	44 SE												SS
KC-648	SS	N 26 E	57 SE												SS
KC-649	MUSC-SS	N 73 E	60 SE												SS
KC-650	BGN/MGW	N 79 E	48 SE			50	N 70 E	N 85 E	67 NW	110			N 52 W	64 NE	SS
						33	S 77 W	N 72 E	73 NW	110			N 33 E	54 NW	SS
KC-651	SS-SAP	N 10 W	35 SW												SS
KC-652	SCH/GG-SAP	N 50 E	41 SE												SS
KC-653	SCH/MGW	N 30 E	80 SE												SS
KC-654	SS	N 45 E	65 SE												SS
KC-655	SCH/MGW-MIG	N 44 E	39 SE			14	N 2 E	N 10 E	45 SE	5		NW	N 63 E	78 SE	SS
						37	N 72 E	N 53 E	33 SE	100		NW			SS
KC-656	MGW-MIG	N 17 W	73 NE										N 82 W	78 SW	SS
KC-657	GSS	N 30 W	42 NE												SS
KC-658	SS/MGW					21	S 20 E	N 42 W	44 SW	100					SS
KC-659	MGW	N 30 W	46 NE												SS
KC-660	SS/MGW-MIG	N 90 E	46 NW												SS
KC-661	SS-MIG	N 2 W	56 NE												SS
KC-662	MGW	N 59 E	52 SE												SS
KC-663	GSS/MGW	N 10 W	52 NE												SS
KC-664	BAG/GG	N 5 W	39 NE												SS
KC-665	GSS	N 37 E	50 SE										N 62 W	80 NE	SS
KC-666	GG/GMGW-SCH	N 23 E	48 SE												SS
KC-667	WT-MYLON& GSS	N 46 E	68 SE										N 23 W	70 SW	SS
KC-668	SS	N 24 W	48 NE												SS
KC-669	GSS	N 17 E	52 SE												SS
KC-670	WT	N 56 W	48 SW												WT
KC-617	WT	N 55 E	52 SE												WT
KC-672	G-WT	N 70 E	37 NW			31	N 66 E	N 71 E	63 NW	30					WT
KC-673	WT	N 45 E	35 SE												WT
KC-674	WT	N 66 E	62 NW												WT
KC-675	GSS/MGW	N 51 W	55 SW												SS
KC-676	WT	N 13 E	39 SE												WT
KC-677	WT	N 2 E	64 SE												WT
KC-678	MGW/SCH	N 3 W	60 NE												SS
KC-679	SS	N 84 E	80 SE												SS
KC-680	GSS	N 47 E	71 SE												SS
KC-681	GSS	N 76 E	80 SE												SS
KC-682	GSS/MGW-MIG	N 40 E	50 NW												SS
KC-683	WT-MYLON	N 27 E	66 SE												WT
KC-684	GG	N 28 E	40 SE												SS
KC-685	MGW/SCH	N 3 W	58 NE										N 45 E	90 SE	SS
KC-686	MGW/SCH	N 53 E	69 SE												SS
KC-687	SS	N 23 E	80 SE												SS
KC-688	SS/MGW	N 12 W	61 NE												SS

		Foliation		Lineation		Fold Axis		Axial Surface		IL	Amp.	Fold	Joint		Map
Station	Lithology	Strike	Dip	Plunge	Bearing	Plunge	Bearing	Strike	Dip	Angle	(m)	Verg.	Strike	Dip	Unit
KC-689	SS-MIG	N 58 E	36 SE										N 10 W	72 SW	SS
KC-690	R-E-BGN	N 7 E	30 SE												RE
KC-691	R-E-BGN	N 43 E	28 SE												RE
KC-692	R-E-BGN	N 31 E	31 SE												RE
KC-693	SS/BAG	N 30 E	58 SE										N 34 W	83 SW	SS
KC-694	SS/MGW-MIG	N 35 E	48 SE												SS
KC-695	SS/MGW	N 70 E	51 SE			32	N 35 E	N 31 W	27 NE	30		NW	N 15 E	90 SE	SS
		N 11 W	33 NE			18	N 37 E	N 18 E	33 SE						SS
KC-696	MGW	N 74 W	58 NE												SS
KC-697	G-AMPH	N 28 E	45 SE												SS
KC-698	MGW&AMPH	N 50 E	48 SE										N 2 W	80 SW	SS
KC-699	SS/MGW/AMPH/BAG					36	N 75 W	N 53 W	62 NE	70		SW			SS
						54	N 60 W	N 54 W	62 NE	50		NW			SS
KC-700	G-BGN/MGW	N 37 E	61 SE												SS
KC-701	SS	N 57 E	55 SE										N 33 W	75 SW	SS
KC-702	GSS	N 57 E	66 SE										N 30 W	78 S W	SS
KC-703	SS/MGW	N 20 E	58 SE												SS
KC-704	SS	N 52 E	45 NW												SS
KC-725	R-E-BGN	N 27 E	25 SE										N 2 E	82 NW	SS
KC-726	AMPH/MGW-WEATH	N 21 E	45 SE												SS
KC-727	BGN	N 37 E	42 SE												RE
KC-728	HRE/MGW/AMPH-S	N 36 E	44 SE												SS
KC-729	AMPH	N 37 E	60 SE												SS
KC-730	AMPH	N 39 E	63 SE												SS
KC-731	SCH	N 65 E	56 SE										N 14 W	88 NE	SS
KC-732	BAG			30	N 30 E	13	N 90 W	N 90 W	76 NE	60			N 83 W	70 SW	SS
						17	S 7 W	N 40 E	31 SE	100					SS
						15	S 8 W	N 5 E	66 SE	160					SS
						14	S 50 W	N 50 E	40 SE	10					SS
KC-733	BGG/BSCH~50%	N 16 E	65 SE			41	S 88 E	N 15 E	51 SE	20					SS
KC-734	SCH/MGW-MIG	N 49 E	62 SE												SS
KC-735	SS	N 35 E	32 SE										N 85 E	75 NW	SS
KC-736	R-E-BGN- SCHISTY	N 43 E	47 SE												SS
KC-737	AMPH	N 55 W	39 NE												SS
KC-738	SS	N 33 E	56 SE												SS
KC-739	OCHRE-MGW	N 31 E	45 SE												SS
KC-740	BGN	N 49 E	33 SE										N 24 W	76 SW	SS
KC-741	SS	N 61 E	66 SE												SS
KC-742	AMPH?														SS
KC-743	GSS	N 26 E	55 SE												SS
KC-744	MGW/SCH/R-E-BGN	N 5 E	63 SE										N 10 E	66 NW	SS
KC-745	MGW/SCH/R-E-BGN	N E	60 SE										N 18 W	86 NE	SS
KC-746	R-E-BGN	N 12 E	23 SE												RE
KC-747	R-E-BGN	N 69 E	70 SE										N 20 W	80 NE	RE
KC-748	R-E-BGN	N 69 E	34 NW												RE
KC-749	R-E-BGN	N 16 E	50 SE												RE
KC-750	R-E-BGN	N 54 E	35 SE										N 9 E	82 SE	RE
KC-762	BGN	N 87 E	41 SE												RE
KC-763	SCH	N 30 E	46 SE												SS
KC-764	MGW	N 54 E	45 SE												SS
KC-765	MGW/GG	N 38 E	55 SE												SS
KC-766	BGN	N 72 E	56 NW												SS
KC-767	SS	N 33 E	51 SE												SS
KC-768	SS-MIG	N 41 E	59 SE										N 63 W	74 SE	SS
KC-769	WT	N 69 E	62 SE												WT
KC-770	GMGW-MIG	N 87 E	70 SE										N 0 E	50 SE	SS
KC-771	MGW-SCH	N 54 E	60 SE												SS
KC-772	SCH-BGN	N 76 E	63 SE												SS
KC-773	SCH-MIG	N 58 E	38 SE										N 12 W	63 SW	SS
KC-774	SS	N 29 E	36 SE	44	N 78 E								N 21 W	59 SW	SS
KC-775	GG	N 61 E	60 SE										N 9 E	77 NW	RE
KC-776	GG/WT?~15%	N 67 E	54 SE												SS
KC-777	BGN-SAP	N 80 W	52 NE												SS
KC-778	BGN-SAP	N 59 E	76 SE										N 2 W	87 NE	SS
KC-779	WT	N 26 E	83 NW												WT
KC-780	WT-MYLON	N 31 E	50 SE												WT
KC-781	GAR-GG														SS
KC-782	MGW-SCH	N 83 E	75 SE												SS
KC-783	BGN/MGW-F.G.	N 84 E	51 SE										N 15 W	86 SW	SS
KC-784	WT	N 35 E	47 NW												WT
KC-785	LEUCO-GG	N 53 E	50 SE												RE
KC-786	SCHSAP-R-E-BGN?	N 48 E	71 SE												RE
KC-787	R-E-BGN	N 53 E	77 SE												RE
KC-788	AMPH/R-E-BGN	N 50 E	69 SE												RE
KC-789	MGW-SCH	N 29 E	61 SE												RE
KC-790	SS	N 52 E	70 SE												RE
KC-791	R-E-BGN	N 57 E	76 SE												RE
KC-792	R-E-BGN	N 50 E	47 SE										N 1 W	80 NE	RE
KC-793	MGW/R-E-BGN	N 66 E	68 SE										N 3 W	82 SW	RE
KC-794	SS	N 58 E	70 SE												SS
KC-795	WT-MYLON	N 47 E	49 SE												WT
KC-796	WT	N 26 W	31 NE												WT
KC-797	SCH	N 50 E	30 SE										N 75 E	72 NW	SS
KC-798	MGW-SCH	N 70 W	38 NE												SS

		Foliation		Lineation		Fold Axis		Axial Surface		IL	Amp.	Fold	Joint		Map
Station	Lithology	Strike	Dip	Plunge	Bearing	Plunge	Bearing	Strike	Dip	Angle	(m)	Verg.	Strike	Dip	Unit
KC-813	R-E-BGN	N 43 E	40 SE	27	N 73 E								N 70 W	69 SW	RE
													N 37 W	72 SW	RE
KC-814	R-E-BGN	N 54 E	45 SE										N 33 W	82 SW	RE
KC-815	AMPH-TG	N 49 E	56 SE										N 45 W	44 SW	RE
KC-816	R-E-BGN	N 30 E	55 SE												RE
KC-817	GG/BGN/AMPH	N 8 W	44 NE										N 14 W	31 SW	RE
KC-818	R-E-BGN	N 28 E	35 SE												RE
KC-823	SAP	N 48 E	54 SE												RE
KC-850	SS	N 52 E	51 SE												SS
KC-851	SS	N 55 E	56 SE												SS
KC-852	WT-MYLON	N 79 E	53 SE												WT
KC-853	MGW-SCH	N 19 E	60 SE												SS
KC-854	SS	N 62 E	55 SE										N 22 W	86 SW	SS
KC-855	SS/MGW	N 26 E	44 SE												SS
		N 16 E	72 SE												SS
KC-856	R-E-BGN	N 10 E	42 SE												RE
KC-857	R-E-BGN	N 15 E	63 SE												RE
KC-858	R-E-BGN	N 16 W	47 NE												RE
KC-859	R-E-BGN	N 18 E	38 SE												RE
KC-860	R-E-BGN	N 10 E	33 SE												RE
KC-861	R-E-BGN-AMPH	N 42 E	53 SE												RE
KC-862	R-E-BGN	N 50 E	62 SE												RE
KC-863	R-E-BGN	N 26 E	61 SE												RE
KC-864	R-E-BGN	N 36 E	53 NW												RE
KC-865	R-E-BGN														RE
KC-866	R-E-BGN	N 43 E	41 SE										N 65 E	73 NW	RE
KC-867	R-E-BGN	N 53 E	66 SE												RE
KC-868	R-E-BGN-SCH	N 24 W	20 NE												RE
KC-869	R-E-BGN	N 51 E	65 SE												RE
KC-870	R-E-BGN	N 44 E	63 SE												RE
KC-871	R-E-BGN	N 48 E	61 SE												RE
KC-872	MGW-SCH-SAP	N 58 E	61 SE												SS
KC-873	SILL-MGW/SCH	N 59 E	64 SE												SS
KC-874	SS	N 42 E	61 SE										N 34 W	84 SW	SS
KC-875	MGW	N 36 E	72 NW												SS
KC-876	SS-SAP	N 74 E	70 SE												SS
KC-877	SS	N 42 E	42 SE	17	N 72 E										SS
KC-878	SS	N 44 E	29 SE												SS
KC-879	SILLMGW-SAP	N 78 E	62 SE												SS
KC-880	WT?	N 48 E	18 SE												WT
KC-881	MGW/SS-SAP	N 68 E	65 SE												SS
KC-882	SS	N 69 W	39 NE												SS
KC-883	SS	N 55 E	57 SE	13	N 45 E										SS
KC-884	SS-MIG	N 13 W	59 NE												SS
KC-885	BGN/MGW	N 21 E	77 SE												SS
KC-886	GG	N 28 W	64 SW												SS
KC-887	SS	N 75 E	82 SE	25	N 75 E										WT
KC-888	WT-MYLON	N 70 E	74 NW												WT
KC-889	WT-MYLON	N 49 E	71 SE												WT
KC-890	MGW-SCH	N 82 E	27 SE												SS
	WT-MYLON	N 63 E	76 NW												SS
KC-891	SS	N 21 E	81 SE										N 88 W	86 SW	SS
KC-892	SS-MIG	N 54 E	53 SE												SS
KC-893	SS	N 2 E	63 SE										N 25 W	48 SW	SS
		N 43 W	49 NE												SS
	GG-INTRUSION	N 34 E	67 SE												SS
KC-894	SS/MGW-MIG	N 59 E	52 SE										N 35 W	62 SW	SS
KC-895	GG-INTRUSION	N 70 E	64 SE										N 22 W	33 SW	SS
KC-896	SS/MGW	N 54 E	77 SE												SS
KC-897	SS	N 58 E	67 SE												SS
KC-898	BGN-M.G.	N 19 E	47 NW												SS
KC-899	SS-MIG	N 39 E	54 SE												SS
KC-900	SS-MIG	N 34 E	37 SE												SS
KC-901	SS/MGW	N 37 E	52 SE										N 28 W	84 SW	SS
KC-907	SS/MGW	N 71 E	57 SE										N 4 W	86 NE	SS
KC-908	R-E-BGN	N 43 E	28 SE												RE
KC-909	R-E-BGN	N 45 E	30 NW												RE
KC-910	R-E-BGN	N 67 E	45 NW												RE
KC-911	R-E-BGN	N 57 E	50 SE										N 10 W	68 NE	RE
KC-912	R-E-BGN	N 33 E	46 SE										N 28 W	66 SW	RE
KC-913	R-E-BGN	N 63 E	56 SE										N 28 W	84 NE	RE
KC-914	R-E-BGN	N 60 E	27 SE	32	S 86 E								N 4 W	75 NE	RE
KC-915	R-E-BGN	N 0 E	62 NW												RE
KC-916	R-E-BGN	N 67 E	47 SE										N 9 W	86 NE	RE
KC-917	AMPH														TG
KC-920	BGG~50%	N 61 E	34 SE												TG
KC-921	R-E-BGN	N 50 E	44 SE										N 49 W	49 NE	RE
													N 80 W	37 SW	RE
KC-922	R-E-BGN/AMPH	N 43 E	46 SE												RE
KC-923	BIO-SS	N 77 W	20 SW												RE
KC-924	R-E-BGN	N 75 E	23 SE										N 44 W	50 NE	RE
KC-925	R-E-BGN	N 40 E	43 SE										N 0 E	90 SE	RE
KC-926	R-E-BGN	N 63 E	39 SE												RE
KC-927	R-E-BGN	N 68 E	50 SE										N 8 W	44 SW	RE

		Foliation		Lineation		Fold Axis		Axial Surface		IL	Amp.	Fold	Joint		Map
Station	Lithology	Strike	Dip	Plunge	Bearing	Plunge	Bearing	Strike	Dip	Angle	(m)	Verg.	Strike	Dip	Unit
KC-928	R-E-BGN	N 28 E	47 SE												RE
KC-929	R-E-BGN	N 62 E	42 SE												RE
KC-930	GG	N 58 E	53 SE										N 30 W	57 SW	RE
KC-931	R-E-BGN	N 30 E	43 SE												RE
KC-932	R-E-BGN	N 85 E	55 SE										N 12 W	84 NE	RE
KC-933	R-E-BGN/AMPH	N 59 E	62 SE												RE
KC-934	SS	N 85 W	48 NE										N 50 W	70 NE	RE
KC-935	R-E-BGN	N 69 E	50 SE										N 6 E	77 NW	RE
KC-936	R-E-BGN	N 64 E	43 SE												RE
KC-940	R-E-BGN	N 60 E	34 SE												RE
KC-941	R-E-BGN	N 32 E	32 SE												RE
KC-943	R-E-BGN	N 32 E	57 SE												RE
KC-944	R-E-BGN/AMPH	N 28 E	66 SE												RE
KC-945	R-E-BGN	N 90 E	40 SE												RE
KC-947	GG	N 80 E	28 SE										N 11 W	58 NE	RE
KC-948	GG	N 64 E	57 SE										N 13 E	81 SE	RE
KC-977	R-E-BGN	N 75 E	42 SE												RE
KC-978	R-E-BGN	N 54 E	40 SE												RE
KC-979	R-E-BGN	N 64 E	6 S E												RE
KC-980	R-E-BGN	N 28 E	32 SE										N 48 W	50 SW	RE
KC-981	R-E-BGN	N 49 E	67 SE										N 19 W	86 NE	RE
KC-982	R-E-BGN	N 35 E	42 SE										N 5 W	57 SW	RE
KC-983	R-E-BGN	N 69 E	22 SE										N 72 E	74 NW	RE
													N 5 W	83 NE	RE
KC-984	SCH	N 90 E	32 SE			17	S 75 E	N 75 W	82 NE	OPEN					RE
KC-985	R-E-BGN	N 4 E	25 SE	39	S 35 E								N 9 E	68 N W	RE
KC-986	R-E-BGN	N 26 E	44 SE										N 29 W	68 N E	RE
KC-987	MUCH-BIO-SCH	N 21 E	37 SE												RE
KC-988	MICA-SAP	N 88 E	27 SE												RE
KC-989	SCH	N 78 E	14 SE												RE
KC-990	SCH/MGW?	N 50 E	24 SE												RE
KC-991	R-E-BGN	N 20 E	31 SE												RE
KC-994	GG/AMPH	N 51 E	41 SE												RE
KC-996	R-E-BGN	N 85 E	60 SE										N 9 E	73 NW	RE
KC-997	R-E-BGN	N 55 E	68 SE												RE
KC-998	SS	N 64 E	88 SE										N 20 W	67 SW	RE
KC-999	R-E-BGN	N 42 E	65 SE												RE
KC-1000	R-E-BGN	N 42 E	40 SE										N 10 W	41 SW	RE
KC-1001	R-E-BGN	N 66 E	40 SE										N 11 W	71 SW	RE
KC-1002	R-E-BGN	N 35 E	57 SE										N 19 W	66 S W	RE
KC-1003	R-E-BGN	N 17 E	58 SE												RE
KC-1004	SS	N 37 E	56 SE										N 5 W	71 SW	RE
KC-1005	R-E-BGN-SAP	N 44 E	74 SE										N 20 W	56 SW	RE
													N 16 W	60 SW	RE
KC-1006	R-E-BGN	N 44 E	46 SE										N 0 E	81 SE	RE
KC-1007	R-E-BGN	N 58 E	34 SE										N 3 E	80 SE	RE
KC-1008	R-E-BGN	N 48 E	56 SE										N 6 W	74 SW	RE
KC-1009	R-E-BGN	N 78 E	40 SE			30	S 37 W	N 78 E	40 SE						RE
KC-1010	R-E-BGN	N 60 E	60 SE												RE
KC-1011	R-E-BGN	N 59 E	44 SE												RE
KC-1012	R-E-BGN	N 70 E	50 SE												RE
KC-1013	R-E-BGN	N 51 E	56 SE												RE
KC-1014	R-E-BGN	N 63 E	61 SE												RE
KC-1015	R-E-BGN	N 28 E	58 SE												RE
KC-1016	SS/MGW	N 31 E	76 NW												SS
KC-1017	WT	N 50 E	55 SE												WT
KC-1018	GSS/MGW	N 9 E	55 SE										N 51 W	39 SW	SS
KC-1019	SILL-MUSC-SCH	N 37 W	47 NE												SS
KC-1020	MGW	N 50 E	45 SE												SS
KC-1021	SCH-MIG					61	S 50 E	N 64 W	90 SW	OPEN					SS
KC-1022	GBGN	N 34 E	44 SE										N 63 W	70 NE	SS
KC-1023	SS/MGW														SS
KC-1024	SS/MGW	N 18 E	57 SE										N 74 E	65 NW	SS
KC-1025	SS	N 43 W	68 NE	45	S 75 E	40	N 47 E	N 43 E	81 NW	160					SS
KC-1026	GSS	N 58 E	74 SE												SS
KC-1027	SS/MGW-MIG	N 37 W	43 NE										N 22 W	52 SW	SS
KC-1028	SS/MGW-MIG	N 7 E	46 SE										N 73 E	40 NW	SS
KC-1029	SS/MGW	N 73 E	40 NW												SS
KC-1030	BGG-fine grained	N 16 W	64 NE												SS
KC-1031	BGN	N 54 E	65 SE										N 7 W	75 NE	SS
KC-1032	WT	N 50 E	22 SE										N 46 E	57 NW	WT
KC-1033	WT	N 56 E	33 S E												WT
KC-1034	BGN	N 21 E	49 SE										N 76 W	82 SW	SS
KC-1035	WT	N 25 E	3 S										N 2 W	82 SW	WT
KC-1036	WT	N 51 E	76 SE												WT
KC-1037	WT	N 38 E	41 SE										N 71 E	62 NW	WT
KC-1038	WT	N 30 E	35 SE										N 19 W	66 SW	WT
KC-1039	WT	N 54 E	67 SE												WT
KC-1040	QZ-BGN	N 78 E	63 SE												SS
KC-1041	SS/MGW	N 63 E	23 SE												SS
KC-1042	LEUCO-GG	N 20 E	72 SE										N 64 W	86 NE	SS
		N 55 E	73 SE												SS
KC-1043	GSS	N 65 E	33 NW										N 5 W	57 SW	SS
KC-1044	SCH	N 36 W	29 NE												SS

		Foliation		Lineation		Fold Axis		Axial Surface		IL	Amp.	Fold	Joint		Map
Station	Lithology	Strike	Dip	Plunge	Bearing	Plunge	Bearing	Strike	Dip	Angle	(m)	Verg.	Strike	Dip	Unit
KC-1045	SS/MGW	N 14 E	46 NW												SS
		N 73 E	49 NW												SS
KC-1046	SCH	N 6 E	38 SE			62	N 85 E	N 85 E	75 NW	175					SS
KC-1047	GSS/MGW	N 55 E	66 SE												SS
KC-1048	R-E-BGN	N 50 E	51 SE										N 68 E	32 NW	RE
													N 84 W	74 NE	RE
KC-1049	R-E-BGN	N 4 E	66 SE												RE
KC-1050	SS	N 41 E	61 SE												RE
KC-1051	SS	N 47 E	67 SE										N 5 W	69 SW	RE
KC-1052	R-E-BGN	N 53 E	59 SE												RE
KC-1053	R-E-BGN	N 49 E	39 SE												RE
KC-1054	SS	N 56 E	58 SE												RE
KC-1055	R-E-BGN	N 44 E	22 SE												RE
KC-1056	R-E-BGN	N 55 E	52 SE										N 4 W	69 SW	RE
KC-1057	R-E-BGN	N 82 E	45 SE										N 13 W	69 SW	RE
KC-1058	R-E-BGN	N 68 E	66 SE										N 1 W	50 SW	RE
KC-1059	SS-SAP	N 75 E	65 NW												RE
KC-1060	RE-SAP	N 75 E	77 SE												RE
KC-1061	WT	N 45 E	48 SE										N 50 W	79 NE	WT
KC-1062	R-E-BGN	N 61 E	52 SE												RE
KC-1063	WT	N 66 E	69 SE												WT
KC-1064	SCH	N 28 E	74 SE										N 20 W	60 SW	RE
KC-1065	SCH/MGW	N 54 E	44 SE												RE
KC-1066	WT	N 19 E	65 SE										N 71 W	81 NE	WT
KC-1067	SCH	N 66 E	52 SE												SS
KC-1068	MGW-AUGEN	N 74 W	33 NE										N 80 E	52 NW	SS
KC-1069	GSS	N 59 E	67 SE	28	N 78 E										SS
KC-1070	MGW-SCH	N 14 E	28 SE												SS
KC-1071	WT	N 12 E	48 SE										N 61 E	70 NW	WT
KC-1072	R-E-BGN	N 41 E	47 SE												RE
KC-1073	R-E-BGN	N 35 E	58 SE												RE
KC-1074	RE-SAP/AMPH	N 46 E	28 SE												RE
KC-1075	R-E-BGN	N 73 E	58 SE												RE
KC-1076	RE/AMPH	N 36 E	60 SE												RE
KC-1077	RE-MIG	N 42 E	50 SE												RE
KC-1078	PHYLL-SCH	N 65 E	59 SE										N 13 W	78 SW	RE
KC-1079	S-RE-MYLON	N 54 E	60 SE	34	N 68 E										WT
KC-1080	RE-WEATH	N 29 E	30 SE										N 58 E	60 NW	SS
													N 18 W	54 SW	SS
KC-1081	R-E-BGN	N 11 E	34 SE										N 6 E	54 NW	SS
KC-1082	SS/MGW	N 75 E	54 SE												SS
KC-1083	SS/MGW-MIG	N 52 E	41 SE												SS
KC-1084	SS/MGW-MIG	N 70 E	53 SE												SS
KC-1085	BGN/MGW	N 78 E	40 SE												SS
KC-1086	R-E-BGN	N 61 E	45 SE												SS
KC-1087	BGG-50%	N 60 E	41 SE												RE
KC-1088	RE/AMPH	N 44 E	33 SE										N 30 W	61 NE	RE
KC-1089	RE-75%	N 63 E	51 SE										N 6 E	80 SE	RE
KC-1090	BAG	N 75 E	42 SE												RE
KC-1091	BAG/RE	N 19 E	31 SE												RE
KC-1092	SS	N 85 E	65 SE			74	S 2 W	N 3 E	87 SE	170			N 21 W	86 SW	SS
KC-1093	SS	N 61 E	61 SE												SS
KC-1094	SS-MIG	N 77 W	72 NE												SS
KC-1095	SS	N 76 E	73 SE			43	S 32 W	N 29 E	77 NW						SS
KC-1096	SS-MIG	N 9 E	49 SE	14	N 82 E										SS
KC-1097	SCH/GG	N 84 E	52 SE												SS
KC-1098	SCH	N 16 W	46 NE										N 79 W	32 SW	BGN
													N 54 E	44 NW	BGN
KC-1099	LEUCO-GG	N 21 E	36 SE												BGN
KC-1100	MICA-GG-SAP	N 22 E	20 SE												BGN
KC-1101	GG	N 63 E	38 SE												BGN
KC-1102	SS	N 35 W	24 NE										N 14 W	81 SW	SS
KC-1103	SS-MIG	N 84 E	68 SE	54	S 66 E										SS
KC-1104	SS	N 71 E	36 SE												SS
KC-1105	SS-MIG	N 68 E	42 SE												SS
KC-1106	SS-MIG	N 78 E	45 SE										N 23 E	88 NW	SS
KC-1107	GG	N 72 E	19 SE												BGN
KC-1108	SS-MIG	N 3 W	46 NE												SS
KC-1109	SS														SS
KC-1110	SS	N 20 E	28 SE												SS
KC-1111	SS	N 34 W	50 NE										N 18 W	78 SW	SS
KC-1112	SS	N 77 E	42 SE	NTIFORM									N 37 E	50 NW	SS
		N 56 W	28 NE												SS
KC-1113	SS	N 17 E	35 SE			40	N 78 E	N 73 W	52 NE	30			N 13 E	80 NW	SS
KC-1114	SCH-MIG	N 62 E	28 SE										N 21 W	72 SW	SS
		N 39 E	43 SE										N 74 E	81 NW	SS
KC-1115	SS-MIG	N 40 E	44 SE												SS
KC-1116	SCH-MIG	N 54 W	45 NE												SS
KC-1117	MGW/SCH	N 5 E	18 SE			23	S 13 W	N 25 E	58 SE	5					SS
KC-1118	MGW/SCH	N 54 E	45 SE										N 46 E	34 NW	SS
													N 65 W	69 NE	SS
KC-1119	MGW/SCH	N 66 E	66 SE										N 13 W	46 NE	SS
KC-1120	SS-MIG	N 13 E	25 SE												SS
KC-1121	SS	N 42 E	29 SE										N 25 W	69 SW	SS

		Foliation		Lineation		Fold Axis		Axial Surface		IL	Amp.	Fold	Joint		Map
Station	Lithology	Strike	Dip	Plunge	Bearing	Plunge	Bearing	Strike	Dip	Angle	(m)	Verg.	Strike	Dip	Unit
KC-1122	SS-MIG	N 49 E	38 SE												SS
KC-1123	MGW	N 42 E	42 SE										N 15 W	81 NE	SS
													N 79 W	58 NE	SS
KC-1124	SS	N 6 E	30 SE			6	N 73 E	N 55 E	21 SE	45					SS
		N 10 W	22 NE												SS
KC-1125	SS-MIG	N 17 E	20 SE										N 8 W	76 NE	SS
KC-1126	SCH-MIG	N 49 W	50 NE										N 22 E	75 NW	SS
		N 5 E	3 6SE										N 6 E	85 NW	SS
KC-1127	SCH-MIG/GG	N 51 W	31 N E										N 11 E	85 NW	SS
KC-1128	GG	N 86 E	50 S E												SS
KC-1129	SS/GG	N 73 W	46 N E			57	S 72 W	N 24 W	51 NE	15-20		SE			SS
KC-1130	SS	N 85 E	41 SE												SS
KC-1131	SS-MIG	N 50 E	48 SE												SS
KC-1132	SS	N 66 E	64 SE			46	S 17 W	N 17 E	90 SE	30-40					SS
KC-1133	SS	N 70 E	63 SE	28	S 28 W										SS
KC-1134	SS-MIG	N 83 W	66 S W			36	S 30 E	N 76 W	64 NE	40					SS
KC-1135	SS-MIG	N 81 W	65 SW												SS
		N 57 E	61 SE												SS
KC-1136	SS	N 70 E	37 SE												SS
KC-1137	SS-MIG	N 81 E	52 SE			32	S 68 E	N 35 E	26 SE	40			N 3 E	74 NW	SS
						41	S 52 E	N 52 W	86 NE	140					SS
KC-1138	SS	N 63 E	30 SE			18	S 31 W	N 26 E	30 SE	OPEN					SS
KC-1139	SS-MIG	N 55 E	42 SE										N 73 W	57 NE	SS
KC-1140	SS	N60 E	49 SE										N 32 W	79 NE	SS
KG1 4	SS	N 41 E	61 SE			36	S 18 E	N 18 W	78 NE	170-175					SS
KC-1142	SS-MIG	N 7 3	E40 SE										N 55 E	66 NW	SS
KC-1143	SS-MIG	N 62 E	45 SE												SS
KC-1144	LEUCO-GG	N 50 E	17 SE												BGN
KC-1145	LEUCO-GG	N 38 E	43 SE												BGN
KC-1146	GG	N 11 W	17 NE												BGN
KC-1147	GG/SS	N 66 E	31 SE												BGN
		N 5 E	42 SE												BGN
KC-1148	BGG	N 81 W	38 SW										N 26 E	86 SE	BGN
KC-1149	LEUCO-GG	N 64 E	26 SE												BGN
KC-1150	SS	N 7 E	36 SE												SS
KC-1151	SS	N 72 E	55 SE												SS
KC-1152	SS	N 87 E	72 SE												SS
KC-1153	SS/LEUCO-GG	N 80 E	42 SE												BGN
KC-1154	GG	N 89 E	34 SE												BGN
KC-1155	BGG/BAG/MGW	N 60 E	54 SE												BGN
KC-1156	WT														WT
KC-1157	SS-MIG	N 13 W	26 NE										N 6 W	77 SW	SS
KC-1158	SS	N 28 W	18 NE			19	N 78 E	N 80 E	47 SE	45			N 64 E	80 SE	SS
													N 24 W	87 SW	SS
KC-1159	BGN/MGW	N 50 W	28 NE										N 7 W	86 SW	BGN
													N 81 E	80 NW	BGN
KC-1160	MGW/GG	N 44 W	34 NE			22	N 50 E	N 50 E	90 SE	165			N 30 W	34 NE	BGN
KC-1161	QZ-SILL-MGW	N 62 W	27 NE	36	N 52 E								N 28 E	79 NW	BGN
KC-1162	QZ-BGN	N 15 E	45 SE										N 7 W	35 SW	BGN
KC-1163	GG C.G.	N 66 W	27 NE										N 46 W	76 SW	BGN
													N 71 E	68 SE	BGN
KC-1164	GG	N 8 E	19 SE												BGN
KC-1165	BAG	N 62 W	46 NE										N 36 E	64 SE	BGN
KC-1166	GSS	N 72 E	26 SE			26	N 71 W	N 71 W	90 SW	110			N 26 W	81 NE	SS
KC-1167	SS	N 70 W	35 NE												SS
KC-1168	SS/GG****	N 30 W	19 NE			21	N 13 W								SS
		N 74 W	64 NE			27	N 5 E	N 38 E	33 NW						SS
KC-1169	GG-C.G /PEG	N 18 W	45 NE										N 68 E	73 SE	BGN
KC-1170	GG/C.G.	N 78 W	60 NE												BGN
KC-1171	GG/C.G.	N 45 W	29 NE										N 10 E	72 NW	BGN
KC-1172	GG/SCH	N 28 W	17 NE												BGN
KC-1173	MICA-GG	N 13 W	18 NE												BGN
KC-1174	GG-SAP-C.G.	N 50 E	16 SE										N 36 W	85 SW	BGN
													N 64 E	90 SE	BGN
KC-1175	GG/MGW-SAP	N 37 W	42 NE										N 63 E	68 SE	BGN
KC-1176	GG/BGN-MGW-F.G.	N 46 W	32 NE												BGN
KC-1177	N/MGW-F.G. // CALC	N 65 W	46 NE			21	N 80 E	N 80 E	72 NW	170					BGN
KC-1178	GG/C.G.	N 50 W	37 NE												BGN
KC-1179	MGW	N 85 W	22 NE												BGN
KC-1180	B-SCH-SAP	N 88 W	12 NE												BGN
KC-1181	GG/C.G.	N 76 W	14 NE										N 25 W	68 NE	BGN
													N 64 E	79 SE	BGN
KC-1182	BGG-M.G.	N 50 E	41 SE										N 37 E	53 NW	BGN
KC-1183	GG	N 64 E	35 SE												BGN
KC-1184	GG/M.G.	N 48 E	17 NW										N 70 E	70 SE	BGN
KC-1185	GG/C.G.	N 71 E	28 SE												BGN
KC-1186	CALC-SILL														BGN
KC-1187	GG/M.G.	N 36 W	46 NE												BGN
KC-1188	GG/C.G.	N 15 W	36 NE												BGN
KC-1189	N/F.G./MGW/CALC-S	N 49 W	86 NE												BGN
KC-1190	GG	N 44 W	10 NE												BGN
KC-1191	GG/C.G.	N 84 W	45 NE												BGN
KC-1192	SS-MIG/CALC-SIL	N 25 W	42 NE										N 2 W	86 SW	BGN?
KC-1193	SS/MGW	N 75 W	34 NE												BGN

		Foliation		Lineation		Fold Axis		Axial Surface		IL	Amp.	Fold	Joint		Map
Station	Lithology	Strike	Dip	Plunge	Bearing	Plunge	Bearing	Strike	Dip	Angle	(m)	Verg.	Strike	Dip	Unit
KC-1194	BGG/MGW~60%	N 10 E	28 SE										N 81 E	79 SE	BGN
KC-1195	MGW-F G	N 28 E	31 SE												BGN
KC-1196	RE-FL?														WT
KC-1197	GBAG-MYLON	N 74 W	45 NE												WT
KC-1198	GBAG-MYLON	N 30 W	45 NE												
KC-1199	BAG-MYLON	N 84 E	44 NW										N 80 W	48 SW	WT
													N 8 W	86 NE	WT
KC-1200	WT	N 66 W	60 NE										N 10 E	61 SE	WT
KC-1201	BGN/M G	N 81 E	30 SE										N 6 W	82 SW	BGN
KC-1202	CALC-SIL														BGN
KC-1203	BGN/MGW~40%	N 79 E	57 NW												BGN
KC-1204	BGN/MGW	N 57 E	35 SE												BGN
KC-1205	AMPH-GN	N 10 E	38 SE										N 28 E	90 SE	BGN
KC-1206	BGN/M G	N 46 E	40 NW										N 42 W	57 NE	BGN
KC-1207	GBGN	N 13 W	69 NE										N 55 E	78 SE	BGN
KC-1208	BAG-MYLON	N 59 W	44 NE												BGN
KC-1209	MGW	N 37 W	39 NE												BGN
KC-1210	CALC-SIL	N 73 W	59 NE												BGN
KC-1211	GG/MGW-LEUCO					15	N 76 E	N 76 E	90 SE	140					BGN
KC-1212	MGW														BGN
KC-1213	LEUCO-GG/C G	N 50 W	16 NE										N 4 E	82 SE	BGN
KC-1214	MGW-SAP	N 82 W	60 NE												BGN
KC-1215	MGW-SAP					3	S 22 E	N 0 E	5 SE	35559					BGN
KC-1216	BGN/MGW/RE	N 60 W	39 NE												WT
KC-1217	RE?	N 82 W	50 NE												SS
KC-1218	GSS-MIG	N 81 E	61 SE										N 3 E	59 NW	SS
KC-1219	GSS/MGW	N 65 W	35 NE										N 7 W	56 SW	SS
KC-1220	SS-MIG	N 60 W	36 NE	40	N 38 E	17	N 65 E	N 73 E	59 NW	140			N 53 E	71 SE	SS
				16	N 45 E	28	N 15 E	N 10 E	74 NW	160					SS
KC-1221	SS	N 60 W	25 NE												SS
KC-1222	SS/MGW	N 44 W	40 NE										N 21 E	24 NW	SS
		N 5 E	57 SE										N 82 E	75 SE	SS
KC-1223	GSS/MGW	N 51 E	60 NW										N 45 W	80 SW	SS
KC-1224	GSS-MIG	N 83 E	66 NW										N 22 W	69 SW	SS
KC-1225	GSS	N 75 E	43 SE												SS
KC-1226	GSS	N 78 E	44 SE										N 16 W	76 SW	SS
KC-1227	SS	N 86 E	63 NW												SS
KC-1228	B-SS-MIG	N 79 E	38 SE	44	N 6 E	30	N 37 E	N 50 W	43 NE	20		SW			SS
		N 83 E	65 NW												SS
KC-1229	GSS-MIG	N 71 E	30 SE										N 11 W	71 NE	SS
													N 88 W	59 NE	SS
KC-1230	BSS	N 75 E	42 NW												SS
KC-1231	SS-MIG	N 72 E	48 SE												SS
KC-1232	LEUCO-GG/BAG	N 69 E	65 NW												WT
KC-1233	WT-FLT														WT
KC-1234	BGN/F G	N 34 E	60 SE												SS
KC-1235	SS-MICA-MIG	N 82 E	70 NW										N 25 W	50 SW	SS
KC-1236	SS-MIG	N 72 W	68 NE												SS
KC-1237	LEUCO-GG	N 79 W	32 NE												SS
KC-1238	SS	N 38 W	34 NE										N 24 E	86 SE	SS
KC-1239	GSS-MIG	N 70 E	52 SE										N 17 W	90 SW	SS
KC-1240	BGN	N 75 E	50 NW										N 17 W	78 SW	MGW-MIG
KC-1241	GG/C G	N 59 E	55 SE												MGW-MIG
KC-1242	GSS/MGW	N 79 E	54 SE										N 31 E	56 SW	MGW-MIG
KC-1243	BGNGG~50%	N 30 W	42 NE										N 63 W	64 NE	MGW-MIG
KC-1244	MGW														MGW-MIG
KC-1245	MGW	N 74 E	78 NW												MGW-MIG
KC-1246	MGW/BGN	N 59 E	57 SE										N 37 W	59 SW	SS
KC-1247	WT-MYLON/RE	N 70 E	52 NW												WT
		N 20 E	45 SE												WT
KC-1248	R-E-BGN	N 77 W	67 NE												SS
KC-1249	GSS	N 60 W											N 77 W	70 SW	SS
													N 18 W	71 SW	SS
KC-1250	GSS/MGW	N 78 W	55 NE										N 20 W	68 SW	SS
KC-1251	SS	N 72 E	45 SE	8	S 87 E										SS
KC-1252	SS	N 80 W	47 NE										N 17 W	68 SW	SS
KC-1253	WT-MYLON	N 25 W	32 NE												WT
KC-1254	WT-MYLON	N 44 W	21 NE												WT
KC-1255	WT	N 70 E	51 SE												WT
KC-1256	WT	N 57 E	65 SE												WT
KC-1257	WT	N 61 E	65 SE												WT
KC-1258	WT	N 54 E	56 SE										N 19 W	72 SW	WT
KC-1259	R-E-BGN	N 51 W	31 NE												RE
KC-1260	R-E-BGN	N 59 E	51 SE										N 12 W	66 SW	RE
KC-1261	R-E-BGN	N 22 E	50 SE												RE
KC-1262	R-E-BGN	N 77 E	68 SE										N 2 W	74 SW	RE
KC-1263	R-E-BGN	N 54 E	46 SE										N 3 W	50 SW	RE
KC-1264	R-E-BGN	N 55 E	55 SE												RE
KC-1265	MGW/SS	N 17 W	17 NE										N 81 W	78 SW	SS
KC-1266	GSS-MIG	N 65 E	43 SE			35	N 64 E	N 58 E	17 SE	15-50					SS
KC-1267	WT	N 63 E	46 SE												WT
KC-1268	MGW/BGN	N 77 E	37 NW												BGN
KC-1269	BAG~70-80%	N 78 W	43 NE										N 5 W	85 SW	WT
KC-1270	MGW/SCH	N 83 E	54 NW										N 4 W	80 SW	SS

		Foliation		Lineation		Fold Axis		Axial Surface		IL	Amp.	Fold	Joint		Map
Station	Lithology	Strike	Dip	Plunge	Bearing	Plunge	Bearing	Strike	Dip	Angle	(m)	Verg.	Strike	Dip	Unit
KC-1271	GSS-MIG	N 30 W	43 SW										N 77 W	44 NE	SS
													N 35 W	68 NE	MGW-MIG
KC-1272	MGW-F.G.-MIG	N 70 W	18 NE										N 5 E	78 NW	MGW-MIG
KC-1273	GG/PEG	N 8 E	17 NW												MGW-MIG
KC-1274	MGW/BGN-MYLON?	N 48 W	28 SW										N 32 E	38 NW	MGW-MIG
KC-1275	SS	N 76 W	30 NE												MGW-MIG
KC-1276	SS/MGW-MIG	N 70 W	41 NE												MGW-MIG
KC-1277	LEUCO-GG	N 4 W	39 NE												RE
		N 39 E	62 SE												RE
KC-1278	R-E-BGN	N 30 E	50 SE												RE
KC-1279	R-E-BGN	N 67 W	55 NE												RE
KC-1280	R-E-BGN	N 39 E	43 SE												RE
KC-1281	WT-OVAL?	N 59 E	40 SE												WT
KC-1282	WT	N 27 W	56 NE												WT
KC-1283	BGN/MGW	N 74 E	45 SE												SS
KC-1284	MGW/SS	N 80 E	46 SE										N 12 E	64 NW	SS?
KC-1285	RE/WT??	N 73 E	22 SE												WT
KC-1286	MGW/CALC-SIL-SAI	N 64 W	68 NE												WT
KC-1287	WT-OVAL/MYLON?	N 19 E	32 SE												WT
KC-1288	SILL-BGN-MIG	N 65 E	14 SE												RE
KC-1289	SILL-BGN-MIG	N 25 W	43 NE										N 78 E	67 SE	RE
KC-1290	R-E-BGN	N 60 W	42 NE										N 7 W	67 SW	RE
KC-1291	EUCO-GG/SCH-SA	N 65 E	31 SE												RE
KC-1292	RE-SAP	N 77 E	54 SE												RE
KC-1293	R-E-BGN	N 80 W	21 NE												RE
KC-1294	R-E-BGN	N 61 E	55 SE										N 42 W	81 NE	RE
KC-1295	R-E-BGN	N 20 E	30 SE										N 51 W	51 SW	RE
KC-1296	R-E-BGN	N 60 E	49 SE												RE
KC-1297	R-E-BGN	N 61 E	50 SE												RE
KC-1298	R-E-BGN	N 45 E	57 SE												RE
KC-1299	R-E-BGN	N 48 E	79 SE												RE
KC-1300	RE-SILL	N 6 W	45 NE												RE
KC-1301	R-E-BGN	N 33 E	41 SE												RE
KC-1302	R-E-BGN	N 20 E	53 SE										N 83 E	76 NW	RE
KC-1304	R-E-BGN	N 47 E	47 SE										N 60 E	46 NW	RE
KC-1305	BGN-DARK	N 63 W	34 NE												WT
KC-1306	WT	N 35 W	33 NE												WT
KC-1307	SS	N 52 E	40 SE												SS
KC-1308	MUSC-SCH	N 88 E	56 NW												SS
KC-1309	RE	N 68 W	68 NE												SS
KC-1310	RE/WT	N 77 E	48 NW												WT
KC-1311	MUSC-SILL-SCH	N 69 W	29 NE	33	N 67 E								N 23 W	72 SW	SS
KC-1312	MUSC-SILL-SCH	N 88 W	50 NE												SS
KC-1313	MGW-F.G./GG	N 57 E	36 SE										N 15 W	62 SW	MGW-MIG
KC-1314	LEUCO-GG	N 5 W	32 NE										N 36 W	62 SW	MGW-MIG
KC-1315	MGW/GG?	N 5 E	28 SE												MGW-MIG
KC-1316	MGW-M.G./AUGEN	N 80 E	63 NW										N 80 E	63 NW	MGW-MIG
KC-1317	GSS	N 68 W	40 NE	34	N 79 E								N 34 W	55 SW	SS
KC-1318	SILL-MGW/SCH-MIC	N 60 E	67 SE												SS
KC-1319	SILL-MGW	N 36 W	42 SW												SS
KC-1320	MUSC-SILL-MGW	N 33 W	46 SW												SS
KC-1321	SS/MGW	N 30 E	21 SE												SS
KC-1322	MGW-MIG/PEG	N 21 W	33 NE												MGW-MIG
KC-1323	MGW/GG	N 33 W	25 NE										N 3 W	21 NE	MGW-MIG
KC-1324	MGW/GG	N 30 W	30 NE												MGW-MIG
KC-1325	BGG/MGW	N 72 E	32 SE			19	N 66 E	N 66 E	70 SE	150					MGW-MIG
KC-1326	WT-MYLON	N 26 W	21 NE												WT
		N 57 W	34 NE												WT
KC-1327	SS/MGW	N 75 W	35 NE												SS
KC-1328	LEUCO-GG/C.G.	N 53 E	28 SE												
KC-1329	GBMGW	N 8 W	17 NE										N 19 E	58 NW	
KC-1330	LEUCO-GG/C.G.	N 83 W	30 NE												
KC-1331	BGG-20%	N 10 E	34 SE												
KC-1332	MGW/GG	N 30 E	64 NW			47	N 43 W	N 25 W	67 SW	80					SS
						45	N 60 W	N 11 E	39 NW						SS
KC-1333	WT-MYLON	N 18 E	55 SE												WT
KC-1334	WT	N 48 E	39 SE										N 19 W	64 SW	WT
KC-1335	SS/MGW	N 50 E	38 SE										N 28 W	76 SW	SS
KC-1336	SS	N 21 E	37 SE	37	N 88 E										SS
KC-1337	SS/MGW	N 54 W	26 NE										N 60 E	82 NW	SS
KC-1338	SS	N 53 W	31 NE												SS
KC-1339	SS	N 50 W	14 NE										N 20 W	75 SW	SS
KC-1340	SILL-MGW/GG	N 70 E	24 SE										N 40 W	90 SW	SS
KC-1341	L-MGW/WT-?-MYL	N 49 W	38 NE												WT
KC-1342	SS	N 72 W	53 NE												SS
KC-1343	MUSC-SS	N 83 W	34 NE												SS
KC-1344	SCH-MIG	N 68 E	28 NW												SS
KC-1345	MGW-C.G.	N 72 E	40 SE										N 83 E	60 NW	MGW-MIG
KC-1346	SS	N 79 E	37 NW										N 45 W	8 5NE	SS
KC-1347	LEUCO-GG	N 67 E	32 SE										N 3 W	57 SW	MGW-MIG
KC-1348	SS/MGW	N 43 W	36 NE												SS
KC-1349	SS-MIG	N 67 E	27 SE												SS
KC-1350	SS-MIG	N 78 E	48 SE												SS
KC-1351	SS-MIG	N 59 W	35 NE			27	N 35 W	N 35 W	90 SW	OPEN					SS

		Foliation		Lineation		Fold Axis		Axial Surface		IL	Amp.	Fold	Joint		Map
Station	Lithology	Strike	Dip	Plunge	Bearing	Plunge	Bearing	Strike	Dip	Angle	(m)	Verg.	Strike	Dip	Unit
		N 15 E	47 NW												SS
KC-1352	MGW	N 5 E	57 SE												SS
KC-1353	MICA-SS-MIG	N 1 E	46 SE										N 53 W	60 SW	SS
													N 22 E	8 NW	SS
KC-1354	SS/MGW-F G	N 37 E	51 SE										N 33 W	71 SW	SS
													N 57 E	89 SE	SS
KC-1355	SS-GG-C G	N42 E	40 SE												SS
KC-1356	MGW	N 63 E	59 NW										N 29 W	88 NE	BGN
KC-1357	SS	N 77 E	51 NW										N 18 E	74 SE	SS
KC-1358	T -MYLON/ GMGW/	N 38 W	48 NE	41	N 88 E	37	S 72 E	N 28 W	57 NE	20-30			N 53 W	30 NE	WT
		N 53 W	30 NE												WT
KC-1359	MGW/SS	N 35 E	52 SE										N 75 W	80 NE	SS
KC-1360	MYLON-WT/RE	N 14 E	18 SE												WT
KC-1361	SS/MGW-MIG	N 40 W	31 NE										N 17 E	85 NW	SS
KC-1362	-SILL-MGW/BGN/M	N 34 E	25 SE										N 55 W	76 SW	WT
KC-1363	SS-MIG	N 17 W	64 NE												SS
KC-1364	SIL-MGW/BGN-C G	N 44 E	17 SE										N 8 W	81 SW	MGW-MIG
KC-1365	MUSC-BIO-MGW/SC	N 74 E	20 SE										N 2 E	90 SE	MGW-MIG
KC-1366	GMGW	N 35 E	16 SE										N 14 W	55 NE	MGW-MIG
													N 84 E	65 SE	MGW-MIG
													N 16 W	86 SW	MGW-MIG
KC-1367	GSS	N 41 E	30 SE												SS
KC-1368	GSS/GG-FLT	N 49 E	41 SE												SS
KC-1369	GSS/MGW-MIG	N 47 E	41 SE												SS
KC-1370	MGW/SS&GG														MGW-MIG
KC-1371	GG-PEG	N 5 E	36 SE												MGW-MIG
KC-1372	MUSC-SS	N 47 E	22 SE	21	N 67 E								N 24 W	81 NE	SS
KC-1373	SS/MGW	N 90 E	78 SE												SS
KC-1374	BGN/SCH-MIG	N 68 E	28 SE												SS
KC-1375	SILL-MUSC-SCH	N 65 W	19 NE												SS
KC-1382	SS/MIG	N 51 W	37 NE												SS
KC-1383	SS-MIG	N 51 W	37 NE			50	N 19 E	N 13 W	62 NE	25		W			SS
						39	N 24 W	N 9 W	78 SW	80					SS
KC-1384	SS-MIG	N 15 W	43 NE	60	N 40 E										SS
KC-1385	SILL-MICA-SCH	N 38 W	15 NE			44	S 15 W	N 55 W	55 SW	20-30			N 30 W	86 NE	SS
													N 60 E	83 NW	SS
KC-1386	GG-MIG/CALC-SIL	N 87 E	27 NW												BGN
KC-1387	BGN/GRANITE	N 4 W	43 NE										N 14 E	66 SE	BGN
KC-1388	SS-MIG	N 28 W	38 NE			23	N 51 E	N 46 E	90 SE	80					SS
KC-1389	SS-MIG	N 85 E	35 SE												SS
KC-1390	SS	N 65 W	40 NE			20	S 71 E	N 28 W	22 NE	5		NW			SS
						32	N 45 E	N 45 E	90 SE	120					SS
KC-1391	SS	N 49 W	33 NE										N 77 E	82 NW	SS
KC-1392	SS	N 2 W	43 NE			39	S 57 E	N 21 E	38 SE	25					SS
KC-1393	SS	N 83 E	44 SE			24	S 53 E	N 28 W	33 NE	30		SW			SS
KC-1394	MGW/SS	N 15 E	21 SE												SS
KC-1395	SS/MGW	N 5 E	69 SE			53	S 46 E	N 45 W	66 NE	100-120					SS
KC-1396	SCH-MIG	N 9 W	48 SW										N 52 W	84 SW	SS
KC-1397	SS	N 31 E	39 SE	22	S 20 E										SS
KC-1398	MUSC-SILL-SCH	N 53 W	56 NE												SS
KC-1399	SS/MGW/MIG	N 68 W	55 NE												SS
KC-1400	LEU-GG/C G	N 69 E	46 NW												SS
KC-1401	SS-MIG	N 68 E	48 SE												SS
KC-1402	SS-MIG	N 53 E	42 SE										N 83 E	77 NW	SS
KC-1403	SS-MIG	N 24 E	47 SE										N 6 W	83 SW	SS
KC-1404	MUSC/BIO/SS	N 11 E	25 SE			20	N 12 E	N 35 W	19 NE	100		SW			SS
KC-1405	SS-MIG/MGW	N 15 E	79 SE												SS
KC-1406	SS-MIG/MUSC	N 16 E	52 SE												SS
KC-1407	MUSC-SS-MIG	N 31 E	33 SE										N 77 E	80 SE	SS
													N 10 W	58 SW	SS
KC-1408	SS-MIG	N 6 E	28 SE										N 64 E	78 NW	SS
KC-1409	MICA-SS-MIG	N 51 E	26 SE												SS
KC-1410	MGW/LEU-GG					33	N 10 E	N 23 E	67 SE	135			N 7 E	53 NW	BGN
KC-1411	MGW	N 68 E	46 SE										N 77 E	90 SE	BGN
KC-1412	GG-C G	N 29 E	37 SE										N 10 W	41 SW	BGN
													N 78 W	74 SW	BGN
															BGN
KC-1413	BGG~40%	N 63 E	57 SE												BGN
KC-1414	MUSC-SILL-SCH	N 7 E	19 SE	8	S 11 W								N 81 E	80 NW	SS
KC-1415	SS-MIG	N 5 W	41 NE	56	S 57 E	34	N 55 E	N 31 E	69 SE	90					SS
KC-1416	MUSC-SILL-SCH	N 4 E	32 SE												SS
KC-1417	G-MUSC-SS	N 20 W	53 NE										N 24 E	75 NW	SS
KC-1418	MGW	N 23 W	42 NE										N 85 E	86 NW	SS
KC-1419	SS/MGW	N 24 W	45 NE			53	S 54 E	N 24 W	45 NE	5					SS
KC-1420	GSS-MIG	N 13 W	56 NE												SS
KC-1421	SS/MGW	N 17 E	65 SE												SS
KC-1422	SS/MGW	N 3 E	62 SE												SS
KC-1423	SS	N 20 W	44 SE			16	S 41 E	N 44 W	84 SW	80					SS
KC-1424	SS-MIG	N 78 W	74 SW												SS
KC-1425	SCH-MIG	N 0 E	34 SE												SS
		N 78 E	72 SE												SS
KC-1426	MUSC-SILL-SCH	N 63 E	52 SE												SS
KC-1427	SS/MGW	N 45 E	41 SE												SS
KC-1428	MUSC-GG/SCH-MIG	N 35 W	56 NE										N 84 E	60 SE	SS

		Foliation		Lineation		Fold Axis		Axial Surface		IL	Amp.	Fold	Joint		Map
Station	Lithology	Strike	Dip	Plunge	Bearing	Plunge	Bearing	Strike	Dip	Angle	(m)	Verg.	Strike	Dip	Unit
KC-1429	SS	N 64 E	52 SE												SS
KC-1430	SIL-MICA-SCH	N 80 E	31 SE												SS
KC-1431	BIO-SILL-SCH-MIG	N 37 W	22 NE										N 85 E	75 SE	SS
KC-1432	MGW-MIG	N 53 E	38 SE												SS
		N 57 E	27 SE										N 44 W	77 NE	SS
KC-1433	SS	N 64 E	59 SE												SS
KC-1434	MUSC-SS-MIG	N 73 E	33 SE												SS
KC-1435	SS-MIG	N 28 W	49 NE												SS
KC-1436	MUSC-SILL-SCH	N 12 E	23 SE												SS
KC-1437	MUSC-SS-MIG	N 16 E	24 SE			41	S 67 E	N 78 E	65 SE	25			N 13 W	82 SW	SS
KC-1438	MUSC-SILL-SCH	N 39 E	48 SE										N 63 E	90 SE	SS
													N 69 W	80 NE	SS
KC-1439	SS	N 22 E	39 SE												SS
KC-1440	MUSC-SS-MIG	N 38 E	54 SE			48	S 84 E	N 38 E	54 SE	10					SS
KC-1441	MUSC-SS-MIG	N 63 E	36 SE			34	S 47 E	N 12 W	39 NE	30					SS
KC-1442	MUSC-SS-MIG	N 48 E	52 SE	17	S 82 E										SS
KC-1443	SS-MIG	N 83 E	36 SE	15	S 78 E										SS
KC-1444	SS-MIG	N 53 E	78 SE			55	N 72 E	N 50 W	49 NE	130					SS
KC-1445	MUSC-SS-MIG	N 50 E	47 SE			37	S 13 W	N 13 E	90 SE	110			N 57 E	63 NW	SS
KC-1446	MUSC-SS-MIG	N 55 E	37 SE	22	N 73 E										SS
KC-1447	BIO-SILL-SCH-MIG	N 53 W	30 NE										N 84 W	68 NE	SS
KC-1	MIG BGN	N 70 E	48 SE										N 15 W	79 SW	TG
		N 60 E	58 SE												
		N 45 E	57 SE												
KC-2	BGN/GG	N 60 E	20 SE			15	S 40 W	N 60 E	20 SE	50					TG
KC-85	VULCAN QUARY	N 58 E	31 SE										N 22 E	40 NW	TG
KC-86	VULCAN QUARY	N 65 W	36 NE			15	S 52 E						N 35 W	83 SW	TG
KC-497	MGW/SS	N 70 E	80 NW												TG
KC-498	BGG	N 22 E	24 SE										N 87 W	80 NE	TG
KC-499	BGG	N 4 W	31 NE												TG
KC-500	B-AMPH-GN	N 7 E	20 SE	19	N 10 E	25	N 48 W						N 50 E	72 SE	TG
															TG
KC-501	BGN	N 26 W	35 NE	52	S 17 W										TG
KC-502	B-AMPH-GN	N 55 E	19 SE												TG
KC-503	B-AMPH-GN	N 30 W	34 [illegible]												TG
		N 20 E	55 SE												TG
		N 40 E	20 SE												TG
KC-504	BGN/GG	N 58 E	62 SE										N 30 E	77 NW	TG
KC-505	BGN/GG	N 68 E	25 SE												TG
KC-506	B-AMPH-GN	N 50 E	56 SE												TG
KC-507	BGN/GG	N 38 E	40 SE												TG
KC-508	AMPH	N 43 E	70 SE												TG
KC-509	QZ-GG	N 4 E	26 SE												TG
KC-510	GG	N 0 E	46 SE												TG
KC-511	AMPH	N 73 E	76 NW			36	N 84 E	N 73 E	58 SE	35717					TG
KC-512	BGG	N 35 E	48 NW												TG
KC-513	GG/AMPH	N 28 E	37 SE										N 25 W	83 SW	TG
KC-514	GG/AMPH	N 33 E	70 SE												TG
		N 55 E	42 SE												
KC-519	AMPH														TG
KC-520	BGG	N 39 E	48 SE			30	N 45 E						N 53 E	60 SW	TG
KC-521		N 36 E	25 SE												TG
		N 84 E	64 SE												TG
KC-522	BGN-MIG	N 60 E	48 SE												TG
KC-523	BGN-MIG	N 42 E	33 SE												TG
KC-524	B-AMPH-GN	N 22 E	51 SE												TG
KC-525	B-AMPH-GN	N 35 E	61 SE												TG
KC-526	B-AMPH-GN	N 44 E	39 SE			7	S 22 W	N 31 E	22 SE			NW			TG
KC-527	B-AMPH-GN	N 61 E	38 SE												TG
KC-528	BGG	N 50 E	60 SE												TG
KC-540	AMPH/BGG														TG
KC-541	BGG	N 33 E	39 SE												TG
KC-542	B-AMPH-GN	N 32 E	19 SE										N 10 W	68 NE	TG
KC-543	BGG-CG	N 57 E	67 SE												TG
KC-550	B-AMPH-GN-MIG	N 31 E	52 SE			53	S 53 E	N 28 W	65 NE	70					TG
						19	N 22 W	N 24 W	48 NE	20					TG
KC-551	B-AMPH-GN					32	N 72 E	N 35 W	44 NE				N 15 E	70 NW	TG
KC-552	B-AMPH-GN	N 58 E	59 SE										N 18 W	65 NE	TG
KC-553	B-AMPH-GN	N 48 E	74 SE												TG
KC-593	QZ-BGN	N 55 E	68 NW												TG
KC-594	BGN (T G ?)	N 41 E	56 SE										N 45 W	70 NE	TG
KC-595	BGN-C G	N 41 E	38 SE												TG
KC-596	BGG-C G	N 54 E	41 SE												TG
KC-597	BGN-C G -MIG~65%	N 82 E	48 SE			27	S 63 W	N 82 E	48 SE	10		NW			TG
KC-598	R-E-BGN	N 38 E	29 SE												TG
KC-599	R-E-BGN-MYLON?	N 57 E	47 SE												TG
KC-600	R-E-BGN	N 53 E	34 SE												TG
KC-601	BGG/BGN	N 40 E	41 SE												TG
KC-602	GG	N 58 E	39 SE												TG
KC-603	AMPH-GG	N 47 E	43 SE												TG
KC-604	GG-MIG	N 49 E	46 SE												TG
KC-605	BGN	N 45 E	44 SE												TG
KC-606	BGN-C G	N 57 E	64 SE										N 12 W	76 NE	TG
KC-607	GG	N 23 E	35 SE												TG

		Foliation		Lineation		Fold Axis		Axial Surface		IL	Amp.	Fold	Joint		Map
Station	Lithology	Strike	Dip	Plunge	Bearing	Plunge	Bearing	Strike	Dip	Angle	(m)	Verg.	Strike	Dip	Unit
KC-623	GG-SAP	N 18 W	40 NE												TG
KC-624	AMPH-GG	N 32 E	52 SE										N 90 E	57 NW	TG
KC-625	BGG	N 21 E	35 SE												TG
KC-626	R-E-BGN-?														TG
KC-629	BGN~60-70%	N 77 E	42 SE												TG
KC-631	BGN	N 39 E	36 SE												TG
KC-632	BGN-C.G	N 4 E	60 SE												TG
KC-633	BGN	N 67 E	29 SE												TG
KC-635	BGN	N 33 E	32 S E												TG
KC-636	BGN/GG	N 37 E	38 S	21	N 83 E								N 10 W	77 NE	TG
KC-705	BGN	N 42 E	66 SE										N 20 W	63 SW	TG
KC-706	BGN-C.G.	N 20 E	47 SE												TG
KC-707	BGN-C.G.	N 37 E	47 SE												TG
KC-708	BGN/GG	N 49 E	42 SE												TG
KC-709	GG-SAP/ &AMPH	N 55 E	66 SE												TG
KC-710	GG	N 44 E	68 SE										N 40 W	81 NE	TG
KC-711	BGG	N 30 E	46 SE												TG
KC-712	GG	N 23 E	46 SE												TG
KC-713	BGG	N 21 E	40 SE										N 15 W	85 NE	TG
KC-714	AMPH	N 43 E	28 SE												TG
KC-715	BGN	N 62 E	55 SE												TG
KC-716	BGN/GG	N 30 E	30 SE												TG
KC-717	B/AMPG-GN(TG?)	N 28 E	43 SE			25	N 63 E								TG
KC-718	TG	N 35 E	37 SE												TG
KC-719	TG	N 48 E	49 SE										N 20 E	77 NW	TG
KC-720	TG	N 85 W	24 NE												TG
KC-721	TG	N 45 E	41 SE												TG
KC-722	BGG	N 53 E	65 SE												TG
KC-723	BGN(TG)	N 33 E	51 SE												TG
KC-724	BGN(TG)	N 39 E	38 SE												TG
KC-751	TG?	N 28 W	44 NE												TG
KC-752	SCH-MIG-SAP	N 17 E	35 SE												TG
KC-753	OCHRE-SAP	N 44 E	40 SE										N 17 E	83 NW	TG
KC-754	GG-SAP	N 22 E	51 NW												TG
KC-755	GG	N 53 E	31 SE												TG
KC-756	BGG	N 53 E	63 SE												TG
KC-757	AMPH-GG-TG?	N 53 E	63 SE												TG
KC-758	GG-TG?	N 67 E	36 SE										N 5 W	69 NE	TG
KC-759	MGW/SCH-TG	N 54 E	46 SE												TG
KC-760	TG	N 61 E	54 SE												TG
KC-761	GG	N 36 E	38 SE												TG
KC-799	BGG	N 52 E	64 SE												TG
KC-800	BGG~3-5%	N 26 E	32 SE										N 86 E	81 NW	TG
KC-801	BGN	N 55 E	34 SE												TG
KC-802	BGN-C.G.	N 51 E	53 SE										N 39 W	62 SW	TG
KC-903	L-GG	N 53 E	62 SE												TG
KC-804	GG	N 71 E	41 SE												TG
KC-805	TG	N 46 E	58 SE	12	N 58 E								N 43 W	58 SW	TG
KC-806	TG/PEG	N 21 E	42 SE										N 2 W	40 SW	TG
													N 73 E	99 SE	TG
KC-807	BGN	N 68 E	64 SE												TG
KC-808	BGN	N 35 E	32 SE												TG
KC-809	BGN/SCH-SAP	N 30 W	35 NE												TG
KC-810	TG	N 50 E	45 SE										N 0 E	42 NW	TG
KC-811	TG	N 70 W	46 NE			26	S 80 E	N 60 W	24 NE	70		SE?	N 57 W	63 SW	TG
		N 57 E	53 SE			14	N 62 E	N 48 E	18 SE	20		SE			TG
		N 73 E	40 SE			17	N 80 E								TG
KC-812	BGN-DRK	N 48 E	35 SE												TG
KC-819	TG	N 27 E	54 SE												TG
KC-820	TG	N 28 E	46 SE			32	N 66 E	N 66 E	90 SE	OPEN					RE
KC-821	TG	N 47 E	43 SE												RE
KC-822	SAP-GG?	N 28 W	40 NE												TG
KC-824	TG	N 5 E	46 SE			24	N 67 E	N 20 E	28 SE	30			N 18 E	81 NW	TG
KC-825	TG	N 10 E	46 SE												TG
KC-826	GG	N 7 E	43 SE										N 53 E	83 SE	TG
KC-827	TG~10%	N 16 E	46 SE												TG
KC-828	GG	N 6 E	34 SE										N 27 W	71 SW	TG
KC-829	TG	N 12 E	59 SE										N 77 E	84 NW	TG
KC-830	TG	N 70 E	25 NW										N 16 E	75 SE	TG
KC-831	TG	N 87 E	27 SE												TG
KC-832	TG*****	N 49 E	35 SE			17	N 4 W					W	N 66 W	70 NE	TG
						15	N 67 E	N 62 E	31 SE	20		W	N 22 W	75 SW	TG
															TG
KC-833	TG	N 46 E	34 SE										N 23 W	75 SW	G
KC-834	GG-SAP	N 25 E	21 SE												TG
KC-835	AMPH-GG=TG	N 56 E	44 SE			14	N 72 E	N 56 E	44 SE	30			N 19 W	71 NE	TG
KC-836	AMPG-GG-SAP	N 50 E	32 SE												TG
KC-837	GG	N 65 E	30 SE										N 29 W	68 SW	TG
KC-838	GG-SAP	N 20 W	42 NE			10	N 70 E	N 41 E	35 SE	160					TG
						32	N 14 W	N 51 E	38 NW	70					TG
KC-839	GG	N 75 E	30 NW												TG
KC-840	GG	N 36 E	34 SE										N 13 W	73 NE	TG
KC-841	TG	N 83 E	61 SE												TG
KC-842	TG	N 41 E	27 SE										N 6 W	84 SW	TG

		Foliation		Lineation		Fold Axis		Axial Surface		IL	Amp.	Fold	Joint		Map
Station	Lithology	Strike	Dip	Plunge	Bearing	Plunge	Bearing	Strike	Dip	Angle	(m)	Verg.	Strike	Dip	Unit
KC-843	TG	N 19 E	16 SE												TG
KC-844	TG	N 36 E	63 SE										N 2 W	86 SW	TG
KC-845	GG-SAP	N 25 E	27 SE												TG
KC-846	GG-PEG	N 0 E	30 SE										N 1 E	85 SE	TG
													N 37 E	64 SE	TG
KC-847	GG	N 26 E	46 SE										N 4 W	77 NE	TG
KC-848	TG	N 43 E	42 SE												TG
KC-849	GG	N 19 E	31 SE										N 27 E	27 SE	TG
													N 0 E	90 SE	
KC-902	GG	N 30 E	36 SE												TG
KC-903	GG	N 32 E	36 SE												TG
KC-904	GG	N 79 W	58 SW												TG
KC-905	GG	N 49 E	45 SE												TG
KC-906	TG	N 28 W	24 NE												TG
KC-918	AMPH	N 46 E	44 SE										N 70 E	75 NW	TG
KC-919	TG														TG
KC-937	TG~75%														TG
KC-938	TG	N 62 E	50 SE										N 7 E	79 SE	TG
													N 2 E	64 SE	TG
KC-939	TG	N 62 E	50 SE										N 23 E	61 NW	TG
KC-942	GG-PEG	N 40 E	32 SE										N 20 W	82 NE	TG
KC-946	TG??														TG
KC-949	TG	N 43 E	32 SE												TG
KC-950	TG	N 16 E	58 SE	6	N 57 E								N 18 W	86 NE	TG
KC-951	AMPH	N 72 E	57 SE										N 20 W	78 SW	TG
KC-952	GG-SAP	N 47 E	44 SE												TG
KC-953	TG	N 79 E	14 SE										N 13 E	84 SE	TG
KC-954	GG-SAP	N 51 E	66 SE												TG
KC-955	GG-SAP	N 32 E	31 SE												TG
KC-956	GG-C.G.	N 17 W	11 NE												TG
KC-957	GG-SAP	N 15 W	28 NE												TG
KC-958	GG	N 63 E	35 SE												TG
KC-959	RED-SAP	N 28 W	25 NE												TG
KC-960	GG-SAP	N 53 E	40 SE												TG
KC-961	GG-SAP	N 68 E	34 SE												TG
KC-962	GG-SAP/AMPH	N 23 E	42 SE												TG
KC-963	TG														TG
KC-964	TG	N 0 E	33 SE										N 6 E	37 NW	TG
KC-965	TG	N 41 E	47 SE										N 18 W	84 SW	TG
KC-966	RED-SAP	N 3 E	28 SE												TG
KC-967	RED-SAP	N 10 E	29 SE												TG
KC-968	TG	N 0 E	36 SE			36	N 52 E	N 70 W	28 NE	OPEN					TG
KC-969	TG	N 22 W	35 NE										N 7 W	67 SW	TG
		N 8 E	40 SE												TG
KC-970	TG	N 34 E	47 SE										N 44 W	75 SW	TG
KC-971	GG-SAP	N 57 E	17 SE												TG
KC-972	GG-SAP	N 7 E	35 SE												TG
KC-973	TG	N 59 E	46 SE												TG
KC-974	GG	N 27 E	47 SE										N 74 W	86 NE	TG
KC-975	BGG (WT?)	N 70 E	58 SE										N 11 W	82 NE	TG
KC-976	TG	N 56 E	58 SE												TG
KC-992	GG-SAP	N 5 E	72 SE												TG
KC-993	TG	N 28 E	24 NW												TG
KC-995	TG	N 61 E	17 SE			19	S 50 E	N 81 E	17 SE	35559		NW	N 6 E	86 SE	TG
KC-1303	TG	N 40 E	44 SE			16	N 50 E	N 40 E	44 SE	35722					TG
KC-1376	TG-M.G.-C.G.	N 29 E	30 SE												TG
KC-1377	AMPH/TG	N 3 E	16 SE	33	N 72 E										TG
KC-1378	TG-LEU	N 55 E	61 SE												TG
KC-1379	TG-AMPH	N 11 E	43 SE										N 36 E	15 NW	TG
KC-1380	AMPH/GG-C.G.	N 23 E	38 SE			32	N 39 E	N 82 W	39 NE	95					TG
KC-1381	LEU-GG-C.G.	N 39 E	22 SE												TG
KC-1448	LEU-GG	N 34 E	16 SE										N 20 W	90 SW	TG-MIG
KC-1449	CALC-SIL/GG-M.G.	N 52 E	36 SE										N 16 W	74 SW	TG-MIG
KC-1450	MPH/MUSC-SCH-M	N 36 E	24 SE												TG-MIG
KC-1451	LEU-GG-C.G.	N 46 E	34 SE												TG-MIG
KC-1452	GG-C.G./ &CALC-SI	N 64 E	60 SE										N 3 W	85 NE	TG-MIG
KC-1453	AMPH-WEATH	N 15 E	62 SE										N 79 E	71 SE	TG
KC-1454	LEU-GG-C.G.	N 61 E	50 SE												TG
KC-1455	OCHRE-SAP	N 43 E	28 SE										N 2 E	90 SE	TG
KC-1456	DIOR/AMPH														TG
KC-1457	AMPH														TG
KC-1458	TG	N 65 E	46 SE										N 48 W	80 SW	TG
													N 4 W	75 NE	TG
KC-1459	TG	N 5 E	25 SE												TG
KC-1460	TG-SAP	N 57 E	62 SE										N 17 W	42 SW	TG
KC-1461	TG	N 65 E	56 SE										N 7 W	80 NE	TG
KC-1462	AMPH-C.G.	N 24 E	55 SE										N 63 W	76 SW	TG
KC-1463	AMPH-PHENOCRY	N 53 E	58 SE										N 31 E	63 NW	TG
KC-1464	TG-SAP	N 34 E	35 SE												TG
KC-1465	AMPH-WEATH	N 21 E	43 SE										N 37 E	77 SE	TG
													N 33 W	90 SW	TG
													N 77 E	69 SE	TG
KC-1466	TG-MIG	N 53 E	33 SE												TG
KC-1467	WEATH-AMPH	N 14 E	34 SE										N 0 E	73 SE	TG

		Foliation		Lineation		Fold Axis		Axial Surface		IL	Amp.	Fold	Joint		Map
Station	Lithology	Strike	Dip	Plunge	Bearing	Plunge	Bearing	Strike	Dip	Angle	(m)	Verg.	Strike	Dip	Unit
KC-1468	GG/AMPH	N 56 E	64 SE												TG
KC-1469	LEU-GG	N 80 E	43 SE												TG
KC-1470	CHRE-GG-SAP/C	N 65 E	43 SE												TG
KC-1471	TG-MIG	N 89 W	32 SW			15	N 73 W	N 89 W	32 SW	10			N 20 E	71 SE	TG
													N 18 W	81 SW	TG
KC-1472	CHRE/MICA-SCH/	N 42 E	48 SE												TG
KC-1473	TG?	N 81 E	61 SE												TG
KC-1474	AMPH-WEATH	N 64 E	42 SE												TG
KC-1475	AMPH-WEATH	N 82 E	52 NW										N 22 W	77 SW	TG
KC-1476	BGG-C G	N 52 E	60 SE										N 6 E	84 SE	TG-MIG
KC-1477	AMPH-C G	N 68 E	35 SE										N 5 E	77 NW	TG
KC-1478	TG	N 73 E	61 SE												TG
KC-1479	TG-C G	N 82 E	51 SE												TG
KC-1480	TG/AMPH-	N 37 E	35 SE										N 63 W	81 SW	TG
KC-1481	TG/AMPH~40%	N 63 E	42 SE												TG
KC-1482	TG~20%	N 45 E	42 SE										N 52 W	73 SW	TG
KC-1483	TG 3-5%	N 44 E	56 SE												TG
KC-1484	TG-C G	N 37 E	36 SE										N 33 W	80 SW	TG
KC-1485	AMPH	N 33 E	19 SE										N 75 E	78 NW	TG
													N 4 E	79 SE	TG
KC-1486	TG/AMPH	N 57 E	53 SE												TG
KC-1487	LEU-TG~10%	N 75 E	61 NW												TG
KC-1488	TG~20-30%	N 40 E	54 NW										N 39 W	90 SW	TG
KC-1489	TG~20-30%	N 50 E	25 NW										N 37 W	87 NE	TG
KC-1490	TG~6-10%	N 68 E	49 NW										N 32 W	60 SW	TG
KC-1491	TG/AMPH	N 53 E	56 SE												TG
		N 22 E	36 SE												TG
KC-1492	SCH	N 35 E	66 SE												TG
KC-1493	AMPH-WEATH	N 87 E	50 SE										N 22 E	50 NW	TG
KC-1494	LEU-GG	N 36 E	53 SE												TG
KC-1495	TG~20-30%	N 35 E	50 SE										N 30 W	79 SW	TG
KC-1496	TG-CG-SAP	N 60 E	35 SE										N 20 W	77 NE	TG
KC-1497	AMPH	N 11 E	33 SE										N 68 E	52 NW	TG
													N 3 W	38 SW	TG
KC-1498	LEY-GG-C G	N 20 E	32 SE												TG
KC-1499	TG/AMPH	N 52 E	57 SE										N 22 W	79 NE	TG
KC-1500	AMPH	N 55 W	47 NE												TG
KC-1501	GG-SAP/TG	N 76 W	35 NE												TG
KC-1502	TG-AMPH	N 10 E	68 NW												TG
KC-1503	AMPH	N2 W	39 SW												TG
KC-1504	AMPH	N34 E	28 SE												TG
KC-1505	TG	N 13 E	18 SE												TG
KC-1506	TG	N 47 E	48 SE												TG
KC-1507	TG~30%	N 29 E	52 SE										N 17 E	34 NW	TG
KC-1508	AMPH	N 47 E	80 SE										N 29 W	67 SW	TG
KC-1509	TG	N 65 E	58 NW												TG
KC-1510	AMPH/GG	N 70 E	48 SE										N 13 W	65 SW	TG
KC-1511	TG-GG	N 66 E	76 SE												TG
KC-1512	TG-C G	N 47 E	51 SE												TG
KC-1513	LEU-GG	N 40 E	42 SE												TG
KC-1514	TG~50%-C G	N 15 E	52 SE												TG
KC-1515	TG~50%-C G	N 2 E	45 SE												TG
KC-1516	TG	N 53 E	55 SE										N 34 W	79 SW	TG
KC-1517	TG	N 51 E	37 SE												TG
KC-1518	AMPH/GG-F G	N 40 E	58 SE												TG
KC-1519	LEU-GG-C G	N 42 E	47 SE										N 47 W	80 SW	TG
KC-1520	TG/AMPH	N 47 E	54 SE	8	S 35 W										TG
KC-1521	AMPH	N 46 E	73 SE			24	S 42 W	N 53 E	75 SE			NW	N 28 W	62 SW	TG
KC-1522	TG-C G	N 85 E	38 SE												TG
KC-1523	MICA-GN-SAP	N 26 E	37 SE												TG
KC-1524	TG-MESO	N 66 E	45 SE												TG
KC-1525	TG-MESO	N 88 W	30 SW												TG
KC-1526	TG/-BIO-SCH	N 59 E	43 SE												TG
KC-1527	LEU-GG-C G	N 62 E	65 SE												TG
KC-1528	AMPH	N 58 E	77 SE												TG
KC-1529	MICA-SAP	N 74 E	37 NW												TG
KC-1530	TG-SAP	N 17 E	55 SE												TG
KC-1531	TG-SAP	N 33 E	32 SE												TG
KC-1532	TG-MESO	N 76 E	20 NW												TG
KC-1533	TG~50%-C G	N 84 E	58 SE												TG
KC-1534	LEUCO-GG-SAP	N 10 W	40 NE												TG
KC-1535	IO-GRANO-DIORIT	N 67 E	49 SE												TG
KC-1536	TG~50%-C G	N 75 E	23 SE												TG
KC-1537	TG-MESO	N 43 E	62 NW												TG
KC-1538	AMPH-WEATH	N 42 E	59 SE										N 66 W	41 NE	TG
KC-1539	AMPG/TG	N 35 E	48 SE												TG
KC-1540	LEUCO-GG-SAP	N 37 E	46 SE												TG
KC-1541	AMPH	N 34 E	58 SE	25	S 30 W								N 59 W	87 SW	TG
KC-1542	AMPH	N 48 E	40 SE	12	N 62 E								N 47 W	79 SW	TG
KC-1543	AMPH	N 33 E	72 SE										N 10 W	74 NE	TG
KC-1544	TG~50%-C G	N 44 E	32 SE										N 24 W	48 SW	TG
KC-1545	AMPH	N 18 E	57 SE	17	S 5 E								N 67 W	78 SW	TG
KC-1546	TG/AMPH	N 88 E	45 SE												TG
KC-1547	AMPH	N 35 E	38 SE												TG

		Foliation		Lineation		Fold Axis		Axial Surface		IL	Amp.	Fold	Joint		Map
Station	Lithology	Strike	Dip	Plunge	Bearing	Plunge	Bearing	Strike	Dip	Angle	(m)	Verg.	Strike	Dip	Unit
KC-1548	SS	N 34 E	69 SE	24	S 12 W										TG
KC-1549	TG/AMPH	N 41 E	57 SE	8	N 47 E	7	N 50 E	N 43 E	80 NW				N 2 W	84 NE	TG
KC-1550	MICA-SAP	N 6 W	56 NE												TG
KC-1551	TG~30-40%	N 68 E	34 SE												TG
KC-1552	AMPH	N 36 E	27 SE												TG
KC-1553	AMPH	N 8 E	62 SE	11	S 23 W										TG
KC-1554	TG/AMPH	N 18 E	36 SE												TG
KC-1555	AMPH-M.G.	N 80 E	36 SE												TG
KC-1556	BIO-SILL-SCH-SAP	N 22 E	36 SE												TG
KC-1557	AMPH	N 20 E	73 SE	4	S 9 W										TG
KC-1558	AMPH	N 37 E	36 SE												TG
KC-1559	TG~50%-C.G.														TG
KC-1560	TG	N 6 E	57 SE										N 74 E	77 NW	TG
KC-1561	TG	N 48 E	55 SE										N 2 E	77 SE	TG
KC-1562	TG-SAP	N 75 E	28 NW			10	N 74 E	N 75 E	55 NW	165		NW			TG
KC-1563	TG~75%	N 17 E	43 SE												TG
KC-1564	AMPH-C.G.	N 35 E	44 SE	13	N 56 E										TG
KC-1565	AMPH/TG~~60%	N 61 E	61 SE										N 3 E	40 NW	TG
KC-1566	AMPH-M.G.	N 54 E	56 NW												TG
KC-1567	TG/AMPH	N 54 E	49 SE	N 25 W	65 SW										TG
KC-1568	AMPH														TG
KC-1569	TG-M.G.	N 68 E	51 SE												TG
KC-1570	TG~40-50%	N 36 E	20 SE	8	N 49 E										TG
KC-1571	TG~30-40%	N 33 E	57 SE												TG
KC-1572	AMPH														TG
KC-1573	TG-SAP	N 54 E	42 SE												TG
KC-1574	CA-SCH//MYLON-B	N 50 E	47 SE												TG
KC-1575	OCHRE-SAP	N 37 E	50 SE										N 26 W	84 SW	TG
KC-1576	TG~30%	N 50 E	49 SE	10	N 61 E										TG
KC-1577	TG~10%	N 33 E	44 SE												TG
KC-1578	AMPH-WEATH	N 43 E	56 SE										N 31 W	82 NW	TG
KC-1579	AMPH-WEATH	N 34 E	85 SE	31	N 37 E	10	N 60 W	N 64 W	56 NE	165		NA	N 31 E	86 NW	TG
KC-1580	TG/OCHRE-SAP	N 84 E	45 SE												TG
KC-1581	TG-C.G.	N 21 E	80 SE												TG
KC-1582	TG	N 58 E	29 SE												TG
KC-1583	AMPH	N 21 E	68 SE	5	N 28 E										TG
KC-1584	TG-C.G.	N 36 E	41 SE												TG
KC-1585	AMPH	N 37 E	39 SE												TG
KC-1586	TG/AMPH	N 38 E	36 SE												TG
KC-1587	AMPH	N 40 E	67 SE												TG
KC-1588	TG-C.G.	N 61 E	76 SE												TG
KC-1589	AMPH/TG	N 82 E	39 SE												TG
KC-1590	AMPH-C.G.	N 53 E	62 SE												TG
KC-1591	TG/AMPH	N 28 E	71 SE												TG
KC-1592	TG-AMPH	N 42 E	64 SE												TG
KC-1593	TG-AMPH	N 30 E	47 SE												TG
KC-1594	TG	N 73 E	50 SE												TG
KC-1595	OCHRE-SAP	N 19 E	55 SE										N 30 W	84 SW	TG
KC-1596	TG~30-40%/AMPH	N 49 E	47 SE										N 56 E	25 NW	TG
													N 34 W	66 SW	TG
KC-1597	MICA-SAP	N 17 E	54 SE												TG
KC-1598	TG-SAP	N 29 E	65 SE										N 32 W	74 SW	TG
KC-1599	AMPH	N 58 E	56 SE										N 15 W	62 SW	TG
KC-1600	AMPH	N 71 E	70 SE												TG
KC-1601	OCHRE-SAP	N 30 E	53 SE												TG
KC-1602	TG-SAP	N 57 E	13 SE												TG
KC-1603	TG-M.G.	N 37 E	48 SE												TG
KC-1604	TG-SAP	N 5 W	42 NE												TG
KC-1605	TG	N 61 E	46 SE												TG
KC-1606	AMPH~60-70%	N 77 E	39 SE	20	S 47 W								N 61 E	36 NW	TG
KC-1607	TG-C.G.	N 47 E	73 SE												TG
KC-1608	TG/AMPH	N 48 E	70 SE	6	S 46 W										TG
KC-1609	AMPH	N 37 E	52 SE										N 24 W	87 NE	TG
KC-1610	TG	N 66 E	67 SE												TG
KC-1611	TG~50%	N 28 E	55 SE												TG
KC-1612	AMPH	N 27 E	58 SE										N 34 W	77 SW	TG
KC-1613	LEU-GG/AMPH	N 28 E	39 SE												TG
KC-1614	LEU-GG-TG	N 48 E	58 SE												TG
KC-1615	AMPH	N 68 E	51 NW	15	N 55 E										TG
KC-1616	AMPH~50%	N 60 E	36 SE										N 2 E	76 NW	TG
KC-1617	AMPH	N 47 E	60 SE										N 23 W	87 NE	TG
KC-1618	TG/AMPH~60%	N 50 E	47 SE												TG
KC-1619	AMPH/					49	N 4 E	N 7 E	56 NW	90		NE?			TG
KC-1620	TG/AMPH	N 14 E	36 SE												TG
KC-1621	AMPH	N 70 E	49 SE			26	S 31 W	N 43 E	80 SE	35732		W			TG
		N 35 E	77 SE												TG
KC-1622	AMPH/GG-C/G/	N 54 E	42 SE			77	S 50 E	N 39 E	68 SE	0-2		W			TG
KC-1623	AMPH	N 56 E	61 SE										N 33 W	78 SW	TG
KC-1624	AMPH-SAP	N 68 E	35 SE										N 68 E	49 NW	TG
KC-1625	TG-C.G.	N 39 E	38 SE												TG
KC-1626	LEU-GG-TG	N 31 E	40 SE										N 29 E	81 NW	TG
KC-1627	TG~50%	N 84 E	57 NW												TG
KC-1628	TG-MIG/PEG	N 58 E	32 SE												TG
KC-1629	TG-C.G.	N 86 E	53 SE												TG

		Foliation		Lineation		Fold Axis		Axial Surface		IL	Amp.	Fold	Joint		Map
Station	Lithology	Strike	Dip	Plunge	Bearing	Plunge	Bearing	Strike	Dip	Angle	(m)	Verg.	Strike	Dip	Unit
KC-1630	TG	N 66 E	53 SE												TG
KC-1631	TG/AMPH~20%	N 48 E	64 SE												TG
KC-1632	LEUCO-GG~20%	N 74 E	66 SE												TG
KC-1633	AMPH-WEATH	N 73 E	49 SE												TG
KC-1634	TG-C G	N 58 E	45 SE												TG
KC-1635	TG	N 27 E	32 SE										N 7 W	47 SW	TG
KC-1636	TG														TG
KC-1637	TG	N 72 E	50 SE										N 68 E	50 NW	TG
KC-1638	TG-LEU	N 67 E	71 SE										N 13 W	70 NE	TG
KC-1639	TG	N 59 E	68 SE												TG
KC-1640	NONE														TG
KC-1641	AMPH-~50%	N 13 E	52 SE	17	N 37 E										TG
KC-1642	TG-GG	N 25 E	32 SE										N 8 E	57 NW	TG
KC-1643	TG-SAP/AMPH	N 41 E	54 SE										N 66 E	32 NW	TG
KC-1644	TG-MESO	N 47 E	49 SE												TG
KC-1645	AMPH	N 8 E	52 SE			39	S 28 E	N 8 E	52 SE	5		NW			TG
KC-1646	AMPH	N 34 E	42 SE										N 16 W	74 SW	TG
KC-1647	TG/AMPH	N 49 E	59 SE												TG
KC-1648	BGG	N 76 E	47 SE												TG
KC-1649	TG/AMPH	N 7 W	50 NE												TG
KC-1650	TG/AMPH	N 51 E	70 SE										N 27 W	58 SW	TG
KC-1651	OCHRE-SAP	N 65 E	58 SE												TG
KC-1652	OCHRE-SAP	N 36 E	25 SE												TG
KC-1653	TG-MIG/PEG	N 52 E	54 SE										N 57 W	90 SW	TG
		N 37 E	38 SE												TG
KC-1654	MESO-SAP	N 79 E	22 SE												TG
KC-1655	TG/PEG	N 67 E	33 SE												TG
KC-1656	LEU-SAP	N 85 E	40 NW												TG
		N 37 E	53 NW												TG
KC-1657	TG-SAP	N 23 E	31 SE												TG
KC-1658	BGG-C.G.~20-30%	N 58 E	35 SE												TG
KC-1659	TG-MESO	N 67 E	40 SE												TG
KC-1660	TG-GG~30%	N 84 E	34 SE												TG
KC-1661	TG-C.G./AMPH	N 44 E	62 SE												TG
KC-1662	TG	N 73 E	27 SE										N 26 W	75 NE	TG
KC-1663	OCHRE-SAP	N 65 E	47 SE										N 14 W	68 SW	TG
KC-1664	LEU-GG/AMPH	N 25 E	37 SE			3	N 23 E	N 32 E	72 NW	170			N 40 W	82 SW	TG
KC-1665	TG~50%	N 72 E	30 SE												TG
KC-1666	TG-SAP~50%	N 43 E	34 SE												TG
KC-1667	GG/PEG	N 67 E	30 SE												TG
KC-1668	GG-MUSC-10%	N 9 E	37 SE										N 5 W	56 SW	TG
KC-1669	TG	N 2 E	24 SE										N 24 E	41 SE	TG
													N 76 E	66 SE	TG
KC-1670	TG	N 47 E	45 SE	32	N 68 E										TG
KC-1671	TG~30%	N 49 E	47 SE												TG
KC-1672	TG-SAP	N 66 E	26 SE												TG
KC-1673	TG-SAP?	N 58 E	19 SE												TG
KC-1674	LEU-TG-C.G	N 18 E	63 SE												TG
KC-1675	TG	N 68 E	37 SE												TG
KC-1676	OCHRE-SAP	N 2 E	52 SE												TG
KC-1677	TG	N 63 E	52 SE												TG
KC-1678	BIO-TG-SAP	N 27 E	35 SE												TG
KC-1679	TG/AMPH	N 17 E	33 SE	20	N 57 E								N 54 W	84 NE	TG
KC-1680	TG-C.G	N 18 E	20 SE										N 18 W	80 SW	TG
KC-1681	TG-C G					23	S 55 E	N 55 W	90 SW	160					TG
KC-1682	TG	N 58 E	30 SE												TG
KC-1683	AMPG/TG	N 37 E	50 SE	36	N 62 E										TG
KC-1684	AMPG/TG~50%	N 66 E	55 SE												TG
KC-1685	AMPG/TG~50%	N 5 E	53 SE												TG
KC-1686	OCHRE-SAP	N 63 E	42 SE												TG
KC-1687	AMPG/TG~40-50%	N 45 E	70 SE												TG
KC-1688	AMPG/TG~50%/PEG	N 16 E	47 SE												TG
KC-1689	TG/AMPH	N 17 E	49 SE	18	N 52 E								N 63 W	61 SW	TG
KC-1690	TG	N 3 E	26 SE			7	N 37 E	N 37 E	71 SE	90		NW			TG
KC-1691	QZ	N 73 E	82 SE										N 7 W	72 SW	TG
KC-1692	TG-C G	N 36 E	42 SE												TG
KC-1693	AMPH-SAP	N 50 E	36 SE										N 24 W	90 SW	TG
KC-1694	TG-MESO	N 23 E	59 SE												TG
KC-1695	TG-SAP	N 72 E	34 SE												TG
KC-1696	TG/PEG	N 44 E	48 SE												TG
KC-1697	AMPG-TG	N 59 E	72 SE	6	N 68 E										TG
KC-1698	TG~15%	N 56 E	70 SE												TG
KC-1699	TG-MESO	N 28 E	40 SE												TG
KC-1700	TG-MESO	N 26 E	37 SE												TG
KC-1701	TG-SAP	N 49 E	42 SE												TG
KC-1702	BIO-TG-SAP					53	N 24 E	N 13 W	60 NE	30		NW			TG
KC-1703	AMPH	N 41 E	53 SE												TG
KC-1704	TG-SAP	N 53 E	46 SE												TG
KC-1705	TG	N 62 E	63 SE												TG
KC-1706	TG~10-15%	N 56 E	32 SE												TG
KC-1707	TG-MUSC	N 53 E	32 SE												TG
KC-1708	TG-GG	N 42 E	42 SE												TG
KC-1709	AMPH/TG-SAP	N 61 E	30 SE												TG
KC-1710	TG~10%	N 66 E	49 SE												TG

		Foliation		Lineation		Fold Axis		Axial Surface		IL	Amp.	Fold	Joint		Map
Station	Lithology	Strike	Dip	Plunge	Bearing	Plunge	Bearing	Strike	Dip	Angle	(m)	Verg.	Strike	Dip	Unit
KC-1711	TG-MESO	N 40 E	44 SE												TG
KC-1712	TG-MESO/AMPH	N 53 E	43 SE												TG
KC-1713	TG	N 83 E	48 SE										N 9 W	84 SW	TG
KC-1714	TG-MESO	N 34 E	29 SE												TG
KC-1715	TG-C.G./PEG	N 53 E	24 SE												TG
KC-1716	USC-RICH-T.G./AM	N 63 E	53 SE										N 43 W	75 SW	M-SCH
KC-1717	MUSC-LEU-GG/SCH	N 59 E	33 SE										N 65 W	63 SW	M-SCH
KC-1718	AMPH	N 22 E	47 SE												TG
KC-1719	TG	N 29 E	51 SE												TG
KC-1720	AMPH-SAP-F.G.	N 52 E	36 SE												TG
KC-1721	TG~15-20%	N 40 E	49 SE												TG
KC-1722	TG	N 23 E	48 SE												TG
KC-1723	MUSC-SCH	N 48 E	40 SE												TG
KC-1724	MUSC-TG	N 48 E	28 SE												TG
KC-1725	TG/AMPH-SAP	N 29 E	32 SE												TG
KC-1726	AMPH	N 54 E	57 SE												TG
KC-1727	MUSC-TG	N 2 W	44 NE												TG
KC-1728	BIO-MUSC-TG	N 43 E	58 SE												TG
KC-1729	TG~15%	N 48 E	64 SE												TG
KC-1730	LEU-TG-C.G.	N 61 E	59 SE												TG
KC-1731	LEU-BIO-TG	N 62 E	52 SE												TG
KC-1732	OCHRE-SAP/AMPH	N 64 E	51 SE	20	S 63 W								N 14 W	90 SW	TG
KC-1733	LEU/QZ/MUSC-GN	N 60 E	23 SE										N 50 E	45 NW	M-SCH
													N 23 W	77 SW	M-SCH
KC-1734	OG-MYLON	N 11 E	66 SE												OG
KC-1735	MYLON-OG	N 60 E	73 SE												OG
KC-1736	MYLON-OG	N 44 E	68 SE												OG
KC-1737	MUSC-BIO-GAR-SC	N 56 E	53 SE												OG
KC-1738	OG	N 73 E	29 SE												OG
KC-1739	OG	N 54 E	34 SE												OG
KC-1740	OG	N 51 E	49 SE										N 24 W	67 SW	OG
KC-1741	OG	N 35 E	28 SE												OG
KC-1742	OG	N 82 E	41 SE												OG
KC-1743	OG/SCH	N 58 E	30 SE												OG
KC-1744	OG	N 67 E	39 SE												OG
KC-1745	MUSC-BIO-SCH	N 61 E	45 NW												OG
KC-1746	MUSC-SCH	N 55 E	58 SE												OG
KC-1747	OG	N 54 E	45 NW												OG
KC-1748	MUSC-OG	N 15 E	30 SE												OG
KC-1749	OG	N 62 E	43 SE										N 4 W	48 SW	OG
KC-1750	OG	N 57 E	70 SE												OG
KC-1751	OG	N 83 E	53 SE												OG
KC-1752	OG/PEG	N 6 W	43 NE												OG
KC-1753	OG/PEG	N 66 E	30 SE												OG
KC-1754	OG	N 75 E	40 SE										N 25 W	72 NE	OG
													N 37 E	79 SE	OG
KC-1755	OG-SAP?	N 58 E	63 SE												OG
KC-1756	OG-SAP	N 52 E	36 SE												OG
KC-1757	GG	N 59 E	60 SE												OG
KC-1758	MUSC-GAR-SCH	N 45 E	39 SE												M-SCH
KC-1759	MUSC-SCH	N 63 E	52 SE												M-SCH
KC-1760	MUSC/TG?	N 55 E	57 SE												M-SCH
KC-1761	SAP	N 67 E	54 SE												TG
KC-1762	MUSC-SAP/TG	N 41 E	68 SE												TG
KC-1763	AMPH	N 68 E	50 SE										N 10 W	69 SW	TG
KC-1764	TG	N 70 E	49 SE												TG
KC-1765	TG	N 28 E	53 SE												TG
KC-1766	TG	N 27 E	34 SE										N 30 W	90 SW	TG
KC-1767	TG	N 57 E	58 SE												TG
KC-1768	TG-C.G./PEG	N 66 E	30 SE												TG
KC-1769	TG	N 86 E	40 SE												TG
KC-1770	TG-SAP	N 36 E	55 SE												TG
KC-1771	GG	N 32 E	31 NW												TG
KC-1772	TG	N 74 E	45 SE			8	N 45 E	N 55 E	66 NW	90					TG
KC-1773	GG	N 43 E	37 SE										N 74 E	83 NW	TG
KC-1774	B-GG	N 72 E	48 SE										N 64 E	51 NW	TG
KC-1775	C-GG/BGN														TG
KC-1776	C-GG	N 47 E	31 SE												TG
KC-1777	M-BGN	N 30 E	25 SE												TG
KC-1778	T.G. ***	N 70 E	50 SE										N 13 E	66 SE	TG
KC-1779	AMPH	N 74 E	32 SE										N 90 E	44 NW	TG
KC-1780	BGN/GG	N 80 E	30 NW												TG
KC-1781	BGN	N 42 E	43 SE												TG
KC-1782	BGN/PEG	N 35 E	42 SE												TG
KC-1783	GG/BGN/SCH	N 76 E	54 SE			13	N 65 E	N 65 E	50 NW						TG
KC-1784	QZ-SCH/ AMPH	N 62 E	55 SE												TG
KC-1785	DRK-SCH/BGN	N 43 E	54 SE												TG
KC-1786	QZITE					15	S 32 E	N 25 W	90 SW						TG
KC-1787	QZITE/ HW	N 37 E	43 SE												TG
		N 85 W	40 NE												TG
KC-1788	SHEARED-BGN	N 63 E	55 SE												TG
KC-1789	AMPH/ SCH	N 73 E	58 SE												M-SCH
KC-1790	QZITE/ SCH	N 73 E	66 SE										N 12 W	75 NE	M-SCH
KC-1791	GG-SAP	N 82 E	41 SE												OG

		Foliation		Lineation		Fold Axis		Axial Surface		IL	Amp.	Fold	Joint		Map
Station	Lithology	Strike	Dip	Plunge	Bearing	Plunge	Bearing	Strike	Dip	Angle	(m)	Verg.	Strike	Dip	Unit
KC-1792	O.G. BGN	N 11 W	30 SE										N 4 W	90 SW	TG
KC-1793	PEG/ SCH	N 80 E	43 SE												TG
KC-1794	O.G	N 82 E	6 SE												TG
KC-1795	O.G. SCH	N 68 E	55 SE												TG
KC-1796	O.G	N 77 E	47 SE												TG
KC-1797	MGW/BGN/SCH	N 54 E	46 SE												TG
KC-1798	DRK-SCHI	N 52 E	57 SE												TG
KC-1799	O.G. SAP	N 71 E	51 SE												TG
KC-1800	O G	N 76 E	58 SE												TG
KC-1801	AMPH														TG
KC-1802	GG/SCHI	N 66 E	48 SE												M-SCH
KC-1803	BGN (S&P)	N 72 E	55 SE												TG
KC-1804	OCHRE-SAP	N 68 E	56 NW												TG
KC-1805	BGN/ GG	N 52 E	54 SE												TG
KC-1806	GG/SCHI	N 32 E	67 SE												TG
KC-1807	T.G.??	N 55 E	32 SE												TG
KC-1808	QZ -RICH-BGN	N 75 E	55 SE												TG
KC-1809	BGN	N 60 E	29 SE	9	N 67 E								N 21 W	75 SW	TG
													N 66 E	66 NW	TG
KC-1810	BGN-MIG	N 74 E	42 SE												TG
KC-1811	T G.	N 54 E	61 NW												TG
KC-1812	T G -SAP	N 72 E	54 SE												TG
KC-1813	T G	N 66 E	62 SE												TG
KC-1814	PMA	N 35 E	57 SE										N 67 E	47 NW	TG
KC-1815	AMPH	N 41 E	54 SE												TG
KC-1816	T G	N 67 E	38 SE												TG
KC-1817	MESO-&AMPH	N 81 E	34 SE												TG
KC-1818	BGN/T G	N 68 E	40 SE												TG
KC-1819	AMPH/ T G	N 61 E	50 SE												TG
KC-1820	T G / PEG	N 42 E	38 SE										N 16 W	85 SW	TG
KC-1821	GG/ PEG	N 50 E	54 SE												TG
KC-1822	C-Grained-T G	N 52 E	51 SE												TG
KC-1823	OCHRE-SAP	N 70 E	44 SE												TG
KC-1824	GG-SAP	N 77 E	40 SE												TG
KC-1825	B-GG	N 58 E	31 SE												TG
KC-1826	T.G./GG	N 11 E	43 SE												TG
KC-1827	SAP	N 86 E	40 NW												TG
KC-1828	T G (MAFIC)	N 72 E	35 SE												TG
KC-1829	T G (SCHIST)	N 28 E	47 SE												TG
KC-1830	O.G. SCHI?	N 33 E	60 SE												TG
KC-1831	T G ??	N 70 W	39 SW												TG
KC-1832	MUSC-SCH	N 43 E	61 SE												M-SCH
KC-1833	SCH-SAP	N 52 E	53 SE												OG
KC-1834	SCH	N 70 E	66 SE												OG
KC-1835	SCHI	N 63 E	53 SE												OG
KC-1836	O G	N 15 E	45 SE												OG
KC-1837	O G	N 68 W	44 SW												OG
KC-1838	O.G.	N 47 E	37 SE												OG
KC-1839	DRK-SCH	N 34 E	50 SE										N 82 E	62 NW	OG
													N 3 W	45 S W	OG
KC-1840	O.G.	N 20 E	38 SE												OG
KC-1841	O.G.	N 63 E	66 SE												OG
KC-1842	HEN	N 56 E	74 SE										N 20 W	78 SW	HEN
KC-1843	HEN	N 68 E	66 SE												HEN
KC-1844	O.G.	N 63 E	32 SE												OG
KC-1845	O.G.	N 62 E	58 SE												OG
KC-1846	MUSC-BIO-SCH	N 49 E	56 SE												OG
KC-1847	O.G.	N 37 E	51 SE												OG
KC-1848	BGN														OG
KC-1849	O.G.	N 65 E	77SE												OG
KC-1850	fine-gr-SCH/BGN	N 71 E	53 SE												OG
KC-1851	O G	N 66 E	42 SE												OG
KC-1852	O.G.	N 68 E	57 SE										N 60 E	40 NW	OG
KC-1853	O G	N 65 E	49 SE										N 50 E	64 SE	OG
KC-1854	O G	N 56 E	47 SE												OG
KC-1855	O.G.	N 22 E	38 SE												OG
KC-1856	BGG	N 75 E	60 SE												HEN
KC-1857	HEN (W/PEG)	N 47 E	46 SE												HEN
KC-1858	HEN	N 64 E	46 SE										N 32 E	57 SE	HEN
KC-1859	O.G.	N 64 E	43 SE												OG

Vita

James L. Kalbas was born and raised in Brandon, Florida. His scientific career began early with fourth through sixth grade studies of erosion rates of clay-rich, poorly consolidated soils in central Florida. Jay graduated from Brandon High School, where he was a member of the national record-holding varsity wrestling team, Senior class president, and a member of the band, chorus, and orchestra. Jay attended Furman University where he was a member of the Furman Singers and the Bell Tower Boys (a men's a capella group). While at Furman, Jay trained to become an Army officer; he was a member of both an award-winning Ranger team and the specialized Battalion Ranger Company. An injury, obtained while competing in the annual Ranger Challenge competition, and the series of knee surgeries that followed, disqualified him from combat operations. Jay was honorably discharged from U.S. Army Reserve in 1999. Jay graduated from Furman University in the Spring of 2000 after completing two senior theses. The first was a study of the effect of Pliocene climate change on surface water productivity and circulation on Namibian continental shelf, southern Atlantic Ocean. His second research thesis was a mapping-based study of macroscopic structures in the Inner Piedmont belt, South Carolina. He was also an Associate Instructor at Indiana University's Geologic Field Camp in Cardwell, Montana.

On March 16, 2002, Jay married the most wonderful woman he ever met, Jennifer M. Anderson. In Fall, 2002 they moved to Indiana where Jennifer began working on her Master of Divinity degree at Christian Theological Seminary and Jay began work on his Ph.D. at Purdue University. His dissertation topic is active and Cenozoic strike slip deformation in the Alaska Range, south-central Alaska and Cretaceous development of the Kuskokwim Group, southwestern Alaska.

7811 0207 57
11/05/03 MAB

Geologic Map of a portion of the western and eastern Inner Piedmont, North Carolina

Compiled by: James L. Kalbas, Brendan R. Bream, and Sara E. Bier,
Modified by: Arthur J. Merschat
University of Tennessee-Knoxville
Tectonics and Structural Geology Research Group

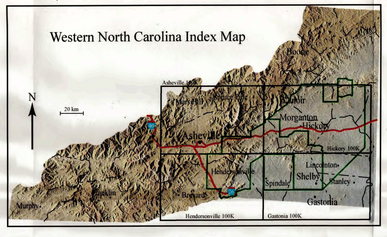

Structure

- Trace of axial surface of F_{2n} overturned, recumbent anticline
- Trace of axial surface of F_{2n} overturned, recumbent synicline
- Hinge of F_2 sheath fold
- Trace of axial surface of F_3 open, upright anticline
- Trace of axial surface of F_3 open, upright synicline
- Normal fault; dashed where inferred, where displacement is known, arrows are used and/or U = upthrown wall, D = downthrown wall
- Thrust fault; teeth on the hanging wall
- Area of intense migmatization
- 1 2002 CGS field trip stop location

Supported by the National Cooperative Mapping Program (EDMAP) under Assistance Awards 97HQAG1720, 98HQAG2026, 99HQAG0026, and 00HQAG0035 to Robert D. Hatcher, Jr.

1993 CGS Field Trip

SCALE 1:100 000
1 CENTIMETER ON THE MAP REPRESENTS 1 KILOMETER ON THE GROUND
Kilometers 0 1 2 3 4 5 6 7 8 9 10 11 12 13 14 15 16 17 18 19 20
Miles 0 1 2 3 4 5 6 7 8 9 10 11 12 13

Correlation of Map Units

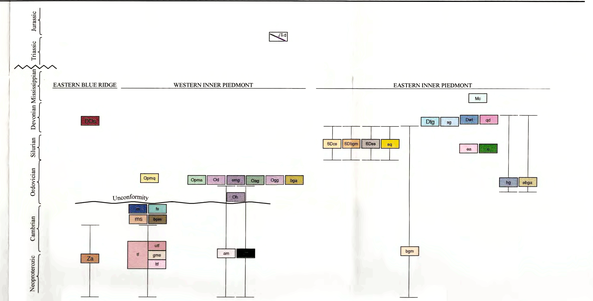
Triassic
Jurassic
Devonian-Mississippian
Silurian
Ordovician
Cambrian
Neoproterozoic
EASTERN BLUE RIDGE
WESTERN INNER PIEDMONT
EASTERN INNER PIEDMONT
Unconformity
Dtg
Dwl
Dbg
Dgr
Dqd
Dsg
Dgn
Dtd
Dmq
Dpm
Dpmq
Dpma
Dpmg
Dqg
Dqp
Dpa
Dsa
Dsgn
Dsm
Dsmg
Dsmq
Dsmp
Dsmm
Dsmv
Dsmt
Dsmh
Dsmc
Dsmd
Dsmn
Dsmw
Dsmk
Dsmr
Dsmb
Dsmf
Dsmz

Plate 2. Geologic map and cross sections of the Kings Creek, North Carolina 7.5-minute quadrangle

James L. Kalbas; December, 2002
Tectonics and Structural Geology Research Group,
University of Tennessee-Knoxville

Western Inner Piedmont

Qal **Alluvium-** poorly sorted, unconsolidated sediments ranging from silt- to boulder-size. Thickness of deposits is typically from ~1 – 3 m.

Ml **Lenoir Quarry migmatite -** dark gray to black, medium-grained, hornblende (33-99 %), quartz (0-27 %), plagioclase (< 1-27 %; An_{24-44}), biotite (0-12 %), epidote (< 1-7 %) gneiss. Also contains light to dark gray, medium- to coarse-grained, quartz (38-68 %), plagioclase (32-36 %; An_{24-34}), biotite (12-14 %), microcline (< 10 %), hornblende (< 5 %), myrmekite (2-3 %), and epidote (1-2 %). Typically migmatitic; contains 1-4 cm quartz, feldspar layers and lenses. Contains numerous boudins of amphibolite, with minor quartz-feldspar layering, ranging in size from 10 cm to >1 m.

Ohg **Henderson Gneiss-** light gray to medium gray, megacrystic, microcline-oligoclase-quartz-biotite-muscovite augen gneiss. Augen are lenticular and are aligned with the foliation defined by a medium-grained matrix composed of feldspars, biotite, quartz, and epidote.

am **Amphibolite-** black, fine- to medium-grained, hornblende-plagioclase (trace)-quartz (trace) gneiss.

gg **Granitoid gneiss-** light gray (frequently stained to a light orange by secondary oxidation), medium- to coarse-grained, poorly foliated to massive, quartz-feldspar, holo-leucocratic to leucocratic, granitic gneiss.

ms **White-mica schist-** light brownish-white to reddish brown, coarse-grained quartz-muscovite-sillimanite schist. Migmatitic with local quartzofeldspathic leucosomes.

bs **Inequigranular biotite gneiss and schist-** dark gray, fine- to medium-grained, inequigranular quartz (34-37 %), biotite (23-30 %), plagioclase (13-24 %; An_{34-44}), muscovite (8-15 %), sillimanite (trace-3%) schist and biotite gneiss. Porphyroclasts are dominantly composite and range in size from 0.1 10 1.0 cm in diameter. Texturally similar to "Hg."

Eastern Inner Piedmont

Qal **Alluvium-** poorly sorted, unconsolidated sediments ranging from silt- to boulder-size. Thickness of deposits is typically from ~1 – 3 m.

Dwt **Walker Top Granite-** light gray to medium gray, megacrystic, plagioclase (18-39 %; An $_{37-40}$), quartz (29-30 %), microcline (16-30 %), biotite (9-18 %), muscovite (trace-5 %), garnet (0-1 %) gneiss. Microcline megacrysts are euhedral to subhedral and are aligned with the dominant foliation. Long axes range in size from ~0.5 to 8.0 cm and display carlesbad twinning. Matrix is medium- to coarse-grained and contains feldspar, biotite, and quartz.

Dtg **Toluca granite-** very light gray to white, medium- to coarse-grained, weakly foliated to massive biotite-garnet-white mica, metagranitoid to granitic gneiss. Includes enclaves of migmatitic biotite gneiss/metagraywacke.

hg **Hibriten orthogneiss-** dark blue- gray to black, medium to coarse-grained, megacrystic plagioclase (32-41 %; An_{33-38}), quartz (2-29 %), biotite (0-27 %), muscovite (0-1 %) gneiss. Megacrysts are dominantly euhedral plagioclase, and range in size from ~0.25 to 1.0 cm in diameter. Local amphibolite boudins.

ss **Sillimanite mica schist-** brown to reddish brown to silvery blue-gray, medium- to coarse-grained porphyroblastic biotite (27-49 %), quartz (13-45 %), sillimanite (9-14 %), muscovite (3-12 %), plagioclase (0-7 %; An_{20}), garnet (trace-7 %) schist. Migmatitic with local quartzofeldspathic layers and leucosomes.

mgw **Metagraywacke-** light to dark gray (weathering to a reddish-brown), fine- to coarse-grained, porphyroblastic, quartz (37-49 %), K-feldspar (2-32 %), biotite (13-18 %), plagioclase (13-28 %; An $_{25-31}$), muscovite (trace-4 %), hornblende (0-2 %), epidote (0-1 %) gneiss. Insubordinate amounts of garnet, biotite schist occur locally. Lacks distinct compositional layering >1-2 cm. Migmatitic, with local quartzofeldspathic leocosomes. Contains interlayers and boudins of light gray to white, fine-grained calc-silicate.

bag **Biotite augen gneiss-** light gray, fine- to medium-grained, megacrystic, K-feldspar-biotite-quartz-muscovite-garnet gneiss. Alkali feldspar megacrysts range in size from ~0.2 – 0.75 cm (long axes) and are aligned parallel to the dominant foliation. Fine- to medium-grained feldspar, biotite, and quartz constitute the matrix.

Note: where percentages are not listed, minerals are listed in descending order of abundance.

STRUCTURAL FEATURES AND SYMBOLS

CONTACTS

- Lithologic contact, dashed where approximately located, solid where exact.
- Thrust fault contact dashed where approximately located, solid where exact. Teeth on hanging wall.

LINEAR STRUCTURES

- Trend and plunge of mineral lineation
- Trend and plunge of crenulation axis
- Trend and plunge of mesoscopic upright open antiform
- Trend and plunge of mesoscopic upright open synform
- Trend and plunge of mesoscopic overturned tight to isoclinal antiform
- Trend and plunge of mesoscopic overturned tight to isoclinal synform

(NOTE: Where structural symbols are combined, the intersection marks the point of observation.)

PLANAR STRUCTURES

- Strike and dip of foliation; inclined, vertical
- Strike and dip of schistosity; inclined, vertical

MAP SYMBOLS

- Vulcan Materials Quarry
- Abandoned prospect pit

SCALE 1:24 000
1 MILE 1000 2000 3000 4000 5000 6000 7000 FEET
1 KILOMETER
CONTOUR INTERVAL 20 FEET
DATUM IS MEAN SEA LEVEL

UTM GRID AND 1970 MAGNETIC NORTH DECLINATION AT CENTER OF SHEET

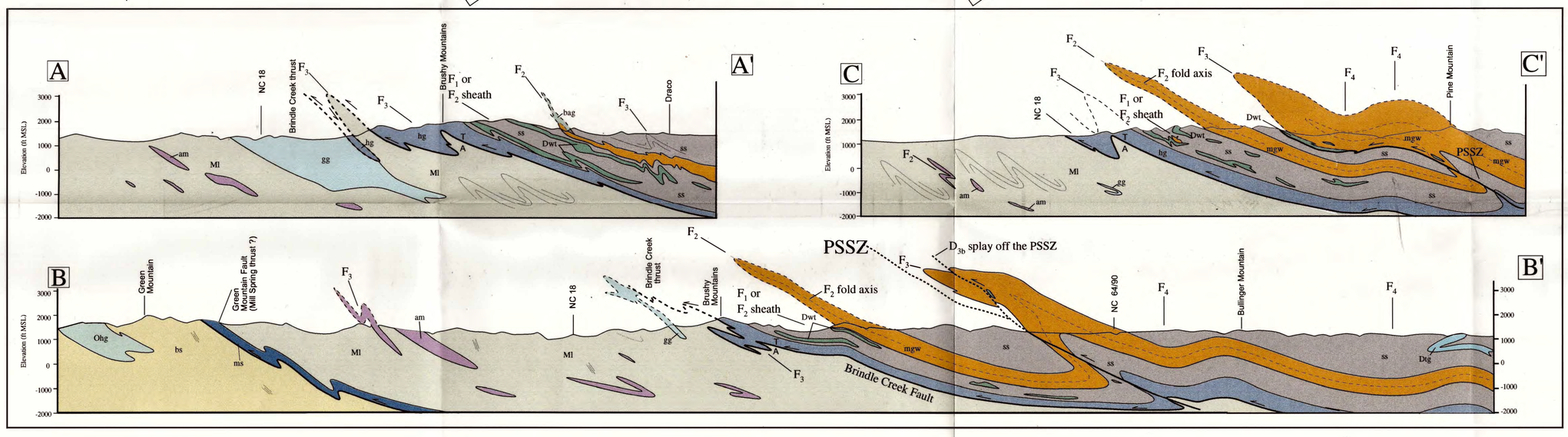

Major Faults

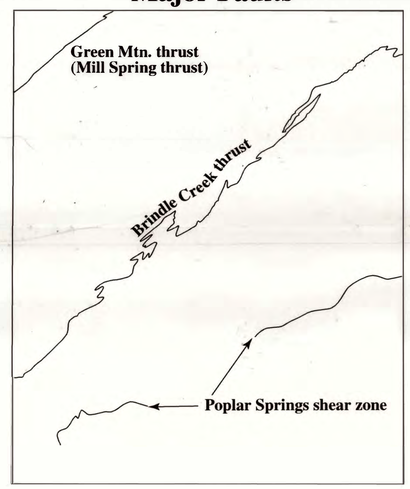

Plate 3. Station locations in the Kings Creek, North Carolina 7.5-minute quadrangle

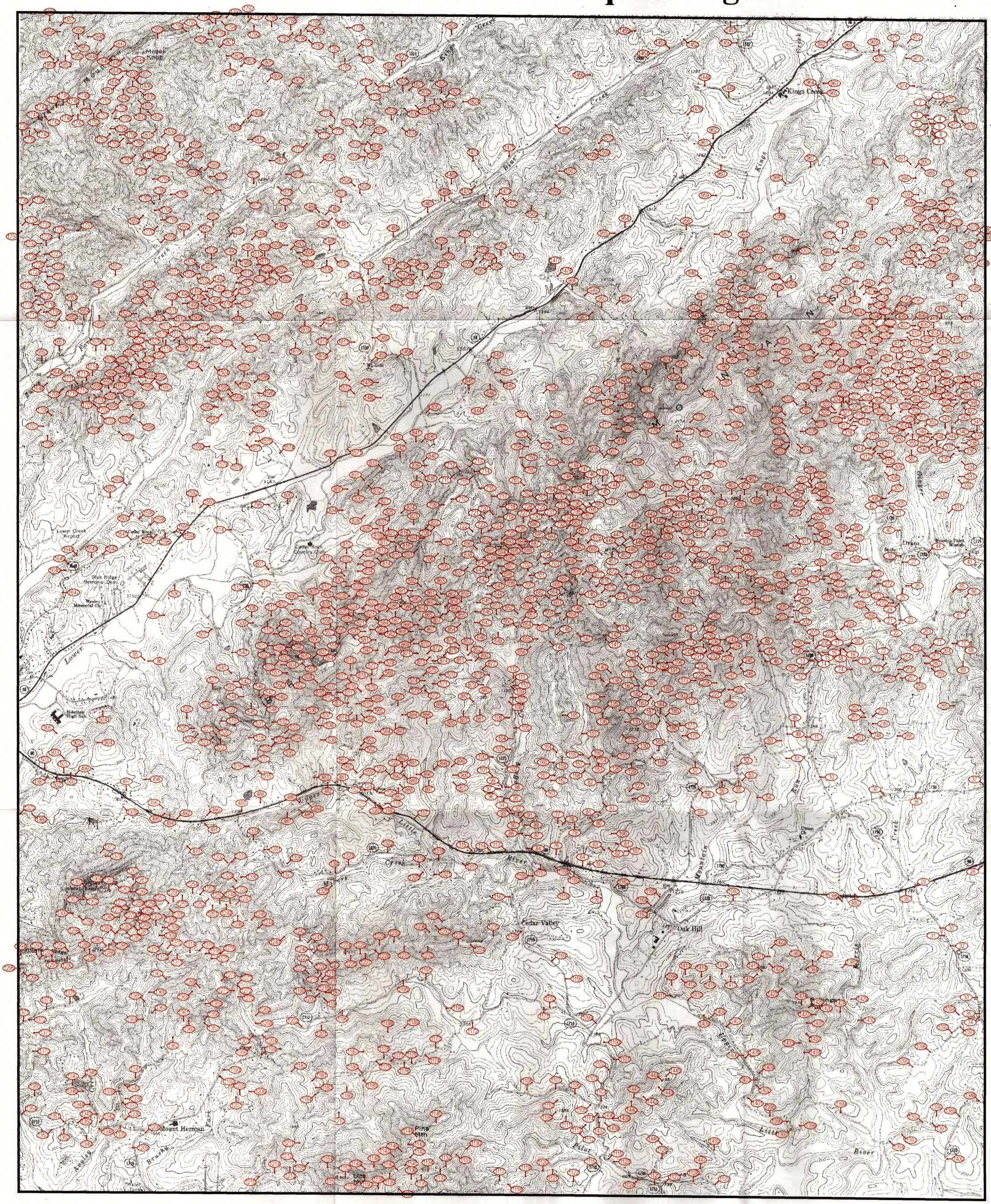

SCALE 1:24 000

1 0 1 MILE

1000 1000 2000 3000 4000 5000 6000 7000 FEET

1 .5 0 1 KILOMETER

CONTOUR INTERVAL 20 FEET

DATUM IS MEAN SEA LEVEL

MN GN

3° 53 MILS 0°15' 4 MILS

UTM GRID AND 1970 MAGNETIC NORTH DECLINATION AT CENTER OF SHEET